

Estimation of Key PCC, Base, Subbase, and Pavement Engineering Properties from Routine Tests and Physical Characteristics

PUBLICATION NO. FHWA-HRT-12-030

AUGUST 2012



U.S. Department of Transportation
Federal Highway Administration

Research, Development, and Technology
Turner-Fairbank Highway Research Center
6300 Georgetown Pike
McLean, VA 22101-2296



FOREWORD

Material characterization is a basic aspect of pavement engineering and is critical for analysis, performance prediction, design, construction, quality control/quality assurance, pavement management, and rehabilitation. Advanced tools like the American Association of State Highway and Transportation Officials *Mechanistic-Empirical Pavement Design Guide, Interim Edition: A Manual of Practice* (MEPDG) can be used to estimate the influence of several fundamental engineering material parameters on the long-term performance of a pavement.⁽¹⁾ Consequently, there is a need for more information about material properties, which are addressed only to a limited extent with currently available resources for performing laboratory and field testing. Reliable correlations between material parameters and index properties offer a cost-effective alternative, and the derived material property values are equivalent to the level 2 inputs in the MEPDG. This study initially verified the adequacy of the Long-Term Pavement Performance (LTPP) data and also made a preliminary assessment of the feasibility of developing the correlation models. In the next phase of the study, prediction models were developed to help practicing engineers estimate proper MEPDG inputs. This report describes the basis for selecting material parameters that need predictive models, provides a review of current LTPP program data, and proposes several statistically derived models to predict material properties. The models developed under this effort have been incorporated into a simple software program compatible with current versions of Microsoft Windows[®] operating system.

Jorge E. Pagán-Ortiz
Director, Office of Infrastructure
Research and Development

Notice

This document is disseminated under the sponsorship of the U.S. Department of Transportation in the interest of information exchange. The U.S. Government assumes no liability for the use of the information contained in this document. This report does not constitute a standard, specification, or regulation.

The U.S. Government does not endorse products or manufacturers. Trademarks or manufacturers' names appear in this report only because they are considered essential to the objective of the document.

Quality Assurance Statement

The Federal Highway Administration (FHWA) provides high-quality information to serve Government, industry, and the public in a manner that promotes public understanding. FHWA uses standards and policies are used to ensure and maximize the quality, objectivity, utility, and integrity of its information. It also periodically reviews quality issues and adjusts its programs and processes to ensure continuous quality improvement.

TECHNICAL REPORT DOCUMENTATION PAGE

1. Report No. FHWA-HRT-12-030	2. Government Accession No.	3. Recipient's Catalog No.	
4. Title and Subtitle Estimation of Key PCC, Base, Subbase, and Pavement Engineering Properties from Routine Tests and Physical Characteristics		5. Report Date August 2012	
		6. Performing Organization Code	
7. Author(s) C. Rao, L. Titus-Glover, B. Bhattacharya, M.I. Darter, M. Stanley, and H. L. Von Quintus		8. Performing Organization Report No.	
9. Performing Organization Name and Address Applied Research Associates, Inc. 100 Trade Centre Drive, Suite 200 Champaign, IL 61820		10. Work Unit No. (TRAIS)	
		11. Contract or Grant No. DTFH61-02-C-00138	
12. Sponsoring Agency Name and Address Office of Infrastructure Research and Development Federal Highway Administration 6300 Georgetown Pike McLean, VA 22101-2296		13. Type of Report and Period Covered Interim Report	
		14. Sponsoring Agency Code	
15. Supplementary Notes The Contracting Officer's Technical Representative (COTR) was Larry Wisner, HRDI LTPP data analysis contract.			
16. Abstract Material characterization is a critical component of modern day pavement analysis, design, construction, quality control/quality assurance, management, and rehabilitation. At each stage during the life of a project, the influence of several fundamental engineering material parameters on the long-term performance of the pavement can be predicted using advanced tools like the American Association of State Highway and Transportation Officials <i>Mechanistic-Empirical Pavement Design Guide, Interim Edition: A Manual of Practice</i> (MEPDG). Consequently, there is a need for more information about material properties, which are addressed only to a limited extent with currently available resources for performing laboratory and field testing. Reliable correlations between material parameters and index properties offer a cost-effective alternative and are equivalent to the level 2 MEPDG inputs. The Long-Term Pavement Performance database provides data suitable for developing predictive models for Portland cement concrete (PCC) materials, stabilized materials, and unbound materials, as well as other design-related inputs for the MEPDG. This report describes the procedure for developing the following models: <ul style="list-style-type: none"> • PCC materials: Compressive strength, flexural strength, elastic modulus, tensile strength, and coefficient of thermal expansion. • Stabilized materials: Elastic modulus of lean concrete base. • Unbound materials: Resilient modulus of fine-grained and coarse-grained materials. • Rigid pavement design features: Pavement curl/wrap effective temperature difference for jointed plain concrete pavement and continuously reinforced concrete pavement designs. 			
17. Key Words Pavements, LTPP, Material properties, MEPDG, Prediction model, Index properties		18. Distribution Statement No restrictions. This document is available to the public through the National Technical Information Service, Springfield, VA 22161.	
19. Security Classification (of this report) Unclassified	20. Security Classification (of this page) Unclassified	21. No. of Pages 214	22. Price

SI* (MODERN METRIC) CONVERSION FACTORS

APPROXIMATE CONVERSIONS TO SI UNITS

Symbol	When You Know	Multiply By	To Find	Symbol
LENGTH				
in	inches	25.4	millimeters	mm
ft	feet	0.305	meters	m
yd	yards	0.914	meters	m
mi	miles	1.61	kilometers	km
AREA				
in ²	square inches	645.2	square millimeters	mm ²
ft ²	square feet	0.093	square meters	m ²
yd ²	square yard	0.836	square meters	m ²
ac	acres	0.405	hectares	ha
mi ²	square miles	2.59	square kilometers	km ²
VOLUME				
fl oz	fluid ounces	29.57	milliliters	mL
gal	gallons	3.785	liters	L
ft ³	cubic feet	0.028	cubic meters	m ³
yd ³	cubic yards	0.765	cubic meters	m ³
NOTE: volumes greater than 1000 L shall be shown in m ³				
MASS				
oz	ounces	28.35	grams	g
lb	pounds	0.454	kilograms	kg
T	short tons (2000 lb)	0.907	megagrams (or "metric ton")	Mg (or "t")
TEMPERATURE (exact degrees)				
°F	Fahrenheit	5 (F-32)/9 or (F-32)/1.8	Celsius	°C
ILLUMINATION				
fc	foot-candles	10.76	lux	lx
fl	foot-Lamberts	3.426	candela/m ²	cd/m ²
FORCE and PRESSURE or STRESS				
lbf	poundforce	4.45	newtons	N
lbf/in ²	poundforce per square inch	6.89	kilopascals	kPa
APPROXIMATE CONVERSIONS FROM SI UNITS				
Symbol	When You Know	Multiply By	To Find	Symbol
LENGTH				
mm	millimeters	0.039	inches	in
m	meters	3.28	feet	ft
m	meters	1.09	yards	yd
km	kilometers	0.621	miles	mi
AREA				
mm ²	square millimeters	0.0016	square inches	in ²
m ²	square meters	10.764	square feet	ft ²
m ²	square meters	1.195	square yards	yd ²
ha	hectares	2.47	acres	ac
km ²	square kilometers	0.386	square miles	mi ²
VOLUME				
mL	milliliters	0.034	fluid ounces	fl oz
L	liters	0.264	gallons	gal
m ³	cubic meters	35.314	cubic feet	ft ³
m ³	cubic meters	1.307	cubic yards	yd ³
MASS				
g	grams	0.035	ounces	oz
kg	kilograms	2.202	pounds	lb
Mg (or "t")	megagrams (or "metric ton")	1.103	short tons (2000 lb)	T
TEMPERATURE (exact degrees)				
°C	Celsius	1.8C+32	Fahrenheit	°F
ILLUMINATION				
lx	lux	0.0929	foot-candles	fc
cd/m ²	candela/m ²	0.2919	foot-Lamberts	fl
FORCE and PRESSURE or STRESS				
N	newtons	0.225	poundforce	lbf
kPa	kilopascals	0.145	poundforce per square inch	lbf/in ²

*SI is the symbol for the International System of Units. Appropriate rounding should be made to comply with Section 4 of ASTM E380. (Revised March 2003)

TABLE OF CONTENTS

EXECUTIVE SUMMARY	1
BACKGROUND	1
MODEL DEVELOPMENT	1
LIST OF MODELS.....	3
CHAPTER 1. INTRODUCTION.....	5
BACKGROUND	5
DATA NEEDS.....	5
Design	5
Construction.....	6
Pavement Management.....	8
OBJECTIVES AND SCOPE	8
SCOPE OF THE REPORT AND ORGANIZATION.....	9
CHAPTER 2. MATERIAL PROPERTIES FOR PREDICTIVE EQUATIONS.....	11
INPUTS FOR MEPDG.....	11
Hierarchical Inputs for MEPDG	11
Input Categories for the MEPDG	12
Correlations Developed/Adapted for the MEPDG	14
SELECTION OF MATERIAL PARAMETERS.....	15
CHAPTER 3. LITERATURE REVIEW	21
CORRELATION BETWEEN PCC MIX MECHANICAL PROPERTIES AND PCC MIX CONSTITUENT PROPORTIONS AND OTHER PCC PROPERTIES.....	21
Compressive Strength	21
Flexural Strength and Splitting Tensile Strength.....	28
Elastic Modulus	31
CTE.....	34
Drying Shrinkage.....	35
PREDICTION OF CHEMICALLY STABILIZED MATERIAL PROPERTIES	36
PREDICTION OF UNBOUND MATERIAL AND SOIL RESILIENT MODULUS....	37
Overview.....	37
Resilient Modulus Prediction Models.....	38
Regression Constant Estimates Based on Soil Properties	46
SELECTION OF INDEPENDENT VARIABLES FOR THE PREDICTION OF MATERIAL ENGINEERING PROPERTIES	56
CHAPTER 4. DATA ASSEMBLY AND MODELING CONSIDERATIONS.....	61
DATA SELECTION FOR CURRENT STUDY	61
DATA REVIEW.....	65
Key Findings From Data Review	65

CHAPTER 5. MODEL DEVELOPMENT.....	69
STATISTICAL ANALYSES METHODS ADOPTED	69
Formulating Data for Statistical Models.....	69
Statistical Criteria for Used for Model Development.....	73
Other Modeling Considerations.....	76
Procedures for Model Development.....	78
PCC MODELS.....	79
Data Used in PCC Models.....	79
PCC Compressive Strength Models.....	81
PCC Flexural Strength Models.....	110
PCC Elastic Modulus Models.....	119
PCC Tensile Strength Models.....	129
PCC CTE Models.....	131
RIGID PAVEMENT DESIGN FEATURES MODELS.....	140
ΔT —JPCP Design.....	140
ΔT —CRCP Design.....	149
Erosion for CRCP Design.....	154
EI for JPCP Design.....	154
STABILIZED MATERIALS MODELS	155
LCB Elastic Modulus Model.....	155
UNBOUND MATERIALS MODELS.....	156
Data Assembly for Resilient Modulus Model Development.....	157
Resilient Modulus Model Development.....	168
PRACTICAL GUIDE AND SOFTWARE PROGRAM.....	175
CHAPTER 6. SUMMARY AND FUTURE WORK	177
SUMMARY	177
PCC MATERIALS	179
PCC Compressive Strength Models.....	179
PCC Flexural Strength Models.....	180
PCC Elastic Modulus Models.....	181
PCC Indirect Tensile Strength Models.....	182
PCC CTE Models.....	182
RIGID PAVEMENT DESIGN FEATURES MODELS.....	183
ΔT —JPCP Design.....	183
ΔT —CRCP Design.....	184
Erosion for CRCP Design.....	184
EI for JPCP Design.....	184
STABILIZED MATERIALS MODELS	184
LCB Elastic Modulus Model.....	184
UNBOUND MATERIALS MODELS.....	185
Resilient Modulus of Unbound Materials.....	185
FUTURE WORK.....	185
REFERENCES.....	187

LIST OF FIGURES

Figure 1. Illustration. MEPDG performance prediction during the design and construction stage	7
Figure 2. Illustration. Summary of factors affecting PCC strength	24
Figure 3. Equation. f_c according to Abrams	27
Figure 4. Equation. f_c according to Neville	27
Figure 5. Equation. f_c according to Colak	27
Figure 6. Equation. f_c according to ACI 318.....	28
Figure 7. Equation. f_c according to Wang et al	28
Figure 8. Equation. MR	29
Figure 9. Equation. MR according to Neville	30
Figure 10. Equation. MR according to Sozen et al	30
Figure 11. Equation. MOR according to NCHRP	30
Figure 12. Equation. f'_{sp}	30
Figure 13. Equation. $f_{ctk,min}$ according to <i>CEB-FIP Model Code 1990</i>	30
Figure 14. Equation. $f_{ctk,max}$ according to <i>CEB-FIP Model Code 1990</i>	30
Figure 15. Equation. $f_{ct,mean}$ according to <i>CEB-FIP Model Code 1990</i>	30
Figure 16. Equation. f'_{sp} according to Mehta and Monteiro.....	31
Figure 17. Equation. f'_{sp} according to NCHRP	31
Figure 18. Equation. E_c where constants are defined by various researchers.....	33
Figure 19. Equation. E_c according to ACI 318.....	33
Figure 20. Equation. E_c for normal strength concrete according to Tomosawa et al	33
Figure 21. Equation. E_c according to <i>CEB-FIP Model Code 1990</i>	33
Figure 22. Equation. MR according to Jensen via Irick et al	33
Figure 23. Equation. MR according to Hognestad via Irick et al.....	34
Figure 24. Equation. E_c according to Turkish Standard 500.....	34
Figure 25. Equation. E_c according to Noguchi et al.....	34
Figure 26. Equation. $E_{ct}/E_{c,28}$ according to NCHRP	34
Figure 27. Equation. α_c according to Neekhra	35
Figure 28. Equation. α_{PCC} according to NCHRP	35
Figure 29. Equation. E for lean concrete or cement treated aggregate	36
Figure 30. Equation. E for soil cement	36
Figure 31. Equation. E for lime-cement-flyash	37
Figure 32. Equation. M_r for lime-stabilized soils.....	37
Figure 33. Equation. M_r according to NCHRP Project 1-28A.....	38
Figure 34. Equation. M_r according to Jones and Witczak.....	39
Figure 35. Equation. M_r according to Thompson and LaGrow	39
Figure 36. Equation. M_r according to Thompson and Robnett	39
Figure 37. Equation. M_r according to Carmichael and Stuart for fine subgrade soils containing clay and silts.....	39
Figure 38. Equation. M_r according to Carmichael and Stuart for coarse granular soils and aggregate bases	40
Figure 39. Equation. M_r according to Elliot et al. with deviator stress of 4 psi.....	40
Figure 40. Equation. M_r according to Elliot et al. with deviator stress of 8 psi	40
Figure 41. Equation. M_r according to Rahim for fine-grained soils.....	40

Figure 42. Equation. M_r according to Rahim for coarse-grained soils.....	40
Figure 43. Equation. M_r according to Farrar and Turner	40
Figure 44. Equation. M_r according to Hudson et al.....	40
Figure 45. Equation. M_r according to Li and Selig.....	40
Figure 46. Equation. M_r according to Gupta et al	41
Figure 47. Equation. M_r according to Berg et al	41
Figure 48. Equation. M_r according to Pezo and Hudson	41
Figure 49. Equation. Correlation between M_r and CBR according to Heukelom and Klomp.....	42
Figure 50. Equation. Correlation between M_r and CBR according to Powell et al	42
Figure 51. Equation. Correlation between M_r and CBR according to George	42
Figure 52. Equation. Correlation between M_r and CBR according to the Asphalt Institute.....	42
Figure 53. Equation. Correlation between M_r and R-value according to AASHTO	42
Figure 54. Equation. Correlation between M_r and R-value according to Buu.....	42
Figure 55. Equation. Correlation between M_r and R-value according to Yeh and Su.....	43
Figure 56. Equation. Correlation between M_r and R-value according to MEPDG	43
Figure 57. Equation. Correlation between M_r and unconfined compressive strength according to Thompson and Robnett	43
Figure 58. Equation. Correlation between M_r and shear strength according to Lee et al	43
Figure 59. Equation. Correlation between M_r and DCP test method according to Hassan	43
Figure 60. Equation. Correlation between M_r and DCP test method according to Chen et al.....	43
Figure 61. Equation. Correlation between M_r and DCP test method for coarse-grained sandy soils according to George and Uddin.....	43
Figure 62. Equation. Correlation between M_r and DCP test method for fine-grained clays according to George and Uddin	43
Figure 63. Equation. Correlation between M_r and DCP test method according to Chen et al	44
Figure 64. Equation. Correlation between M_r and DCP test method DCPI only according to Mohammad et al	44
Figure 65. Equation. Correlation between M_r and DCP test method DCPI and soil properties according to Mohammad et al.....	44
Figure 66. Equation. Correlation between M_r and CPT test method in situ conditions according to Mohammad et al.....	44
Figure 67. Equation. Correlation between M_r and CPT test method traffic loading conditions according to Mohammad et al.....	45
Figure 68. Equation. M_r of Mississippi materials for fine-grained soils.....	46
Figure 69. Equation. k_1 of Mississippi materials for fine-grained soils.....	46
Figure 70. Equation. k_2 of Mississippi materials for fine-grained soils.....	47
Figure 71. Equation. M_r of Mississippi materials for coarse-grained soils.....	47
Figure 72. Equation. k_1 of Mississippi materials for coarse-grained soils.....	47
Figure 73. Equation. k_2 of Mississippi materials for coarse-grained soils.....	47
Figure 74. Equation. M_r of Georgia materials	47
Figure 75. Equation. k_1 of Georgia materials.....	48
Figure 76. Equation. k_2 of Georgia materials.....	48
Figure 77. Equation. k_3 of Georgia materials.....	48
Figure 78. Equation. M_r of Louisiana materials.....	48
Figure 79. Equation. k_1 of Louisiana materials.....	49

Figure 80. Equation. k_2 of Louisiana materials.....	49
Figure 81. Equation. k_3 of Louisiana materials.....	49
Figure 82. Equation. M_r of LTPP materials.....	49
Figure 83. Equation. k_1 of LTPP materials—crushed stone.....	50
Figure 84. Equation. k_2 of LTPP materials—crushed stone.....	50
Figure 85. Equation. k_3 of LTPP materials—crushed stone.....	50
Figure 86. Equation. k_1 of LTPP materials—crushed gravel.....	51
Figure 87. Equation. k_2 of LTPP materials—crushed gravel.....	51
Figure 88. Equation. k_3 of LTPP materials—crushed gravel.....	51
Figure 89. Equation. k_1 of LTPP materials—uncrushed gravel.....	51
Figure 90. Equation. k_2 of LTPP materials—uncrushed gravel.....	51
Figure 91. Equation. k_3 of LTPP materials—uncrushed gravel.....	51
Figure 92. Equation. k_1 of LTPP materials—sand.....	51
Figure 93. Equation. k_2 of LTPP materials—sand.....	51
Figure 94. Equation. k_3 of LTPP materials—sand.....	52
Figure 95. Equation. k_1 of LTPP materials—coarse-grained soil-aggregate mixture.....	52
Figure 96. Equation. k_2 of LTPP materials—coarse-grained soil-aggregate mixture.....	52
Figure 97. Equation. k_3 of LTPP materials—coarse-grained soil-aggregate mixture.....	52
Figure 98. Equation. k_1 of LTPP materials—fine-grained soil-aggregate mixture.....	52
Figure 99. Equation. k_2 of LTPP materials—fine-grained soil-aggregate mixture.....	52
Figure 100. Equation. k_3 of LTPP materials—fine-grained soil-aggregate mixture.....	52
Figure 101. Equation. k_1 of LTPP materials—fine-grained soil.....	53
Figure 102. Equation. k_2 of LTPP materials—fine-grained soil.....	53
Figure 103. Equation. k_3 of LTPP materials—fine-grained soil.....	53
Figure 104. Equation. k_1 of LTPP materials—coarse-grained gravel soils.....	53
Figure 105. Equation. k_2 of LTPP materials—coarse-grained gravel soils.....	53
Figure 106. Equation. k_3 of LTPP materials—coarse-grained gravel soils.....	53
Figure 107. Equation. k_1 of LTPP materials—coarse-grained sand soils.....	53
Figure 108. Equation. k_2 of LTPP materials—coarse-grained sand soils.....	53
Figure 109. Equation. k_3 of LTPP materials—coarse-grained sand soils.....	53
Figure 110. Equation. k_1 of LTPP materials—fine-grained silt soils.....	54
Figure 111. Equation. k_2 of LTPP materials—fine-grained silt soils.....	54
Figure 112. Equation. k_3 of LTPP materials—fine-grained silt soils.....	54
Figure 113. Equation. k_1 of LTPP materials—fine-grained clay soils.....	54
Figure 114. Equation. k_2 of LTPP materials—fine-grained clay soils.....	54
Figure 115. Equation. k_3 of LTPP materials—fine-grained clay soils.....	54
Figure 116. Equation. k_1 of Wisconsin materials—fine-grained soils.....	55
Figure 117. Equation. k_2 of Wisconsin materials—fine-grained soils.....	55
Figure 118. Equation. k_3 of Wisconsin materials—fine-grained soils.....	55
Figure 119. Equation. k_1 of Wisconsin materials—non-plastic coarse-grained soils.....	55
Figure 120. Equation. k_2 of Wisconsin materials—non-plastic coarse-grained soils.....	55
Figure 121. Equation. k_3 of Wisconsin materials—non-plastic coarse-grained soils.....	55
Figure 122. Equation. k_1 of Wisconsin materials—plastic coarse-grained soils.....	55
Figure 123. Equation. k_2 of Wisconsin materials—plastic coarse-grained soils.....	56
Figure 124. Equation. k_3 of Wisconsin materials—plastic coarse-grained soils.....	56
Figure 125. Equation. C_p	74

Figure 126. Equation. MSE_f	74
Figure 127. Equation. VIF	74
Figure 128. Equation. f_c linear model form with no transformation.....	78
Figure 129. Equation. $E_{c,t}$ nonlinear model form with no transformation	78
Figure 130. Equation. k_1 linear model form with transformation	78
Figure 131. Equation. k_1 nonlinear model form with transformation	78
Figure 132. Equation. f_c model form.....	82
Figure 133. Graph. Predicted versus measured for 28-day cylinder compressive strength model.....	90
Figure 134. Graph. Residual error plot for 28-day cylinder compressive strength model	91
Figure 135. Equation. Prediction model 1 for $f_{c,28d}$	91
Figure 136. Graph. 28-day compressive strength model sensitivity to w/c ratio	92
Figure 137. Graph. 28-day compressive strength model sensitivity to CMC.....	92
Figure 138. Equation. Prediction model 2 for $f_{c,t}$	93
Figure 139. Graph. Predicted versus measured for short-term cylinder compressive strength model.....	94
Figure 140. Graph. Residual errors for short-term cylinder compressive strength model	94
Figure 141. Graph. Short-term cylinder compressive strength sensitivity to CMC	95
Figure 142. Graph. Short-term cylinder compressive strength sensitivity to w/c ratio	95
Figure 143. Graph. Short-term cylinder compressive strength sensitivity to age.....	95
Figure 144. Graph. Comparison of core and cylinder strengths for SPS sections.....	96
Figure 145. Equation. Prediction model 3 for $f_{c,t}$	97
Figure 146. Graph. Predicted versus measured for short-term core compressive strength model.....	99
Figure 147. Graph. Residual errors for short-term core compressive strength model.....	99
Figure 148. Graph. Short-term core compressive strength sensitivity to CMC.....	99
Figure 149. Graph. Short-term core compressive strength sensitivity to unit weight	100
Figure 150. Graph. Short-term core compressive strength sensitivity to MAS.....	100
Figure 151. Graph. Short-term core compressive strength sensitivity to w/c ratio	100
Figure 152. Graph. Short-term core compressive strength sensitivity to fine aggregate FM.....	101
Figure 153. Graph. Short-term core compressive strength sensitivity to age.....	101
Figure 154. Equation. Prediction model 4 for $f_{c,t}$	101
Figure 155. Graph. Predicted versus measured for all ages core compressive strength model.....	103
Figure 156. Graph. Residual errors for all ages core compressive strength model	103
Figure 157. Graph. All ages core compressive strength sensitivity to w/c ratio	103
Figure 158. Graph. All ages core compressive strength sensitivity to CMC.....	104
Figure 159. Graph. All ages core compressive strength sensitivity to unit weight	104
Figure 160. Graph. All ages core compressive strength sensitivity to age	104
Figure 161. Equation. Prediction model 5 for $f_{c,LT}$	105
Figure 162. Graph. Predicted versus measured for long-term core compressive strength model.....	106
Figure 163. Graph. Residual errors for long-term core compressive strength model.....	106
Figure 164. Graph. Model compressive strength prediction for varying CMC.....	107
Figure 165. Graph. Model compressive strength prediction for varying w/c ratio.....	107
Figure 166. Graph. Model compressive strength prediction for varying unit weights	108

Figure 167. Graph. Strength gain in the short-term predicted by three models.....	108
Figure 168. Graph. Long-term strength gain predicted by the models	109
Figure 169. Equation. M_r	110
Figure 170. Graph. Predicted versus measured for validating 0.5 power flexural strength model.....	111
Figure 171. Graph. Predicted versus measured for validating 0.667 power flexural strength model.....	111
Figure 172. Equation. Prediction model 6 for MR_t	112
Figure 173. Graph. Predicted versus measured values for flexural strength model based on compressive strength.....	113
Figure 174. Graph. Residuals errors for flexural strength model based on compressive strength.....	113
Figure 175. Graph. Comparison of flexural strength models based on compressive strength ...	114
Figure 176. Equation. Prediction model 7 for MR_t	114
Figure 177. Graph. Predicted versus measured values for flexural strength model based on age, unit weight, and w/c ratio	116
Figure 178. Graph. Residuals errors for flexural strength model based on age, unit weight, and w/c ratio.....	116
Figure 179. Equation. Prediction model 8 for MR_t	116
Figure 180. Graph. Predicted versus measured values for flexural strength model based on age, unit weight, and CMC	118
Figure 181. Graph. Residuals errors for flexural strength model based on age, unit weight, and CMC.....	118
Figure 182. Graph. Sensitivity of flexural strength predictions to CMC.....	118
Figure 183. Graph. Sensitivity of flexural strength predictions to w/c ratio	119
Figure 184. Graph. Sensitivity of flexural strength predictions to unit weight	119
Figure 185. Graph. Sensitivity of flexural strength predictions to age.....	119
Figure 186. Equation. E_c as a function of square root of compressive strength	120
Figure 187. Equation. Model form for E as a function of compressive strength with slope and intercept.....	120
Figure 188. Equation. E_c	121
Figure 189. Equation. E as function of unit weight and compressive strength	121
Figure 190. Equation. Prediction model 9 for E_c	122
Figure 191. Equation. E	124
Figure 192. Graph. Predicted versus measured for elastic modulus model based on aggregate type	124
Figure 193. Graph. Residual errors for elastic modulus model based on aggregate type.....	125
Figure 194. Equation. Prediction model 10 for $E_{c,t}$	125
Figure 195. Graph. Predicted versus measured for elastic modulus model based on age and compressive strength.....	126
Figure 196. Graph. Residual errors for elastic modulus model based on age and compressive strength.....	127
Figure 197. Equation. Prediction model 11 for $E_{c,t}$	127
Figure 198. Graph. Predicted versus measured for elastic modulus model based on age and 28-day compressive strength.....	128

Figure 199. Graph. Residual errors for elastic modulus model based on age and 28-day compressive strength.....	129
Figure 200. Equation. Prediction model 12 for f_t	129
Figure 201. Graph. Predicted versus measured for tensile strength model	130
Figure 202. Graph. Residuals error plot for tensile strength model.....	131
Figure 203. Graph. Sensitivity of tensile strength prediction model to change compressive strength.....	131
Figure 204. Graph. Comparison of average values from other sources and recommended CTE values based on aggregate type from LTPP data	134
Figure 205. Equation. CTE_{PCC}	136
Figure 206. Equation. CTE_{PCC} as a function of volumetric proportion	136
Figure 207. Equation. CTE_{PCC} as a function of coarse aggregate volumetric proportio	136
Figure 208. Equation. Prediction model 14 for CTE_{PCC}	136
Figure 209. Graph. Predicted versus measured for CTE model based on mix volumetrics	138
Figure 210. Graph. Residual errors for CTE model based on mix volumetrics	138
Figure 211. Graph. Comparison of CTE model prediction with average values reported in literature for each aggregate rock type.....	139
Figure 212. Graph. CTE model prediction versus average values reported in literature for each aggregate rock type.....	139
Figure 213. Graph. Sensitivity of the CTE model to coarse aggregate content.....	139
Figure 214. Equation. Prediction model 15 for ΔT /inch	142
Figure 215. Graph. Predicted versus measured for JPCP ΔT gradient model.....	144
Figure 216. Graph. Residual errors for JPCP ΔT gradient model	144
Figure 217. Graph. Predicted versus measured ΔT based on the JPCP ΔT gradient model.....	145
Figure 218. Graph. Sensitivity of predicted ΔT to temperature range during month of construction	145
Figure 219. Graph. Sensitivity of predicted ΔT to slab width.....	146
Figure 220. Graph. Sensitivity of predicted ΔT to slab thickness	146
Figure 221. Graph. Sensitivity of predicted ΔT to PCC slab unit weight	146
Figure 222. Graph. Sensitivity of predicted ΔT to PCC w/c ratio.....	147
Figure 223. Graph. Sensitivity of predicted ΔT to latitude of the project location	147
Figure 224. Graph. Predicted ΔT for different locations in the United States	147
Figure 225. Equation. Prediction model 16 for ΔT /inch	150
Figure 226. Graph. Predicted versus measured for CRCP ΔT model	151
Figure 227. Graph. Residual errors for CRCP ΔT model.....	152
Figure 228. Graph. Effect of maximum temperature on CRCP ΔT prediction model	152
Figure 229. Graph. Effect of temperature range on CRCP ΔT prediction model	153
Figure 230. Graph. Effect of slab thickness on CRCP ΔT prediction model	153
Figure 231. Graph. Effect of geographic location on CRCP ΔT prediction.....	153
Figure 232. Equation. Prediction model 17 for E_{LCB}	155
Figure 233. Graph. Predicted versus measured for the LCB elastic modulus model	156
Figure 234. Graph. Residual errors for the LCB elastic modulus model	156
Figure 235. Graph. Mean percent clay fraction for unbound material types included in the model development database	158

Figure 236. Graph. Mean percent coarse sand fraction for unbound material types included in the model development database	158
Figure 237. Graph. Mean percent fine sand fraction for unbound material types included in the model development database	159
Figure 238. Graph. Mean percent silt fraction for unbound material types included in the model development database	159
Figure 239. Graph. Mean hydraulic conductivity for unbound material types included in the model development database	160
Figure 240. Graph. Plot of bulk stress versus lab tested resilient modulus for section 45_1025 (base layer).....	160
Figure 241. Graph. Percent passing No. 4 sieve for unbound material types included in the model development database	161
Figure 242. Graph. Percent passing No. 40 sieve for unbound material types included in the model development database	161
Figure 243. Graph. Percent passing No. 200 sieve for unbound material types included in the model development database	162
Figure 244. Graph. Liquid limit for unbound material types included in the model development database	162
Figure 245. Graph. Plasticity index for unbound material types included in the model development database	163
Figure 246. Graph. Maximum dry density for unbound material types included in the model development database	163
Figure 247. Graph. Optimum moisture content for unbound material types included in the model development database	164
Figure 248. Equation. M_r	165
Figure 249. Graph. Resilient modulus parameter k_1 for unbound material types included in the model development database	166
Figure 250. Graph. Resilient modulus parameter k_2 for unbound material types included in the model development database	166
Figure 251. Graph. Resilient modulus parameter k_3 for unbound material types included in the model development database	167
Figure 252. Graph. Plot of measured versus calculated resilient modulus (using k_1 , k_2 , and k_3 computed from constitutive model).....	168
Figure 253. Equation. Prediction model 18 for k_1	169
Figure 254. Equation. Prediction model 19 for k_2	170
Figure 255. Equation. Prediction model 20 for k_3	170
Figure 256. Graph. Measured versus predicted resilient modulus (using k_1 , k_2 , and k_3 from figure 70 through figure 72).....	171
Figure 257. Graph. Predicted and measured resilient modulus versus bulk stress for fine- and coarse-grained soils.....	171
Figure 258. Graph. Effect of material type (AASHTO soil class) on predicted resilient modulus.....	172
Figure 259. Graph. Effect of percent passing 0.5-inch sieve on predicted resilient modulus	173
Figure 260. Graph. Effect of liquid limit on predicted resilient modulus.....	173
Figure 261. Graph. Effect of optimum moisture content on predicted resilient modulus	174
Figure 262. Graph. Effect of No. 80 sieve on predicted resilient modulus	174

Figure 263. Graph. Effect of gravel content on predicted resilient modulus.....	175
Figure 264. Graph. Effect of effective size on predicted resilient modulus	175
Figure 265. Equation. Prediction model 1 for $f_{c,28d}$	179
Figure 266. Equation. Prediction model 2 for $f_{c,t}$	179
Figure 267. Equation. Prediction model 3 for $f_{c,t}$	179
Figure 268. Equation. Prediction model 4 for $f_{c,t}$	179
Figure 269. Equation. Prediction model 5 for $f_{c,LT}$	180
Figure 270. Equation. Prediction model 6 for MR	180
Figure 271. Equation. Prediction model 7 for MR_t	180
Figure 272. Equation. Prediction model 8 for MR_t	180
Figure 273. Equation. Prediction model 9 for E_c	181
Figure 274. Equation. Prediction model 10 for $E_{c,t}$	181
Figure 275. Equation. Prediction model 11 for $E_{c,t}$	182
Figure 276. Equation. Prediction model 12 for f_t	182
Figure 277. Equation. Prediction model 14 for CTE_{PCC}	183
Figure 278. Equation. Prediction model 15 for $\text{delta}T/\text{inch}$	183
Figure 279. Equation. Prediction model 16 for $\text{delta}T/\text{inch}$	184
Figure 280. Equation. Prediction model 17 for E_{LCB}	184
Figure 281. Equation. M_r	185
Figure 282. Equation. Prediction model 18 for k_1	185
Figure 283. Equation. Prediction model 19 for k_2	185
Figure 284. Equation. Prediction model 20 for k_3	185

LIST OF TABLES

Table 1. Major material types for the MEPDG.....	13
Table 2. PCC material inputs beyond strength considered by the MEPDG for JPCP and CRCP	14
Table 3. PCC material properties and rigid pavement design features considered for generating predictive models	16
Table 4. Chemically stabilized materials properties considered for generating predictive models.....	18
Table 5. Unbound material properties considered for generating predictive models.....	19
Table 6. Potential or likely independent variables to derive prediction models for PCC material properties or design features for rigid pavements.....	57
Table 7. Independent variables to derive prediction models for stabilized materials.....	58
Table 8. Independent variables to derive prediction models for unbound materials	59
Table 9. LTPP sections selected to review data for each category.....	63
Table 10. LTPP data tables queried to obtain data for review and future analyses.....	64
Table 11. Summary of data availability for material property predictive models.....	67
Table 12. Summary of MEPDG calibration sections to develop predictive models for rigid pavement design features.....	68
Table 13. Model types used to derive predictive relationships for PCC material properties or design features for rigid pavements	72
Table 14. Model types used to derive predictive relationships for stabilized materials.....	72
Table 15. Model types used to derive predictive relationships for unbound materials	73
Table 16. C_p selection method for 28-day cylinder compressive strength model	83
Table 17. Regression statistics for the four-variable model suggested by C_p analysis with subset of data that were available for all parameters evaluated.....	87
Table 18. Regression statistics for the four-variable model suggested by C_p analysis with complete dataset available for the parameters selected	87
Table 19. Regression statistics for the three-variable model suggested by C_p analysis	88
Table 20. Regression statistics for the two-variable model suggested by C_p analysis	88
Table 21. Regression statistics for selected prediction model for 28-day PCC cylinder strength.....	90
Table 22. Range of data used for 28-day PCC cylinder strength.....	90
Table 23. Regression statistics for short-term cylinder strength model.....	93
Table 24. Range of data used for short-term cylinder strength model.....	93
Table 25. Paired t -test results for comparison of core and cylinder strengths in SPS data	97
Table 26. Regression statistics for short-term core strength model.....	98
Table 27. Range of data used for short-term core strength model.....	98
Table 28. Regression statistics for all ages core strength model	102
Table 29. Range of data used for all ages core strength model	102
Table 30. Regression statistics for long-term core strength model.....	105
Table 31. Range of data used for long-term core strength model.....	105
Table 32. Power models developed for flexural strength prediction using LTPP data for validation.....	111
Table 33. Regression statistics for flexural strength model based on compressive strength.....	112
Table 34. Range of data used for flexural strength model based on compressive strength.....	112

Table 35. Regression statistics for flexural strength model based on age, unit weight, and w/c ratio.....	115
Table 36. Range of data used for flexural strength model based on age, unit weight, and w/c ratio.....	115
Table 37. Regression statistics for flexural strength model based on age, unit weight, and CMC.....	117
Table 38. Range of data used for flexural strength model based on age, unit weight, and CMC.....	117
Table 39. Regression statistics for elastic modulus model based on aggregate type.....	123
Table 40. Range of data used for elastic modulus model based on aggregate type.....	124
Table 41. Regression statistics for elastic modulus model based on age and compressive strength.....	126
Table 42. Range of data used for elastic modulus model based on age and compressive strength.....	126
Table 43. Regression statistics for elastic modulus model based on age and 28-day compressive strength.....	128
Table 44. Range of data used for elastic modulus model based on age and 28-day compressive strength.....	128
Table 45. Model statistics for tensile strength prediction model.....	130
Table 46. Range of data used for tensile strength prediction model.....	130
Table 47. Prediction model 13 PCC CTE based on aggregate type ($\times 10^{-6}$ inch/inch/ $^{\circ}$ F).....	134
Table 48. Statistical analysis results for CTE model based on mix volumetrics.....	137
Table 49. Range of data used for CTE model based on mix volumetrics.....	137
Table 50. Summary of field measured distress and predicted distress for section 1_3028.....	141
Table 51. Error calculations for section 1_3028.....	141
Table 52. Determining optimal ΔT	142
Table 53. Regression statistics for JPCP ΔT model.....	143
Table 54. Range of data used for JPCP ΔT model.....	143
Table 55. Regression statistics for CRCP ΔT model.....	150
Table 56. Range of data used for CRCP ΔT model.....	151
Table 57. Model 13. CTE based on aggregate type.....	182

LIST OF ABBREVIATIONS AND SYMBOLS

AASHTO	American Association of State Highway and Transportation Officials
AC	Asphalt concrete
ACI	American Concrete Institute
ANOVA	Analysis of variance
CBR	California bearing ratio
CEB-FIP	Committee Euro-International du Beton
CMC	Cementitious materials content
CRCP	Continuously reinforced concrete pavement
CTE	Coefficient of thermal expansion
DCP	Dynamic cone penetrometer
EI	Erodibility Index
EICM	Enhanced integrated climatic model
FEA	Finite element analysis
FHWA	Federal Highway Administration
FM	Fineness modulus
FWD	Falling weight deflectometer
GLM	Generalized linear model
GPS	General Pavement Studies
HMA	Hot mix asphalt
HRIS	Highway Research Information Service
IRI	International Roughness Index
ITZ	Interfacial zone
JPCP	Jointed plain concrete pavement
JRCP	Jointed reinforced concrete pavement
LCB	Lean concrete base
LEA	Layered elastic analysis
LTPP	Long-term pavement performance
MAS	Maximum aggregate size
M-E	Mechanistic-empirical
MEPDG	<i>Mechanistic-Empirical Pavement Design Guide</i>
MPT	Maximum paste thickness

<i>MR</i>	Modulus of rupture
NCHRP	National Cooperative Highway Research Program
PCA	Portland Cement Association
PCC	Portland cement concrete
PRS	Performance-related specification
QA	Quality assurance
QC	Quality control
RMSE	Root mean square error
SEE	Standard error of estimate
SCM	Supplemental cementitious material
SHA	State highway agency
SHRP	Strategic Highway Research Program
SPS	Specific Pavement Studies
TFHRC	Turner-Fairbank Highway Research Center
UCS	Unified Classification System
VIF	Variance inflation factor

EXECUTIVE SUMMARY

BACKGROUND

The goal of this study was to develop predictive models to estimate material properties and pavement engineering properties for use in routine practice. The study focused on rigid pavement and relevant material types, primarily Portland cement concrete (PCC) materials, stabilized materials, and unbound materials, including subgrade soils. As such, the objectives of this study were as follows:

- Identify a set of material engineering properties for which predictive relationships would be useful in pavement design, construction quality control/quality assurance (QC/QA), and pavement management applications.
- Establish and/or validate relationships between the identified engineering properties and routine test results, index properties, and other readily available information.
- Develop a practical guide accompanied by user friendly software incorporating the recommendations.

In recent years, pavement engineering practices have emphasized the importance of proper material characterization to optimize pavement performance. Procedures like the *Mechanistic-Empirical Pavement Design Guide* (MEPDG) use various material property inputs for pavement performance prediction.⁽²⁾ The greater need for estimating material properties is being addressed only to a limited extent with the currently available resources. Reliable correlations between material parameters and index properties offer a cost-effective alternative and are equivalent to the level 2 MEPDG inputs. These models can also support agencies in improving QC/QA specifications and pavement management functions.

MODEL DEVELOPMENT

The Long-Term Pavement Performance (LTPP) study database, which contains material property test results and material index properties, provided the necessary data to develop the models in this study. The most recent version of the LTPP database that was available at the time of the study, *Standard Data Release 23.0*, was used.⁽³⁾ Material properties and pavement engineering properties for which develop predictive models were developed were selected based on the following:

- Material inputs requirements for the MEPDG design procedure and the sensitivity of the specific parameter for performance prediction.
- Typical agency needs for determining material properties during QA.
- Typical agency needs for determining material properties during routine pavement management functions.
- Data availability in the LTPP database.

Predictive models were developed for PCC compressive strength, PCC flexural strength, PCC elastic modulus, PCC tensile strength, lean concrete base (LCB) modulus, and unbound materials resilient modulus. In addition, rigid pavement design feature input properties were developed using the MEPDG calibration data. These include the jointed plain concrete pavement (JPCP) and continuously reinforced concrete pavement (CRCP) ΔT parameters, where ΔT is defined as the equivalent temperature differential that corresponds to the effective permanent curl-warp locked into the pavement. For all PCC material properties, multiple models were developed for use in different project situations and also provided users with prediction model alternatives depending on the extent of mix design information available.

In developing the models, a uniform set of statistical criteria were used to select independent parameters to define a relationship as well as to mathematically formulate prediction functions. The analyses examined several statistical parameters in choosing the optimal model and in determining the predictive ability of the model. In general, the optimal set of independent variables (through the Mallows coefficient, C_p), the interaction effects (through the variance inflation factor (VIF)), the significance of the variable (through the p -value), and the goodness of fit (through the R^2 value) were verified. Additionally, the study validated or refined existing models and developed new relationships. In the analyses, the following general observations were made:

- PCC compressive strength could be correlated to several index properties. It was found to increase with decreasing water/cement (w/c) ratio and increasing cementitious materials content (CMC), curing time, and unit weight while decreasing maximum aggregate size (MAS) for a given level of w/c ratio and fineness modulus (FM) of the sand.
- PCC flexural strength could be correlated to the compressive strength using a power model. These relationships were validated and refined using the LTPP data. It also could be correlated to the w/c ratio, unit weight, CMC, and curing time. The correlation was improved significantly in the new models with the additional parameters. The flexural strength increased proportionally with all parameters listed except w/c ratio, with which it had an inverse relationship.
- PCC elastic modulus could be correlated to the compressive strength and unit weight using a power model, as has been done in past studies. These relationships were validated and verified with the data used in this study. Predictions could be made based on aggregate type, unit weight, compressive strength, and age with improved correlation. The elastic modulus increased with an increase in magnitude of all parameters listed.
- PCC tensile strength was found to correlate well with the compressive strength using a power relationship.
- The coefficient of thermal expansion (CTE) of PCC was most sensitive to the coarse aggregate type and the volumetrics of the mix design.
- JPCP ΔT negative gradient increased with an increase in temperature range at the project location for the month of construction and slab width and increased with a decrease in PCC thickness, unit weight, w/c ratio, and latitude of the project location.

- CRCP ΔT negative gradient increased with an increase in maximum temperature at the project location for the month of construction and maximum temperature range and decreased with the use of chert, granite, limestone, and quartzite.
- The modulus of LCB correlated well with its 28-day compressive strength based on a power model.
- The prediction of resilient modulus was possible using parameters k_1 , k_2 , and k_3 of the constitutive model as follows:
 - The parameter k_1 increased with decreasing percent passing the $1/2$ -inch sieve, increasing liquid limit, and decreasing optimum moisture content.
 - The parameter k_2 increased with decreasing percent passing the No. 80 sieve, decreasing liquid limit and percent gravel, and increasing maximum particle size of the smallest 10 percent of the soil sample.
 - The parameter k_3 was dependent on the soil classification (coarse-grained versus fine-grained materials).

LIST OF MODELS

The following models have been developed under this study.

PCC compressive strength models include the following:

- Compressive strength model 1—28-day cylinder strength model.
- Compressive strength model 2—Short-term cylinder strength model.
- Compressive strength model 3—Short-term core strength model.
- Compressive strength model 4—All ages core strength model.
- Compressive strength model 5—Long-term core strength model.

PCC flexural strength models include the following:

- Flexural strength model 1—Flexural strength based on compressive strength.
- Flexural strength model 2—Flexural strength based on age, unit weight, and w/c ratio.
- Flexural strength model 3—Flexural strength based on age, unit weight, and CMC.

PCC elastic modulus models include the following:

- Elastic modulus model 1—Model based on aggregate type.
- Elastic modulus model 2—Model based on age and compressive strength.
- Elastic modulus model 3—Model based on age and 28-day compressive strength.

PCC indirect tensile strength model is as follows:

- PCC indirect tensile strength model—Model based on compressive strength.

PCC CTE models include the following:

- CTE model 1—CTE based on aggregate type (level 3 equation for MEPDG).
- CTE model 2—CTE based on mix volumetrics (level 2 equation for MEPDG).

The JPCP design ΔT model is as follows:

- JPCP ΔT model—JPCP ΔT gradient based on temperature range, slab width, slab thickness, PCC unit weight, w/c ratio, and latitude.

The CRCP design ΔT model is as follows:

- CRCP ΔT model—CRCP ΔT gradient based on maximum temperature, maximum temperature range, and aggregate type.

The lean concrete base elastic modulus is as follows:

- Elastic modulus model—Elastic modulus based on 28-day compressive strength.

The unbound materials resilient modulus is as follows:

- Resilient modulus model—Resilient modulus using constitutive model based on gradation, Atterberg limits, optimum moisture content, and soil classification.

CHAPTER 1. INTRODUCTION

BACKGROUND

Material characterization is vital to pavement analyses and has received increasing focus as it forms a critical component in recent improvements to engineering practices. This pertains to all aspects of pavement engineering—analysis, design, construction, QC/QA, pavement management, and rehabilitation. At each stage during the life of a project, the influence of several fundamental engineering material parameters on the long-term performance of the pavement has been recognized. There is a greater emphasis for optimizing the performance of concrete pavements, which involves a detailed understanding of the variables that affect pavement behavior and the properties of concrete that correspond to the desired performance.

Consequently, there is a need for more information about material properties so that they can be characterized accurately for predicting performance or for verifying their quality during the construction phase. With limited resources for performing laboratory and field tests to determine material properties, the need for a secondary means to obtain these material property values (i.e., through correlations or predictive models based on data from routine or less expensive tests) is obvious. Additionally, the American Association of State Highway and Transportation Officials (AASHTO) MEPDG offers users the option of using inputs obtained through correlations.^(2,4,1) The MEPDG defines level 2 inputs as those obtained from correlations between the primary inputs (level 1 measured) and other parameters that are material-specific or are measured through simpler tests. The LTPP database provides an excellent source of information to develop these correlations using material properties of field sections.⁽⁵⁾

The current report addresses critical data needs for design, construction, and pavement management operations under the LTPP Data Analysis Technical Support contract. This project focuses on developing predictive models to estimate PCC and unbound material properties using LTPP data.

DATA NEEDS

Material property data needs in the context of this study are grouped into the following three categories:

- Inputs during the design stage.
- QC/QA during construction.
- Scheduling maintenance and rehabilitation in a pavement management program.

Design

In both empirical and mechanistic-empirical (M-E) design systems, material property inputs are essential to characterize pavement behavior and to predict pavement responses, such as the magnitudes of stress, strain, and displacement, when subjected to applied traffic loads and environmental conditions. Furthermore, major pavement distresses are associated directly with

the material properties of a component (or layer) of the pavement structure. For example, in JPCP, transverse cracking is influenced by PCC flexural strength. Faulting can be related to the erodibility of the underlying base/subbase material. Punchout development in CRCP can be related to PCC tensile strength.

The MEPDG, developed under National Cooperative Highway Research Program (NCHRP) Project 1-37A and subsequently improved under NCHRP 1-40D, allows users to model the effects of project-specific climate, traffic loads, materials, design features, and construction practices mechanistically to predict pavement performance based on distress models calibrated with LTPP field sections.^(2,4) The MEPDG is considered a significant improvement over current pavement design procedures, and in November 2007, it received the status of an AASHTO interim standard.⁽¹⁾ The publication *User Manual and Local Calibration Guide for the Mechanistic-Empirical Pavement Design Guide and Software* developed under NCHRP 1-40B provides guidance to State highway agencies (SHAs) that are considering implementing the MEPDG.⁽⁶⁾ It is expected that SHAs will adopt locally calibrated distress models that are representative of their specific materials and design conditions.

The need for a variety of material inputs is being recognized as agencies evaluate the MEPDG and streamline efforts for implementation. They continue to face challenges in estimating material parameter inputs and understanding their impact on pavement performance. For example, agencies do not have measured test data or access to databases and the necessary engineering expertise to develop correlations for their needs. Furthermore, due to a lack of familiarity with several input categories, they have come to rely on default values to characterize their typical materials. These default parameters are often a gross approximation of the true value, which may lead to erroneous distress and International Roughness Index (IRI) predictions. As another example, the permanent curl/warp gradient in the national calibration was set at -10 °F through the slab, as it was not possible to obtain an accurate value for this parameter, which depends on construction-related conditions. Analysis of selected LTPP data made it possible to derive an improved way to estimate this important input for design.

This study provides much needed procedures to obtain several inputs and provide correlations to determine the whole range of material properties based on routine test results and physical characteristics. These correlations will supplement the *User Manual and Local Calibration Guide for the Mechanistic-Empirical Pavement Design Guide and Software* to support MEPDG implementation efforts.⁽⁶⁾

Construction

Pavement construction practices are being enhanced continually for faster and more efficient processes. In addition, new materials and material types are being introduced. For example, cement compositions and cement types have changed considerably over the years, resulting in PCC properties and durability characteristics that are different from the past.

The focus of QC/QA procedures is now on identifying more reliable and faster QC/QA tests and determining material properties that are related directly to performance. The MEPDG enables performance prediction of the as-built pavement in addition to that of the as-designed pavement, as long as deviations from design assumptions (material properties or construction practices such

as curing or temperature during construction) are identified during the construction process (see figure 1). For example, although the density of an unbound material is a good indicator of construction quality, the more fundamental resilient modulus is an indicator of performance and is a key input to the MEPDG. The ability to predict resilient modulus from index properties measured during construction will make the QA process address both construction quality and pavement performance issues. Note that in figure 1, material properties measured during construction can be used to predict performance in the field and might be different from the design/target performance.

Also, performance-related specifications (PRSs) for concrete pavements have been developed in recent years. Irick et al., under a Federal Highway Administration (FHWA) study to demonstrate PRS system for rigid pavement construction, considered three key performance indicators: PCC strength, PCC slab thickness, and initial serviceability.⁽⁷⁾ Several relationships for the prediction of PCC properties were evaluated under this study. Irick et al. provide a comprehensive literature summary of models to predict concrete strength parameters. PRSs have also been implemented on several projects that required many correlations between pavement properties and performance.^(8,9)

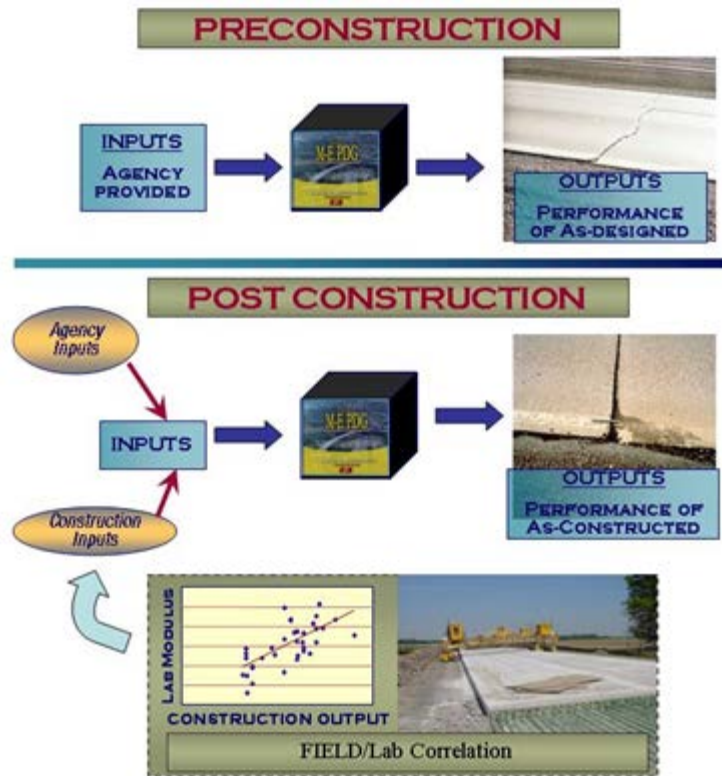


Figure 1. Illustration. MEPDG performance prediction during the design and construction stage.

This study will bridge the gaps in current knowledge regarding the estimation of more fundamental material parameters that influence performance based on index properties or other commonly measured properties during construction.

Pavement Management

One of the key needs in managing pavements is an estimation of remaining life. Several SHAs use this parameter to program rehabilitation treatments. Various models (including the MEPDG models) are useful in that they can be utilized to predict the remaining life until critical levels of each distress and IRI are reached. Also, agencies are now considering the integration of construction quality databases with pavement management databases to track the effect of design and construction quality on long-term performance.⁽¹⁰⁾ Such efforts lend themselves to more accurate performance predictions, whereby the performance of the as-constructed pavement can be used for scheduling maintenance and rehabilitation programs (see figure 1). However, many model inputs are needed related to the existing pavement, including inputs to characterize materials accurately. Index properties from construction QA data can be used to predict fundamental material properties that are related to performance.

In summary, the MEPDG provides a tool to specify material characteristics during the design and construction processes to achieve desired performance. The same models used in the MEPDG for design and construction analyses can be used in the future management of the pavement to estimate its remaining structural and functional life. For example, the inputs for a 10-year-old pavement could be measured from the existing pavement and estimated from the MEPDG models to project future slab cracking. The curve can be adjusted to match today's actual performance to improve the prediction. The slab cracking curve can be projected into the future to determine when it reaches a critical value to estimate its remaining life. The same could be done with joint faulting and IRI.

Therefore, the design, construction, and pavement management stages share a common need for determining a variety of material properties based on correlations from index properties and/or properties determined from more routine test procedures. This practice has been used in past AASHTO pavement design procedures and likely will increase in the future due to the more complex fundamental inputs required for the MEPDG procedure.

OBJECTIVES AND SCOPE

This study utilized LTPP data to develop correlations for SHAs to characterize PCC, subbase, and subgrade materials as necessary for design, QC/QA, and pavement management. It is expected that the findings from this study will assist an agency's materials selection procedures, materials specification, pavement design, and pavement management practices.

To accomplish this overall goal, this research sought to address the following three objectives:

1. Identify a set of material engineering properties for which predictive relationships would be useful in pavement design, construction QC/QA, and pavement management applications.
2. Establish and/or validate relationships between these engineering properties and routine test results, index properties, and/or other readily available information.

3. Develop a practical guide accompanied by user-friendly software for applying the results of the aforementioned tasks in pavement design, construction QC/QA, and pavement management.

This project provides the necessary guidance for agencies to use more accurate values for material properties in design, construction, and pavement management. The correlations developed as part of this study are based on actual data from LTPP sections and, therefore, are more reliable than default or typical values currently being used. The full potential of the MEPDG to predict performance accurately can be realized by providing more accurate input values to the procedure. This also supports improvements in material specifications for use in pavement construction, particularly for PRS. Eventually, these models can be implemented into the *PaveSpec* PRS software and used for construction.⁽¹¹⁾ In particular, the following major benefits will be obtained from this study:

- Support in local calibration of MEPDG models.
- Support in future use of MEPDG.
- Improved designs.
- Improved QC/QA and specifications.
- Improved pavement management.

Most of the data used in the development of prediction models to estimate material properties were obtained from the LTPP *Standard Data Release 23.0*.⁽³⁾

SCOPE OF THE REPORT AND ORGANIZATION

This report documents the work performed under this project and presents the models developed to characterize materials and estimate material inputs. The report consists of five chapters. Chapter 2 describes the selection procedure to identify material properties that require predictive models. Chapter 3 provides a summary of literature reviewed for this study and concludes with a list of index properties (independent variables) used to characterize the material properties identified in chapter 2. Chapter 4 explains the data analyses procedures and discusses the developed models. Chapter 5 provides a summary of the report and presents the conclusions.

CHAPTER 2. MATERIAL PROPERTIES FOR PREDICTIVE EQUATIONS

The primary engineering material properties considered for indepth evaluation in this study were those required for pavement analysis and design using the MEPDG. The MEPDG considers the effects of a comprehensive set of material properties in the structural design of JPCP and CRCP. Its capability to consider strength, modulus, thermal, and other materials properties is the foundation for designing for performance under traffic loads and climatic conditions. Also, the MEPDG procedure can accommodate various material types and uniquely model each material's response to load, temperature, and moisture and predict their effects on performance. Therefore, the research approach was to develop a list of material properties that likely could be estimated based on the availability of data in the LTPP database and the needs of the MEPDG performance prediction models.

INPUTS FOR MEPDG

Hierarchical Inputs for MEPDG

The MEPDG adopts a hierarchical input level scheme to accommodate the designer's knowledge of the input parameter. Inputs can be provided at three different levels. Level 1 inputs represent the greatest knowledge about the input parameter and typically are obtained from a project-specific data collection or test effort. Level 2 represents a moderate level of knowledge of the input parameter and is often calculated from correlations with other site-specific data or a less expensive measure. Level 3 represents the least knowledge of the input parameter and is based on "best-estimated" or default values. For example, level 1 data for concrete flexural strength would involve a flexural beam test, level 2 would be a flexural strength value estimated using a compressive strength test and correlation to flexural strength, and level 3 would be a default value for concrete strength used by a particular SHA. Most agencies have adequate information in their materials and construction quality databases to develop agency-specific default values for immediate implementation of the MEPDG (based on current knowledge and surveys conducted by Rao et al.).⁽¹⁰⁾

During the development of the MEPDG, the need for correlation equations to determine some input values was recognized. Many designs must be created years in advance of construction, and little is known of the exact materials that will be used. However, it is highly desirable to have the best estimates of these inputs possible based on available information. The MEPDG therefore supports the use of level 2 or 3 data in the absence of level 1 laboratory test data. This adaptability is critical to the model types developed in this study and is further discussed in chapter 5 of this report.

Input Categories for the MEPDG

Table 1 provides a list of major material types considered in the MEPDG. Bolded information reflects the material types that are relevant in this project. Each material type requires a variety of material inputs (not all easily available) during local calibration efforts and after the procedure is implemented. As an example, the various PCC material-related inputs considered by the MEPDG are presented in table 2 under the following three categories:

- Material properties required for computing pavement responses.
- Additional material inputs to the distress/transfer functions.
- Additional material inputs required for climatic modeling.

Table 1. Major material types for the MEPDG.⁽²⁾

<p>Asphalt Materials:</p> <ul style="list-style-type: none"> • Stone matrix asphalt. • Hot mix asphalt (HMA). <ul style="list-style-type: none"> ○ Dense graded. ○ Open graded asphalt. ○ Asphalt stabilized base mixes. ○ Sand asphalt mixtures. • Cold mix asphalt. <ul style="list-style-type: none"> ○ Central plant processed. ○ In-place recycled. <p>PCC Materials:</p> <ul style="list-style-type: none"> • Intact slabs—PCC. <ul style="list-style-type: none"> ○ High-strength mixes. ○ Lean concrete mixes. • Fractured slabs. <ul style="list-style-type: none"> ○ Crack/seal. ○ Break/seal. ○ Rubblized. <p>Chemically Stabilized Materials:</p> <ul style="list-style-type: none"> • Cement stabilized aggregate. • Soil cement. • Lime cement fly ash. • Lime fly ash. • Lime stabilized soils. • Open graded cement stabilized aggregate. 	<p>Non-Stabilized Granular Base/Subbase:</p> <ul style="list-style-type: none"> • Granular base/subbase. • Sandy subbase. • Cold recycled asphalt (used as aggregate). <ul style="list-style-type: none"> ○ Recycled asphalt pavement (includes millings). ○ Pulverized in-place. • Cold recycled asphalt pavement (HMA plus aggregate base/subbase). <p>Subgrade Soils:</p> <ul style="list-style-type: none"> • Gravelly Soils (A-1 and A-2). • Sandy Soils. <ul style="list-style-type: none"> ○ Loose sands (A-3). ○ Dense sands (A-3). ○ Silty sands (A-2-4 and A-2-5). ○ Clayey sands (A-2-6 and A-2-7). • Silty soils (A-4 and A-5). <ul style="list-style-type: none"> ○ Clayey soils, low plasticity. ○ Clays (A-6). ○ Dry-hard. ○ Moist stiff. ○ Wet/sat-soft. • Clayey soils, high plasticity clays (A-7) <ul style="list-style-type: none"> ○ Dry-hard. ○ Moist stiff. ○ Wet/sat-soft. <p>Bedrock:</p> <ul style="list-style-type: none"> • Solid, massive, and continuous. • Highly fractured, weathered.
---	---

Note: Bolded information reflects the material types that are relevant in this project.

Table 2 reflects the additional significance of other material engineering properties beyond strength properties for PCC materials in the analysis process. As an example, while concrete modulus of rupture (*MR*) was the main material input for the AASHTO 1993 rigid pavement design procedure (along with the modulus of elasticity), the MEPDG allows correlations through level 2 inputs with compressive strength and requires other volumetric properties such as shrinkage, CTE, specific heat, and thermal conductivity for analysis.⁽¹²⁾ In addition, strength parameters that are used in the analysis include compressive strength, modulus of elasticity, and tensile strength for CRCP. The modulus of elasticity has a much greater effect on performance with the MEPDG than with the AASHTO 1993 procedure. In other words, the MEPDG offers a framework to optimize mix designs to balance a range of strength, modulus, CTE, shrinkage, and other engineering properties for improved performance.⁽¹³⁾

Table 2. PCC material inputs beyond strength considered by the MEPDG for JPCP and CRCP.

Material Inputs Required for Critical Response Computations	Material Inputs Required for Distress/Transfer Functions	Material Inputs Required for Climatic Modeling
<ul style="list-style-type: none"> • Static modulus of elasticity (E) adjusted with time. • Poisson’s ratio. • Unit weight. • CTE. 	<ul style="list-style-type: none"> • MR over time. • Split tensile strength (CRCP only). • Ultimate shrinkage.* • Amount of reversible shrinkage. • Time to achieve 50 percent of ultimate shrinkage. • PCC zero-stress temperature.** 	<ul style="list-style-type: none"> • Surface shortwave absorptivity. • Thermal conductivity. • Heat capacity.

*Estimated from compressive strength, cement type, curing type, cement content, and w/c ratio.

**Estimated from cement content and mean monthly temperatures at the project location.

Likewise, unbound materials are characterized by material parameters that account for the changing stress state in the material with seasonal changes in moisture conditions in a specific location. The gradation of the soil, maximum dry density, and optimum moisture content are key inputs to the procedure.

The MEPDG also requires the input of construction and field-specific parameters that are critical to performance. These construction or site features are not restrictive to a particular material, but they are associated with specific material index properties, climatic conditions, and construction practices. For example, base erodibility is a function of base material properties such as the strength of the base layer, the amount of fines, and site conditions such as the level of precipitation and traffic load repetitions.

Correlations Developed/Adapted for the MEPDG

The calibration of the rigid pavement distress models utilized several inputs from levels 2 and 3 based on the best information available from literature and LTPP databases. The following is a partial list of correlations used in the MEPDG models:

- The default concrete strength gain models in the MEPDG were derived from two decades of Portland Cement Association (PCA) research and the LTPP Specific Pavement Studies (SPS)-2 time series data.
- The ultimate shrinkage calculation model is based on Bazant’s model and was derived as a function of compressive strength, cement type, curing type, cement content, and w/c ratio.⁽¹⁴⁾ Other shrinkage inputs, such as time to 50 percent of ultimate shrinkage, were adopted from the American Concrete Institute (ACI) recommended models.
- CTE defaults by coarse aggregate type were established based on testing and petrography performed under the LTPP program.⁽¹⁵⁾

- Correlations between several of the PCC strength and modulus terms are based on work done under the LTPP program.⁽¹⁶⁾
- Erosion of the base layer under a CRCP was calculated using an empirical model that considers the climatic conditions and the properties of the base layer to determine the extent of erosion and voids under the slab.
- Erodibility Index (EI) for JPCP design is based on the base type and was established during the calibration process.
- Resilient modulus at optimum moisture content, which is a key material input for unbound layers, was determined through an iterative process by matching the subgrade *k*-value backcalculated from falling weight deflectometer (FWD) test data with the subgrade *k*-value for the same calendar month as determined by the MEPDG analysis.
- Friction coefficients of the slab/base layer in CRCP (mean friction coefficient for each type of base course) were determined by matching the predicted and field measured transverse crack spacing.
- ΔT in rigid pavement design was set at -10 °F for the calibration of the MEPDG distress models. Since it was not possible to determine the actual magnitude of this parameter, it was found that a value of -10 °F optimized the transverse cracking prediction over the numerous calibration sections. The MEPDG recommends -10 °F for this parameter as a default value and is more or less considered a level 3 default.

SELECTION OF MATERIAL PARAMETERS

A preliminary list of material properties was prepared for developing predictive models based on inputs required for the MEPDG and their level of significance in performance prediction as well as their importance during the design, construction, or pavement management phases. The materials are classified broadly as PCC materials, stabilized materials, and unbound materials. Note that unbound materials include both coarse-grained and fine-grained soils, which have different mechanical behavior in response to applied stress states. The preliminary material properties are listed in table 3 through table 5 for PCC, stabilized, and unbound materials. These tables list all input variables, identify the conventional source of data for SHAs, and indicate whether a predictive model can be developed for the parameter.

Table 3. PCC material properties and rigid pavement design features considered for generating predictive models.

Material Property	Constant or Time Dependent	Source	Recommended Test Protocol or Data Source	Predictive Model Possibility Yes(Y)/ No(N)	Project Stage: Design (D), QC/QA (C), or Pavement Management (PM)	Level of Significance for Performance
Rehabilitation of New PCC Slabs						
Compressive strength	Time dependent	Test	AASHTO T 22 ⁽¹⁷⁾	Y	D, C, PM	High
Elastic modulus	Time dependent	Test	ASTM C 469 ⁽¹⁸⁾	Y	D, PM	High
Poisson's ratio*	Constant	Test	ASTM C 469 ⁽¹⁸⁾	N	D	Low
Flexural strength	Time dependent	Test	AASHTO T 97 ⁽¹⁹⁾	Y	D, PM	High
Indirect tensile strength (CRCP only)	Time dependent	Test	AASHTO T 198 ⁽²⁰⁾	Y	D	High
Unit weight*	Constant	Test	AASHTO T 121 ⁽²¹⁾	N	D, C	Medium or high
Air content*	Constant	Test	AASHTO T 152 ⁽²²⁾ or AASHTO T 196 ⁽²³⁾	N	C	Medium (affects durability)
CTE	Constant	Test	AASHTO TP 60 ⁽²⁴⁾	Y	D, PM	High
Surface shortwave absorptivity***	N/A	Estimate	MEPDG default ⁽²⁾	N	D	Low
Thermal conductivity***	N/A	Test	ASTM E1952 ⁽²⁵⁾ or MEPDG default ⁽²⁾	N	D	Low
Heat capacity***	N/A	Test	ASTM D2766 ⁽²⁶⁾ or MEPDG default ⁽²⁾	N	D	Low

PCC zero-stress temperature	N/A	Estimate	MEPDG model ⁽²⁾	Y	D, PM	Medium (JPCP); high (CRCP)
Ultimate shrinkage*	Time dependent	Estimate	MEPDG predictive model ⁽²⁾	Y	D, PM	Medium (JPCP); high (CRCP)
<i>deltaT</i> in JPCP and CRCP design**	Time dependent	Estimate	MEPDG calibrated with default (-10 °F) ⁽²⁾	Y	D, C, PM	High
Erosion in CRCP design**	Time dependent	Estimate	MEPDG predictive model ⁽²⁾	Y	D	High
EI for JPCP design**	N/A	Estimate	MEPDG recommendation for base type ⁽²⁾	Y	D	Medium
Rehabilitation of Existing PCC Slabs						
Compressive strength	Time dependent	Test	AASHTO T 22 ⁽¹⁷⁾ (extracted cores)	Y	D, C, PM	High
Elastic modulus	Time dependent	Test	ASTM C 469 ⁽¹⁸⁾ (extracted cores)	Y	D, PM	High
			ASTM D 4694 ⁽²⁷⁾ (NDT deflection testing)			
Poisson's ratio*	Constant	Test	ASTM C 469 ⁽¹⁸⁾ (extracted cores)	N	D	Low
Flexural strength	Time dependent	Test	AASHTO T 97 ⁽¹⁹⁾ (extracted beam)	Y	D, PM	High

N/A = Not applicable.

*Parameter was not selected for model development.

**Considered a design feature input to rigid pavement design process.

Table 4. Chemically stabilized materials properties considered for generating predictive models.

Material Type	Material Property	Constant or Time Dependent	Source	Recommended Test Protocol or Data Source	Predictive Model Possibility Yes (Y)/ No (N)	Project Stage: Design (D), QC/QA (C), or Pavement Management (PM)	Level of Significance for Performance
Lean concrete and cement-treated aggregate	Elastic modulus	Constant	Test	ASTM C 469 ⁽¹⁸⁾	Y	D, PM	Medium-high
	Flexural strength (for HMA pavement)	Constant	Test	AASHTO T 97 ⁽¹⁹⁾	Y	D, PM	Medium-high
Lime-cement-fly ash	Resilient modulus	Time dependent	Estimate	MEPDG predictive model ⁽²⁾	Y	D, PM	Medium-high
Soil cement	Resilient modulus	Time dependent	Test	AASHTO T 307 ⁽²⁸⁾	Y	D, PM	Medium-high
Lime stabilized soil	Resilient modulus	Time dependent	Estimate	MEPDG predictive model ⁽²⁾	Y	D, PM	Medium-high
All above material types	Unconfined compressive strength	Time dependent	Test	MDTP, AASHTO T 307 ⁽²⁸⁾	Y	D, C, PM	Medium-high

Table 5. Unbound material properties considered for generating predictive models.

Material Property	Constant or Time Dependent	Source	Recommended Test Protocol or Data Source	Predictive Model Possibility Yes (Y)/ No (N)	Project Stage: Design (D), QC/QA (C), or Pavement Management (PM)	Level of Significance for Performance
Resilient modulus determined using two options:	Time dependent	Test	AASHTO T 307 ⁽²⁸⁾ or NCHRP Project 1-28A ⁽²⁹⁾	Y	D, C, PM	High
1. Regression coefficients k_1 , k_2 , and k_3 for the constitutive model that defines resilient modulus as a function of stress state			Resilient modulus = f (bulk stress, major principal stresses, octahedral shear stress, normalizing stress)			
2. Determine resilient modulus for expected in-place stress state from laboratory tests			Model coefficients are different for coarse-grained and fine-grained soils			
Poisson's ratio*	N/A	Estimate	No standard test; use default values.	N	D	Low
Maximum dry density*	Constant	Test	AASHTO T 180 ⁽³⁰⁾	N	D, C	High
Optimum moisture content*	Constant	Test	AASHTO T 180 ⁽³⁰⁾	N	D	High
Specific gravity*	Constant	Test	AASHTO T 100 ⁽³¹⁾	N	D	Low
Saturated hydraulic conductivity*	Constant	Test	AASHTO T 215 ⁽³²⁾	N	D	Medium
Soil water characteristic curve parameters*	N/A	Test	AASHTO T 99, T 100, and T 180 ^(33,31,30)	N	D	High
Rehabilitation of Existing Pavement and Properties of Soil to Be Left In-Place						
Modulus (backcalculated)	Time dependent	Test	ASTM D 4694 ⁽²⁷⁾ and D 5858 ⁽³⁴⁾	N	D	High
Poisson's ratio*	Time dependent	Estimate	MEPDG default ⁽²⁾	N	D	Low

N/A = Not applicable.

*Parameter was not selected for model development.

In selecting the material properties that require predictive models, the following factors were considered:

- The selected parameters are not index properties of the material or they are not part of mix design information and hence would require a predictive model to determine its value. In other words, these parameters are not independent variables for the material, and their values depend on the individual properties of constituent materials.
- Routine test procedures are not sufficient to determine the value of these parameters, and they require either expensive or time-consuming tests to determine their values. CTE and resilient modulus of unbound base materials are examples of such parameters.
- The material parameter exists in the LTPP database, and the required data are available for developing the model. For example, PCC shrinkage and modulus of stabilized base materials were not part of the database. In fact, they were never intended to be included in the LTPP tests when the experiments were designed.
- The engineering property is of significance to pavement performance.
- The material property is not affected significantly by construction factors or by parameters that cannot be determined prior to the design stage. For example, the unit weight of a material is an important parameter for pavement performance. It contributes to the total stresses developed in the PCC slab and is an indicator of the quality of consolidation achieved during construction that has a direct impact on the strength and durability characteristics. However, unit weight cannot be predicted using index properties, as it is also a function of aggregate gradation and packing achieved in the field.
- The likelihood of actual value of the material property deviating from the assumed defaults and its implications on design or performance is significant. For example, Poisson's ratio of PCC or specific heat of PCC would not qualify as an engineering property requiring a predictive relationship because these parameters do not vary significantly from the recommended/typical default values. Additionally, within a realistic range, their effects on performance are not large.

Accordingly, several variables in table 3 to table 5 were not selected for model development.

The selected parameters from table 3 to table 5 as well as predictive models to estimate their values were the focus of the literature review performed in this study. The literature review sought to identify independent variables (index properties) that could be used to determine the values of the selected material parameters. A list of index properties that can serve as independent variables in the prediction models is provided at the end of chapter 3.

CHAPTER 3. LITERATURE REVIEW

This chapter summarizes the literature review performed to investigate the correlations proposed by researchers and practitioners to estimate mechanical properties of pavement materials from simpler material index or constituent properties. The material types covered in this review are PCC and unbound aggregate and soils.

The literature was compiled from the following sources:

- FHWA and U.S. Department of Transportation publications (including those from the United States Army Corps of Engineers, United States Air Force, and United States Navy), PCA, American Concrete Pavement Association, and SHAs.
- Searches of Internet-based library systems (e.g., the University of Illinois, Transportation Research Information Service, and National Technical Information Service).
- Published proceedings of the American Society of Civil Engineers, the Transportation Research Board, the Federal Aviation Administration, the International Society for Concrete Pavements, and other agencies.
- Textbooks covering the material types of interest.

CORRELATION BETWEEN PCC MIX MECHANICAL PROPERTIES AND PCC MIX CONSTITUENT PROPORTIONS AND OTHER PCC PROPERTIES

PCC mix mechanical properties such as compressive strength (f'_c), flexural strength (also called modulus of rupture), tensile strength (f_t), elastic modulus (E), CTE, and drying shrinkage were among the most commonly studied and discussed in the literature, as they directly impact pavement performance. PCC mix constituent properties such as w/c ratio and coarse aggregate characteristics appeared to be the more commonly used properties to predict these PCC mix mechanical properties.

Other PCC properties, such as temperature at set, unit weight, thermal conductivity, heat capacity, and specific heat, which have come into sharper focus since the advent of the MEPDG and other pavement modeling programs such as the FHWA's HIGH PERFORMANCE Concrete PAVing (HIPERPAV[®]) software, were not very well documented in the literature.⁽³⁵⁾

The following discussion summarizes the factors affecting some of the commonly cited PCC mix properties and typical correlations proposed.

Compressive Strength

Compressive strength of concrete is the most frequently used measure of concrete quality in design and QA during construction. This parameter, most easily determined through a laboratory uniaxial compressive loading test and standardized in ASTM C 39, is considered a fundamental strength property.⁽³⁶⁾ PCC has a high compressive strength, and most structures are designed to take advantage of this property. The 28-day compressive strength is a widely accepted strength

index, especially for initial design. PCC strength increases with time and can affect opening strength, as well as rehabilitation designs in the long term. The compressive strength is also used frequently as an index for other strength types. As will be discussed in chapters 4 and 5, emphasis was placed on developing prediction models for compressive strength in this study.

In a majority of materials, including PCC, strength has been found to correlate strongly with its intrinsic porosity. Although considered a homogeneous material, concrete contains void spaces of various sizes in the matrix and in the interfacial zone (ITZ). Voids in the ITZ are responsible for the development of microcracks in the material. The failure modes initiated in the material vary with the type of loading applied. The formation of cracks in the matrix under a uniaxial compressive load requires greater energy compared to failures resulting from other forms of loading. A stable system of cracks exists in the ITZ up to 50 or 60 percent of the failure loads. At higher stress levels, cracks initiate and progress through the matrix, combine with those in the ITZ, and a failure plane develops 20 to 30 degrees from the direction of load. The failure is typically more brittle with high-strength concrete.

Concrete strength is influenced by the complex interaction of the characteristics and proportions of the individual materials, the consolidation provided (construction factors), the curing condition, and the rate/type of loading. Ozyildirim and Carino provide a comprehensive summary of the test procedures to determine each strength parameter (i.e., type of loading) and the parameters that are most significant.⁽³⁷⁾ It can be difficult to isolate the effect of a single parameter because of the inherent interaction and their confounding effects. The following list summarizes the influence of key parameters:

- **w/c ratio**—Strength varies inversely with w/c ratio, provided strength is evaluated for a given degree of hydration. Low w/c ratios produce lower paste porosity and result in higher strengths in low- to medium-strength mixes. However, with high-strength mixes, a small reduction in the w/c ratio (especially at levels below 0.3) results in a drastic increase in the strength essentially due to the improved strength of the ITZ.
- **Air content**—For a given level of hydration, when air is incorporated into a concrete mix, either entrapped or entrained air, the paste porosity and the strength decrease. However, the effect of air on concrete strength is influenced by the cement content and w/c ratio. At higher w/c ratios and cement contents, the effect is less pronounced than at low w/c ratios and cement contents.
- **Cement type and content**—The effect of cement type is most pronounced with the use of type III cement, which contains higher amounts of calcium aluminates and is more finely ground. Mixes with type III cements show higher strength, especially during early ages (1 to 7 days). Also, mixes with types IV and V cements produce lower strengths at early ages but have more or less similar strength characteristics at 28 days. Conventional mix design principles also typically use higher cement content to increase strength, and this holds true for a certain range of cement contents or CMC while holding other parameters constant. However, mix designs can incorporate many other means to improve strength. In fact, with the current push for sustainability in design and construction, the use of less cement (combined with other mix design practices) is recommended to improve strength and durability.

- **Aggregate type**—The coarse aggregate type has a significant effect on strength for high strength and for mixes with lightweight aggregate. The aggregate particle being several times stronger than the paste, failure in concrete is controlled by the paste strength for normal strength concrete. However, with high-strength concrete, as the paste is relatively stronger, aggregate type can be a factor affecting strength. Also, the hardness of the aggregate influences the deformational characteristics, which are more critical for modulus of elasticity and flexural strength. Crushed aggregates provide a stronger bond with the aggregate particles, improving the strength of ITZ.
- **Aggregate size distribution**—For a given cement content in a mix, larger aggregates (qualified by MAS from the gradation) tend to reduce the strength of the concrete. Larger aggregates have a weaker ITZ and form microcracks that initiate failures at lower load levels. PCC tensile strength and flexural strength are more sensitive to changes in aggregate size because the ITZ characteristics are critical to the loading pattern used in these tests.
- **Mineral and chemical admixtures**—Chemical admixtures that are designed to alter the rate of strength gain, commonly known as set accelerators or retarders, clearly have a significant effect on early strength of the mix. The use of supplementary cementitious materials also reduces early age strength but results in similar or higher strength in the long term. Mineral admixtures, also referred to as supplemental cementitious materials (SCMs), improve the tensile strength of concrete because of reduced porosity in ITZ.
- **Unit weight**—For a given mix, higher unit weights are indicative of a higher degree of consolidation or better construction in the field. High unit weight can also signal low entrained air. Since unit weight directly reduces the porosity of the mix, this condition results in higher strength. Compressive strengths are more sensitive to unit weight than tensile or flexural strengths.
- **Curing conditions**—Conditions that support better hydration in general increase the strength, and strength increases with time. Hence, age is generally defined in quantifying concrete strength. Higher relative humidity and temperature accelerate the chemical processes involved in hydration. The availability of moisture is a necessary condition for hydration to proceed regardless of the temperature conditions or the time allowed for concrete to gain strength. More recently, the significance of initial curing conditions (i.e., accelerated curing, curing temperature, etc.) has been better understood for predicting long-term strengths.⁽³⁸⁾
- **Loading conditions**—The rate of loading and the size of the specimen have an effect on strength. There is an apparent increase in strength (or modulus of elasticity) at higher loading rates. Therefore, standard procedures to determine concrete strength standardize the rate of load application.

Irick et al. conducted a pilot PRS study in which they developed a comprehensive summary of all PCC material property prediction models. The predictor variables used in that study were generally in agreement with the list and discussion above.⁽⁷⁾

Figure 2 illustrates the summary of factors and specific properties that affect concrete strength. In developing predictive models, every effort was made to evaluate the effect of parameters from this list that were available in the LTPP database. Furthermore, unless the data exhibited the effects discussed here, the parameter would not be recognized as significant in the statistical analyses.

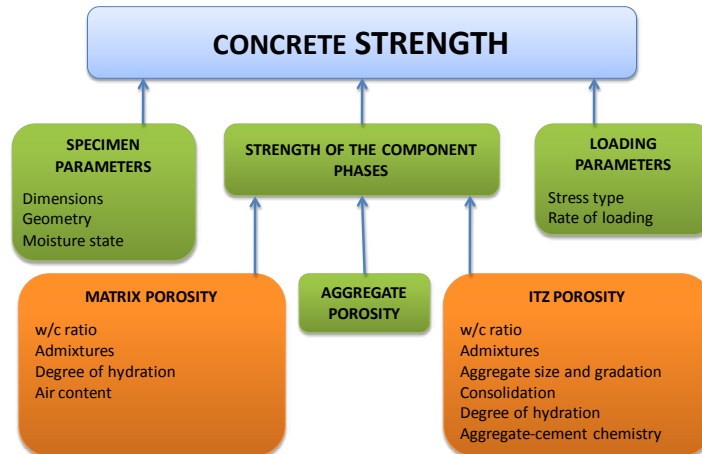


Figure 2. Illustration. Summary of factors affecting PCC strength.⁽³⁹⁾

Compressive Strength Prediction Models

The porosity of concrete, which includes paste porosity and ITZ porosity, cannot be determined realistically. Therefore, no empirical correlations exist to compare concrete porosity and strength. Other surrogate parameters that affect porosity or strength have been used to model compressive strength.

Compressive strength has been related mainly to the w/c ratio. Neville reported about Feret's work in 1896 that correlates mix volumetrics to strength.⁽⁴⁰⁾ Abrams' work proposed a ratio law for concrete strength based on a more thorough investigation of other parameters and stated that the strength of the concrete was solely controlled by the ratio of cement to free water in the plastic mixture (i.e., the w/c ratio) as long as the cement type, conventional aggregates, placement conditions, curing conditions, and test conditions remained constant.⁽⁴¹⁾

The empirical coefficients relating PCC compressive strength to w/c ratio depend on the units, materials, test methods used, age of testing, and the conditions of validity for Abrams' law. Further, Abrams suggested the following conclusions:⁽⁴¹⁾

- Compressive strengths are lower with higher w/c.
- Compressive strengths are higher with lower w/c.
- Compressive strengths are identical with the same w/c.
- The strengths of comparable concrete depend solely on their w/c ratios regardless of their compositions.

Research suggests that Abrams' law is valid, provided that the following assumptions hold:

- The strength-developing capabilities of the cements used are identical.
- The quantities and strength influencing effects of the admixtures used are identical.
- The concrete specimens are prepared, cured, and tested under the same conditions.
- The concrete ingredients are distributed evenly.
- Air contents are the same, air voids are distributed uniformly, and none of the voids are too large relative to the specimen size.
- Aggregate particles are stronger than the matrix (which suggests that high-strength concrete with typically higher paste strength could be more sensitive to aggregate properties).
- The bonds between aggregate surfaces and the matrix are strong. The bond can transfer the stresses to the aggregate before loading crushes the matrix.
- The strength affecting physical and chemical processes (i.e., drying, aggregate reactivity, etc.) are the same and are not overwhelming (hydration).
- The composite nature of the concrete affects the strength of the compared concretes to the same extent.
- The contribution of the aggregate skeleton is the same in the various concretes.

In 2006, Colak presented a model for strength prediction based on only w/c ratio.⁽⁴²⁾ However, Abrams' assumptions are not true, especially in the case of high-strength concrete, for which the mechanical properties of the aggregate become important.⁽⁴¹⁾ However, Alexander and Mindess found that no universal or meaningful mathematical relationships were derived to predict concrete strength as a function of both paste and aggregate variables.⁽⁴³⁾ This suggests that mix-specific empirical correlations will possibly need to be developed while considering key cement, cement paste, and aggregate attributes of interest to the concrete compressive strength.

The first studies of the effects of aggregates on concrete strength were conducted by Gilkey as well as Bloem and Gaynor.^(44,45) Gilkey presented a review of the limitations of the Abrams w/c ratio theory. He proposed that Abrams' law must be extended to include such parameters as the ratio of cement to aggregate, stiffness and maximum size of aggregate, and surface texture. According to Gilkey, Abrams' law could be generalized into a series of relationships represented by a family of approximately parallel strength curves.

The work of Bloem and Gaynor concentrated mainly on the effect of maximum size of concrete aggregate on compressive strength.⁽⁴⁵⁾ They found that strength decreased as aggregate size increased over the full range of w/c ratio. Their relationships are of limited significance for widespread use because the impact on compressive strength of the different types of aggregates can be larger than impact of maximum size of aggregate.

In the United Kingdom, Kaplan investigated the impact of aggregate surface texture, aggregate shape, and modulus of elasticity on compressive strength.⁽⁴⁶⁾ Aggregate strength within the limits of Kaplan's tests had no effect on concrete strength, which is where the target strength of the mix design is of significance, as discussed previously.

In work performed by Bennett and Khilji in the United Kingdom, an empirical relationship between concrete strength and the following variables was developed: w/c ratio, static modulus of elasticity of coarse aggregate, coarse aggregate/cement ratio, angularity number, and the aggregate impact value.⁽⁴⁷⁾ These researchers found that the modulus of elasticity of the coarse aggregate had a considerable effect on the strength, exceeded only by w/c ratio.

De Larrard and Bellock developed a semi-empirical method for defining compressive strength of concrete.⁽⁴⁸⁾ They suggested the concept of maximum paste thickness (MPT), which can be interpreted as the mean distance between aggregate particles and is described in terms of three important mix variables: the maximum size of aggregate, the aggregate volume concentration, and packing density of aggregate. They established that the strength of concrete depends on MPT, and they developed the empirical equation between concrete compressive strength and matrix strength, which was determined from the paste strength. According to this equation, for very high matrix strengths, the composite strength of concrete is controlled by the intrinsic strength of the rock. For low matrix strengths (or alternatively very high aggregate strengths), the strength of the composite is proportional to the matrix strength, with coefficients depending on the bond between the paste and the aggregate.

De Larrard and Bellock's equations, while based on sound concepts and helpful for theoretical strength prediction, do not provide a universally applicable approach to the problem of compressive strength prediction. For example, they do not account for the effects of aggregate elastic modulus, shape, and texture, as in Kaplan's investigations. Also, De Larrard and Bellock's results can be applied only to high-strength concrete where it is possible to measure paste strength with a reasonable degree of certainty.

The results of a comprehensive study of compressive strength were presented by Namyong et al.⁽⁴⁹⁾ This study used 1,442 compressive strength test results obtained from specimens with a range of w/c ratios and cement/aggregate ratios. Based on the results of correlation analysis, Namyong et al. developed empirical equations for predicting compressive strength of in situ concrete.

Time effects on compressive strength gain or strength at a given time have been predicted by several models. ACI and the Committee Euro-International du Beton (CEB-FIP) provided models to predict strength at a given time after hydration.^(50,51) The ACI model is applicable only to moist-cured samples cast with type I cement, and the CEB-FIP model is applicable only for specimens cured at 70 °F. FHWA's HIPERPAV[®] concrete compressive strength model is based on generalized Abrams theory.⁽⁵²⁾ The HIPERPAV[®] compressive strength prediction model accounts for the influence of w/c ratio, pozzolans, and aggregate contents in addition to concrete age. The main limitation of the HIPERPAV[®] compressive strength model is that it assumes all the conditions required to apply Abrams' rule are satisfied. Also, this model was calibrated only for fly ash as the mineral admixture. Wang et al. used historical concrete mix design

and strength test data in Iowa and developed statistical models to predict strength and other concrete properties.⁽⁵³⁾

Powers' approach for compressive strength for hardening concrete (time generalization of Abrams' law) has been used wherein the compressive strength was predicted as a function of the gel/space ratio, which, in turn, was found to be a function of degree of hydration and the w/c ratio.⁽⁵⁴⁾ Tango's model uses the additional time-dependent parameter, the degree of hydration, when considering concrete age.⁽⁵⁵⁾ This model was used successfully in the prediction of concrete strength in the Brazilian IPT concrete mixture design method. Irick et al. provided a comprehensive literature summary of models to predict concrete strength parameters.⁽⁷⁾

The equations in figure 3 through figure 7 summarize a few key models for compressive strength, f_c . These models are significant from the standpoint of fundamental theories and those that are relevant to the context of the current study.

$$f_c = \left(\frac{k_1}{k_2^{w/c}} \right)$$

Figure 3. Equation. f_c according to Abrams.⁽⁴¹⁾

Where:

k_1, k_2 = Empirical constants for a mix.

w/c = water/cement ratio.

$$f_c = K \left(\frac{c}{c + w + a} \right)^2$$

Figure 4. Equation. f_c according to Neville.⁽⁴⁰⁾

Where:

K = Empirical constant.

c, w, a = Cement, water, and air content volumetric proportions.

$$f_c = \frac{\alpha \frac{w}{c}}{\left(\beta + \lambda \frac{w}{c} \right)^n}$$

Figure 5. Equation. f_c according to Colak.⁽⁴²⁾

Where:

$\alpha, \beta, \lambda, n$ = Constants.

$$f_c(t) = f_{c,28} \left(\frac{t}{4 + 0.85t} \right)$$

Figure 6. Equation. f_c according to ACI 318.⁽⁴⁹⁾

Where:

$f_c(t)$ = Compressive strength at time, t days.

$f_{c,28}$ = Compressive strength at 28 days.

t = Time in days.

$$f_c = A + B \times w/b + C \times uw + D \times CMF + E \times \log(t) - F \times w/b \times uw - G \times uw \times CMF$$

Figure 7. Equation. f_c according to Wang et al.⁽⁵³⁾

Where:

A, B, C, D, E, F, G = Empirical constants.

w/b = w/c ratio.

uw = Unit weight.

CMF = Cementitious materials factor.

t = Time after hydration or age in days.

Flexural Strength and Splitting Tensile Strength

The flexural strength or MR and split tensile strength of concrete are the most commonly used indices to define the tensile capacity of PCC. Concrete is typically not tested under direct tension because the test apparatus and the loading mechanism introduce secondary stresses that are not easy to compensate for. Since the factors that affect these two strength estimates share some similarities in the nature of failure introduced along with a limited set of dissimilarities, the factors affecting their values are quite similar. Like compressive strength, MR is influenced by mix design parameters including w/c ratio, cement type, cement content, and aggregate properties (aggregate type, maximum size, gradation, and surface texture). In general, the material characteristics affect MR in the same manner as compressive strength. However, parameters that affect ITZ porosity are more sensitive to flexural strength. Literature published in the last decade suggests that the most important factor governing concrete tensile capacity is the aggregate matrix bond.^(56,57)

The flexural strength of concrete is defined as the maximum tensile strength at rupture at the bottom of a simply supported concrete beam during a flexural test with third point loading, as standardized in ASTM C 78-02.⁽⁵⁸⁾ Failure in the region between the loads applied at third points, or the region of maximum moment, is considered to be acceptable for this test. In other words, this test measures the tensile capacity of the material in bending or flexure. MR of a fully supported slab is far greater than the flexural strength of a simply supported beam. MR is the basis for estimating flexural fatigue in concrete. In the MEPDG, the damage calculated for the estimation of transverse cracking is a function of the flexural strength of the concrete. A true estimation of MR , therefore, would improve the accuracy of cracking prediction.

Kaplan developed a regression equation for flexural strength after statistical analysis of test data.^(46,59) He associated MR with aggregate elastic modulus, void percents, and surface texture

roughness. According to Kaplan, the elastic modulus of the aggregate is the most important factor affecting flexural strength.

The split tensile strength, commonly referred to as the indirect tensile strength or simply the tensile strength of PCC, is estimated using the ASTM C 496-90 test, which involves subjecting a concrete cylinder to compressive loads along two diametrically opposite axial lines.⁽⁶⁰⁾ The compressive load applied on the side of a cylindrical specimen causes a uniform tensile stress along the vertical diameter until the specimen fails. The indirect tensile strength is used in the CRCP distress prediction models of the MEPDG. This strength parameter has a direct influence on the transverse crack spacing, which, in turn, affects the crack widths, the load transfer efficiency of the crack, and eventually damage leading to punchout development.

Prediction Models and Interrelationship Between Tensile Capacity and Other Strength Parameters

Of all the PCC mechanical properties listed, compressive strength is the easiest and, not surprisingly, the most commonly tested parameter. Consequently, several researchers have developed relationships between this parameter and the three other PCC strength/modulus parameters—flexural strength, tensile strength, and elastic modulus. A summary of the flexural strength models is presented in figure 8 through figure 11, and a summary of the tensile strength correlations to compressive strength is presented in figure 12 through figure 17.

Various researchers have found that the relationship follows a power curve model. This is mainly because as the compressive strength of the concrete increases, the ratio between the tensile strength and compressive strength decreases, as does the ratio between the flexural strength and compressive strength.⁽³⁹⁾

$$MR = a \times f_c^b$$

Figure 8. Equation. *MR*.

Where:

$$a = 9.0, b = 0.5 \text{ (psi).}^{(61)}$$

$$a = 7.5, b = 0.5 \text{ (psi); } a = 0.62, b = 0.5 \text{ (MPa).}^{(50)}$$

$$a = 8.3, b = 0.5 \text{ (psi).}^{(62)}$$

$$a = 9.6, b = 0.5 \text{ (psi).}^{(63)}$$

$$a = 11.7, b = 0.5 \text{ (psi) (for high-strength mixes).}^{(64)}$$

$$a = 12.93, b = 0.4543 \text{ (psi).}^{(53)}$$

$$a = 0.3, b = 0.66 \text{ (MPa).}^{(51)}$$

$$a = 2.63, b = 0.66 \text{ (psi).}^{(65)}$$

$$MR = k_2 \times (f'_c)^{k_1}$$

Figure 9. Equation. MR according to Neville.⁽⁴⁰⁾

Where:

k_2 ranges from 3 to 6 psi.

k_1 ranges from 0.3 to 0.8 psi.

$$MR = \frac{3000}{4 + 12000 / f'_c}$$

Figure 10. Equation. MR according to Sozen et al.⁽⁶⁶⁾

$$MOR(t) = \left[1 + \log_{10} \left(\frac{t}{0.0767} \right) - 0.01566 \log_{10} \left(\frac{t}{0.0767} \right)^2 \right] \times MOR_{28d}$$

Figure 11. Equation. MOR according to NCHRP.⁽²⁾

Where:

$MOR(t)$ = The flexural strength at age t years.

MOR_{28d} = The 28-day flexural strength.

$$f'_{sp} = a * f'_c{}^b$$

Figure 12. Equation. f'_{sp} .

Where:

f'_{sp} = Tensile strength.

$a = 4.34, b = 0.55$ (psi).⁽⁶⁷⁾

$a = 0.53, b = 0.7$ (MPa).⁽⁴⁰⁾

$a = 7.11, b = 0.5$ (psi) (high strength mixes).⁽⁶⁸⁾

$a = 0.89$ to $1.7, b = 0.67$ to 0.71 (MPa). (See references 69–72.)

$a = 1.019, b = 0.7068$ (psi).⁽⁵³⁾

$a = 1.56, b = 0.67$ (MPa).⁽⁵¹⁾

$$f_{ctk,min} = 0.95 \left(\frac{f_{ck}}{f_{cko}} \right)^{2/3}$$

Figure 13. Equation. $f_{ctk,min}$ according to CEB-FIP Model Code 1990.⁽⁵¹⁾

$$f_{ctk,max} = 1.85 \left(\frac{f_{ck}}{f_{cko}} \right)^{2/3}$$

Figure 14. Equation. $f_{ctk,max}$ according to CEB-FIP Model Code 1990.⁽⁵¹⁾

$$f_{ct,mean} = 1.40 \left(\frac{f_{ck}}{f_{cko}} \right)^{2/3}$$

Figure 15. Equation. $f_{ct,mean}$ according to CEB-FIP Model Code 1990.⁽⁵¹⁾

Where:

f_{ck} = Compressive strength, MPa.

f_{cko} = 10 MPa.

$$f'_{sp} = a * MR$$

Figure 16. Equation. f'_{sp} according to Mehta and Monteiro.⁽³⁹⁾

Where:

a is a correlation coefficient and ranges from 0.48 to 0.68.

$$f'_{sp}(t) = \left[\beta_1 + \beta_2 \log_{10}(t) - \beta_3 \log_{10}(t)^2 \right] \times f'_{sp,28d}$$

Figure 17. Equation. f'_{sp} according to NCHRP.⁽²⁾

Where:

$f'_{sp}(t)$ = Tensile strength at age t years.

$f'_{sp,28d}$ = Tensile strength at 28 days.

$\beta_1, \beta_2, \beta_3$ = Empirical constants for a mix design.

Tensile strength is typically linear, with MR and estimated tensile strength being between 0.6 and 0.7 of MR . This is mostly because only a small volume of the material is under tension in the MR test compared to the entire volume in the tensile strength test. Also, the flexural strength test assumes a linear stress strain relationship across the depth of the beam. For very low-strength concretes, the tensile strength is nearly half the flexural strength.

Mallela et al. evaluated these models with the 2000 data release of the LTPP materials data.⁽¹⁶⁾ The following broad conclusions were drawn:

- Relationships between compressive and flexural strength: The ACI model, described by the relationship in figure 8 with coefficients of 7.5 and 0.5 for a and b , respectively, produced conservative estimates.
- Tensile/flexural strength relationships were on target.

The MEPDG provides a model form to develop strength gain relationships for agencies implementing the procedure.⁽²⁾ Based on flexural strength data analyzed in the calibration of the MEPDG models, the flexural strength at any age, t (years), can be calculated based on the 28-day strength. This generalized relationship is included in figure 7, and it can be modified for specific mix designs using test data at different ages. Likewise, the tensile strength gain can be calculated using the model form included in figure 17.

Elastic Modulus

Elastic modulus measures material stiffness and is a ratio of the applied stress to measured strain. This is determined using the ASTM C 496-90 test procedure, wherein the chord modulus is

measured in a concrete cylinder loaded in longitudinal compression at a relatively slow constant rate.⁽⁶⁰⁾ This test procedure also is used to determine Poisson's ratio.

The concrete elastic modulus is an important variable in pavement design, as it controls the overall slab deflections from traffic loading and slab curling stresses. Historically, in pavement applications, this value has not been rigorously estimated; typical values are assumed because it is perceived to have little effect. However, newer design methods such as the MEPDG have brought the importance of this parameter to the forefront. Generally, PCC elastic modulus increases as compressive strength increases, and it was found that in general, the material characteristics affect the elastic modulus in the same manner as the compressive strength. However, elastic modulus is more sensitive to aggregate characteristics and volumes.

Early works in this area established that concretes having the same compressive strength may have different moduli of elasticity if different aggregates are used. Additionally, concretes of different proportions may have different compressive strength for the same elastic modulus. Finally, for equal compressive strength, the elastic modulus increases with increasing aggregate/cement ratio.^(59,73)

The properties of aggregates also influence the modulus of elasticity—the higher the modulus of elasticity of the aggregate, the higher the modulus of the concrete.⁽⁷⁴⁾ The shape of coarse aggregate particles and their surface characteristics may also influence the value of the modulus of elasticity of concrete.⁽⁴⁰⁾ The aforementioned are very significant findings, suggesting that the strength-modulus relationship should be mixture specific.

Mathematical expressions to predict elastic modulus have been developed based on concrete being modeled as a two-phase material, a matrix phase and aggregate phase. (See references 75–79.)

Elastic Modulus Prediction Models

Several relationships between elastic modulus and compressive strength are presented in the literature. (See references 39, 40, 67, and 80.) All these relations are valid for specific samples of data and are affected by the condition of the specimen at the time of testing.

Extensive pavement-specific studies to predict material properties from index properties were conducted in the 1990s as part of FHWA's PRS development for concrete pavements.⁽⁸⁾ Mix design factors were compared against PCC strength and modulus to evaluate the effects of coarse aggregate type, cement content, air content, and w/c ratio. It was found that elastic modulus and flexural strength were most sensitive to a change in w/c ratio. The analyses conducted with the 2000 release of LTPP materials data showed that the compressive strength-static elastic modulus relationships produced no consistent trend.⁽¹⁶⁾

The relationship between modulus of elasticity and strength also depends on the mix proportions and on the age of the specimen. At later ages, the modulus increases more rapidly than strength.⁽⁴⁰⁾

In general, the elastic modulus of concrete is influenced by the stiffness of the paste and aggregate phases, their volume concentrations, and interface characteristics or the ITZ. The

stiffer the individual phases, the higher the elastic modulus. Concrete elastic modulus also increases with increases in the stiffer phase (usually the aggregate). Also of significance is the moisture state of the specimen. For a given aggregate, elastic modulus increases with the strength of the concrete. The significant influence of aggregates on concrete elastic modulus was confirmed in a study of 23 aggregate types conducted by Alexander and Davis.^(81,82) Each aggregate type produces a different age-dependent relationship. Likewise, Noguchi et al. developed a model for high-strength concrete mixes as a function of aggregate type and admixtures used.⁽⁸³⁾

The various models developed for the prediction of elastic modulus as well as the MEPDG recommended model for the estimation of modulus at any age are presented in figure 18 through figure 26. In these equations, E_c is the PCC secant elastic modulus in psi (GPa), ρ is the PCC unit weight in pounds per cubic foot (kg/m^3), and f'_c is the PCC compressive strength of a standard 5.85- x 11.7-inch cylinder in psi.

$$E_c = af'_c{}^b$$

Figure 18. Equation. E_c where constants are defined by various researchers.

Where:

$$a = 57,000, b = 0.5 \text{ (psi).}^{(50)}$$

$$a = 275,538, b = 0.33 \text{ (psi).}^{(51)}$$

$$a = 77,173, b = 0.46 \text{ (psi).}^{(71,72)}$$

$$a = 80811, b = 0.4659 \text{ (psi).}^{(53)}$$

$$E_c = \rho^{1.5} * 33 * f'_c{}^{0.5}$$

Figure 19. Equation. E_c according to ACI 318.⁽⁴⁹⁾

$$E_c = 2.1 * 10^5 * \left(\frac{\gamma}{2.3}\right)^{1.5} * \left(\frac{f'_c}{200}\right)^{\frac{1}{2}}$$

Figure 20. Equation. E_c for normal strength concrete according to Tomosawa et al.⁽⁸⁴⁾

$$E_c = a \left(\frac{\rho}{b}\right) (f'_c + c)^d$$

Figure 21. Equation. E_c according to CEB-FIP Model Code 1990.⁽⁵¹⁾

Where:

$$a = 9.1, b = 2,300, c = 0, d = 0.33.$$

$$a = 9.5, b = 2,400, c = 8, d = 0.33.$$

$$MR = \frac{6000000}{1 + 2000/f'_c}$$

Figure 22. Equation. MR according to Jensen via Irick et al.⁽⁷⁾

$$MR = 1,800,000 + 460 \times f'_c$$

Figure 23. Equation. MR according to Hognestad via Irick et al.⁽⁷⁾

$$E_c = 39,150(f'_c)^{0.50} + 2,030,528$$

Figure 24. Equation. E_c according to Turkish Standard 500.⁽⁸⁵⁾

$$E_c = k_1 \times k_2 \times 3.35 \times 10^4 \times \left(\frac{\rho}{2,400}\right)^2 \times \left(\frac{\sigma_b}{60}\right)^{\frac{1}{3}} \quad (\text{Units in MPa})$$

or

$$E_c = k_1 \times k_2 \times 4,860 \times \left(\frac{\rho}{150}\right)^2 \times \left(\frac{\sigma_b}{8.7}\right)^{\frac{1}{3}} \quad (\text{Units in ksi})$$

Figure 25. Equation. E_c according to Noguchi et al.⁽⁸³⁾

Where k_1 and k_2 are constants, and their values depend on the coarse aggregate type and the admixture.

$$\frac{E_{ct}}{E_{c,28}} = [\alpha_1 + \alpha_2 \log_{10}(t) - \alpha_3 \log_{10}(t)^2]$$

Figure 26. Equation. $E_{ct}/E_{c,28}$ according to NCHRP.⁽²⁾

CTE

CTE has received much attention recently since it appears to have a huge impact on the pavement design methodology proposed in the MEPDG. Its importance has been recognized since Westergaard's 1927 study from a pavement analysis standpoint.⁽⁸⁶⁾ The concrete CTE parameter directly influences the magnitudes of temperature-related pavement deformations. These deformations, in combination with the restraint offered by the base layer and slab weight, affect the resulting curling stresses in the slab. CTE is found to be most influenced by the coarse aggregate rock type as well as the internal relative humidity of the paste.

A protocol for CTE measurement of concrete, AASHTO TP 60, *Standard Test Method for the Coefficient of Thermal Expansion of Hydraulic Cement Concrete*, was adopted and the method is standardized now as a full AASHTO test procedure, AASHTO T 336, which has modified calibration requirements consistent with the 2010 LTPP data release.^(24,87) The older AASHTO TP 60 should be used with earlier CTE data releases.⁽²⁴⁾

Mallela et al. presented results of CTE testing conducted by FHWA as part of the LTPP material testing.⁽¹⁵⁾ CTE of the concrete was found to vary widely depending on the predominant aggregate type used in the concrete. This was in agreement with the CTE values reported by Irick et al. by aggregate type.⁽⁷⁾ The Mississippi Department of Transportation, in its efforts to implement the MEPDG, conducted PCC material property tests, including CTE on a range of mixes used in Mississippi.⁽⁸⁸⁾ In addition to several PCC material test results, it also presented CTE test results. In general, the effect of aggregate type was significant on reported CTE values.

CTE Prediction Models

CTE of concrete is predicted empirically by CTE of cement paste and aggregate. Aggregate type has the greatest influence on the value of thermal expansion due to the high volume content of coarse and fine aggregate in concrete.^(89,90) Neekhra developed prediction models to estimate the CTE of coarse aggregates and PCC based on the CTE of their individual components.⁽⁹¹⁾ Individual components are defined as the individual minerals for the estimation of aggregate CTE and mortar-aggregate phases for the estimation of PCC CTE. (The estimation of aggregate CTE is not of particular relevance to this study, and thus this review discusses only Neekhra's findings regarding the CTE of PCC.) PCC CTE is predicted based on the percent volume fraction, CTE, and modulus of elasticity of coarse aggregates and the mortar. In deriving the CTE model, Neekhra assumed that the PCC follows the Hirsch composite model, and the predictions are based on a 50-50 split in the fraction of material in series and parallel alignments. CTE measurements were made using the dilatometer, and the model was verified using nine different mixes that contained different aggregate types. A level 2 equation based on mix volumetrics has been proposed in the MEPDG to predict PCC.⁽²⁾ The models are provided in figure 27 and figure 28.

$$\alpha_c = X \times (\alpha_m V_m + \alpha_a V_a) + (1 - X) \times \left(\frac{\alpha_m V_m E_m + \alpha_a V_a E_a}{V_m E_m + V_a E_a} \right)$$

Figure 27. Equation. α_c according to Neekhra.⁽⁹¹⁾

Where:

α_c and α_a = CTE of mortar and aggregate.

V_m and V_a = Volume fraction of mortar and aggregate.

E_m and E_a = Elastic modulus of mortar and aggregate.

X = Relative proportion of material conforming with the upper and lower bound solution (assumed as 0.5).

Note that $X = 0$ implies series arrangement, and $X = 1$ implies parallel arrangement of constituent phases in the Hirsch model.

$$\alpha_{PCC} = \alpha_{agg} * V_{agg} + \alpha_{paste} * V_{paste}$$

Figure 28. Equation. α_{PCC} according to NCHRP.⁽²⁾

Where:

α_{PCC} , α_{agg} , and α_{paste} = CTE of PCC, aggregate, mortar, and paste.

V_{agg} and V_{paste} = Volume fraction of aggregate and paste.

Drying Shrinkage

Drying shrinkage of hardened concrete is an important factor affecting the performance of PCC pavements. The magnitude of drying shrinkage depends on numerous factors, including water per unit volume, aggregate type and cement, ambient relative humidity and temperature, and curing conditions.⁽⁴⁰⁾ The size and grading of aggregate influences the magnitude of shrinkage.

Larger aggregate permits the use of a leaner mix and results in lower shrinkage. Clay minerals in the -200 fraction can also increase shrinkage.

Powers demonstrated a significant impact of aggregate volume content on concrete shrinkage.⁽⁹²⁾ For the high values of aggregate content, concrete shrinkage was small in comparison with cement paste shrinkage. In general, sandstone aggregates tend to produce higher shrinkage in concrete than other aggregates. However, Troxell et al. demonstrated that it is not possible to generalize the effects of different aggregate types on concrete shrinkage.⁽⁹³⁾

The current ACI equation for ultimate shrinkage is based on a large database of mix designs and is a function of cement type, concrete strength, and curing practices.^(14,94) This equation has been incorporated into the MEPDG and HIPERPAV[®].^(2,35)

The LTPP database does not contain shrinkage test results; therefore, within the scope of the current project, no prediction models were developed for PCC shrinkage.⁽⁵⁾ Consequently, the various shrinkage models are not discussed in detail in this report. However, it is an important parameter and influences the performance of CRCP and JPCP.

PREDICTION OF CHEMICALLY STABILIZED MATERIAL PROPERTIES

Several types of chemically stabilized materials are used under pavements as base courses, subbase courses, or treated subgrade. These include lean concrete, cement stabilized or treated aggregate, soil cement, lime-cement flyash, and lime-stabilized materials. Typically, the compressive strength of these materials is used for construction QA and modulus and flexural strength for pavement design. However, compressive strength testing is more common than resilient/elastic modulus testing and flexural strength testing. Industry groups and individual researchers have published several correlations to estimate chemically stabilized base elastic modulus and flexural strength from the compressive strength as shown in figure 29 through figure 32. The more common or feasible of these correlations are presented in figure 32. Resilient modulus (M_r) can be estimated conservatively as 20 percent of the unconfined compressive strength (q_u).⁽⁹⁵⁾

The LTPP database does not contain modulus test results for stabilized materials. Limited data were available for modulus tests of LCB layers, which were utilized for model development. Therefore, the discussion on stabilized materials in this report is brief.

$$E = 57,000 \sqrt{f'_c}$$

Figure 29. Equation. E for lean concrete or cement treated aggregate.⁽⁹⁶⁾

Where:

E = Modulus of elasticity, psi.

f'_c = Compressive strength, psi tested in accordance with AASHTO T 22.⁽¹⁷⁾

$$E = 1,200 * q_u$$

Figure 30. Equation. E for soil cement.⁽⁹⁶⁾

Where:

E = Modulus of elasticity, psi.

q_u = Unconfined compressive strength, psi tested in accordance with ASTM D 1633.⁽⁹⁷⁾

$$E = 500 + q_u$$

Figure 31. Equation. E for lime-cement-flyash.⁽⁹⁸⁾

Where:

E = Modulus of elasticity, psi.

q_u = Unconfined compressive strength, psi tested in accordance with ASTM C 593.⁽⁹⁹⁾

$$M_r = 0.124q_u + 9.98$$

Figure 32. Equation. M_r for lime-stabilized soils.⁽¹⁰⁰⁾

Where:

M_r = Resilient modulus, ksi.

q_u = Unconfined compressive strength, psi tested in accordance with ASTM D 5102.⁽¹⁰¹⁾

PREDICTION OF UNBOUND MATERIAL AND SOIL RESILIENT MODULUS

Overview

Resilient modulus of unbound materials and soils is a required input in most pavement design procedures. It has a significant effect on the computed pavement responses and, hence, pavement performance. Resilient modulus can be tested directly from the laboratory, backcalculated using nondestructive test data, or obtained through the use of correlations with other material strength and index properties such as the California bearing ratio (CBR), R -value, dynamic cone penetrometer (DCP) value, soil Atterberg limit and gradation properties, AASHTO soil class, etc.

As a result of extensive research into the characterization of resilient modulus characterization conducted over the past four decades, it is now widely recognized that resilient modulus exhibits stress-state dependency, material dependency, and moisture and temperature dependency. About 54 percent of State transportation departments use resilient modulus in routine pavement design.⁽¹⁰²⁾ Ideally, resilient modulus should be obtained from laboratory measurements; however, standard test procedures such as AASHTO T 307 and NCHRP 1-28A require substantial time and resources and are not used in routine engineering practice, especially beyond the design phase of the project.^(28,103)

Of the several approaches put forth to estimate resilient modulus in the laboratory for design purposes, the one that has gained considerable traction over time is using a universal constitutive model as proposed in NCHRP 1-28A (see figure 33).⁽¹⁰³⁾ The strength of this approach is that two of the resilient modulus dependencies, stress-state and material type, can be handled by this model form, which is an improvement over previously used discrete models for coarse- and fine-grained soils which require knowledge of material behavior prior to applying a function to characterize it.

The nonlinear elastic coefficients and exponents of the constitutive model are determined by using linear or nonlinear regression analyses to fit the model to laboratory generated resilient modulus test data.

$$M_r = k_1 \left(\frac{\theta}{P_a} \right)^{k_2} \left(\frac{\tau_{\text{oct}}}{P_a} \right)^{k_3}$$

Figure 33. Equation. M_r according to NCHRP Project 1-28A.⁽¹⁰³⁾

Where:

M_r = Resilient modulus, psi.

θ = Bulk stress ($\sigma_1 + \sigma_2 + \sigma_3$).

σ_1 = Major principal stress.

σ_2 = Intermediate principal stress = σ_3 for M_r test on cylindrical specimen.

σ_3 = Minor principal stress/confining pressure.

τ_{oct} = Octahedral shear stress.

$$\tau_{\text{oct}} = \frac{1}{3} \sqrt{(\sigma_1 - \sigma_2)^2 + (\sigma_1 - \sigma_3)^2 + (\sigma_2 - \sigma_3)^2}$$

P_a = Normalizing stress (atmospheric pressure).

$k_1, k_2,$ and k_3 = Regression constants (obtained by fitting M_r test data to this equation).

Resilient Modulus Prediction Models

There have been numerous attempts to estimate resilient modulus as a function of soil index or soil strength properties over time. One of the first studies of the resilient properties of soil with the objective of developing correlation equations for predicting resilient modulus from basic soil test data was conducted by Carmichael and Stuart.⁽¹⁰⁴⁾ They used the Highway Research Information Service (HRIS) database and developed two regression models, one for fine-grained soils and another for coarse-grained soils.⁽¹⁰⁴⁾ Regression models were developed for individual soil types according to the Unified Classification System (UCS). Variables used in the models for coarse-grained soils included moisture content and bulk stress. For fine-grained soils, plasticity index, confining, and deviatoric stresses were used as predictive variables.

Drumm et al. conducted a resilient modulus study of cohesive soils based on AASHTO soil classification.⁽¹⁰⁵⁾ They used deviator stress as the main model parameter. The model coefficients were derived as functions of liquid limit of soil, degree of saturation, and unconfined compressive strength.

Two resilient modulus regression models—one each for fine-grained and coarse-grained Mississippi soils—were developed by George.⁽¹⁰⁶⁾ Variables used to predict fine-grained soil resilient modulus included soil dry density, liquid limit, moisture content, and percentage passing the No. 200 sieve. Variables for the coarse-grained soil resilient modulus model included dry density, moisture content, and percentage passing the No. 200 sieve.

A potential benefit of estimating the resilient modulus from physical properties is that seasonal variations in resilient modulus can be estimated from seasonal changes in a material's physical

properties. A few of the models from phenomenological studies that relate resilient modulus to soil properties are presented in figure 34 to figure 48.

Other soil strength parameters have also been used to estimate resilient modulus. Due to its historical significance in pavement design, CBR is the most commonly used soil strength parameter for correlation. Direct correlations between resilient modulus and CBR are included in the MEPDG.⁽²⁾ Simple correlation equations were developed to predict resilient modulus from standard CBR by several researchers. (See references 107–110.) All these equations are purely empirical and do not depend on soil properties and stress state. Figure 49 through figure 58 present a list of correlations between resilient modulus and other strength parameters.

One should exercise caution in using these correlations because they may not produce the required input to the MEPDG. The resilient modulus input is required to be at optimum moisture content and density of the soil. Most of these correlations do not predict this resilient modulus at optimum moisture content.

The resilient modulus also has been correlated to indices determined from other test devices. A summary of correlations with in-place test methods is presented in figure 59 to figure 67.

$$\log(M_R) = -0.111w + 0.0217S + 1.179$$

Figure 34. Equation. M_r according to Jones and Witzak.⁽¹¹¹⁾

Figure 34 was developed for clay type A-7-6. The deviator stress is 6 psi, the confining pressure is 2 psi, and M_r is measured in ksi.

$$M_R(ksi) = 4.46 + 0.098(C) + 0.12(PI)$$

Figure 35. Equation. M_r according to Thompson and LaGrow.⁽¹¹²⁾

Figure 35 was developed for compacted subgrades. The additional moisture susceptibility correction factor is 0.7 for clay, silty clay, and silty clay loam; 1.5 for clay loam; and 2.1 for loam.

$$M_r(ksi) = 6.37 + 0.034(\%CLAY) + 0.45(PI) - 0.0038(\%SILT) - 0.244(CLASS)$$

Figure 36. Equation. M_r according to Thompson and Robnett.⁽¹¹³⁾

Figure 36 was developed for fine-grained cohesive soils. The deviator stress is 6 psi, and there is no confinement.

$$M_r(ksi) = 37.4 - 0.45(PI) - 0.62(w) - 0.14(S200) + 0.18(\sigma_3) - 0.32(\sigma_d) + 36.4(CH) + 17.1(MH)$$

Figure 37. Equation. M_r according to Carmichael and Stuart for fine subgrade soils containing clay and silts.⁽¹⁰⁴⁾

Figure 37 was developed for fine subgrade soils containing clay and silts. It was developed using the HRIS database for individual UCS soil types.

$$M_r(\text{ksi}) = 0.523 - 0.0225(\%W) + 0.544(\log \theta) + 0.173(SM) + 0.197(GR)$$

Figure 38. Equation. M_r according to Carmichael and Stuart for coarse granular soils and aggregate bases.⁽¹⁰⁴⁾

Figure 38 was created for coarse granular soils and aggregate bases. It was developed using the HRIS database for individual UCS soil types.

$$M_r(\text{ksi}) = 11.21 + 0.17(\%CLAY) + 0.20(PI) - 0.73(w_{opt})$$

Figure 39. Equation. M_r according to Elliot et al. with deviator stress of 4 psi.⁽¹¹⁴⁾

Figure 39 was developed using cohesive subgrades.

$$M_r(\text{ksi}) = 9.81 + 0.13(\%CLAY) + 0.16(PI) - 0.60(w_{opt})$$

Figure 40. Equation. M_r according to Elliot et al. with deviator stress of 8 psi.⁽¹¹⁴⁾

Figure 40 was developed using cohesive subgrades.

$$M_r(\text{MPa}) = 17.29 \left(\frac{LL}{w_c + 1} \gamma_{dr} \right)^{2.18} + \left(\frac{P_{200}}{100} \right)^{-0.609}$$

Figure 41. Equation. M_r according to Rahim for fine-grained soils.⁽¹¹⁵⁾

Figure 41 was developed using undisturbed field samples.

$$M_r(\text{MPa}) = 324.14 \left(\frac{\gamma_{dr}}{w_c + 1} \right)^{0.8998} \left(\frac{P_{200}}{\log c_u} \right)^{-0.4652}$$

Figure 42. Equation. M_r according to Rahim for coarse-grained soils.⁽¹¹⁵⁾

Figure 42 was developed using undisturbed field samples.

$$M_r(\text{psi}) = 30280 - 359(S) - 325(\sigma_d) + 237(\sigma_c) + 86(PI) + 107(S_{200})$$

Figure 43. Equation. M_r according to Farrar and Turner.⁽¹¹⁶⁾

Figure 43 was developed using 13 types of fine-grained soils.

$$\log(M_r) = 46.93 + 0.018(\sigma_d) + 0.033(\Delta\gamma_d) - 0.114(LI) + 0.468(S) + 0.0085(CLASS)^2 - 0.0033(\Delta w)^2 - 0.0012(\sigma_c)^2 + 0.0001(PL)^2 - 0.0278(LI)^2 - 0.0017(S)^2 - 38.44(\log S) - 0.2222(\log \sigma_d)$$

Figure 44. Equation. M_r according to Hudson et al.⁽¹¹⁷⁾

Figure 44 was developed using cohesive subgrade soil types A4 through A7-6.

$$M_r = \left(0.98 - 0.28(\Delta w) + 0.29(\Delta w)^2 \right) M_{Ropt}$$

Figure 45. Equation. M_r according to Li and Selig.⁽¹¹⁸⁾

Figure 45 was developed for cohesive soils.

$$M_r (kPa) = -54,105 + 57,898(\log\psi)$$

Figure 46. Equation. M_r according to Gupta et al.⁽¹¹⁹⁾

Figure 46 was developed for cohesive soils. The valid for bulk stress is 83 kPa, and the octahedral shear stress is 19.3 kPa.

$$M_r (psi) = 1.518 \times 10^{30} [f(S)]^{-13.85} [f(\sigma)]^{-0.272}$$

Figure 47. Equation. M_r according to Berg et al.⁽¹²⁰⁾

Figure 47 was developed using fine-grained and coarse-grained soils from the Minnesota Road Research Project test site; applicable only to cohesive soils.

$$M_r = F_0 \times F_1 \times F_2 \times F_3 \times F_4 \times F_5 \times F_6$$

Figure 48. Equation. M_r according to Pezo and Hudson.⁽¹²¹⁾

Figure 48 was developed for Texas subgrade data. It is valid for silty to clayey subgrades, and correction factors are provided.

The definitions of the terms used in figure 34 through figure 48 are as follows:

%CLAY = C = Clay content in percent.

%SILT = Silt content in percent.

%W = $w = w_c$ = Moisture content.

$\Delta\gamma_d$ = Deviation from the Standard Proctor maximum dry density in pounds per cubic foot.

Δw = Deviation from the optimum water content in percent.

γ_{dr} = Ratio of dry density to maximum dry density.

$\sigma_c = \sigma_3$ = Confining stress.

σ_d = Deviator stress.

θ = Bulk stress.

ψ = Soil suction.

$CH = 1$ for CH type (clay and high plasticity) soil; 0 otherwise.

CLASS = Soil classification (e.g., soil type A7-6 use 7.6 in expression).

c_u = Uniformity coefficient.

$f(S)$ = Normalized saturation by a unit saturation of 1 percent.

$f(\sigma)$ = Normalized octahedral shear stress by a unit stress of 1 psi.

$F_0 = 9.8$ ksi.

F_1 = Moisture content correction factor.

F_2 = Relative compaction correction factor.

F_3 = Soil plasticity correction factor.

F_4 = Age correction factor.

F_5 = Confining pressure correction factor.

F_6 = Deviator stress correction factor.

$GR = 1$ for gravelly soils (silty gravel, well-graded gravel, clay gravel, and poorly graded gravel); 0 otherwise.

LI = Liquidity index in percent.
 LL = Liquid limit in percent.
 MH = 1 for elastic silt type soil; 0 otherwise.
 M_{Ropt} = Resilient modulus at optimum water content.
 PI = Plasticity index.
 PL = Plastic limit.
 S = Degree of saturation in percent.
 SM = 1 for silty sand type soil; 0 otherwise.
 $S_{200} = P_{200}$ = Percent material passing the No. 200 sieve.
 w_{opt} = Optimum water content.

$$M_r(\text{psi}) = 1500(\text{CBR})$$

Figure 49. Equation. Correlation between M_r and CBR according to Heukelom and Klomp.⁽¹⁰⁷⁾

Figure 49 shows reasonable estimates for fine-grained soils with CBR less than or equal to 10.

$$M_r(\text{psi}) = 2554(\text{CBR})^{0.64}$$

Figure 50. Equation. Correlation between M_r and CBR according to Powell et al.⁽¹²²⁾

Figure 50 is currently included in the MEPDG.

$$M_r = 3116(\text{CBR})^{0.478}$$

Figure 51. Equation. Correlation between M_r and CBR according to George.⁽¹⁰⁶⁾

Figure 51 was developed for cohesionless soils and is recommended for medium clay sands.

$$M_r(\text{MPa}) = 10.3(\text{CBR})$$

Figure 52. Equation. Correlation between M_r and CBR according to the Asphalt Institute.⁽¹²³⁾

$$M_r(\text{psi}) = A + B(R)$$

Figure 53. Equation. Correlation between M_r and R-value according to AASHTO.⁽¹²⁾

Where:

A = 772 to 1,155; recommended 1,000.

B = 369 to 555; recommended 555.

$$M_r(\text{ksi}) = 1.6 + 0.038(R)$$

Figure 54. Equation. Correlation between M_r and R-value according to Buu.⁽¹²⁴⁾

Figure 54 was developed for fine-grained soils. The deviator stress is 6 psi, the confinement stress is 2 psi, and the valid for R-value is greater than 20.

$$M_r (\text{psi}) = 3,500 + 125(R)$$

Figure 55. Equation. Correlation between M_r and R-value according to Yeh and Su.⁽¹¹⁰⁾

$$M_r (\text{psi}) = 1,150 + 555(R)$$

Figure 56. Equation. Correlation between M_r and R-value according to MEPDG.⁽²⁾

Figure 56 is currently included in the MEPDG. The R-value is between 2.3 and 11.

$$M_r (\text{ksi}) = 0.86 + 0.31(q_u)$$

Figure 57. Equation. Correlation between M_r and unconfined compressive strength according to Thompson and Robnett.⁽¹¹³⁾

Figure 57 was developed assuming a bilinear M_r versus deviator stress behavior.

$$M_r (\text{kPa}) = a(S_{u,1\%})$$

Figure 58. Equation. Correlation between M_r and shear strength according to Lee et al.⁽¹²⁵⁾

Figure 58 was developed for clayey subgrade soils and is valid for cohesive soils only where:

a = Level of deviator stress.

$S_{u,1\%}$ = Undrained shear strength at 1 percent axial strain.

$$M_r (\text{psi}) = 7013 - 2040.8(\ln DCPI)$$

Figure 59. Equation. Correlation between M_r and DCP test method according to Hassan.⁽¹²⁶⁾

Where DCPI is the DCP index in inches per blow.

$$M_r (\text{ksi}) = 338(DCPI)^{-0.39}$$

Figure 60. Equation. Correlation between M_r and DCP test method according to Chen et al.⁽¹²⁷⁾

Figure 60 was developed for subgrade materials using backcalculated FWD modulus values. DCPI is in millimeters per blow.

$$M_r (\text{MPa}) = 235.3(DCPI)^{-0.48}$$

Figure 61. Equation. Correlation between M_r and DCP test method for coarse-grained sandy soils according to George and Uddin.⁽¹²⁸⁾

For figure 61, DCPI is in millimeters per blow.

$$M_r (\text{MPa}) = 532.1(DCPI)^{-0.49}$$

Figure 62. Equation. Correlation between M_r and DCP test method for fine-grained clays according to George and Uddin.⁽¹²⁸⁾

For figure 62, DCPI is in millimeters per blow.

$$M_r (ksi) = 78.05(DCPI)^{-0.67}$$

Figure 63. Equation. Correlation between M_r and DCP test method according to Chen et al.⁽¹²⁹⁾

Figure 63 was developed for both base and subgrade soils materials. DCPI is in millimeters per blow.

$$M_r (MPa) = \frac{151.8}{(DCPI)^{1.096}}$$

Figure 64. Equation. Correlation between M_r and DCP test method, DCPI only according to Mohammad et al.⁽¹³⁰⁾

Figure 64 was developed for soil types A-4, A-6, A-7-5, and A-7-6. A field DCP test and laboratory test were correlated through statistical analysis. DCPI is in millimeters per blow.

Where:

γ_d = Dry unit weight in kN/m³.
 w = Water content in percent.

$$M_r (MPa) = 165.5 \left(\frac{1}{DCPI^{1.147}} \right) + 0.0966 \left(\frac{\gamma_d}{w} \right)$$

Figure 65. Equation. Correlation between M_r and DCP test method, DCPI, and soil properties according to Mohammad et al.⁽¹³⁰⁾

Figure 65 was developed for soil types A-4, A-6, A-7-5, and A-7-6. Field DCP test and laboratory test were correlated through statistical analysis. DCPI is in millimeters per blow.

Where:

γ_d = Dry unit weight in kN/m³.
 w = Water content in percent.

$$\frac{M_r}{\sigma_c^{0.55}} = \frac{1}{\sigma_v} \left(31.8(q_c) + 74.8 \left(\frac{f_s}{w} \right) \right) + 4.08 \left(\frac{\gamma_d}{\gamma_w} \right)$$

Figure 66. Equation. Correlation between M_r and CPT test method, in situ conditions according to Mohammad et al.⁽¹³¹⁾

Figure 66 was developed for silty clay and heavy clayey cohesive soils.

Where:

q_c = Tip resistance (MPa).
 f_s = Frictional resistance (MPa).
 u_t = Total pore pressure.

$$\frac{M_r}{\sigma_3^{0.55}} = \frac{1}{\sigma_1} \left(47.0(q_c) + 170.4 \left(\frac{f_s}{w} \right) \right) + 1.70 \left(\frac{\gamma_d}{\gamma_w} \right)$$

Figure 67. Equation. Correlation between M_r and CPT test method traffic loading conditions according to Mohammad et al.⁽¹³¹⁾

Figure 67 was developed for silty clay and heavy clayey cohesive soils.

Where:

$\sigma_c = \sigma_3$ = Confining stress (kPa).

σ_v = Vertical stress (kPa).

w = Water content.

γ_d = Dry unit weight (kN/m³).

γ_w = Unit weight of water (kN/m³).

Recently, the resilient modulus has been predicted using a two-step approach. First, models to predict parameters k_1 , k_2 , and k_3 of the constitutive equation are developed. Next, the constitutive equation is used to estimate the resilient modulus. Von Quintus and Killingsworth, Dai and Zollars, and Santha developed prediction equations by regressing the coefficients of selected constitutive equations and relating them to soil physical properties.^(132–134) It was observed that the most influential parameters are moisture content, liquid limit, plasticity index, and percent passing the No. 200 sieve.

One of the most comprehensive reviews of the resilient modulus test data measured on pavement materials and soils was made in the LTPP program.⁽¹³⁵⁾ A total of 2,014 resilient modulus laboratory tests that passed all the QC checks of the LTPP database (i.e., level E data status, 2000 data release) were used in this review. The study verified that the response characteristics correlate to a form of the constitutive model presented in figure 33. The study correlated resilient modulus data to the physical properties of the materials and found that the physical properties that influenced the resilient modulus varied between the different materials and soils. No one physical property was highly correlated to the modulus. For example, the liquid limit, plasticity index, and the amount of material passing the smaller sieve sizes were found to be important for the lower strength unbound aggregate base/subbase materials, while the moisture content and density were important as related to higher strength materials. Furthermore, the amount of material passing the larger sieve sizes was important for the unbound aggregate base/subbase materials with larger MASs. It also was found that percent clay and test specimen moisture content or density were important for all soil groups, while percent silt was important for all soil groups except gravel. It was also found that to improve correlations, the sample locations (depth) had to be matched while comparing test results for the same test section or site. Based on the quality of correlations developed in this study, it was recommended that the results need to be verified and confirmed after all resilient modulus tests have been completed. Future model refinement was suggested with a more comprehensive dataset.

Appendix CC in the MEPDG presents a detailed discussion of moisture and temperature regime influences on resilient modulus.⁽²⁾ The values of the resilient moduli at any location and time within a given pavement structure are calculated in the MEPDG as a function of the soil moisture and freeze-thaw influences. The impact of temporal variations in moisture and temperature on

resilient modulus are considered through the composite environmental adjustment factor, F_{env} . The Enhanced Integrated Climatic model (EICM) is integral to the MEPDG software (the publication by Larson and Dempsey deals with all environmental factors and provides soil moisture, suction, and temperature as a function of time, at any location in the unbound layers from which F_{env} can be determined).⁽¹³⁶⁾ This moisture prediction capability of the EICM was improved by Zapata and Houston.⁽¹³⁷⁾ The resilient modulus at any time or position within the pavement structure is then determined by multiplying the value at optimum with F_{env} (i.e., $M_r = F_{env}M_{ropt}$).

F_{env} is an adjustment factor, and M_{ropt} is the resilient modulus at optimum conditions (maximum dry density and optimum moisture content) at any state of stress. Variations of resilient modulus with stress and variations of modulus with environmental factors (i.e., moisture, density, and freeze-thaw conditions) are assumed to be independent.

Using the latest testing protocol to measure resilient modulus, AASHTO T 307, Titi et al. performed a comprehensive investigation to estimate the resilient modulus of various Wisconsin subgrade soils and develop basic models to estimate the resilient modulus from soil properties.^(28,138) Also, a laboratory testing program was conducted on common subgrade soils to characterize their physical properties. The resilient modulus constitutive equation was used to determine model factors k_1 , k_2 , and k_3 . Titi et al. compared the predictive capability of these models with those developed by Yau and Von Quintus using LTPP data and concluded that the two sets of models did not agree.^(138,135) Differences in the test procedures, test equipment, sample preparation, and other conditions involved with development of the LTPP models and the models of this study were cited as potential factors for this lack of correlation. Key prediction models to estimate resilient modulus from soil properties are summarized below.

Regression Constant Estimates Based on Soil Properties

Prediction Model—Mississippi Materials

Based on the results of repeated triaxial load tests performed on 12 fine-grained and coarse-grained Mississippi subgrades, stress ratios were used in a bulk stress log-log model to describe their behavior. Subsequently, soil properties of the same materials were incorporated in the regression constants of the models. Then, the models were verified using a separate subset of nine different Mississippi subgrades with good correlation.^(106,139) The resulting equations and constants are shown in figure 68 through figure 73.

$$M_R = k_1 P_a \left(1 + \frac{\sigma_d}{1 + \sigma_c} \right)^{k_2}$$

Figure 68. Equation. M_r of Mississippi materials for fine-grained soils.

$$k_1 = 1.12 (\gamma_{dr})^{1.996} \left(\frac{LL}{w_c} \right)^{0.639}$$

Figure 69. Equation. k_1 of Mississippi materials for fine-grained soils.

$$k_2 = -0.27(\gamma_{dr})^{1.04}(w_{cr})^{1.46}\left(\frac{LL}{\#200}\right)^{0.47}$$

Figure 70. Equation. k_2 of Mississippi materials for fine-grained soils.

$$M_R = k_1 P_a \left(1 + \frac{\theta}{1 + \sigma_d}\right)^{k_2}$$

Figure 71. Equation. M_r of Mississippi materials for coarse-grained soils.

$$k_1 = 0.12 + 0.90(\gamma_{dr}) - 0.53(w_{cr}) - 0.017(\#200) + 0.314(\log c_u)$$

Figure 72. Equation. k_1 of Mississippi materials for coarse-grained soils.

$$k_2 = 0.226(\gamma_{dr} w_{cr})^{1.2385} \left(\frac{\#200}{\log c_u}\right)^{0.124}$$

Figure 73. Equation. k_2 of Mississippi materials for coarse-grained soils.

The definitions of the parameters used in figure 68 through figure 73 are as follows:

P_a = Atmospheric pressure.

σ_d = Deviator stress = $\sigma_1 - \sigma_3$.

σ_1 = Major principal stresses.

σ_3 = Minor principal stresses.

σ_c = Confining stress.

γ_{dr} = Ratio of dry density to maximum dry density.

LL = Liquid limit in percent.

w_c = Moisture content in percent.

w_{cr} = Ratio of moisture content to optimum moisture content.

#200 = Percent material passing the No. 200 sieve.

θ = Bulk stress = $\sigma_1 + \sigma_2 + \sigma_3$.

σ_2 = Intermediate principal stress.

c_u = Uniformity coefficient.

Prediction Model—Georgia Materials

The following equation was developed as a combination of the bulk and deviator stress models in an effort to improve the predicted response of resilient modulus test results by including both axial and shear effects.

$$M_R = k_1 P_a \left(\frac{\theta}{P_a}\right)^{k_2} \left(\frac{\sigma_d}{P_a}\right)^{k_3}$$

Figure 74. Equation. M_r of Georgia materials.

Santha estimated values for the regression constants in terms of soil properties using a multiple correlation analysis.⁽¹³⁴⁾ The resulting constants for the analyzed Georgia granular soils are shown in figure 75 to figure 77.

$$\log k_1 = 3.479 - 0.07(w_c) + 0.24(w_{cratio}) + 3.681(COMP) + 0.011(\%SILT) + 0.006(\%CLAY) - 0.025(SW) - 0.039\gamma_s + 0.004\left(\frac{SW^2}{\%CLAY}\right) + 0.003\left(\frac{\gamma_s^2}{P_{40}}\right)$$

Figure 75. Equation. k_1 of Georgia materials.

$$k_2 = 6.044 - 0.053(w_{opt}) - 2.076(COMP) + 0.0053(SATU) - 0.0056(\%CLAY) + 0.0088(SW) - 0.0069(SH) - 0.027\gamma_s + 0.012(CBR) + 0.003\left(\frac{SW^2}{\%CLAY}\right) - 0.31\left(\frac{SW + SH}{\%CLAY}\right)$$

Figure 76. Equation. k_2 of Georgia materials.

$$k_3 = 3.752 - 0.068(w_c) + 0.309(w_{cratio}) - 0.006(\%SILT) + 0.0053(\%CLAY) + 0.026(SH) - 0.033\gamma_s - 0.0009\left(\frac{SW^2}{\%CLAY}\right) + 0.00004\left(\frac{SATU^2}{SH}\right) - 0.0026(CBR \times SH)$$

Figure 77. Equation. k_3 of Georgia materials.

Where:

w_c = Moisture content.

w_{opt} = Optimum moisture content.

$w_{cratio} = w_c / w_{opt}$.

$COMP$ = Degree of compaction.

$SATU$ = Percent saturation.

$\%SILT$ = Silt content in percent.

$\%CLAY$ = Clay content in percent.

SW = Percent swell.

SH = Percent shrinkage.

CBR = California bearing ratio.

γ_s = Dry density.

P_{40} = Material passing No. 40 sieve in percent.

Prediction Model—Louisiana Materials

An equation similar to Uzan's model using the octahedral normal stress instead of the bulk stress was used to study eight types of Louisiana soils.⁽¹⁴⁰⁾ Figure 79 shows the resilient modulus of Louisiana materials.

$$M_R = k_1 P_a \left(\frac{\sigma_{oct}}{P_a} \right)^{k_2} \left(\frac{\tau_{oct}}{P_a} \right)^{k_3}$$

Figure 78. Equation. M_r of Louisiana materials.

Linear regression was then applied to estimate the values of the regression constants in terms of soil properties. The resulting equations are shown in figure 79 through figure 81.

$$\log k_1 = -0.679 + 0.00922(w_c) + 0.00559(\gamma_s) + 3054 \left(\frac{\gamma_s}{\gamma_{opt}} \right) + 2.57(w_{cratio}) + 0.00676(LL) + 0.0116(PL) + 0.022(\%SAND) + 0.0182(\%SILT)$$

Figure 79. Equation. k_1 of Louisiana materials.

$$\log k_2 = -0.887 + 0.0044(w_c) + 0.0093(\gamma_s) + 0.264 \left(\frac{\gamma_s}{\gamma_{opt}} \right) + 0.305(w_{cratio}) + 0.00877(LL) + 0.00665(PL) + 0.0116(\%SAND) + 0.00429(\%SILT)$$

Figure 80. Equation. k_2 of Louisiana materials.

$$\log k_3 = -0.638 + 0.00252(w_c) + 0.00207(\gamma_s) + 0.61 \left(\frac{\gamma_s}{\gamma_{opt}} \right) + 0.152(w_{cratio}) + 0.00049(LL) + 0.00416(PL) + 0.00311(\%SAND) + 0.00143(\%SILT)$$

Figure 81. Equation. k_3 of Louisiana materials.

Where:

$$\sigma_{oct} = \text{Octahedral normal stress} = \frac{1}{3}(\sigma_1 + \sigma_2 + \sigma_3).$$

$$\tau_{oct} = \text{Octahedral shear stress} = \frac{1}{3} \sqrt{(\sigma_1 - \sigma_2)^2 + (\sigma_2 - \sigma_3)^2 + (\sigma_3 - \sigma_1)^2}.$$

w_c = Moisture content.

w_{opt} = Optimum moisture content.

$w_{cratio} = w_c / w_{opt}$.

LL = Liquid limit.

PL = Plastic limit.

$\%SILT$ = Silt content in percent.

$\%SAND$ = Sand content in percent.

γ_s = Dry density in kN/m^3 .

γ_{opt} = Optimum density in kN/m^3 .

Prediction Model—LTPP Materials

Figure 82 has gained considerable acceptance over time and is the constitutive model using the same parameters as in figure 33 and proposed in NCHRP Project 1-28A.⁽¹⁰³⁾

$$M_r(\text{psi}) = k_1 P_a \left(\frac{\theta}{P_a} \right)^{k_2} \left(\frac{\tau_{oct}}{P_a} + 1 \right)^{k_3}$$

Figure 82. Equation. M_r of LTPP materials.

The strength of this equation is its ability to handle two of the resilient modulus dependencies, stress-state and material type. Santha compared a log-log bulk stress model to figure 82 in modeling Georgia granular subgrade soils and concluded that the model presented in figure 82 provided a better representation of laboratory measurements of resilient modulus.⁽¹³⁴⁾

One of the most comprehensive validations of figure 82 using LTPP resilient modulus test data was performed by Yau and Von Quintus.⁽¹³⁵⁾ The authors first identified anomalous data, verified if the response characteristics correlated to the constitutive model presented in figure 82, subsequently explored the effect of material type and sampling technique, and performed a nonlinear regression analysis to establish relationships between the k regression constants in figure 82 and various material properties. The resulting regression equations for unbound and subgrade materials are presented in figure 83 through figure 115. The definitions of the variables used in the figures are as follows:

- $P_{3/8}$ = Percent material passing $3/8$ -inch sieve.
- P_4 = Percent material passing No. 4 sieve.
- P_{40} = Percent material passing No. 40 sieve.
- P_{200} = Percent material passing No. 200 sieve.
- %*SILT* = Silt content in percent.
- %*CLAY* = Clay content in percent.
- LL* = Liquid limit in percent.
- PI* = Plasticity index.
- W_{opt} = Optimum water content in percent.
- W_s = Water content of the test specimen in percent
- γ_{opt} = Maximum dry unit weight of soil in kg/m^3 .
- γ_s = Dry density of the test specimen in kg/m^3 .

Unbound Base and Subbase Materials

Figure 83 through figure 85 show equations for crushed stone (LTPP material code 303) as follows:

$$k_1 = 0.736 + 0.0084(P_{3/8}) + 0.0088(LL) - 0.0371(W_{opt}) - 0.0001\gamma_{opt}$$

Figure 83. Equation. k_1 of LTPP materials—crushed stone.

$$k_2 = 2.2159 - 0.0016(P_{3/8}) + 0.0008(LL) - 0.038(W_{opt}) - 0.0006\gamma_{opt} + 2.4 \times 10^{-7} \left[\frac{\gamma_{opt}^2}{P_{40}} \right]$$

Figure 84. Equation. k_2 of LTPP materials—crushed stone.

$$k_3 = -1.172 - 0.0082(LL) - 0.0014(w_{opt}) + 0.0005\gamma_{opt}$$

Figure 85. Equation. k_3 of LTPP materials—crushed stone.

Figure 86 through figure 88 show equations for crushed gravel (LTPP material code 304) as follows:

$$k_1 = -0.8282 - 0.0065 \left(P_{3/8} \right) + 0.0114(LL) + 0.0004(PI) - 0.0187(W_{opt}) + 0.0036(W_s) + 0.0013\gamma_s - 2.6 \times 10^{-6} \left(\frac{\gamma_{opt}^2}{P_{40}} \right)$$

Figure 86. Equation. k_1 of LTPP materials—crushed gravel.

$$k_2 = 4.9555 - 0.0057(LL) - 0.0075(PI) - 0.0470(W_s) - 0.0022\gamma_{opt} + 2.8 \times 10^{-6} \left[\frac{\gamma_{opt}^2}{P_{40}} \right]$$

Figure 87. Equation. k_2 of LTPP materials—crushed gravel.

$$k_3 = -3.514 + 0.0016\gamma_s$$

Figure 88. Equation. k_3 of LTPP materials—crushed gravel.

Figure 89 through figure 91 show equations for uncrushed gravel (LTPP material code 302) as follows:

$$k_1 = -1.8961 + 0.0014(\gamma_s) - \left(\frac{W_s}{W_{opt}} \right)$$

Figure 89. Equation. k_1 of LTPP materials—uncrushed gravel.

$$k_2 = 0.4960 - 0.0074(P_{200}) - 0.0007\gamma_s + 1.6972 \left(\frac{\gamma_s}{\gamma_{opt}} \right) + 0.1199 \left(\frac{W_s}{W_{opt}} \right)$$

Figure 90. Equation. k_2 of LTPP materials—uncrushed gravel.

$$k_3 = -0.5979 + 0.0349(W_{opt}) + 0.0004\gamma_{opt} - 0.5166 \left[\frac{W_s}{W_{opt}} \right]$$

Figure 91. Equation. k_3 of LTPP materials—uncrushed gravel.

Figure 92 through figure 94 show equations for sand (LTPP material code 306) as follows:

$$k_1 = -0.2786 + 0.0097 \left(P_{3/8} \right) + 0.0219(LL) - 0.0737(PI) + 1.8 \times 10^{-7} \left(\frac{\gamma_{opt}^2}{P_{40}} \right)$$

Figure 92. Equation. k_1 of LTPP materials—sand.

$$k_2 = 1.1148 - 0.0053(P_{3/8}) - 0.0095(LL) + 0.0325(PI) + 7.2 \times 10^{-7} \left(\frac{\gamma_{opt}^2}{P_{40}} \right)$$

Figure 93. Equation. k_2 of LTPP materials—sand.

$$k_3 = -0.4508 + 0.0029 \left(P_{3/8} \right) + 0.0185(LL) - 0.0798(PI)$$

Figure 94. Equation. k_3 of LTPP materials—sand.

Figure 95 through figure 97 show equations for coarse-grained soil-aggregate mixture (LTPP material code 308) as follows:

$$k_1 = -0.5856 + 0.0130 \left(P_{3/8} \right) - 0.0174(P_4) + 0.0027 (P_{200}) + 0.0149(PI) + 1.6 \times 10^{-6} \\ \left(\gamma_{opt} \right) - 0.0426(W_s) + 1.6456 \left(\frac{\gamma_s}{\gamma_{opt}} \right) + 0.3932 \left(\frac{W_s}{W_{opt}} \right) - 8.2 \times 10^{-7} \left(\frac{\gamma_{opt}}{P_{40}} \right)$$

Figure 95. Equation. k_1 of LTPP materials—coarse-grained soil-aggregate mixture.

$$k_2 = 0.7833 - 0.0060(P_{200}) - 0.0081(PI) + 0.0001(\gamma_{opt}) - \\ 0.1483 \left(\frac{W_s}{W_{opt}} \right) - 2.7 \times 10^{-7} \left(\frac{\gamma_{opt}^2}{P_{40}} \right)$$

Figure 96. Equation. k_2 of LTPP materials—coarse-grained soil-aggregate mixture.

$$k_3 = -0.1906 + 0.0026(P_{200}) + 8.1 \times 10^{-7} \left(\frac{\gamma_{opt}^2}{P_{40}} \right)$$

Figure 97. Equation. k_3 of LTPP materials—coarse-grained soil-aggregate mixture.

Figure 98 through figure 100 show equations for fine-grained soil-aggregate mixture (LTPP material code 307) as follows:

$$k_1 = -0.7668 + 0.0051(P_4) + 0.0128(P_{200}) + 0.0030(LL) - 0.0510(W_{opt}) + 1.1729 \left(\frac{\gamma_s}{\gamma_{opt}} \right)$$

Figure 98. Equation. k_1 of LTPP materials—fine-grained soil-aggregate mixture.

$$k_2 = 0.4951 - 0.0141(P_4) - 0.0061(P_{200}) + 1.3941 \left(\frac{\gamma_s}{\gamma_{opt}} \right)$$

Figure 99. Equation. k_2 of LTPP materials—fine-grained soil-aggregate mixture.

$$k_3 = 0.9303 + 0.0293(P_{3/8}) + 0.0036(LL) - 3.8903 \left(\frac{\gamma_s}{\gamma_{opt}} \right)$$

Figure 100. Equation. k_3 of LTPP materials—fine-grained soil-aggregate mixture.

Figure 101 through figure 103 show equations for fine-grained soil (LTPP material code 309) as follows:

$$k_1 = 0.8409 + 0.0004(P_{40}) + 0.0161(PI)$$

Figure 101. Equation. k_1 of LTPP materials—fine-grained soil.

$$k_2 = 0.6668 - 0.0007(P_{40}) - 0.0139(PI)$$

Figure 102. Equation. k_2 of LTPP materials—fine-grained soil.

$$k_1 = -0.1667 - 0.0207(PI)$$

Figure 103. Equation. k_3 of LTPP materials—fine-grained soil.

Subgrade Soils

Figure 104 through figure 106 show equations for coarse-grained gravel soils as follows:

$$k_1 = 1.3429 - 0.0051(P_{3/8}) + 0.0124(\%CLAY) + 0.0053(LL) - 0.0231(W_s)$$

Figure 104. Equation. k_1 of LTPP materials—coarse-grained gravel soils.

$$k_2 = 0.3311 + 0.0010(P_{3/8}) - 0.0019(\%CLAY) - 0.0050(LL) - 0.0072(PI) + 0.0093(W_s)$$

Figure 105. Equation. k_2 of LTPP materials—coarse-grained gravel soils.

$$k_3 = 1.5167 - 0.0302(P_{3/8}) + 0.0435(\%CLAY) + 0.0626(LL) + 0.0377(PI) - 0.2353(W_s)$$

Figure 106. Equation. k_3 of LTPP materials—coarse-grained gravel soils.

Figure 107 through figure 109 show equations for coarse-grained sand soils as follows:

$$k_1 = 3.2868 - 0.0412(P_{3/8}) + 0.0267(P_4) + 0.0137(\%CLAY) + 0.0083(LL) - 0.0379(W_{opt}) - 0.0004(\gamma_s)$$

Figure 107. Equation. k_1 of LTPP materials—coarse-grained sand soils.

$$k_2 = 0.5670 + 0.0045(P_{3/8}) - 2.98 \times 10^{-5}(P_4) - 0.0043(\%SILT) - 0.0102(\%CLAY) - 0.0041(LL) + 0.0014(W_{opt}) - 3.41 \times 10^{-5}(\gamma_s) - 0.4582 \left(\frac{\gamma_s}{\gamma_{opt}} \right) + 0.1779 \left(\frac{W_s}{W_{opt}} \right)$$

Figure 108. Equation. k_2 of LTPP materials—coarse-grained sand soils.

$$k_3 = -3.5677 + 0.1142 \left(P_{3/8} \right) - 0.0839(P_4) - 0.1249(P_{200}) + 0.1030(\%SILT) + 0.1191(\%CLAY) - 0.0069(LL) - 0.0103(W_{opt}) - 0.0017(\gamma_s) + 4.3177 \left(\frac{\gamma_s}{\gamma_{opt}} \right) - 1.1095 \left(\frac{W_s}{W_{opt}} \right)$$

Figure 109. Equation. k_3 of LTPP materials—coarse-grained sand soils.

Figure 110 through figure 112 show equations for fine-grained silt soils as follows:

$$k_1 = 1.0480 + 0.0177(\%CLAY) + 0.0279(PI) - 0.370W_s$$

Figure 110. Equation. k_1 of LTPP materials—fine-grained silt soils.

$$k_2 = 0.5097 - 0.0286(PI)$$

Figure 111. Equation. k_2 of LTPP materials—fine-grained silt soils.

$$k_3 = -0.2218 + 0.0047(\%SILT) + 0.0849(PI) - 0.1399(W_s)$$

Figure 112. Equation. k_3 of LTPP materials—fine-grained silt soils.

Figure 113 through figure 115 show equations for fine-grained clay soils as follows:

$$k_1 = 1.3577 + 0.0106(\%CLAY) - 0.0437(W_s)$$

Figure 113. Equation. k_1 of LTPP materials—fine-grained clay soils.

$$k_2 = 0.5193 - 0.0073(P_4) + 0.0095(P_{40}) - 0.0027(P_{200}) - 0.0030(LL) - 0.0049(W_{opt})$$

Figure 114. Equation. k_2 of LTPP materials—fine-grained clay soils.

$$k_3 = 1.4258 - 0.0288(P_4) + 0.0303(P_{40}) + 0.0251(\%SILT) + 0.0535(LL) - 0.0672(W_{opt}) - 0.0026\gamma_{opt} + 0.0025(\gamma_s) - 0.6055\left(\frac{W_s}{W_{opt}}\right)$$

Figure 115. Equation. k_3 of LTPP materials—fine-grained clay soils.

Prediction Model—Wisconsin Materials

Titi et al. evaluated the model presented in figure 82 using repeated triaxial test results performed on various Wisconsin subgrade soils and developed correlations between the model's regression constants and soil properties.⁽¹³⁸⁾ Good results were achieved when the statistical analysis was performed for fine-grained and coarse-grained soils separately. Researchers also used the LTPP data to compare their correlations to those developed by Yau and Von Quintus.⁽¹³⁵⁾ It was discovered that the two sets of models did not agree. Differences in the test procedures, test equipment, sample preparation, and other conditions involved with development of the LTPP models versus the ones used in the study were cited as potential factors for this lack of agreement. The equations developed by Titi et al. are provided in figure 116 through figure 124.⁽¹³⁸⁾ The definitions of the terms used in the figures are as follows:

P_4 = Percent material passing No. 4 sieve.

P_{40} = Percent material passing No. 40 sieve.

P_{200} = Percent material passing No. 200 sieve.

$\%SAND$ = Sand content in percent.

$\%SILT$ = Silt content in percent.

$\%CLAY$ = Clay content in percent.

LL = Liquid limit.

PL = Plastic limit.

PI = Plasticity index.

LI = Liquidity index.

w = Water content.

w_{opt} = Optimum water content.

γ_d = Dry unit weight.

γ_{dmax} = Maximum dry unit weight.

Figure 116 through figure 118 show equations for fine-grained soils as follows:

$$k_1 = 404.166 + 42.933(PI) + 52.260(\gamma_d) - 987.353 \left(\frac{w}{w_{opt}} \right)$$

Figure 116. Equation. k_1 of Wisconsin materials—fine-grained soils.

$$k_2 = 0.25113 - 0.0292(PI) + 0.5573 \left(\frac{w}{w_{opt}} \right) \left(\frac{\gamma_d}{\gamma_{max}} \right)$$

Figure 117. Equation. k_2 of Wisconsin materials—fine-grained soils.

$$k_3 = -0.20772 + 0.23088(PI) + 0.00367(\gamma_d) - 5.4238 \left(\frac{w}{w_{opt}} \right)$$

Figure 118. Equation. k_3 of Wisconsin materials—fine-grained soils.

Figure 119 through figure 121 show equations for non-plastic coarse-grained soils as follows:

$$k_1 = 809.547 + 10.568(P_4) - 6.112(P_{40}) - 578.337 \left(\frac{w}{w_{opt}} \right) \left(\frac{\gamma_d}{\gamma_{dmax}} \right)$$

Figure 119. Equation. k_1 of Wisconsin materials—non-plastic coarse-grained soils.

$$k_2 = 0.5661 + 0.006711(P_{40}) - 0.02423(P_{200}) + 0.05849(w - w_{opt}) + 0.001242(w_{opt})(\gamma_{dmax})$$

Figure 120. Equation. k_2 of Wisconsin materials—non-plastic coarse-grained soils.

$$k_3 = -0.5079 - 0.041411(P_{40}) + 0.14820(P_{200}) - 0.1726(w - w_{opt}) - 0.01214(w_{opt})(\gamma_{dmax})$$

Figure 121. Equation. k_3 of Wisconsin materials—non-plastic coarse-grained soils.

Figure 122 through figure 124 show equations for plastic coarse-grained soils as follows:

$$k_1 = 8642.873 + 132.643(P_{200}) - 428.067(\%SILT) - 254.685(PI) + 197.230(\gamma_d) - 381.400 \left(\frac{w}{w_{opt}} \right)$$

Figure 122. Equation. k_1 of Wisconsin materials—plastic coarse-grained soils.

$$k_2 = 2.3250 - 0.00853(P_{200}) + 0.02579(LL) - 0.06224(PI) - 1.73380\left(\frac{\gamma_d}{\gamma_{d\max}}\right) + 0.20911\left(\frac{w}{w_{opt}}\right)$$

Figure 123. Equation. k_2 of Wisconsin materials—plastic coarse-grained soils.

$$k_3 = -32.5449 + 0.7691(P_{200}) - 1.1370(\%SILT) + 31.5542\left(\frac{\gamma_d}{\gamma_{d\max}}\right) - 0.4128(w - w_{opt})$$

Figure 124. Equation. k_3 of Wisconsin materials—plastic coarse-grained soils.

SELECTION OF INDEPENDENT VARIABLES FOR THE PREDICTION OF MATERIAL ENGINEERING PROPERTIES

The information collected from literature was used to identify the independent variables or index properties used to predict the material engineering properties identified in chapter 2. The independent variables that the researchers considered most likely to be included in deriving the prediction models for PCC, stabilized, and unbound materials are listed in table 6 through table 8, respectively.

It was envisioned that more than one prediction model might be required or might be derived with the data available in the LTPP database. Multiple models are significant for use in different projects (e.g., new design versus rehabilitation versus pavement management) or stages of pavement life. For example, flexural strength correlations for PCC materials will be derived using index properties that can be useful during the design stage if mix design or optimization is performed. However, a correlation to compressive strength from a core would be useful for predicting the performance of the as-constructed pavement during the QA stage or in pavement management applications.

Data selection, analyses, and statistical modeling are discussed in detail in chapters 4 and 5 of this report. Predictive models can be based on lab or field test data, such as with the prediction of flexural strength based on compressive strength or index properties. Alternatively, correlations can be drawn to categorical variables, such as with PCC CTE. CTE can be a function of mix components and proportioning or a function of aggregate type. The latter option provides SHAs with the opportunity to recommend default values for CTE (as is being done for the MEPDG).

MEPDG calibration data were included as inputs to develop prediction models for design feature inputs (see chapter 5 for further discussion). These variables include the following:

- ΔT for JPCP designs.
- ΔT for CRCP designs.
- Erosion in CRCP design.
- EI for JPCP design.

Table 6. Potential or likely independent variables to derive prediction models for PCC material properties or design features for rigid pavements.

Material Property	Constant or Time Dependent	Independent Variables		Comments
		Primary Model	Secondary Model	
Rehabilitation of New PCC Slab				
Compressive strength	Time dependent	Aggregate type, cement content, air content, w/c, unit weight, gradation, admixtures, SCMs, and age	N/A	Prediction for 28-day strength and long-term strength in separate models; strength gain model to be updated
Elastic modulus	Time dependent	Aggregate type, cement content, air content, w/c, unit weight, admixtures, and SCMs	Compressive strength/ flexural strength	Prediction for 28-day value and long-term values in separate models
Flexural strength	Time dependent	Aggregate type, cement content, air content, w/c, unit weight, admixtures, and SCMs	Compressive strength	Prediction for 28-day strength and long-term strength in separate models; strength gain model to be updated
Indirect tensile strength (CRCP only)	Time dependent	Compressive strength/flexural strength	N/A	
CTE	Constant	Coarse and fine aggregate type, aggregate CTE, coarse and fine aggregate volume, paste volume, and w/c ratio	Aggregate type	Default PCC CTE for each aggregate type and model based on mix design
<i>deltaT</i> for JPCP and CRCP design*	Time dependent	Base type, construction time, PCC index properties, and climatic variables	N/A	Data in MEPDG JPCP and CRCP calibration to be used
Erosion in CRCP design**	Time dependent	Base type, index properties and strength of base, and climate (precipitation)	N/A	Data in MEPDG CRCP calibration models to be used
EI—JPCP**	N/A	Base type, base properties, and climate (precipitation)	N/A	Data in MEPDG JPCP calibration models to be used

Rehabilitation of Existing PCC Slab		
Compressive strength	Time dependent	Same as for parameters used in new design
Elastic modulus	Time dependent	Same as for parameters used in new design
Flexural strength	Time dependent	Same as for parameters used in new design

N/A = Not applicable.

*Construction dependent.

**Base dependent but listed in PCC properties because it is considered a design feature for JPCP or CRCP design.

Table 7. Independent variables to derive prediction models for stabilized materials.

Material Type	Material Property	Constant or Time Dependent	Independent Variables
Lean concrete and cement-treated aggregate	Elastic modulus	Constant	Compressive strength
	Flexural strength* (for HMA pavement design)	Constant	Compressive strength
Lime-cement-fly ash	Resilient modulus	Time dependent	Unconfined compressive strength or index properties (soil type, Atterberg limits, and gradation)
Soil cement	Resilient modulus	Time dependent	Unconfined compressive strength or index properties (soil type, Atterberg limits, and gradation)
Lime-stabilized soil	Resilient modulus	Time dependent	Unconfined compressive strength or index properties (soil type, Atterberg limits, and gradation)
All material types listed above	Unconfined compressive strength	Time dependent	Soil type, Atterberg limits, and gradation

*Construction dependent.

Table 8. Independent variables to derive prediction models for unbound materials.

Material Property	Constant or Time Dependent	Independent Variables	Comments
Resilient modulus determined using the following two options: <ul style="list-style-type: none"> • Regression coefficients k_1, k_2, and k_3 for the generalized constitutive model that defines resilient modulus as a function of stress state and regressed from lab resilient modulus tests. • Determine the average design resilient modulus for the expected in-place stress state from laboratory resilient modulus tests. 	Time dependent	Soil type, Atterberg limits, maximum dry density, optimum moisture content, gradation, and the percent passing the #200 sieve, P_{200} .	Analyses will verify several options and combinations of grouping data

CHAPTER 4. DATA ASSEMBLY AND MODELING CONSIDERATIONS

Data extraction and assembly are key steps to any model development exercise. Depending on the specific types of investigation involved or the particular needs of the analyses involved, the data extraction and assembly process could control the efficiency of data manipulations that are performed during analyses. Model development is an iterative process and involves stepwise evaluation of the significance of several parameters individually, in combination, and their interactive effects. Therefore, assembling data in a versatile manner that is amenable to model revisions and multiple evaluations is of paramount importance.

The relationships developed in this study were based primarily on data from the LTPP database. The key steps in developing the statistical models were as follows:

1. Identify and assemble all relevant data from the LTPP database.
2. Evaluate the quality of the assembled data by reviewing the assembled data for inconsistencies and possible errors, while also identifying missing/suspect data items.
3. Develop methods and procedures for estimating important missing data elements and clean data by resolving anomalies and outliers in a consistent manner.
4. Select the appropriate prediction model form and identify variables that emerge as significant variables.
5. Evaluate the reasonableness of the model formulated and verify whether the predicted correlations are meaningful from an engineering standpoint.
6. Ascertain statistical correctness and suggest tentative prediction models.
7. Perform sensitivity analysis to validate the tentative models. If validation is not satisfactory, revise the model in step 4.
8. Confirm final prediction model(s).

This approach has been used successfully in previous studies and has resulted in practical prediction models. Note that steps 4 through 8 are an iterative process; therefore, the data extraction and assembly process should allow multiple revisions to the selected variables and model forms.

DATA SELECTION FOR CURRENT STUDY

Data in the LTPP program exist for two complementary experiments, General Pavement Studies (GPS) and SPS. GPS experiments usually exist in service pavements incorporated into the LTPP program, while the SPS experiments are mostly newly constructed or rehabilitated pavements or pavements subjected to various maintenance activities at the time they were added to the LTPP program.

The GPS and SPS experiments are as follows:

- GPS-1: Asphalt concrete (AC) on granular base.
- GPS-2: AC on bound base.
- GPS-3: Jointed plain concrete.
- GPS-4: Jointed reinforced concrete.
- GPS-5: Continuously reinforced concrete.
- GPS-6A: Existing AC overlay on AC pavements.
- GPS-6B: New AC overlay on AC pavements.
- GPS-7A: Existing AC overlay on PCC pavements.
- GPS-7B: New AC overlay on PCC pavements.
- GPS-9: Unbonded PCC overlays on PCC pavements.
- SPS-1: Strategic study of structural factors for flexible pavements.
- SPS-2: Strategic study of structural factors for rigid pavements.
- SPS-3: Preventive maintenance effectiveness of flexible pavements.
- SPS-4: Preventive maintenance effectiveness of rigid pavements.
- SPS-5: Rehabilitation of AC pavements.
- SPS-6: Rehabilitation of jointed PCC pavements.
- SPS-7: Bonded PCC overlays on concrete pavements.
- SPS-8: Study of environmental effects in the absence of heavy loads.
- SPS-9A: Validation of Strategic Highway Research Program (SHRP) asphalt specification and mix design.

Each GPS test site consists of a single 500-ft test section over which all factors remain constant. SPS-1 and SPS-2 sites usually consist of a series of adjacent 500-ft test sections with different design and material characteristics or maintenance treatments and rehabilitation strategies. The test section layouts and the material data formats in the various LTPP data tables are reported elsewhere.⁽¹⁴¹⁾

The GPS and SPS experimental sections have different data availability. Relative to SPS sections, GPS sections are older pavement projects and were not intentionally built for collecting data under the LTPP program. SPS sections, in contrast, offer more detailed information on materials and construction. Further, the materials used in GPS sections are not necessarily representative of current materials, as several elements of the material manufacturing process and material specifications have changed. With the likelihood that GPS and SPS section data could produce different models, the data extraction and data assembly processes were tailored to analyze these data in two separate groups. Data for the various models by material type were taken from the GPS and SPS sections as shown in table 9.

Table 9. LTPP sections selected to review data for each category.

Material Category	Selected SPS Sections	Selected GPS Sections
PCC materials	SPS-2, SPS-7, and SPS-8	GPS-3, GPS-4, GPS-5, GPS-7, and GPS-9
Stabilized materials	All	All
Unbound materials	All	All

The following additional points offer reasons for the selection of materials data collected for PCC models:

- GPS-1, GPS-2, and GPS-6 projects were not included because they do not include PCC layers.
- SPS-1, SPS-3, SPS-5, and SPS-9 projects were not included because they do not include PCC layers.
- SPS-4 projects contain older rigid pavements with preventive maintenance, and it was found that the data relative to index properties were less accurate than for the newer SPS projects. These data were included with the GPS experiment data because the underlying pavement data were recovered from the original GPS projects.
- SPS-6 projects consist of underlying PCC layers that have been rehabilitated and sometimes cracked or rubblized. The data for the PCC layers are in the original inventory database. As with the SPS-4 underlying PCC slab data, these data were included in the GPS data tables assembled for this study.
- Data for the overlay only were included from the SPS-7 projects because the underlying slab information is relatively less comprehensive.

Table 10 shows the LTPP data tables that were queried to obtain the data necessary for developing the prediction models. The table also lists the data elements that were obtained from each table.

Table 10. LTPP data tables queried to obtain data for review and future analyses.

Data Category	LTPP Data Table	Material or Index Properties
PCC materials	TST_PC01	Compressive strength of cores and cylinders and test date
	TST_PC02	Tensile strength and test date
	TST_PC03	CTE, aggregate type, and test date
	TST_PC04	Elastic modulus, Poisson's ratio, unit weight, and test date
	TST_PC09	<i>MR</i> and test date
	SPS2_PCC_MIXTURE_DATA	Mix design, cement type, admixture type and quantity, aggregate type, and gradation for SPS-2
	SPS2_PCC_PLACEMENT_DATA	Construction date and curing method for SPS-2
	RHB_PCCO_AGGR	Aggregate type for SPS-7
	RHB_PCCO_MIXTURE	Mix design, cement type, admixture type and quantity, and aggregate type for SPS-7
	RHB_PCCO_CONSTRUCTION	Air temperature at time of construction, curing method, and date for SPS-7
	SPS8_PCC_MIXTURE_DATA	Mix design, cement type, admixture type and quantity, and aggregate type for SPS-8
	SPS8_PCC_PLACEMENT_DATA	Curing method and construction date for SPS-8
	INV_PCC_MIXTURE	Mix design, cement type and content, entrained air content, and curing method for GPS
	INV_AGE	Construction date for GPS
Stabilized materials	TST_TB02	Compressive strength
Unbound materials	TST_SS01_UG01_UG02	Gradation
	TST_SS02_UG03	Hydrometer analysis
	TST_SS04_UG08	AASHTO soil classification
	TST_SS11 TST_UG09	Hydraulic conductivity
	TST_UG04_SS03	Atterberg's limits
	TST_UG05_SS05	Maximum laboratory dry density
	TST_UG05_SS05	Optimum laboratory moisture content
TST_UG07_SS07_WKSHT_SUM	Average resilient modulus	
Climate data	CLW_VWS_HUMIDITY_ANNUAL	Local precipitation, humidity, and temperature for all sections in the MEPDG calibration files
	CLW_VWS_HUMIDITY_ANNUAL	
	CLW_VWS_HUMIDITY_ANNUAL	

DATA REVIEW

The data review process sought to verify data availability for the predictive models based on the dependent and independent variables identified in chapters 2 and 3 of this report. The assembled data were reviewed to identify anomalies and missing data elements. The review evaluated whether the following occurred:

- All required data were available.
- Available data were reasonable (i.e., trends and values of the data are as expected according to literature and engineering knowledge).
- Missing data items and the number of missing datasets significantly impaired the ability to develop required models for this study.
- Missing data items could be computed, assumed, or obtained from other readily available sources.

To enable such an evaluation, data were assembled for each 500-ft section in the database. As explained earlier, the data for each GPS section correspond to the test site. However, for SPS sections, it was reasonable to use the index properties of a given material from each site to correlate the data to the material properties from multiple test sections that were constructed using the same material. The treatment of PCC data from SPS-2 sections are discussed in detail in the PCC model development section in chapter 5 of this report.

Also included in developing the reference system were layer number, layer type, and construction number.

Key Findings From Data Review

A detailed unpublished report summarizing the results of the data review process was completed in phase I of this study and submitted to FHWA. The following conclusions were presented:

- All key data elements required for model development according to the literature were available.
- For PCC materials, SPS sections have more extensive data than GPS sections, as expected. This necessitates different model considerations and the inclusions of different parameters in the models using these two datasets.
- While independent variables exist for most predictive models, there are no dependent variable values in the database for parameters that are representative of the construction or site conditions. These parameters include PCC zero-stress temperature, EI for JPCP design, erosion in CRCP design, base friction coefficient for CRCP design, and ΔT for JPCP and CRCP designs. These parameters were never intended for inclusion in the LTPP database and are not typically measured in the field during construction. These variables are specific to MEPDG inputs and were estimated through correlations during

the development of the MEPDG. It was therefore necessary to use MEPDG calibration data to verify or refine these models.

- Most stabilized materials are referred to as treated bases in the LTPP database, and only compressive strength data exist for these materials. Index properties were not included in the database. Predictive models therefore were not developed for a majority of the stabilized base materials. However, the following materials data for LCB layers in SPS-2 sections are more comprehensive:
 - LTPP *Standard Data Release 23.0*, which was evaluated during phase II of this project, contained no elastic modulus data for LCB materials.⁽³⁾
 - LTPP *Standard Data Release 24.0*, released after this study was initiated, contained elastic modulus data for LCB layers in SPS-2 sections.⁽¹⁴²⁾
- LTPP *Standard Data Release 23.0* contains data beyond that utilized in a previous LTPP study investigating various models and predictive variables to estimate resilient modulus of unbound materials.^(3,135)

All data available were of adequate quality and completeness for use in model development. However, some missing data and data anomalies were also identified. The specific issues encountered and the methods used to overcome them is discussed in chapter 5 for each material type and material property. A summary of data availability is presented in table 11 for each material type and in table 12 for models to predict rigid pavement design features.

Table 11. Summary of data availability for material property predictive models.

Material Type	Material Property	Number of Sections Available for Model		Comment	
		GPS	SPS*		
PCC materials	Compressive strength	250	SPS-2 - LS	84	Does not include supplementary sections for SPS-2
			SPS-2 - HS	83	
			SPS-7	26	
			SPS-8	10	
			Total	203	
	Elastic modulus	344	SPS-2 - LS	77	
			SPS-2 - HS	76	
			SPS-7	11	
			SPS-8	8	
			Total	172	
	Flexural strength	349	SPS-2 - LS	50	
			SPS-2 - HS	51	
			SPS-7	15	
			SPS-8	5	
			Total	121	
Tensile strength	95	15		Only for CRCP, SPS data for SPS-7	
CTE	214	SPS-2 - LS	4	No comments	
		SPS-2 - HS	7		
		SPS-7	2		
		SPS-8	2		
		Total	15		
Ultimate shrinkage	258	N/A		Only independent variables are in LTPP database. Predictive model uses MEPDG calibration data. See table 12 discussion in chapter 5	
Zero-stress temperature	245	N/A			
EI for JPCP design	N/A	N/A			
Erosion in CRCP design	N/A	N/A			
ΔT for JPCP and CRCP designs	N/A	N/A			
Stabilized materials	N/A**	N/A**	57		Includes only LCB in SPS-2
Unbound materials	Resilient modulus	1,416	712		No comments

N/A = Not applicable; LS = Low strength; HS = High strength.

*SPS data have been summarized by experiment type. SPS-2-LS and SPS-2-HS refer to SPS-2 sections that have been built with low-strength and high-strength concrete mixes.

**Stabilized material data contain only compressive strength data and elastic modulus data for LCB materials.

Table 12. Summary of MEPDG calibration sections to develop predictive models for rigid pavement design features.

Calibration Sections	Number of CRCP Sections	Number of JPCP Sections
Non-LTPP sections	33	15
LTPP sections	71	285
Total	104	300

CHAPTER 5. MODEL DEVELOPMENT

This chapter discusses the statistical analyses performed to develop the predictive models and the sensitivity analyses used to validate the models. All statistical analyses were performed using the SAS[®] software program.

STATISTICAL ANALYSES METHODS ADOPTED

After data assembly was completed, predictive relationships for the parameters identified in table 6 through table 8 were considered for statistical analyses. The following approaches/options were considered for developing the various models:

- **Refinement of existing models**—Refinement of existing ACI PCC compressive strength-flexural strength relationship or the MEPDG PCC strength gain model.
- **Development of new models**—A predictive model to determine CTE based on PCC mix constituent properties.
- **Development of empirical models specific to MEPDG performance**—A predictive model to determine ΔT for JPCP design.

Formulating Data for Statistical Models

Data were formulated in three distinct types depending on the nature and extent of data available for each parameter and the intended use of the predicted variable. Within each type, different model forms can be adopted depending on the relationship the dependent parameter holds with the independent variables. The three primary data formulation types adopted are data formulation types 1 through 3 and are discussed in the following sections.

Data Formulation Type 1

- **Model description**—Simple mathematical correlation between a dependent parameter and continuous predictors or independent variables.
- **Dependent variable type and data source**—Continuous variable from the LTPP database.
- **Independent variable type and data source**—Continuous variable from the LTPP database.
- **Correlation**—Direct mathematical correlation between dependent and independent variables.
- **Example predictive model**—Compressive strength of PCC predicted as a function of aggregate type, cement content, air content, w/c ratio, unit weight, admixtures, and SCMs. Additionally, k_1 , k_2 , and k_3 coefficients of the resilient modulus universal

constitutive model for unbound materials and soils are predicted as a function of aggregate gradation parameters and index properties.

- **Model inference space**—Applicable to materials representative of the materials in the LTPP database and limited to the ranges of material properties (i.e., data points) used in the model.

Data Formulation Type 2

- **Model description**—Simple correlation between a dependent parameter and categorical predictors or independent variables.
- **Dependent variable type and data source**—Continuous variable from the LTPP database.
- **Independent variable type and data source**—Categorical variable from the LTPP database.
- **Correlation**—Average value of the predicted value determined from the database for each category of independent variable. A direct correlation between dependent and independent variables still exists.
- **Example predictive model**—CTE predicted as a function of aggregate type.
- **Model inference space**—Applicable to materials representative of the materials in the LTPP database and limited to the ranges of material properties used in the model.

Data Formulation Type 3

- **Model description**—Relationship between a dependent parameter and predictor variables for dependent variable values established by matching field performance to MEPDG predicted performance in LTPP sections used in MEPDG calibration.
- **Dependent variable type and data source**—Parameter established by trial and error for each calibration section so that predicted performance matches field performance for each section.
- **Independent variable type and data source**—Continuous variables from the LTPP database.
- **Correlation**—Dependent variable determined from trial and error correlated to independent variables from the LTPP database through simple mathematical correlation.
- **Example predictive model**—The current MEPDG calibration models have used a uniform value of -10 °F for *deltaT* in JPCP and CRCP designs, as this value was found to provide the least error term overall in the cracking model. This project will determine the *deltaT* term required to minimize the error in prediction for each calibration section individually, which represents the *deltaT* term that best explains the performance of the

pavement based on MEPDG calibration. The array of *deltaT* terms correlates to the independent variables from the LTPP database such as base type, construction time, PCC properties (unit weight, compressive strength, etc.), and climatic variables. Another example for a parameter that can be predicted using a type 3 model is EI in JPCP faulting model prediction. The value resulting in the best faulting prediction can be correlated to material (base material), design (dowels/no dowels), and climate (precipitation) parameters.

- **Model inference space**—Specific to MEPDG performance prediction. The MEPDG distress model calibration is built into the predictive relationship proposed and therefore is applicable only to derive MEPDG-specific inputs. However, relative comparisons are valid. For example, *deltaT* determined from this relationship for different locations will explain the relative potential for developing upward/downward curling at these locations.

Table 13 to table 15 provide summaries of the model types evaluated for developing predictive relationships for PCC, stabilized, and unbound materials, respectively.

Table 13. Model types used to derive predictive relationships for PCC material properties or design features for rigid pavements.

Material Property	Primary Model		Secondary Model	
	Model Variables	Model Type	Model Variables	Model Type
Compressive strength	Aggregate type, cement content, air content, w/c ratio, unit weight, admixtures, and SCMs	1	N/A	N/A
Elastic modulus	Aggregate type, cement content, air content, w/c ratio, unit weight, admixtures, and SCMs	1	Compressive strength/ flexural strength	1
Flexural strength	Aggregate type, cement content, air content, w/c ratio, unit weight, admixtures, and SCMs	1	Compressive strength	1
Indirect tensile strength (CRCP only)	Compressive strength/flexural strength	1	N/A	N/A
CTE	Aggregate type, aggregate volume, cement type, paste volume, and w/c ratio	1	Aggregate type	2
Erosion in CRCP design	Base type, index properties and strength of base, and climate (precipitation)	3	N/A	N/A
EI—JPCP	Base type, base properties, and climate (precipitation)	3	N/A	N/A
ΔT	Base type, construction time, PCC index properties, and climatic variables	3	N/A	N/A

N/A = Not applicable.

Table 14. Model types used to derive predictive relationships for stabilized materials.

Material Type*	Material Property	Constant or Time Dependent	Independent Variables	Model Type Evaluated
Lean concrete and cement-treated aggregate	Elastic modulus	Constant	Compressive strength	1

*All other material types have been excluded from this table, as the database provides data for LCB elastic modulus only.

Table 15. Model types used to derive predictive relationships for unbound materials.

Material Property	Independent Variables	Model Type
Resilient modulus determined using the following two options: <ul style="list-style-type: none"> • Regression coefficients k_1, k_2, and k_3 for the generalized constitutive model that defines resilient modulus as a function of stress state and regressed from lab resilient modulus tests • Determine the average design resilient modulus for the expected in-place stress state from laboratory resilient modulus tests 	Soil type, Atterberg limits, maximum dry density, optimum moisture content, gradation, and P_{200}	1; after grouping data for coarse-grained and fine-grained soils

Statistical Criteria for Used for Model Development

The statistical analyses performed in this study examined several statistical parameters in choosing the optimal model and in determining the accuracy of the model. The process included evaluating various aspects of the model, and the following parameters were generally verified:

- C_p —A statistical term to select the best subset of regressors for a model and an indicator of the collinearity of a regression model.
- **VIF**—A statistical term to evaluate the multicollinearity of the model (i.e., it tracks the interaction effects of the regressors identified).
- ***p*-value**—A probability calculation to ascertain the significance of the regressor in the equation.
- R^2 —A statistic that indicates the goodness of fit of a model and describes how closely the regression line fits the data points.

C_p

Mallows' C_p is often used as the criterion for selecting the most appropriate sub-model of p regressors (or independent variables) from a full model of k regressors, $p < k$.⁽¹⁴³⁾ In the current study, the potential variables that could likely influence the value of the dependent variable were identified from a literature review of specific material parameters. However, it is not clear whether the specific dataset being used to develop the models can suitably show the correlation expected. In other words, the initial attempt in developing the model could likely include more variables or regressors than the model can handle. This can result in forcing variables that are highly correlated and whose effects cannot be independently estimated or isolated by the model. The C_p term that is used in a step-wise regression process helps avoid an over-fit model by identifying the best subset of only the important predictors of the dependent variable.

C_p takes into account the mean square error for the two models and the number of variables in the reduced model as seen in figure 125.

$$C_p = (n - p) \frac{MSE_r}{MSE_f} - n + 2p$$

Figure 125. Equation. C_p .

Where:

n = The sample size.

MSE_r = The mean square error for the regression for the smaller model of p regressors and is expressed as follows:

$$MSE_r = \sum_{i=1}^n (y_i - y_{ri})^2$$

Figure 126. Equation. MSE_r .

MSE_f is the mean square error for the regression on the full model of k regressors. Note that for $p = k$, $MSE_r = MSE_f$ and $C_p = p$.

Sub-models are ordered in SAS[®] based on C_p ; the smaller the C_p value, the better. While it is a reliable measure of the goodness of fit for a model, it is fairly independent of R^2 in determining the number of predictors in the model. SAS[®] also lists R^2 for each model created with data subsets, which greatly enables the selection of a feasible submodel for further evaluation. However, the variables in the reduced model must all be significantly different from zero and cannot be too correlated, which is verified using VIF.

VIF

Generally, VIF can be regarded as the inverse of tolerance. The square root of VIF indicates how much larger the standard error is compared with what it would be if that variable is uncorrelated with the other independent variables in the equation.

If y is regressed on a set of x variables x_1 to x_k , VIFs of all x variables should be created in the following manner:

For variable x_j , VIF is the inverse of $(1 - R_j^2)$ from the regression of x_j on the remainder of the x variables. In other words, x_j regressed on $x_1 \dots x_{j-1}, x_{j+1} \dots x_k$, produces a regression with R^2 as R_j^2 . Therefore, figure 127 was created as follows:

$$VIF(x_j) = \frac{1}{(1 - R_j^2)}$$

Figure 127. Equation. VIF.

VIF is always greater than 1. A VIF value of 10 indicates that 90 percent of x_j is not explained by the other x variables. A common rule of thumb is that if VIF for any variable is greater than 5,

multicollinearity exists for that variable and should be excluded from the model. However, in cases where the parameter is either known to correlate well or other variables do not provide a reasonable model, a cut-off value of 10 is acceptable but less preferred.

R^2

R^2 is the coefficient of determination and is the square of the sample correlation coefficient computed between the outcomes and their predicted values, or, in the case of simple linear regression, between the outcome and the values being used for prediction. R^2 values vary from zero to 1 and are expressed as a percentage. An R^2 of x percent indicates x percent of the variation in the response variable can be explained by the explanatory variable, and $(100 - x)$ percent can be explained by unknown variability. The higher the value of this term, the greater the predictive ability of the model. It is the most commonly used statistic to evaluate the quality of fit achieved with a model.

From the standpoint of using R^2 to select a model, while relationships with higher values are desirable, it is not to be treated as the ultimate criterion to establish the model. R^2 needs to be interpreted with reasonable caution and needs to be combined with the information from the other statistical parameters discussed in this section. In fact, it is not the first check to select a model; instead, it should serve as the final check to establish the model.

The statistical parameters discussed previously do not individually optimize a model; instead, these parameters need to be evaluated in combination to derive the most accurate model. Furthermore, it is imperative in establishing a model that both statistical and engineering aspects be balanced. The accuracy of the model needs to be verified for technical/engineering validity by evaluating each variable in the model and confirming that the observed trends are as expected (verified in literature) and that the effect of the independent variable on the predicted variable is reasonable (verified through sensitivity analyses).

The following list describes the limitations of the C_p , VIF, and R^2 parameters and the methods used to overcome them:

- C_p , VIF, and R^2 do not explain whether the independent variables are a true cause of the changes in the dependent variable or if the trends predicted by the model are accurate. In other words, they do not identify a random correlation between two variables. Engineering knowledge (or knowledge from outside of the modeling exercise) needs to be incorporated in accepting or rejecting regressors or a model form.
- C_p , VIF, and R^2 do not explain whether the model has a bias because of a variable that has been omitted from the list of regressors. As a result, it is important to include, within practical considerations, all variables even remotely known to affect the predicted parameter in the model for a preliminary analysis to determine if the variables are correlated.
- R^2 does not indicate whether the variables included in the model are significant. The p -value should be limited to the level of confidence desired in the model. Typically, a

confidence level of 95 percent is used, such that the values should remain below 0.05. However, in rare cases, this sometimes is limited to 0.1.

- R^2 alone does not indicate whether there is collinearity present in the data or whether the selected independent variables have an interaction effect. It is necessary to verify using C_p and VIF.
- C_p , VIF, and R^2 do not offer any suggestions regarding further scope to improve a model by using transformed versions of the existing set of independent variables. Again, the use of engineering knowledge is necessary to incorporate transformed variables.

Other Modeling Considerations

Interaction Effects of Independent Parameters

Information from the literature points to the influence of independent variables on each material property of interest (the dependent variables) in a general sense, without adequately accounting for the impact other design and site parameters or independent variables may have on the dependent parameters. Therefore, to draw consistent and dependable conclusions on the effect of each independent parameter, it would be ideal to compare scenarios that have all other variables constant or in common, except for the independent variable under consideration, such as the effect of w/c ratio on strength or base type on erosion.

However, in synthesizing information from large databases, as was done in the present study, it is essential to adopt statistical tools to assess the relationships between several independent variables and the dependent variable. Therefore, where necessary, both linear regressions and the generalized linear model (GLM) were utilized to establish a model. GLM can independently examine the influence of an independent variable on a dependent variable despite the presence of other predictor variables in the data sample. In other words, GLM can isolate the effects of one independent variable by normalizing the effect of others, and it predicts whether the effect of each independent variable is statistically significant on a dependent variable using the analysis of variance (ANOVA) method.

GLM is a generalization of the linear regression model and can accommodate the following:

- Non-linear and linear effects of independent variables.
- Categorical predictor variables as well as continuous predictor variables.
- Dependent variables whose distributions follow several special members of the exponential family of distributions (e.g., gamma, Poisson, binomial, etc.), as well as normally distributed dependent variable.

Multilevel ANOVA Models

Multilevel ANOVA models are more complex models used in the design of experiments, and in the context of the current study, they are more appropriate to use when the dataset contains multiple measures or clustered tests. The analyses should account for the fact that the other

regressors in the equation are the same for multiple levels of one of the parameters, which most often is the pavement age parameter in the current study. This also is called a hierarchical model.

An example of such a model is one that compares PCC compressive strength for core and cylinder measurements. The LTPP database contains compressive strength results for cylinders cast during construction and cores taken from the pavement for SPS sections. These cores and cylinders have been tested at 14 days, 28 days, and 1 year. The strengths can be compared for each section and age. A simple way of doing such a comparison would be to perform a paired t -test. However, the number of measurements due to repeated measurements at different ages (i.e., 14 days, 28 days, 1 year, 2 years, etc.) should not be allowed to count as a full data point for sections with more than one age measurement. Therefore, a multilevel ANOVA model featuring State and sections should be used. If the data are balanced so that there are the same number of observations for each age and section, the paired t -test and the multilevel ANOVA would show the same results in the test whether core and cylinder measurements differ. In this example, the dataset is not balanced so the tests are not the same, with the multilevel ANOVA being the more appropriate analysis. Likewise, while developing a model to estimate strength at any age, the age parameter has to be treated in a hierarchical fashion.

All observations have the same fabrication variables at the State by section code level, and these are repeated when sections are tested several times (i.e., at different ages). It is not appropriate that the design values for a section tested four times should be allowed to count four times. Therefore, a multilevel ANOVA model must be used to guarantee that values from each section count only once while the values measured over time are incorporated in the analysis.

Treatment of Outliers

Generally, a true model representing the dataset used should include all natural data in the dataset. In other words, deliberate changes or removal of data artificially alters the inherent model. However, in using large datasets, especially when field data are used or when the data are from a dataset not originally designed to develop the model, values that lie beyond the scope of a field's value range are encountered. Such data, referred to as outliers, cannot be explained by other parameters specific to that case or observation. In statistical models, outliers are given special consideration and treated in a consistent manner for all points in the model so as to not simulate a fabricated dataset.

Outliers are either deleted (treated as missing values) or capped at a minimum or maximum value for each variable. In the current study, to the extent possible, outliers were not deleted from the datasets. However, certain models necessitated the deletion of select data points. When outliers were deleted, the process was based on a consistent criterion. Treatment of outliers is discussed separately for each model.

Grouping of Datasets

Any grouping of datasets performed is discussed separately for each model.

Procedures for Model Development

As part of model development, various combinations of model forms (i.e., mathematical relationships) and transformation of dependent/independent variables were evaluated to determine which combination resulted in the best prediction model. The combinations of model forms and transformation of dependent/independent variables is presented in figure 128 through figure 131.

In general, where past literature agreed on some sort of relationship between dependent and independent variables, the relationships were adopted and applied. Where no such agreements exist, all the combinations presented in figure 128 through figure 131 were applied.

$$f_c = A_0 + A_1 \times W/c + A_2 \times \text{cementitious content}$$

Figure 128. Equation. f_c linear model form with no transformation.

$$E_{c,t} = 375.6 * (f_c^{28\text{-day}})^{1.1} * (\ln(\frac{t}{0.03}))^{0.00524}$$

Figure 129. Equation. $E_{c,t}$ nonlinear model form with no transformation.

$$\ln(k_1) = 1.12 + 2.4 \times (\gamma_d) + 3.6 \times LL$$

Figure 130. Equation. k_1 linear model form with transformation.

$$\ln(k_1) = 1.12 (\gamma_d)^{1.996} \left(\frac{LL}{w_c}\right)^{0.639}$$

Figure 131. Equation. k_1 nonlinear model form with transformation.

Both linear and nonlinear statistical techniques were utilized for model development and calibration of the mathematical equations. The two principal SAS[®] procedures used for model development were REG and NLIN. Other SAS[®] procedures, such as STEP WISE, RSQUARE, and RSREG, were used in selecting the most suitable independent variables for incorporation into the tentative model. In general, using the dependent and independent variables (transformed or otherwise) and mathematical equations representing the model forms identified above, the iterative process in selecting a tentative model was performed as follows:

- **Selection of best combination of independent variables**—Selection of the best combination of independent variables was performed by using the SAS[®] STEP WISE, RSQUARE, RSREG, etc., procedures to determine the best combination of independent variables from the general list of possible independent variables identified as part of the literature review. Selection of the best combination of independent variables was performed based on the p -value of each individual independent variable included in the model. In general, an independent variable with a p -value greater than 5 percent was deemed not significant and was excluded from the model.
- **Selection of submodels**—For each model, using C_p and VIF determines the best combination of significant independent variables to be included in the tentative model. The aim is to limit the total number of independent variables in the models while

minimizing multicollinearity among independent variables, minimizing the error between measured and predicted dependent variable, and maximizing R^2 .

- **Maximize R^2** —The goal is to select independent variables to maximize R^2 without compromising model robustness characterized by C_p and VIF.
- **Minimize error**—The goal is to minimize error in predicted and measured dependent variable without compromising model robustness.

PCC MODELS

The prediction models developed for PCC compressive strength, flexural strength, elastic modulus, tensile strength, and CTE are discussed in detail in this section. The specific tables from which these data were obtained were listed in table 10. The development of the models involved an iterative process, and systematic analyses procedures followed. The process is described in detail for the first model. The various steps are not repeated in great detail for the remaining models, and only results are included.

Data Used in PCC Models

As discussed in chapters 2 and 4, PCC materials data and strength data are available in the LTPP database for both GPS and SPS sections. However, the extent of data available is different for the two experiment types. For the data used for the study, the PCC data come from PCC layers in JPCP, CRCP, and jointed reinforced concrete pavements (JRCPs). All JRCP sections with the exception of one test site belonged to GPS test sites. Also, there was a significant difference in the extent of data available for PCC index properties between the SPS and GPS sections. SPS sections had very detailed mix design information compared to the GPS sections. In addition to the materials information available for GPS sections, the SPS sections contained specific details about the use of SCMs, admixtures, and the gradation of the coarse and fine aggregates.

The following information should be noted about all of the PCC models with regard to data used, data reduction, and assumptions:

- The age at which the test was performed was determined by using the test date and the date of placement.
- Each SPS-2 site consists of 12 rigid pavement sections 500 ft long and constructed with two PCC mix designs in the surface JPCP layer. Six sections were placed using a high-strength mixture with a target flexural strength of 900 psi, and six sections were placed using a low-strength mixture with a target flexural strength of 550 psi. The mix design parameters were the same for all six sections in each strength category. The strength tests were performed at 14 days, 28 days, and 1 year using both cores from the pavement and companion specimens cast during construction. During the data assembly process, data for strengths determined from cores versus cast specimens were separated and averaged for each site and for each age across all sections that represented a given mix. In other words, for a given age, each SPS-2 site provided two data points to the prediction models—one for the low-strength concrete and one for the high-strength concrete. In the

data analysis process, codes of 1 and 2 were assigned for the low-strength and high-strength sections, respectively.

- Short-term strength and modulus data were available for SPS sites for 14 days, 28 days, 1 year, and up to 3 years for some sections. Two SPS sections had 10-year strength data.
- For each age, multiple tests were conducted. The analyses used the average strength for each age for all sections (SPS and GPS).
- For correlations between PCC strength parameters, cores were matched with cores and cylinders with cylinders, as necessary.
- The total amount of cement and other SCMs (typically fly ash) was summed to obtain the amount of CMC in SPS sections because this information was readily available for SPS sections. However, the cement content in GPS sections was considered to be the total CMC.
- For SPS sections, coarse and fine aggregate gradations were used to compute MAS and FM.
- Coarse aggregate type was considered a key variable for inclusion in some of the PCC models given its impact on CTE and modulus. As this variable is not countable, the different coarse aggregate types were considered as categorical variables and assigned values of 1 and zero. The aggregate types were basalt, chert, conglomerate, diabase, dolomite, gabbro, granite, limestone, quartzite, syenite, diorite, peridotite, and sandstone.
- Admixtures were considered categorical variables and assigned a value of 1 or zero for the presence or absence of each admixture type. Admixtures included in the list were air entraining agent, fly ash, water reducer, and retarder. Also included were the amounts used in the mix design.
- The curing method adopted for each section was considered as categorical variables (1 and 0) for none, membrane curing, burlap curing, and insulation.
- Mix design variables included the amounts of cement, water, coarse aggregate, fine aggregate, coarse aggregate specific gravity, and fine aggregate specific gravity.
- Cement type in the mix design was considered a categorical variable and included cement types 1, 2, and 3. The database contained one section with type 3 cement.
- LTPP data tables were merged as required for each analysis. The common referencing elements while merging the tables were STATE_ID, SHRP_ID, averaging code, LAYER_NO, and MATERIAL TYPE.

Limitations of All PCC Models

A fundamental limitation for any model is that the relationship that exists between the predicted parameter and the regressors is only valid for the range of data that has been included in the dataset. The statistical modeling procedures, for most part, assume that the variables are normally distributed within the dataset. For example, the relationships developed for PCC properties (e.g., a compressive strength prediction model) are applicable only for mixes with cement types 1 and 2. While one data point with type 3 cement exists in the database (a JRCP section), compared to 500 datasets with type 1 and type 2 cements, the strength gain pattern of a type 3 cement is outcompeted by the other two cement types in the database. As a result, it might not be evident within this dataset that type 3 cements produce higher strengths, especially in the early ages.

The model will reflect the intrinsic trends of the dataset used. For example, the data used for prediction of the 28-day compressive strength contains target low-strength and high-strength mix designs. If the primary means of achieving higher strengths for the States was to increase the cement content, the model will show a high correlation between CMC and strength. However, there are multiple ways to enhance mix compressive strength, such as the use of lower w/c ratios, water reducing agents, higher strength aggregates, curing at higher temperatures and insulation, and the use of type 3 cements. This is critical when the prediction models are implemented for estimating material properties.

The software program developed under the current study calculates the results for the material properties and includes a tool tip that provides the range of values that can be used for each variable. The interface also has a section which lists the basic limitations of the model.

PCC Compressive Strength Models

As discussed in chapter 3, compressive strength is the simplest of PCC strength tests and the most commonly available strength information for PCC materials. For the same reasons, the LTPP database contains extensive compressive strength data for all SPS and GPS sections. Since SPS and GPS data contain different levels of PCC materials information, it was considered meaningful to attempt to group them in different datasets to evaluate if a different subset of regressors emerged as significant for model development.

Compressive strength is considered a fundamental strength parameter and is used at different stages of a project. Many SHAs specify concrete strength requirements by the concrete's compressive strength, and designers develop pavement layer thicknesses based on compressive strength at 28 days. It is an important qualifier for concrete quality and contractor workmanship. QA testing programs (both contractor QC and agency QA tests) include compressive strength tests on cylinders and cores, and they form the basis for computing strength pay factor in a majority of agencies. Also, the compressive strength of the in situ concrete is used to determine if the pavement can be opened to traffic. Finally, the compressive strength of a core extracted from a pavement ready for rehabilitation is used to estimate the existing structure's structural capacity in overlay design. The age of the concrete is clearly a parameter of significance in all these cases (except the 28-day strength, which is used for design). Given the extent of data

available for PCC materials and compressive strength, the project team considered the following models, which are discussed in detail in this section:

- **28-day cylinder strength model**—Suitable for estimating design strength.
- **Short-term (1 year) cylinder strength model**—Suitable for estimating opening time.
- **Short-term (1 year) core strength model**—Suitable for in situ strength and opening time.
- **All ages core strength model**—Suitable for estimating in situ strength at any age.
- **Long-term core strength model**—Suitable for estimating long-term strength for rehabilitation design.

The procedure used to develop the model is explained in detail for the compressive strength model in the following section. The development of all other models in this study has entailed a similar level of analyses if not more.

Compressive Strength Model 1: 28-Day Cylinder Strength Model

The data used for this model included SPS sections that had 28-day cylinder test results. The data included 42 sets of results after averaging the 28-day cylinder strength for each site and for each mix design.

All material properties discussed in the section, *Data Used in PCC Models*, in chapter 5 of this report were evaluated to verify if they co-vary with the predicted variable. The first statistical procedure was a C_p analysis wherein various submodels were considered for fit using ANOVA, and the resulting C_p and R^2 values are provided at the end of the SAS[®] analysis. The results are listed by SAS[®] in order of the resulting C_p value. Also provided in the results are the number of variables (regressors) used in each model and a listing of the variables. The C_p analysis results are shown in table 16 for the 28-day cylinder strength model.

The C_p analysis summary indicates that 42 observations were read. There were missing data for certain PCC mix parameters. For example, the amount of coarse aggregate in the mix design and the amount of fine aggregate in mix design were missing in 13 cases, while the information on admixtures was missing in 21 cases. A summary indicates that only 21 observations had values for all variables considered in the model. Using a subset of 21 datasets, the potential prediction models created produced the R^2 values as listed in the table. The model form used for the analysis was as follows:

$$f_c = A_0 + A_1x_1 + A_2x_2 + A_3x_3 + A_4x_4 + \dots + A_nx_n$$

Figure 132. Equation. f_c model form.

Where:

A_0 = Model intercept determined through the regression.

A_1 through A_n = Regression coefficients.

x_1 through x_n = Parameters included in each submodel.

These results do not imply that all models listed in table 16 are feasible models. C_p and R^2 , as explained earlier, do not indicate whether the parameters included in the model, or submodel in this case, are significant, exhibit multicollinearity, or physically explain the trend. Each submodel suggested by the C_p analysis needs to be further evaluated and verified individually.

Table 16. C_p selection method for 28-day cylinder compressive strength model.

Number of Parameters in Model	C_p	R^2	Variables in Model
4	1.0058	0.8184	w_c cementitious Coarse_Aggregate_Mix_Design Fine_Aggregate_Mix_Design
4	1.2802	0.8143	w_c cementitious AVG_UNIT_WT_W_c Coarse_Aggregate_Mix_Design Fine_Aggregate_Mix_Design
2	1.5747	0.7493	w_c cementitious Coarse_Aggregate_Mix_Design
3	1.807	0.7761	w_c cementitious Coarse_Aggregate_Mix_Design Fine_Aggregate_Mix_Design
4	1.8277	0.806	w_c MASm15pct_W_c Coarse_Aggregate_Mix_Design Fine_Aggregate_Mix_Design
3	1.8478	0.7755	w_c cementitious Coarse_Aggregate_Mix_Design
3	2.0836	0.7719	w_c cementitious AVG_UNIT_WT_W_c Coarse_Aggregate_Mix_Design
5	2.2057	0.8305	w_c cementitious FM Coarse_Aggregate_Mix_Design Fine_Aggregate_Mix_Design
3	2.3622	0.7677	w_c Coarse_Aggregate_Mix_Design Fine_Aggregate_Mix_Design
4	2.4771	0.7962	w_c cementitious MASm15pct_W_c Coarse_Aggregate_Mix_Design Fine_Aggregate_Mix_Design
5	2.4789	0.8264	w_c cementitious FM AVG_UNIT_WT_W_c Coarse_Aggregate_Mix_Design Fine_Aggregate_Mix_Design
4	2.5453	0.7952	w_c FM Coarse_Aggregate_Mix_Design Fine_Aggregate_Mix_Design
3	2.5577	0.7647	w_c cementitious MASm15pct_W_c Coarse_Aggregate_Mix_Design

5	2.7348	0.8225	w_c cementitious MASm15pct_W_c Coarse_Aggregate_Mix_Design Fine_Aggregate_Mix_Design
5	2.9597	0.8191	w_c cementitious AVG_UNIT_WT_W_c Coarse_Aggregate_Mix_Design Fine_Aggregate_Mix_Design
5	2.9672	0.819	w_c cementitious AVG_UNIT_WT2 Coarse_Aggregate_Mix_Design Fine_Aggregate_Mix_Design
5	2.97	0.819	w_c cementitious AVG_UNIT_WT Coarse_Aggregate_Mix_Design Fine_Aggregate_Mix_Design
5	2.9955	0.8186	cementitious AVG_UNIT_WT2 AVG_UNIT_WT_W_c Coarse_Aggregate_Mix_Design Fine_Aggregate_Mix_Design
5	3.0046	0.8185	cementitious AVG_UNIT_WT AVG_UNIT_WT_W_c Coarse_Aggregate_Mix_Design Fine_Aggregate_Mix_Design
5	3.04	0.8179	w_c MASm15pct_W_c FM Coarse_Aggregate_Mix_Design Fine_Aggregate_Mix_Design
4	3.1679	0.7857	cementitious FM Coarse_Aggregate_Mix_Design Fine_Aggregate_Mix_Design
5	3.2171	0.8152	cementitious MASm15pct_W_c AVG_UNIT_WT_W_c Coarse_Aggregate_Mix_Design Fine_Aggregate_Mix_Design
3	3.4873	0.7507	cementitious FM Coarse_Aggregate_Mix_Design
5	3.4917	0.8111	AVG_UNIT_WT2 MASm15pct_W_c AVG_UNIT_WT_W_c Coarse_Aggregate_Mix_Design Fine_Aggregate_Mix_Design
5	3.4928	0.8111	w_c AVG_UNIT_WT2 MASm15pct_W_c Coarse_Aggregate_Mix_Design Fine_Aggregate_Mix_Design
5	3.4971	0.811	w_c AVG_UNIT_WT MASm15pct_W_c Coarse_Aggregate_Mix_Design Fine_Aggregate_Mix_Design
5	3.5058	0.8109	cementitious MASm15pct_W_c FM Coarse_Aggregate_Mix_Design Fine_Aggregate_Mix_Design

5	3.5095	0.8108	AVG_UNIT_WT MASm15pct_W_c AVG_UNIT_WT_W_c Coarse_Aggregate_Mix_Design Fine_Aggregate_Mix_Design
2	3.5215	0.7199	w_c cementitious
5	3.5431	0.8103	w_c MASm15pct_W_c AVG_UNIT_WT_W_c Coarse_Aggregate_Mix_Design Fine_Aggregate_Mix_Design
3	3.5548	0.7496	cementitious AVG_UNIT_WT2 Coarse_Aggregate_Mix_Design
3	3.5574	0.7496	cementitious AVG_UNIT_WT Coarse_Aggregate_Mix_Design
4	3.6023	0.7792	FM AVG_UNIT_WT_W_c Coarse_Aggregate_Mix_Design Fine_Aggregate_Mix_Design
3	3.6744	0.7478	AVG_UNIT_WT_W_c Coarse_Aggregate_Mix_Design Fine_Aggregate_Mix_Design
2	3.711	0.717	cementitious MASm15pct_W_c
4	3.7405	0.7771	w_c cementitious AVG_UNIT_WT2 Coarse_Aggregate_Mix_Design
4	3.7435	0.777	cementitious AVG_UNIT_WT2 AVG_UNIT_WT_W_c Coarse_Aggregate_Mix_Design
4	3.7458	0.777	MASm15pct_W_c AVG_UNIT_WT_W_c Coarse_Aggregate_Mix_Design Fine_Aggregate_Mix_Design
4	3.7472	0.777	w_c cementitious AVG_UNIT_WT Coarse_Aggregate_Mix_Design
4	3.7504	0.7769	w_c cementitious AVG_UNIT_WT_W_c Coarse_Aggregate_Mix_Design
4	3.757	0.7768	cementitious AVG_UNIT_WT AVG_UNIT_WT_W_c Coarse_Aggregate_Mix_Design
4	3.7817	0.7765	w_c cementitious FM Coarse_Aggregate_Mix_Design
4	3.8069	0.7761	cementitious AVG_UNIT_WT Coarse_Aggregate_Mix_Design Fine_Aggregate_Mix_Design
4	3.807	0.7761	cementitious AVG_UNIT_WT2 Coarse_Aggregate_Mix_Design Fine_Aggregate_Mix_Design
4	3.8079	0.7761	w_c cementitious MASm15pct_W_c Coarse_Aggregate_Mix_Design
2	3.9079	0.7141	cementitious AVG_UNIT_WT_W_c

4	4.0157	0.7729	cementitious FM AVG_UNIT_WT_W_c Coarse_Aggregate_Mix_Design
4	4.034	0.7726	w_c AVG_UNIT_WT_W_c Coarse_Aggregate_Mix_Design Fine_Aggregate_Mix_Design
6	4.0832	0.8324	w_c cementitious MASm15pct_W_c FM Coarse_Aggregate_Mix_Design Fine_Aggregate_Mix_Design

Table 17 to table 20 show examples of submodels evaluated in the selection of the optimized model for the prediction of 28-day compressive strength of PCC cylinders. This procedure typically involves an iterative process and specifically evaluates the following aspects:

- Is it reasonable to assume that the variables selected for the submodel are readily available for use at the intended stage of a project?
 - For the 28-day compressive strength value to be used by a designer at an initial design stage, information regarding the unit weight is perhaps not available. The unit weight is dependent on the consolidation achieved in the field. However, it could be available from field tests during the QA stage or to determine opening time or for long-term strength estimates.
- Do the regressed coefficients for the selected parameters explain the trends expected based on literature review and engineering knowledge?
 - Verify the absolute value and the sign (plus or minus) of the coefficient.
- Is the inclusion of the parameter significant to the prediction model (i.e., is the predictive ability of the model negatively affected by the inclusion of a given parameter)?
 - Verify if the p -value is less than 0.05 for a 95 percent confidence level.
- Does the parameter have an interaction effect with another parameter in the model?
 - Verify if VIF is below 5 (or 10 in exceptional cases).
- Is the model showing reasonable sensitivity to each parameter?
 - Verify using sensitivity analyses.

Table 17. Regression statistics for the four-variable model suggested by C_p analysis with subset of data that were available for all parameters evaluated.

Parameter	Degrees of Freedom (DF)	Estimate	Standard Error	t-Value	$P_r > t $	VIF
Intercept	1	9,907.383	2,732.919	3.63	0.0023	0
<i>w/c</i>	1	-4,893.05	2,532.455	-1.93	0.0712	3.01113
<i>Cementitious content</i>	1	3.30331	1.56188	2.11	0.0505	3.76626
<i>Coarse_Aggregate_Mix_Design</i>	1	-1.67238	0.61169	-2.73	0.0147	1.38486
<i>Fine_Aggregate_Mix_Design</i>	1	-1.51914	0.78059	-1.95	0.0694	1.79848

Note: Italicized text indicates that the parameter and statistic do not satisfy the criteria adopted for model development.

The model statistics for table 17 are as follows:

- Root mean square error (RMSE) = 772 psi.
- $R^2 = 0.8184$ percent.
- $N = 21$.

Table 18. Regression statistics for the four-variable model suggested by C_p analysis with complete dataset available for the parameters selected.

Parameter	DF	Estimate	Standard Error	t-Value	$P_r > t $	VIF
Intercept	1	10,789	2,181.11	4.95	<0 .0001	0
<i>w/c</i>	1	-2,050.86	2,200.846	-0.93	0.3607	2.78251
<i>Cementitious content</i>	1	3.57161	1.36819	2.61	0.0153	3.23079
<i>Coarse_Aggregate_Mix_Design</i>	1	-2.34227	0.51775	-4.52	0.0001	1.25735
<i>Fine_Aggregate_Mix_Design</i>	1	-2.35301	0.64777	-3.63	0.0013	1.39035

Note: Italicized text indicates that the parameter and statistic do not satisfy the criteria adopted for model development.

The model statistics for table 18 are as follows:

- RMSE = 774 psi.
- $R^2 = 0.7688$ percent.
- $N = 29$.

Table 19. Regression statistics for the three-variable model suggested by C_p analysis.

Parameter	DF	Estimate	Standard Error	t -Value	$P_r > t $	VIF
Intercept	1	9,381.832	1,569.631	5.98	< 0.0001	0
Cementitious	1	4.57228	0.84557	5.41	< 0.0001	1.24054
Coarse_Aggregate_Mix_Design	<i>1</i>	<i>-2.50707</i>	0.48533	-5.17	< 0.0001	1.11065
Fine_Aggregate_Mix_Design	<i>1</i>	<i>-2.23659</i>	0.63393	-3.53	0.0016	1.33863

Note: Italicized text indicates that the parameter and statistic do not satisfy the criteria adopted for model development.

The model statistics for table 19 are as follows:

- RMSE = 772 psi.
- $R^2 = 0.7604$ percent.
- $N = 29$.

Table 20. Regression statistics for the two-variable model suggested by C_p analysis.

Parameter	DF	Estimate	Standard Error	t -Value	$P_r > t $	VIF
Intercept	1	4,897.511	1,105.332	4.43	0.0002	0
Cementitious content	1	5.80657	0.92386	6.29	< 0.0001	1.02819
Coarse_Aggregate_Mix_Design	<i>1</i>	<i>-2.0405</i>	0.56042	-3.64	0.0012	1.02819

Note: Italicized text indicates that the parameter and statistic do not satisfy the criteria adopted for model development.

The model statistics for table 20 are as follows:

- RMSE = 927 psi.
- $R^2 = 0.6412$ percent.
- $N = 29$.

In establishing and optimizing a model, each variable selected has to be significant ($p < 0.05$) and not show an interaction effect with other variables ($VIF > 5$). However, the opposite is not true. It is not necessary that a variable with a p -value less than 0.05 and VIF less than 5 be included in a model if it is not meaningful from an engineering standpoint or if it does not show promise based on a sensitivity analysis.

While this evaluation process can be performed in a systematic manner, it cannot be performed in a fully automated manner. Each parameter in each model needs to be assessed manually. Table 17 and table 18 show the regression statistics for the four-variable model shown to produce the best correlation (R^2) in table 16. Note that the number of data points in the model is

different in the two tables ($N = 21$ and $N = 29$ in table 17 and table 18, respectively). Table 17 shows the subset of data that was used in the C_p analysis, wherein 21 observations have data in all fields evaluated; however, 29 observations have data for the parameters selected for the model. R^2 in table 17 matches that shown against the four-parameter model in table 16. However, the regressed coefficients and R^2 in table 18 correspond to the variables selected for this model, and the contents of table 18 are the proper statistics to report for the model.

The results in table 18 indicate the following:

- The w/c ratio is not significant to the model prediction ($p > 0.05$).
- A decrease in w/c ratio and an increase in CMC increases strength. Note the coefficients for these two variables are negative and positive, respectively.
- An increase in coarse and fine aggregate content reduces compressive strength. While this can be true in a certain range of aggregate contents, it is not true for the wide range of aggregate contents used in the analysis or that can be evaluated by a potential user of this model. This could be random correlation or possibly due to the high correlation between strength and CMC or due to a few observations containing mix designs with high aggregate content and low strength. Note that mixes with high aggregate contents (in the range of over 1,800–2,000 lb/yd³ for paving mixes) tend to increase the water demand, reducing the w/c ratio and reducing strength. The dataset used included observations that had coarse aggregates above 2,000 lb/yd³ that could have caused the aggregate contents to emerge as significant variables.

Removal of the w/c ratio parameter in the three-variable model results in regression statistics shown in table 19. Note that the coarse and fine aggregate contents show trends that counter engineering knowledge even though the parameters are significant to the model. The best two-variable model, shown in table 20, also shares the same concern. Thus, the iterative process needs to evaluate several parameters and balance both statistical and engineering needs. Often, a trial and error method has to supplement the pure statistical approach. The model selection is not based solely on the best R^2 value, either.

The final model selected for the estimation of 28-day compressive strength is shown in table 21 and includes the w/c ratio and CMC as the regressors. All 42 observations have been included. The R^2 value is 54.4 percent. Although it is compromised relative to the models discussed above, it provides a more meaningful model with a superior predictive ability. RMSE for the model is 871 psi. Table 22 provides details of the range of data used to develop the model. Figure 133 and figure 134 show the predicted versus measured values and the residuals plot for the model, respectively.

Table 21. Regression statistics for selected prediction model for 28-day PCC cylinder strength.

Variable	DF	Estimate	Standard Error	t-Value	$P_r > t $	VIF
Intercept	1	4028.41841	1681.71576	2.4	0.0215	0
w/c ratio	1	-3486.3501	2152.99857	-1.62	0.1134	2.40903
Cementitious content	1	4.02511	1.32664	3.03	0.0043	2.40903

The model statistics for table 21 are as follows:

- RMSE = 871 psi.
- $R^2 = 0.5444$ percent.
- $N = 42$.

Table 22. Range of data used for 28-day PCC cylinder strength.

Parameter	Minimum	Maximum	Average
w/c ratio	0.27	0.71	0.42
Cementitious content	376	936	664
Compressive strength	3,034	7,611	5,239

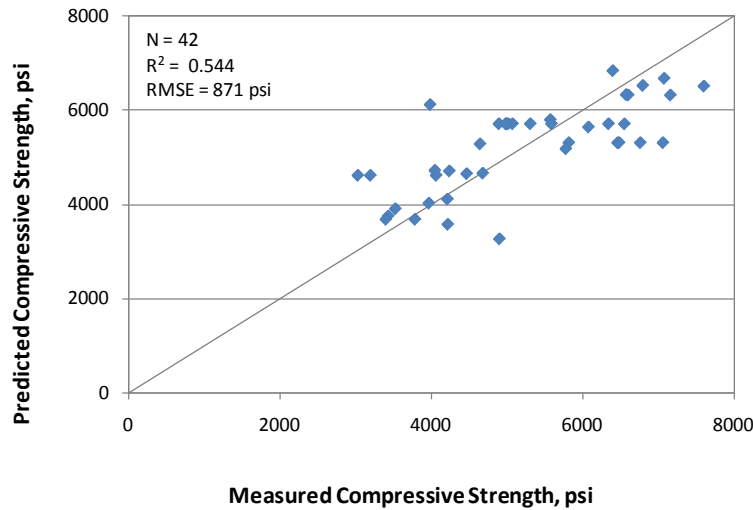


Figure 133. Graph. Predicted versus measured for 28-day cylinder compressive strength model.

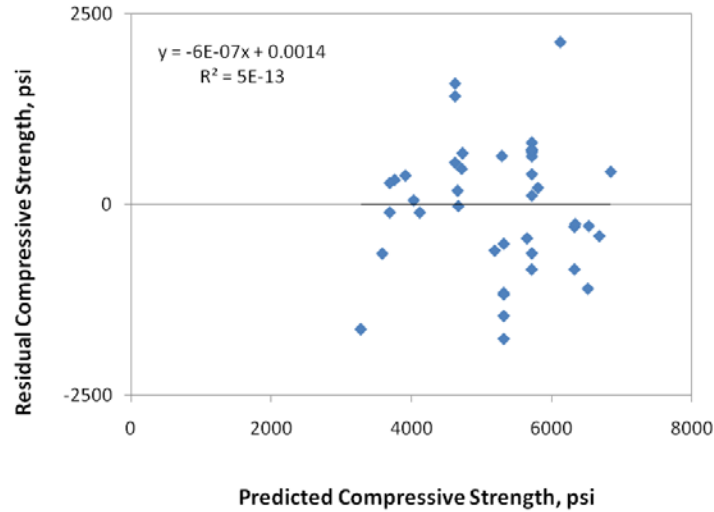


Figure 134. Graph. Residual error plot for 28-day cylinder compressive strength model.

The recommended 28-day compressive strength model is as shown in figure 135.

$$f_{c,28d} = 4,028.41841 - 3,486.3501 \times w/c + 4.02511 \times CMC$$

Figure 135. Equation. Prediction model 1 for $f_{c,28d}$.

Where:

$f_{c,28d}$ = 28-day compressive strength, psi.

w/c = Water to cementitious materials ratio.

CMC = Cementitious materials content, lb/ft³.

Figure 136 and figure 137 show the sensitivity of this model to w/c ratio and CMC . The change in compressive strength appears reasonable for both of the parameters for the range of values evaluated. They are also consistent with the data in the database. Within practical ranges, a change in CMC from 500 to 650 lb/ft³ increases the 28-day strength from approximately 4,700 to 5,300 psi for a w/c ratio of 0.4. Likewise, a decrease in the w/c ratio from 0.5 to 0.35 increases the strength from 4,700 to 5,200 psi.

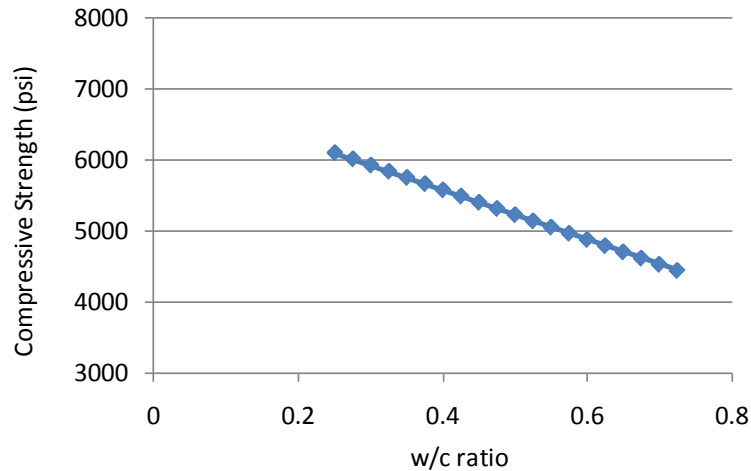


Figure 136. Graph. 28-day compressive strength model sensitivity to w/c ratio.

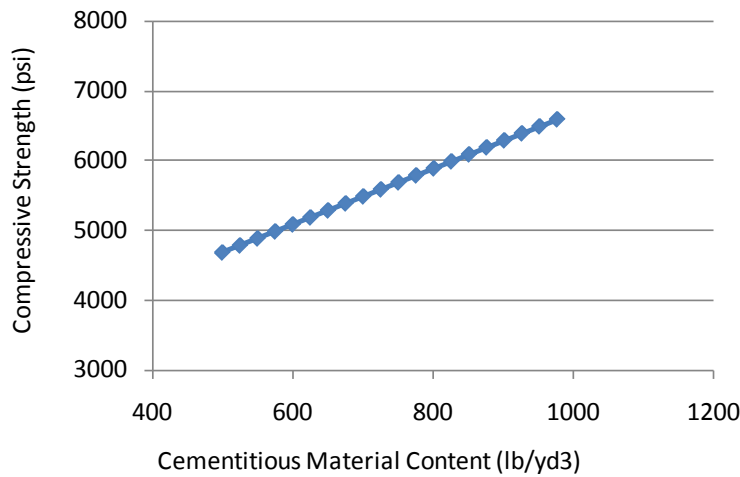


Figure 137. Graph. 28-day compressive strength model sensitivity to CMC.

Compressive Strength Model 2: Short-Term Cylinder Strength Model

Cylinder strength data were available for the SPS sections at pavement ages of 14 days, 28 days, and 1 year for a majority of the sections. Although two sections with strength data at 10 years were available, data in the model were limited for ages up to 1 year. Therefore, this model predicts the strength up to an age of 1 year.

Since this model utilizes only SPS data, a large set of independent variables was available for evaluation. Additionally, it is likely that this model will be used after approval of the mix design for a project or possibly even after initial construction, during which time more mix design parameters will be known for accurate prediction. The model developed includes pavement age as an independent parameter. Because the dataset includes multiple measurements or repeated readings of the same section, this parameter has been treated with a hierarchical modeling approach.

This model was established as shown in figure 138.

$$f_{c,t} = 6358.60655 + 3.53012 * CMC - 34.24312 * w/c * uw + 633.3489 * \ln(t)$$

Figure 138. Equation. Prediction model 2 for $f_{c,t}$.

Where:

- $f_{c,t}$ = Compressive strength at age t years, psi.
- CMC = Cementitious materials content, lb/yd³.
- w/c = Water to cement ratio.
- uw = Unit weight, lb/ft³.
- t = Short-term age, years.

The regression statistics for this model are presented in table 23, and details of the range of data used to develop the model are presented in table 24.

Table 23. Regression statistics for short-term cylinder strength model.

Variable	DF	Estimate	Standard Error	t-Value	$P_r > t $	VIF
Intercept	1	6,358.60655	1,213.09762	5.24	< 0 .0001	0
Cementitious	1	3.53012	0.90968	3.88	0.0002	2.15941
(w/c) × unit weight	1	-34.24312	11.00358	-3.11	0.0026	2.152
Ln(age)	1	633.3489	87.49625	7.24	< 0.0001	1.00604

The model statistics for table 23 are as follows:

- RMSE = 789 psi.
- $R^2 = 0.666$ percent.
- $N = 79$.

Table 24. Range of data used for short-term cylinder strength model.

Parameter	Minimum	Maximum	Average
w/c ratio	0.27	0.69	0.43
Cementitious content	376	936	660
Unit weight	124	151	143
Pavement age	0.0384	1.0000	0.3081
Compressive strength	2,480	10,032	5,256

The model was developed using 79 data points, and the prediction has an R^2 value of 66.6 percent and an RMSE value of 789 psi. The reason for an improved R^2 compared to the 28-day strength model is not clear from these analyses. Figure 139 and figure 140 show the predicted versus measured plot and the residual plot, respectively.

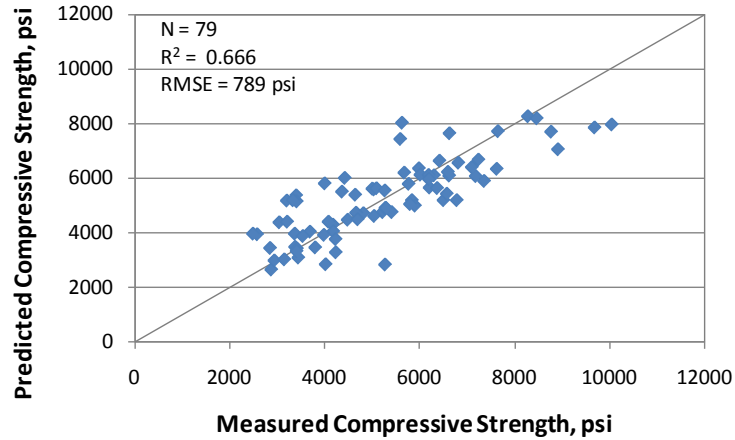


Figure 139. Graph. Predicted versus measured for short-term cylinder compressive strength model.

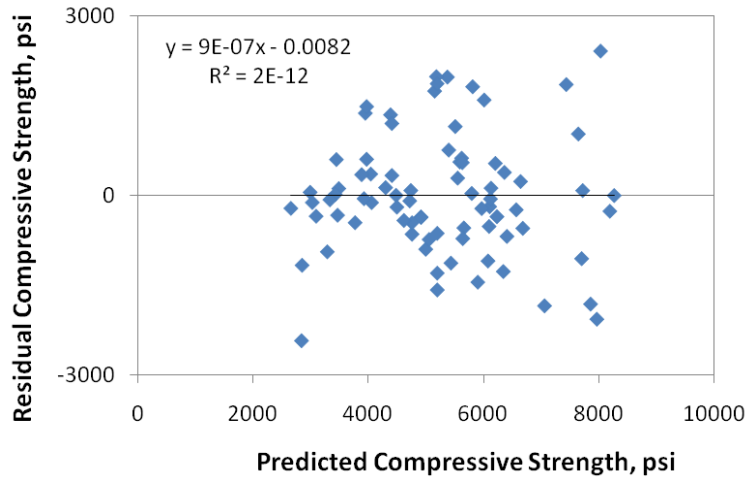


Figure 140. Graph. Residual errors for short-term cylinder compressive strength model.

Figure 141 through figure 143 show the sensitivity of this model to CMC, w/c ratio, and age, respectively. These trends are all reasonable. Figure 141 and figure 142 show the change in compressive strength at two ages, 28 days and 1 year, which are almost at the lower and upper bounds of ages included in this model. The plot in figure 143 can be considered a strength gain curve for typical unit weight and w/c ratios used in mix designs.

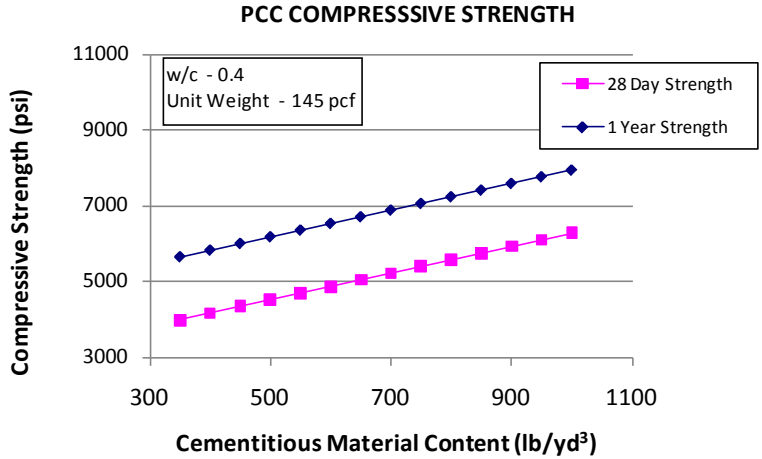


Figure 141. Graph. Short-term cylinder compressive strength sensitivity to CMC.

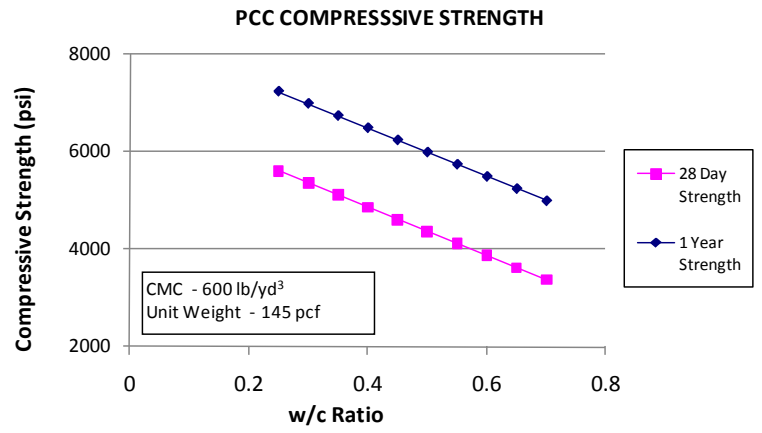


Figure 142. Graph. Short-term cylinder compressive strength sensitivity to w/c ratio.

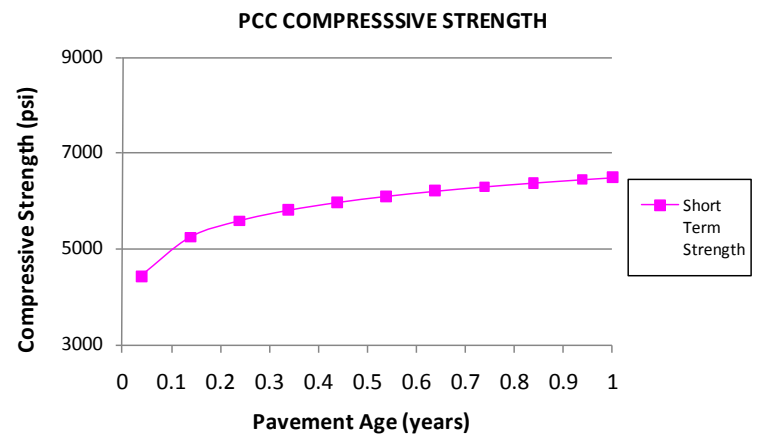


Figure 143. Graph. Short-term cylinder compressive strength sensitivity to age.

Compressive Strength Model 3: Short-Term Core Strength Model

The core strength data in the LTPP database were used for this model. While the materials and test ages are similar to the short-term cylinder strength model, the compressive strength of the cores is representative of the consolidation and quality of construction in the field. An initial comparison of core versus cylinder strengths was performed to determine if there was a significant difference in two strength values. Data were matched by section and age. Data were grouped in several age categories so that strength comparisons could be made at corresponding ages. Generally, each category up to 56 days was grouped for ages of ± 3 days. For ages close to 6 months to 1 year, the results were grouped for ages ± 30 days. The ages at which strength test results were common to both cores and cylinders were 14 days, 21 days, 28 days, 35 days, 41 days, and 1 year.

The comparison showed that there was no significant difference between strength values determined from core or cylinder tests. The paired t -test results shown in table 25 indicate that there is no significant difference between the two strengths ($P < t$ -critical). Figure 144, which has a trend line forced to zero intercept, shows the same results. Note that a trend line with a non-zero intercept produces a higher R^2 (0.67), which is consistent with the Pearson correlation value of 0.82 presented in table 25.

In the development of this model, parameters similar to the cylinder strength model were evaluated. In addition, the effect of curing was considered with greater attention. However, curing did not prove to be a significant variable. As this model attempts to predict the strength up to 1 year in age, the variable accounting for age was treated in a hierarchical fashion.

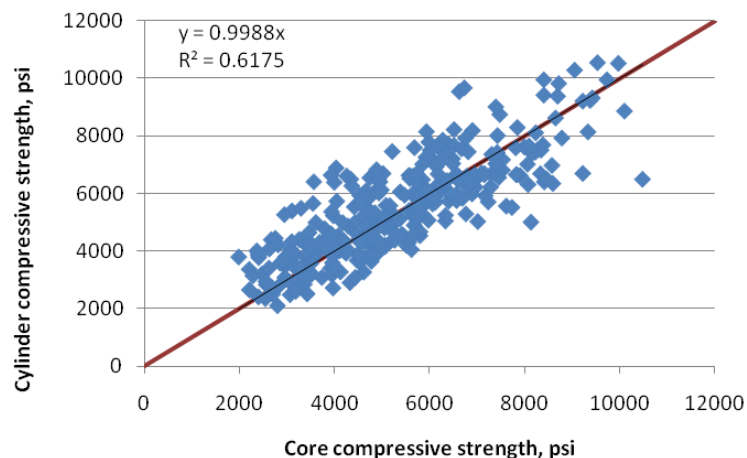


Figure 144. Graph. Comparison of core and cylinder strengths for SPS sections.

Table 25. Paired *t*-test results for comparison of core and cylinder strengths in SPS data.

Parameter	Core	Cylinder
Mean	5345.3	5472.3
Variance	3,307,974.59	3,003,561.77
Observations	312	312
Pearson correlation	0.82	
Hypothesized mean difference	0	
DF	311	
<i>t</i> -Stat	-2.11	
$P(T \leq t)$ one-tail	0.02	
<i>t</i> -critical one-tail	1.65	
$P(T \leq t)$ two-tail	0.04	
<i>t</i> -critical two-tail	1.97	

This model was established as shown in figure 145.

$$f_{c,t} = 98.92962 + 5.70412 * CMC + 28.48527 * uw + 2570.13151 * MAS * w/c - 199.84664 * FM + 611.30879 * \ln(t)$$

Figure 145. Equation. Prediction model 3 for $f_{c,t}$.

Where:

- $f_{c,t}$ = Compressive strength at age t years, psi.
- CMC = Cementitious materials content, lb/yd³.
- uw = Unit weight, lb/ft³.
- MAS = Maximum aggregate size, inch.
- w/c = Water to cementitious materials ratio.
- FM = Fineness modulus of fine aggregate.
- t = Short-term age in years.

The regression statistics for this model are presented in table 26. The model was developed using 294 points, and the prediction has an R^2 value of 67.6 percent and an RMSE value of 1,122 psi. Table 27 provides details of the range of data used to develop the model. Figure 146 and figure 147 show the predicted versus measured plot and the residual plot, respectively. Figure 148 through figure 153 show the sensitivity of this model to CMC, unit weight, MAS, w/c ratio, FM, and age, respectively.

Table 26. Regression statistics for short-term core strength model.

Variable	DF	Estimate	Standard Error	t-Value	$P_r > t $	VIF
Intercept	1	98.92962	1,544.34064	0.06	0.949	0
Cementitious	1	5.70412	0.36589	15.59	< 0.0001	1.23548
Unit weight	1	28.48527	10.59672	2.69	0.0076	1.0182
(MAS) × (w/c ratio)	1	2,570.13151	538.267	-4.77	< 0.0001	1.2201
Fineness modulus (FM)	1	-199.84664	120.68288	-1.66	0.0988	1.01426
Ln(age)	1	611.30879	45.08962	13.56	< 0.0001	1.00026

The model statistics for table 26 are as follows:

- RMSE = 1,122 psi.
- $R^2 = 0.6761$ percent.
- $N = 294$.

Table 27. Range of data used for short-term core strength model.

Parameter	Minimum	Maximum	Average
w/c ratio	0.27	0.69	0.42
Cementitious content	376	999	670
Unit weight	120	163	144
MAS	0.375	1.000	0.683
FM	2.50	4.37	3.05
Pavement age	0.0380	2.2160	0.4230
Compressive strength	1,990	11,350	5,596

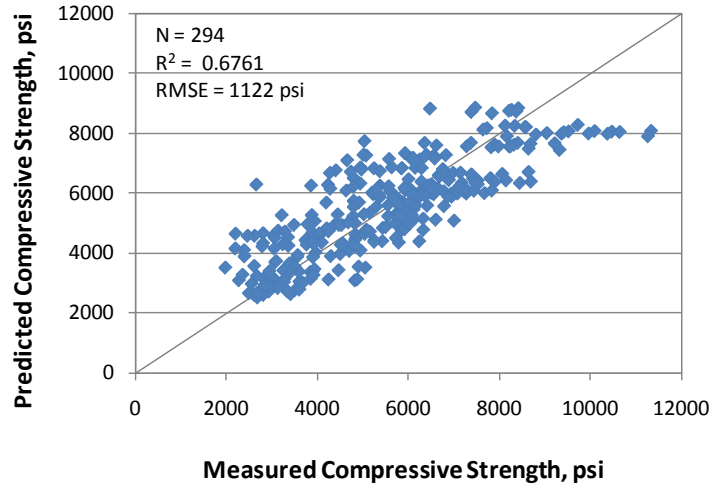


Figure 146. Graph. Predicted versus measured for short-term core compressive strength model.

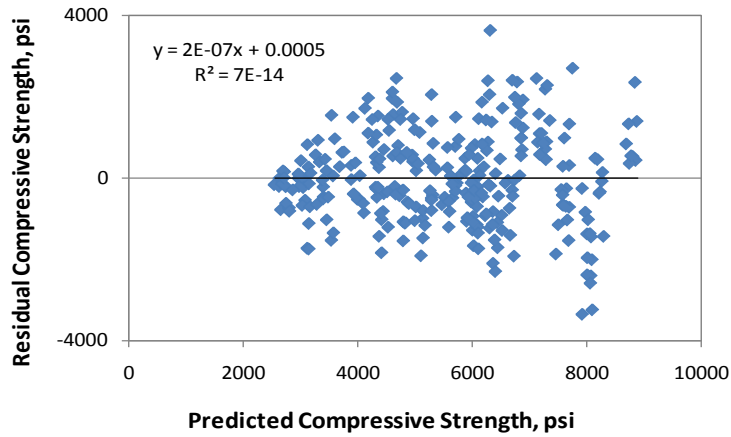


Figure 147. Graph. Residual errors for short-term core compressive strength model.

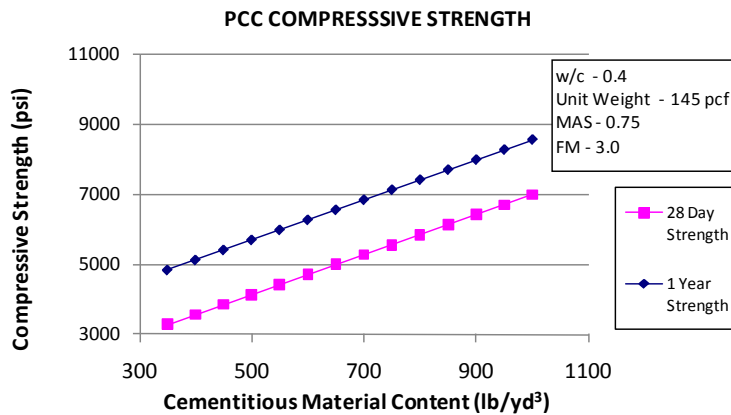


Figure 148. Graph. Short-term core compressive strength sensitivity to CMC.

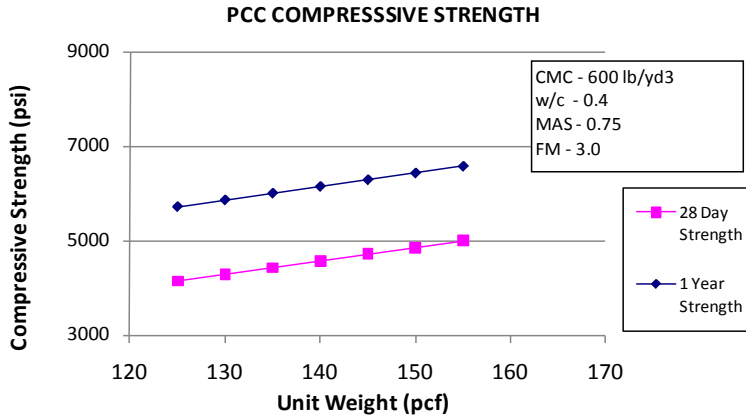


Figure 149. Graph. Short-term core compressive strength sensitivity to unit weight.

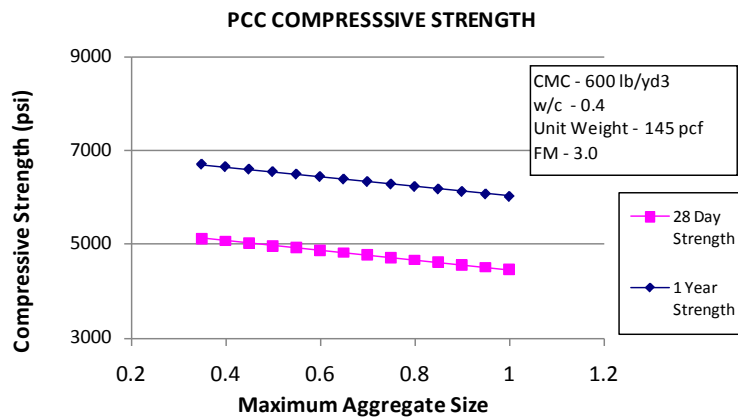


Figure 150. Graph. Short-term core compressive strength sensitivity to MAS.

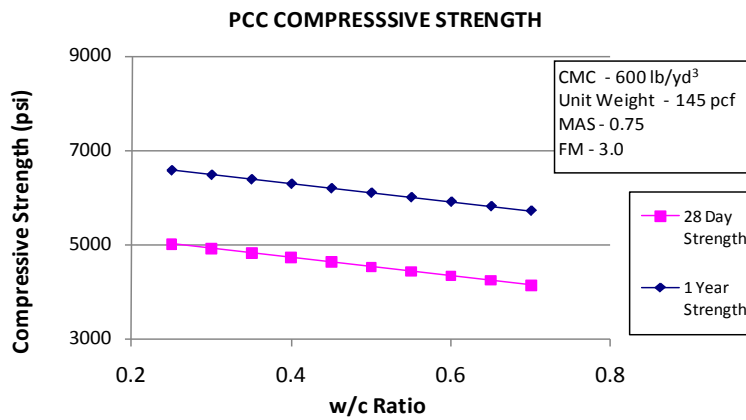


Figure 151. Graph. Short-term core compressive strength sensitivity to w/c ratio.

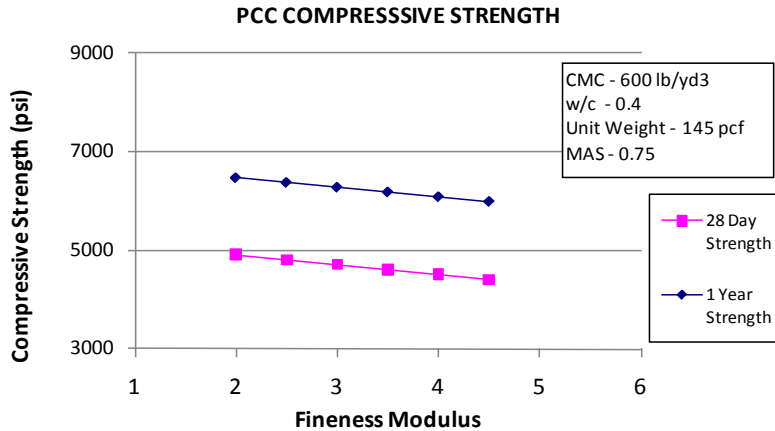


Figure 152. Graph. Short-term core compressive strength sensitivity to fine aggregate FM.

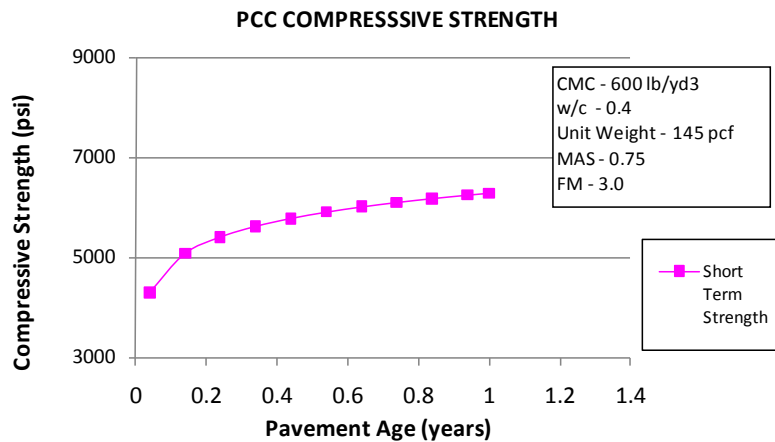


Figure 153. Graph. Short-term core compressive strength sensitivity to age.

Compressive Strength Model 4: All Ages Core Strength Model

The compressive strength model 4 was developed to provide a strength estimate for in situ strength at all ages of a project and covers both short-term and long-term estimates. This model provides the ability to assess the strength development over the entire lifetime of a project and make more realistic estimates of distress development. This necessitates the use of both SPS and GPS section data. The short-term strength data for this model were primarily from SPS sections, and the long-term strength data were controlled by GPS sections. Data from SPS and GPS sections primarily consisted of strength tests for pavement ages less than 3 years and greater than 5 years, respectively. However, this resulted in the use of a limited set of independent parameters for the model. Only information available for GPS sections could be included. For example, gradation parameters of coarse and fine aggregates were not considered when developing this model.

This model can be expressed as follows:

$$f_{c,t} = -6022.44 - 854.46 * w/c + 4.8656 * CMC + 68.5337 * uw + 533.15 * \ln(t)$$

Figure 154. Equation. Prediction model 4 for $f_{c,t}$.

Where:

$f_{c,t}$ = Compressive strength at age t years, psi.

w/c = Water to cement ratio.

CMC = Cementitious materials content, lb/yd³.

uw = Unit weight, lb/ft³.

t = Short-term age, years.

The regression statistics for this model are presented in table 28. The model was developed using 580 data points, and the prediction has an R^2 value of 55.4 percent and an RMSE value of 992 psi. Table 29 provides details of the range of data used to develop the model. Figure 155 and figure 156 show the predicted versus measured plot and the residual plot, respectively. Figure 157 through figure 160 show the sensitivity of this model to w/c ratio, CMC, unit weight, and age, respectively. Again, the sensitivity plots showing the variation in core compressive strength with changes in w/c ratio, CMC, and unit weight are presented for 28 days, 1 year, and 20 years. The rate of strength gain is much higher in the short term (28 days to 1 year) than during the next 19 years in the long term. The use of the logarithmic function for the age parameter is justified, as these trends mimic actual strength gain in the field or in laboratory cast specimens. Figure 160 can be treated as the strength gain relationship representative of a typical mix (w/c of 0.4, cement content of 600 lb/yd³, and unit weight of 145 lb/ft³).

Table 28. Regression statistics for all ages core strength model.

Variable	Estimate	Standard Error	t -Value	$P_r > t $	VIF
Intercept	-6,022.44	2,028.37	-2.97	0.0032	0
w/c ratio	-854.46	675.86	-1.26	0.2069	2.15941
Cementitious	4.8656	0.5737	8.48	< 0.0001	2.152
Unit weight	68.5337	13.4368	5.1	< 0.0001	1.00604
Ln(age)	533.15	22.3343	23.87	< 0.0001	1.00026

The model statistics for table 28 are as follows:

- RMSE = 992 psi.
- $R^2 = 0.5538$ percent.
- $N = 580$.

Table 29. Range of data used for all ages core strength model.

Parameter	Minimum	Maximum	Average
w/c ratio	0.00	0.72	0.43
Cementitious content	354	999	615
Unit weight	120	163	145
Pavement age	0.0380	45.3840	6.4320
Compressive strength	1,990	11,750	6,430

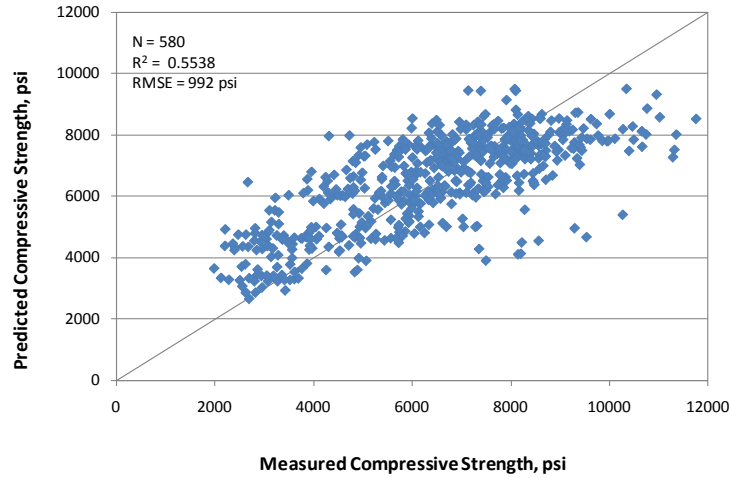


Figure 155. Graph. Predicted versus measured for all ages core compressive strength model.

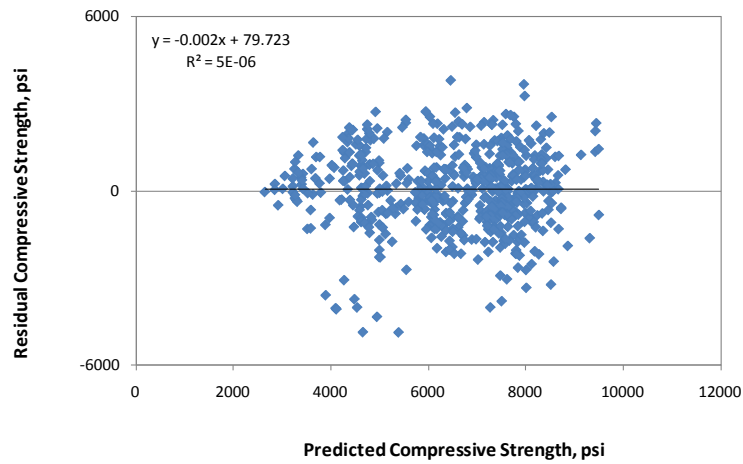


Figure 156. Graph. Residual errors for all ages core compressive strength model.

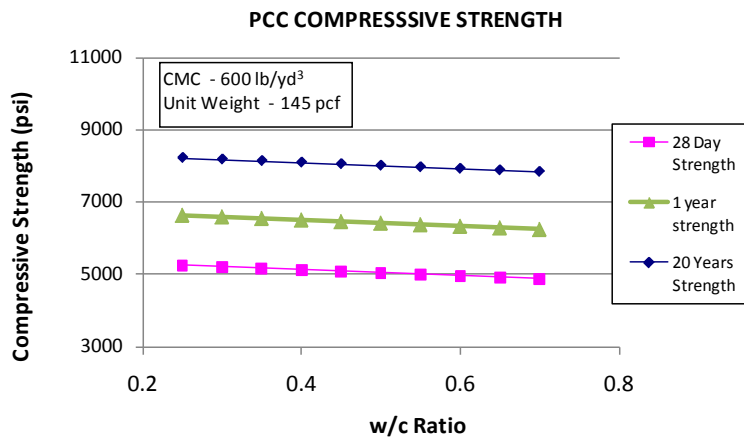


Figure 157. Graph. All ages core compressive strength sensitivity to w/c ratio.

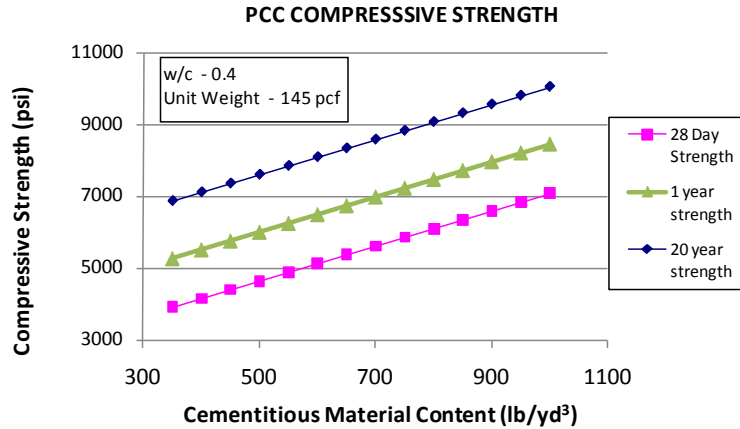


Figure 158. Graph. All ages core compressive strength sensitivity to CMC.

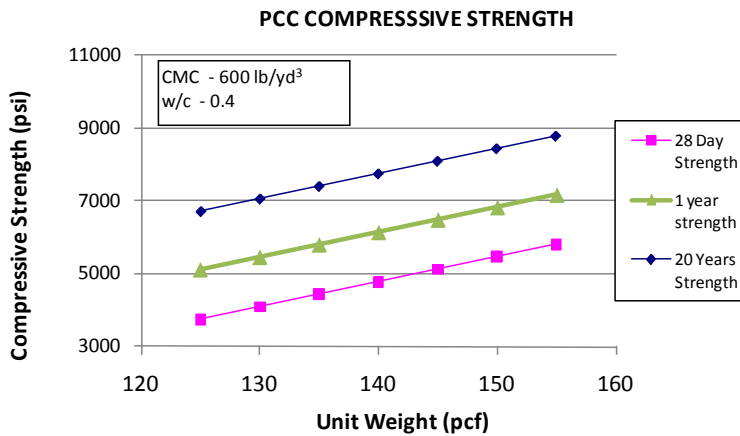


Figure 159. Graph. All ages core compressive strength sensitivity to unit weight.

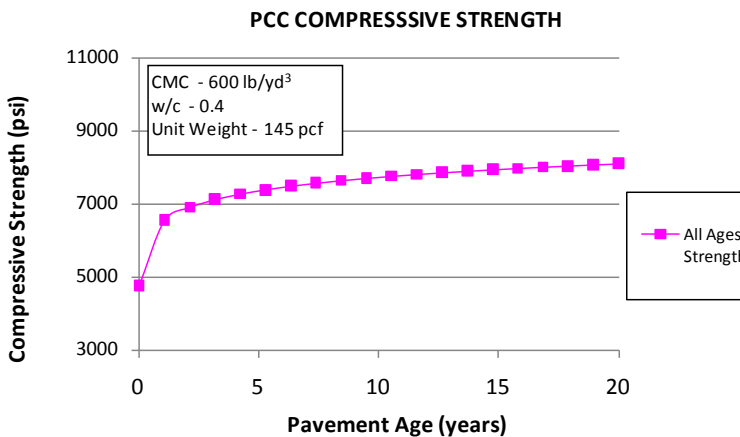


Figure 160. Graph. All ages core compressive strength sensitivity to age.

Compressive Strength Model 5: Long-Term Core Strength Model

This model was developed to estimate the long-term strength of cores taken from a pavement. Data from only the GPS sections were utilized, and they included sections greater than 5 years in age. Strength data at multiple ages were available on some of the sections. A preliminary

analysis indicated that pavement age was not a significant factor in the model. In other words, for pavements that have been in service for several years, the strength was more a function of its material parameters than age. This suggests that strength gain is relatively minimal after 5 years or is not noticed in a statistical sense. It then becomes reasonable, or perhaps even necessary, from a statistical standpoint to average the strengths for each section.

The model selected for the long-term strength can be expressed as follows:

$$f_{c,LT} = -3467.3508 + 3.63452 * CMC + 0.42362 * uw^2$$

Figure 161. Equation. Prediction model 5 for $f_{c,LT}$.

Where:

$f_{c,LT}$ = Long-term compressive strength, psi.

CMC = Cementitious materials content, lb/yd³.

uw = Unit weight, lb/ft³.

The regression statistics for this model are presented in table 30. The model was developed using 201 data points, and the prediction has an R^2 value of 18 percent and an RMSE value of 1,179 psi. Table 31 provides details of the range of data used to develop the model. Figure 162 and figure 163 show the predicted versus measured plot and the residual plot, respectively. From observing figure 162, it is evident that this model does not have a good predictive ability, and while there is no significant bias, the error in prediction is fairly high (see figure 163). This model needs to be used with caution, and other means to verify the value would be necessary, such as core tests.

Table 30. Regression statistics for long-term core strength model.

Variable	DF	Estimate	Standard Error	t-Value	$P_r > t $	VIF
Intercept	1	-3,467.3508	1,720.49637	-2.02	0.0452	0
Cementitious	1	3.63452	1.38354	2.63	0.0093	1.024
(Unit weight) ²	1	0.42362	0.06634	6.39	< 0.0001	1.024

The mode statistics for table 30 are as follows:

- RMSE = 1,179 psi.
- R^2 = 0.1803 percent.
- N = 201.

Table 31. Range of data used for long-term core strength model.

Parameter	Minimum	Maximum	Average
Cementitious content	354	781	550
Unit weight	134	156	147
Compressive strength	4,315	11,750	7,655

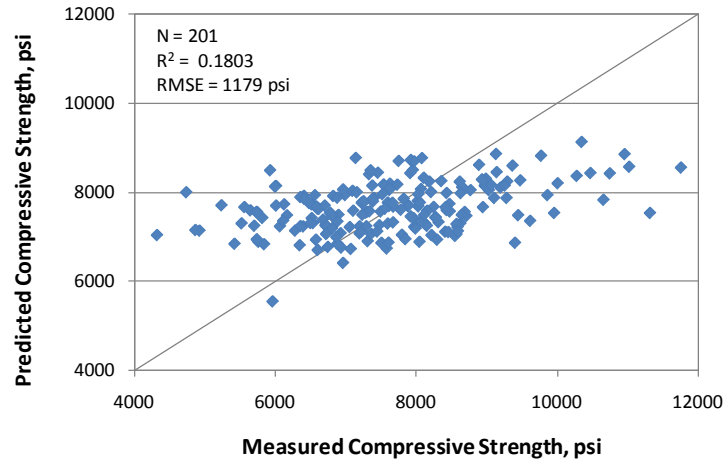


Figure 162. Graph. Predicted versus measured for long-term core compressive strength model.

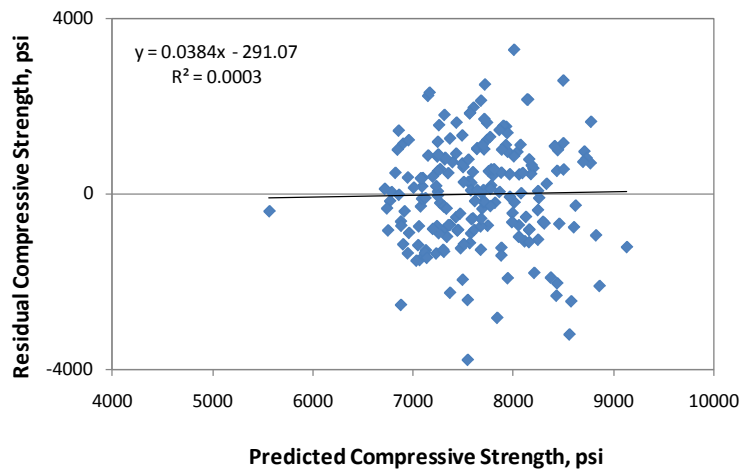


Figure 163. Graph. Residual errors for long-term core compressive strength model.

Relative Comparison of All Compressive Strength Models

The compressive strength models presented in this section reproduce the trends present in the datasets used for each correlation. It is highly recommended that a user estimate the strength based on as many models as possible with the information available at the time of analysis. This might provide a fair assessment of the ranges of compressive strength likely for the project and at different ages.

This section presents a comparison of the various models, and the graphs used for this discussion also include raw data plotted with the various relationships. Figure 164 through figure 168 show the relationship between compressive strength and CMC, w/c ratio, and unit weight, respectively. Figure 167 and figure 168 show the strength gain at short- and long-term ages, respectively. Note that relationships have been plotted for typical values for all variables, and the raw data used in the models do not necessarily lie on the plots.

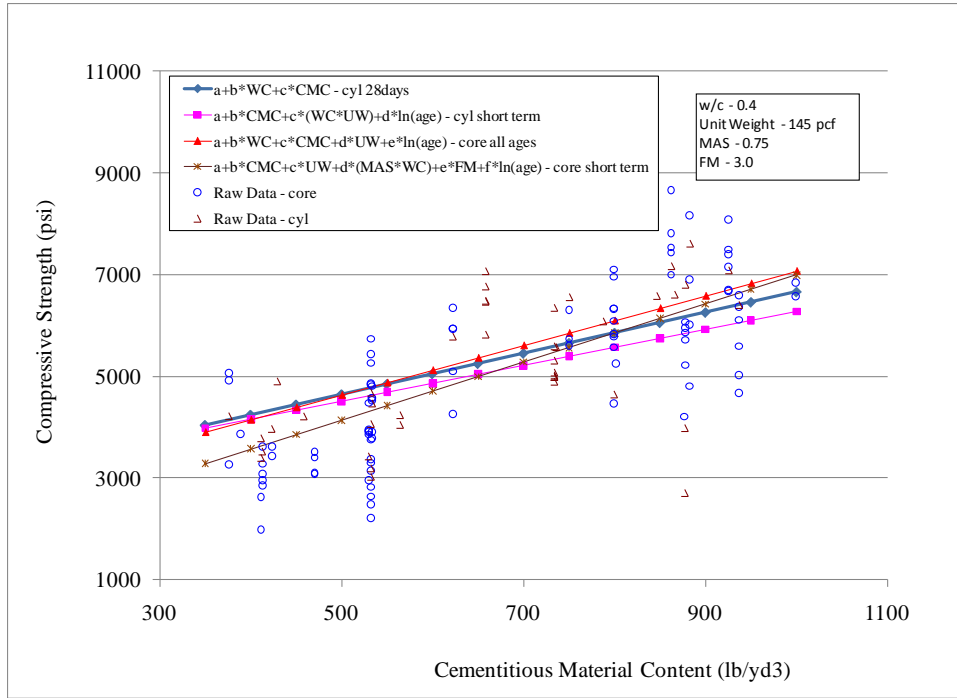


Figure 164. Graph. Model compressive strength prediction for varying CMC.

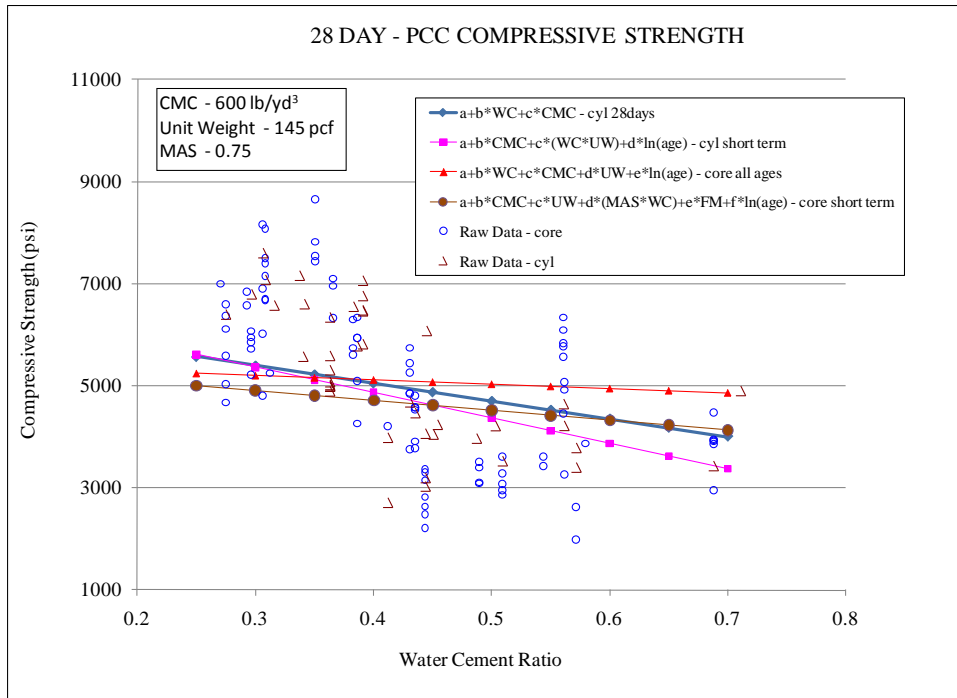


Figure 165. Graph. Model compressive strength prediction for varying w/c ratio.

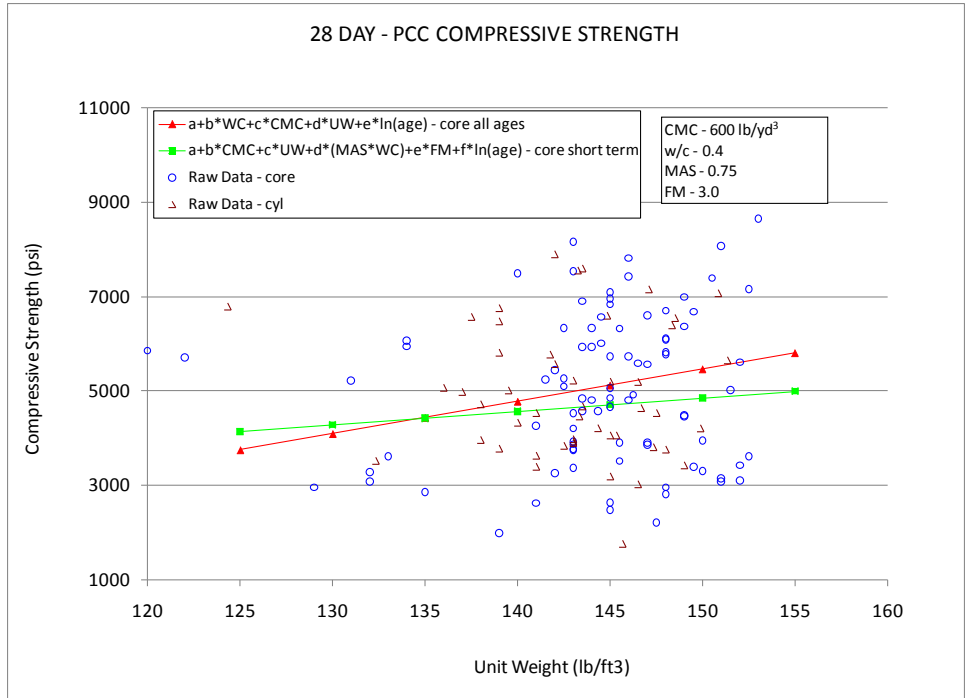


Figure 166. Graph. Model compressive strength prediction for varying unit weights.

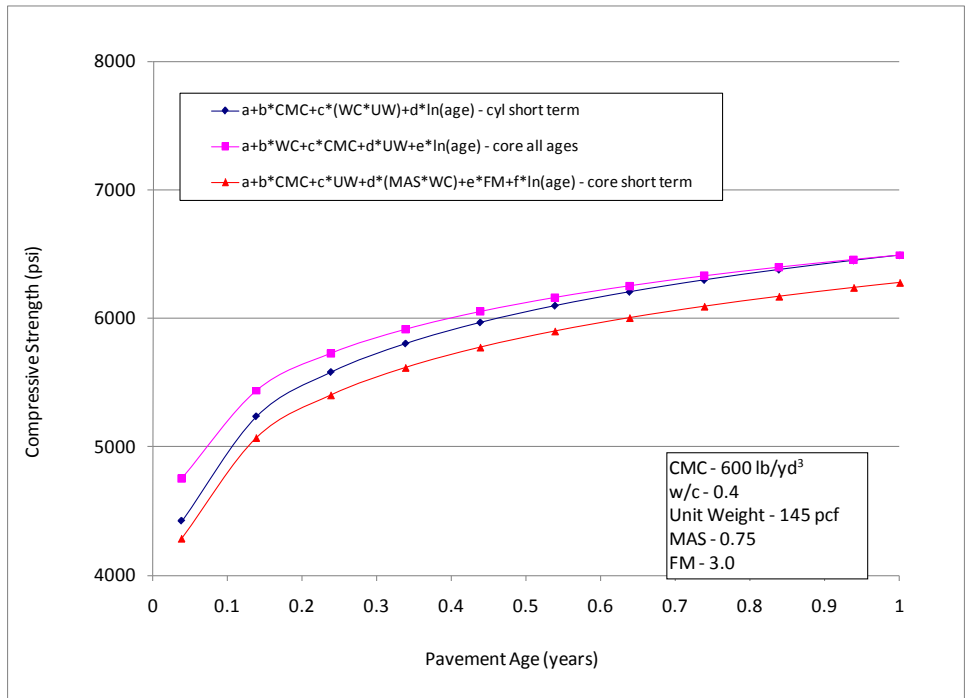


Figure 167. Graph. Strength gain in the short-term predicted by three models.

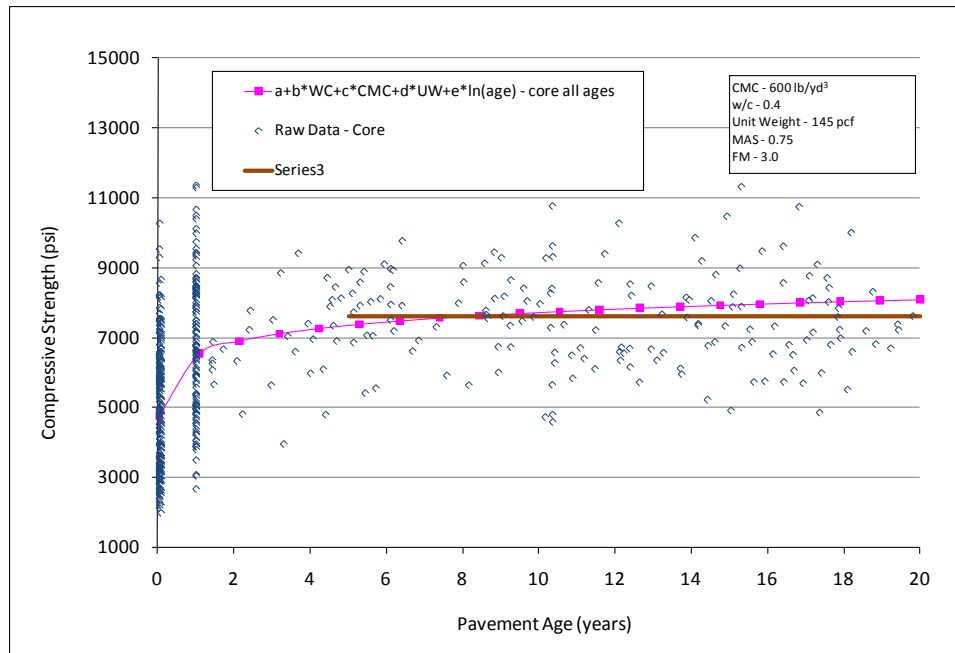


Figure 168. Graph. Long-term strength gain predicted by the models.

The following observations can be made:

- The predictions are within 700 psi of each other for a given CMC (see figure 164). However, for more typical ranges of cement contents, the predictions are within 300 to 400 psi of each other. The short-term core compressive model has the steepest slope for this relationship.
- Figure 165 suggests that the predictions have a range as high as 1,500 psi for a given w/c ratio, especially at very high w/c ratios. However, within typical ranges (0.3 to 0.5), the models predict within a range of 250 to 800 psi. The range slightly increases at lower w/c ratios. The short-term cylinder strength has the highest slope in this case.
- Based on the trend presented in figure 166, for a given level of unit weight, the compressive strength predictions are within 200 to 300 psi for typical ranges of unit weight (140 to 145 lb/ft³). The prediction can vary by about 800 psi for very high unit weight values. Note that the short-term cylinder compressive strength model has not been included in this plot, as the variable appears as a transformed variable in the model, and its effect cannot be isolated.
- Short-term strength predictions by all models that are relevant to short-term strengths show predictions within 200 to 400 psi of each other. The predictions are closer in value at as the age increases from 14 days to 1 year (see figure 167).
- Figure 168 suggests that the long-term strength predicted by the core all ages model is close to the strength predicted by the long-term model. This is essentially because the data used for strengths at ages greater than 5 years were obtained from the same GPS sections.

These observations illustrate the benefit of comparing predictions made by the various models available to obtain the range of strength that each project or observation could develop. Any other information to substantiate or validate the strength predictions should be utilized whenever possible, such as strength values from other projects that have used similar materials and mix design.

PCC Flexural Strength Models

The first step with the development of PCC flexural strength model was to assemble the relevant data in a manner appropriate for model development, followed by the actual statistical analyses. Statistical analyses to develop prediction models for flexural strength involved the validation of existing models and model forms as well as the development of new models to predict flexural strength.

The validation of existing models was a relatively straightforward exercise that involved fitting the data assembled in this study to the most commonly referenced model forms. Flexural strength has been correlated to compressive strength in previous models. Furthermore, in the development of new models, attempts were made to provide relationships as a function of readily available information. This study therefore attempted to develop models based on the compressive strength, as well as material properties and age. This provides options on which models to use, depending on the parameters and mix design information available.

The following are key points to note about flexural strength data:

- Flexural strength test results are available for SPS sections only.
- Test data were collected at 14 days, 28 days, and 1 year. Compressive strength data were also present for these specific ages. The data were matched for these specific age categories.
- Flexural strengths for the SPS-2 sections were predominantly at two levels. Strength results were in two distinct categories representing the two mix designs targeting low (550 psi) and high (900 psi) strengths.

Validation of Existing Models

Previous attempts have been made to correlate PCC flexural strength to the compressive strength, as discussed in chapter 2. These correlations generally have used a power model of the following form:

$$M_r = a * f_c^b$$

Figure 169. Equation. M_r .

Where:

$a = 7.5$ to 11.7 for $b = 0.5$.

$a = 2$ to 2.7 for $b = 0.67$.

The data assembled from the LTPP database was used to develop models with $b = 0.5$ and 0.67 . Table 32 shows a summary of the models developed. The regressed constants, a and b , were found to be within the range of values reported by the other studies discussed in chapter 2. This validation not only provides feasible models, but it also confirms that the data being used in this study can reasonably represent the broad range considered in the various studies. The correlations are presented in figure 170 and figure 171 for the power models with exponents of 0.5 and 0.67 , respectively.

Table 32. Power models developed for flexural strength prediction using LTPP data for validation.

Model	a	b	R^2	N
$M_r = a * f_c^b$	10.3022	0.5	0.446	185
	2.4277	0.67	0.449	185

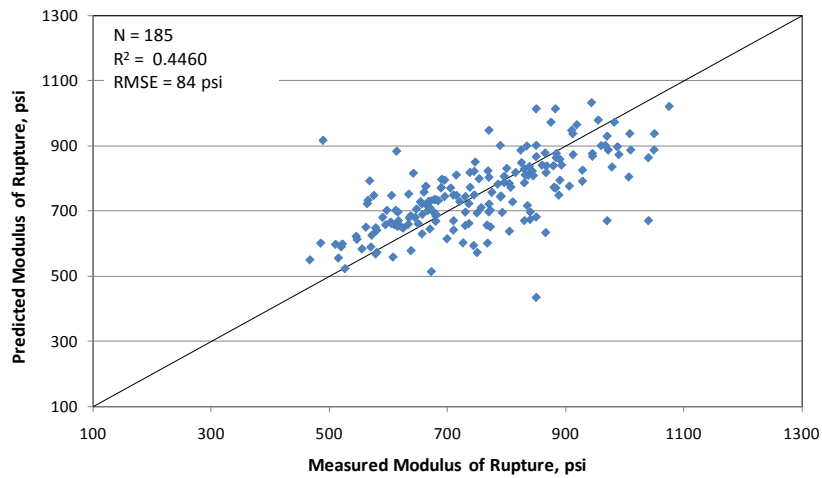


Figure 170. Graph. Predicted versus measured for validating 0.5 power flexural strength model.

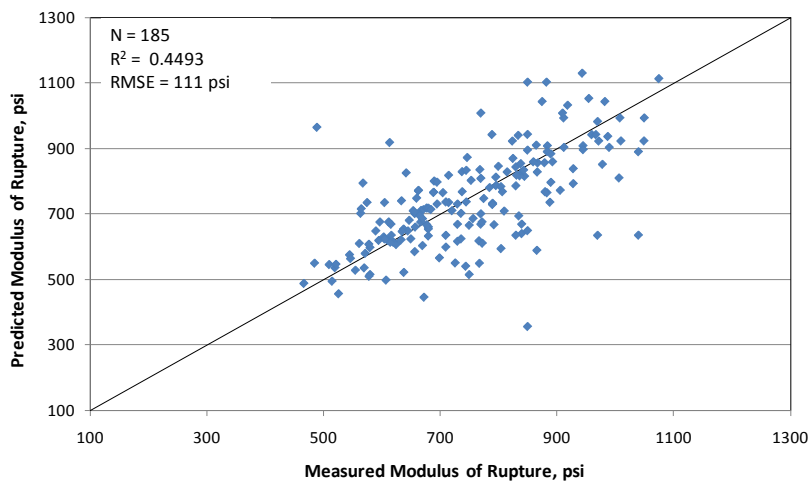


Figure 171. Graph. Predicted versus measured for validating 0.667 power flexural strength model.

Flexural Strength Model 1: Flexural Strength Based on Compressive Strength

The flexural strength model 1 provides the best correlation between compressive strength and flexural strength with the LTPP data. The model form utilizes the power equation. This model will be most useful for cases when the compressive strength of the PCC has been determined through a routine cylinder break.

This model can be expressed as follows:

$$MR = 22.7741 * f'_c{}^{0.4082}$$

Figure 172. Equation. Prediction model 6 for MR.

Where:

MR = Flexural strength, psi.

f'_c = Compressive strength determined at the same age, psi.

The regression statistics for this model are presented in table 33. The model was developed using 185 data points, and the prediction has an R^2 value of 45.2 percent and an RMSE value of 69 psi. Table 34 provides details of the range of data used to develop the model. The confidence limits are both within acceptable ranges for both the regressed coefficients (i.e., limits are positive numbers). Figure 173 and figure 174 show the predicted versus measured plot and the residual plot, respectively.

Table 33. Regression statistics for flexural strength model based on compressive strength.

Parameter	Estimate	Standard Error	Approximate 95 Percent Confidence Limits
<i>a</i>	22.7741	6.6362	9.6807 to 35.8674
<i>b</i>	0.4082	0.0338	0.3416 to 0.4748

The model statistics for table 33 are as follows:

- RMSE = 69 psi.
- $R^2 = 0.452$ percent.
- $N = 185$.

Table 34. Range of data used for flexural strength model based on compressive strength.

Parameter	Minimum	Maximum	Average
Compressive strength	1,770	10,032	5,431
Flexural strength	467	1,075	754

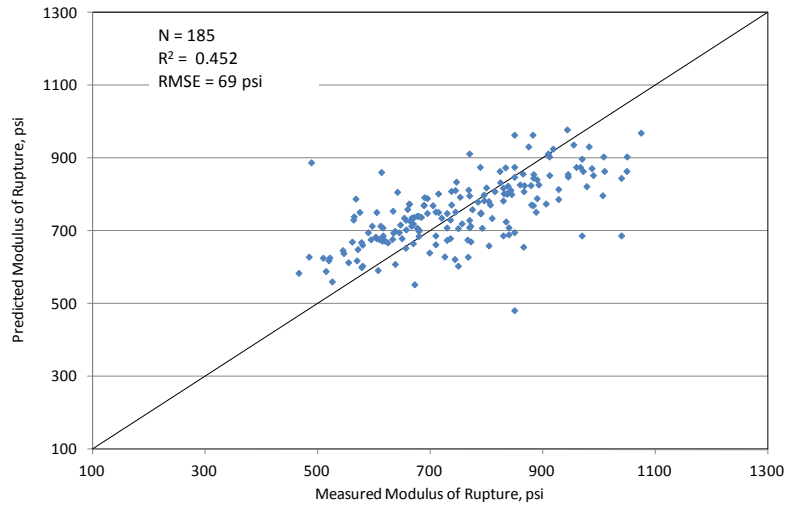


Figure 173. Graph. Predicted versus measured values for flexural strength model based on compressive strength.

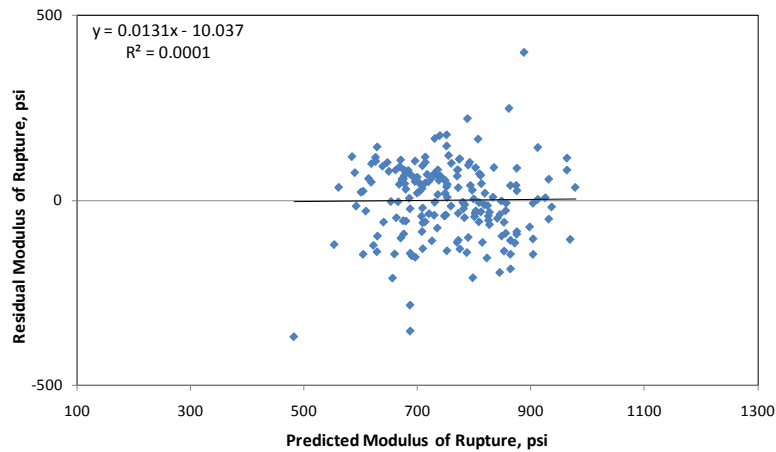


Figure 174. Graph. Residuals errors for flexural strength model based on compressive strength.

Figure 175 shows a comparison of the power models used to validate the data and also to develop a new correlation. Note that the three power models (the new equation developed for this study as well as the validation models) provide close estimates (within 50 psi) in the 4,500- to 5,500-psi compressive strength range.

The ACI and PCA models are plotted for comparison. Also plotted in figure 175 are the raw data that were used in the model. Clearly, the ACI equation is very conservative for this data. It also has been found to give a conservative estimate for several large datasets that have been used in flexural strength model prediction. Conversely, the PCA model fits the LTPP data more closely. The reasons for this lack of fit of the current data with the previous models may be too many to fully explain. The data used in models from prior studies often came from mixes batched under controlled laboratory experiments and were typical of paving and structural concrete. The mixes used in the current model developed from LTPP data relies on only mixes proportioned for typical paving operations. Furthermore, the LTPP data used are from many projects widely

dispersed around the United States. This in itself makes the models more robust than any previous data used to make similar correlations.

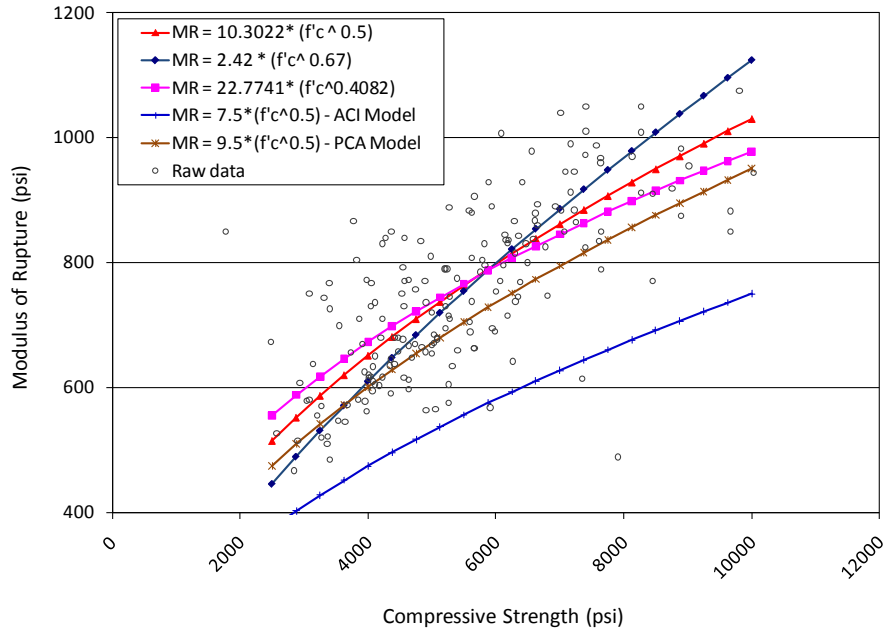


Figure 175. Graph. Comparison of flexural strength models based on compressive strength.

The spread in the raw data about the prediction model in figure 175 indicates that there are factors other than compressive strength that influence the flexural strength of PCC. Among the various factors influencing flexural strength are the mix design parameters and age of the concrete. These variables were considered in the other models developed in this study.

Flexural Strength Model 2: Flexural Strength Based on Age, Unit Weight, and w/c Ratio

Flexural strength model 2 provides a correlation between flexural strength and mix design parameters, specifically the unit weight and w/c ratio. Age is also a parameter in this model, which helps reduce some of the variability seen in the prediction relative to the predictions shown in figure 175. This model will be most useful for cases when the compressive strength of the PCC is not determined but mix design information is available. Also, the user has the option of predicting the 28-day strength value for design or estimating the strength at traffic opening time.

This model can be expressed as follows:

$$MR_t = 676.0159 - 1,120.31 \times w/c + 4.1304 \times uw + 35.74627 \times \ln(t)$$

Figure 176. Equation. Prediction model 7 for MR_t .

Where:

MR_t = Flexural strength at age t years, psi.

w/c = Water to cement ratio.

uw = Unit weight, lb/ft³.

t = Pavement age, years.

The regression statistics for this model are presented in table 35. The model was developed using 62 data points, and the prediction has an R^2 value of 61.1 percent and an RMSE value of 69 psi. Table 36 provides details of the range of data used to develop the model. Figure 177 and figure 178 show the predicted versus measured plot and the residual plot, respectively.

Table 35. Regression statistics for flexural strength model based on age, unit weight, and w/c ratio.

Variable	DF	Estimate	Standard Error	t-value	$P_r > t$	VIF
Intercept	1	676.0159	277.7887	2.43	0.0181	0
w/c	1	-1,120.31	141.3573	-7.93	< 0.0001	1.00591
Unit weight	1	4.1304	1.88934	2.19	0.0329	1.00311
Ln(age)	1	35.74627	8.78516	4.07	0.0001	1.00619

The model statistics for table 35 are as follows:

- RMSE = 91 psi.
- R^2 = 0.6111 percent.
- N = 62.

Table 36. Range of data used for flexural strength model based on age, unit weight, and w/c ratio.

Parameter	Minimum	Maximum	Average
w/c ratio	0.27	0.58	0.40
Unit weight	124	151	142
Pavement age	0.0384	1.0000	0.3169
Flexural strength	467	978	742

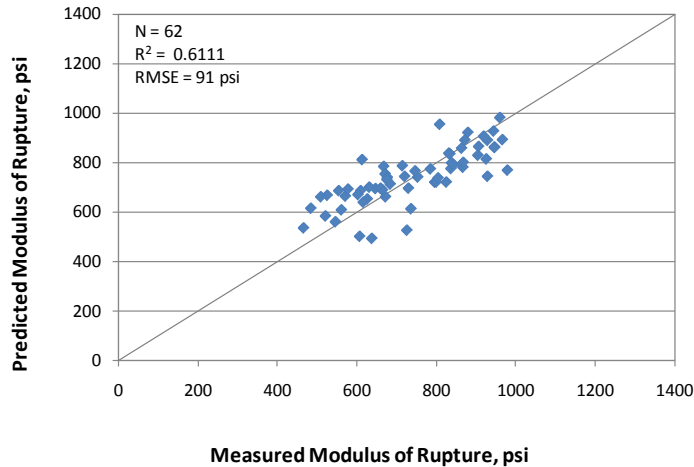


Figure 177. Graph. Predicted versus measured values for flexural strength model based on age, unit weight, and w/c ratio.

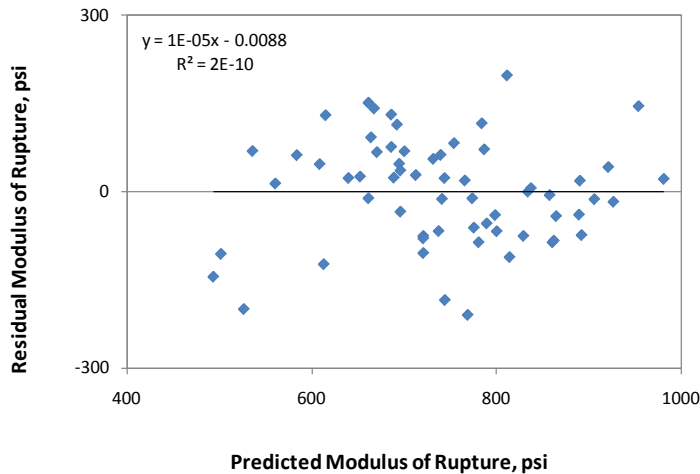


Figure 178. Graph. Residuals errors for flexural strength model based on age, unit weight, and w/c ratio.

Flexural Strength Model 3: Flexural Strength Based on Age, Unit Weight, and CMC

The data used in the previous model also provided a good correlation by replacing the w/c ratio parameter with CMC. The model is expressed as follows:

$$MR_t = 24.15063 + 0.55579 \times CMC + 2.96376 \times uw + 35.54463 \times \ln(t)$$

Figure 179. Equation. Prediction model 8 for MR_t .

Where:

MR_t = Flexural strength at age t years, psi.

CMC = Cementitious materials content, lb/yd³.

uw = Unit weight, lb/ft³.

t = Pavement age, years.

The regression statistics for this model are presented in table 37. The model was developed using 62 data points, and the prediction has an R^2 value of 70.2 percent and an RMSE value of 80 psi. Table 38 provides details of the range of data used to develop the model. Figure 180 and figure 181 show the predicted versus measured plot and the residual plot, respectively.

Figure 182 to figure 185 present the sensitivity of the mix design-based flexural strength models to CMC, w/c ratio, unit weight, and age. Figure 182 and figure 183 show that prediction models in figure 176 and figure 179 do not show any sensitivity to CMC and w/c ratio. For typical values of these parameters, the flexural strength prediction from these two models could show a difference of about 200 psi for extreme values of w/c ratios. However, within a typical range of 0.35 to 0.45, the flexural strength prediction is within 50 psi. Similar trends are evident for the w/c ratio parameter. Therefore, if all details about a mix design are available, it is highly recommended that both models be used to predict flexural strength so that the user has a fair estimate of the MR range. Figure 184 shows that the predictions are close from both models. Likewise, figure 185, which is more or less a flexural strength gain model for a typical mix design, shows close predictions from both models.

Table 37. Regression statistics for flexural strength model based on age, unit weight, and CMC.

Variable	DF	Estimate	Standard Error	t -value	$P_r > t$	VIF
Intercept	1	24.15063	236.7606	0.1	0.9191	0
CMC	1	0.55579	0.05563	9.99	< 0.0001	1.01522
Unit weight	1	2.96376	1.66087	1.78	0.0796	1.01253
Ln(age)	1	35.54463	7.68504	4.63	< 0.0001	1.00573

The model statistics for table 37 are as follows:

- RMSE = 80 psi.
- $R^2 = 0.7023$ percent.
- $N = 62$.

Table 38. Range of data used for flexural strength model based on age, unit weight, and CMC.

Parameter	Minimum	Maximum	Average
CMC	388	936	668
Unit weight	124	151	142
Pavement age	0.0384	1.0000	0.3169
Flexural strength	467	978	742

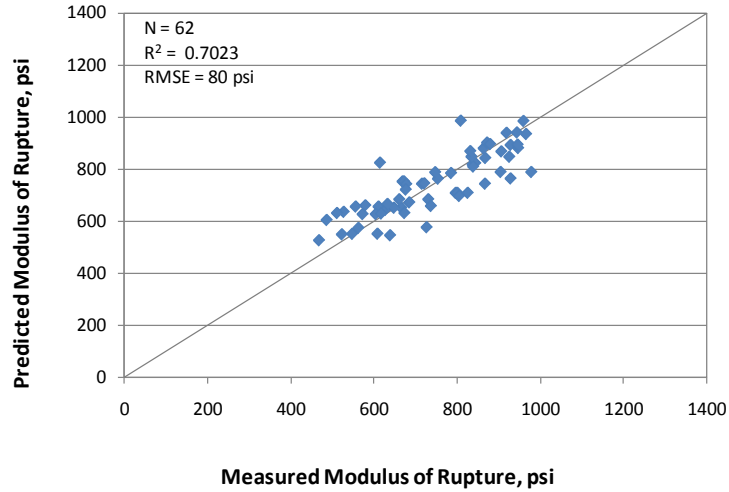


Figure 180. Graph. Predicted versus measured values for flexural strength model based on age, unit weight, and CMC.

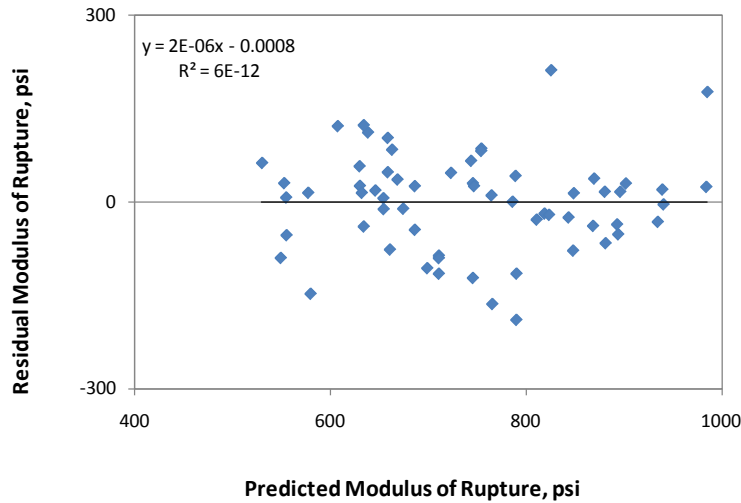


Figure 181. Graph. Residuals errors for flexural strength model based on age, unit weight, and CMC.

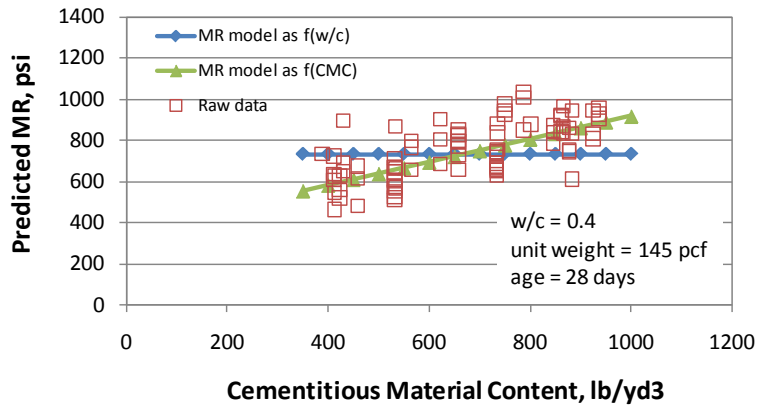


Figure 182. Graph. Sensitivity of flexural strength predictions to CMC.

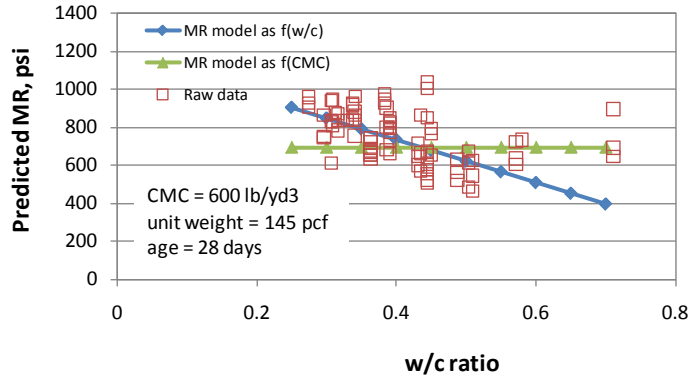


Figure 183. Graph. Sensitivity of flexural strength predictions to w/c ratio.

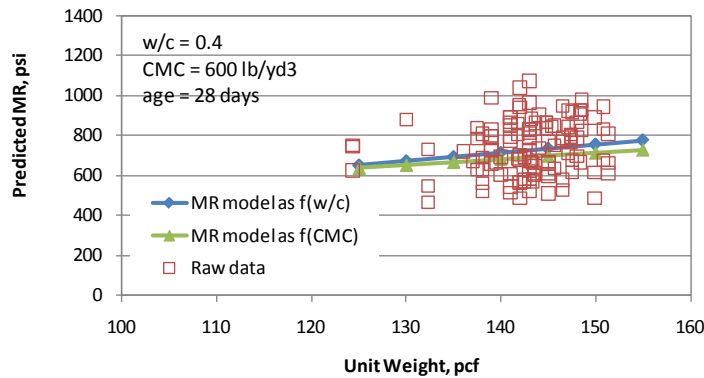


Figure 184. Graph. Sensitivity of flexural strength predictions to unit weight.

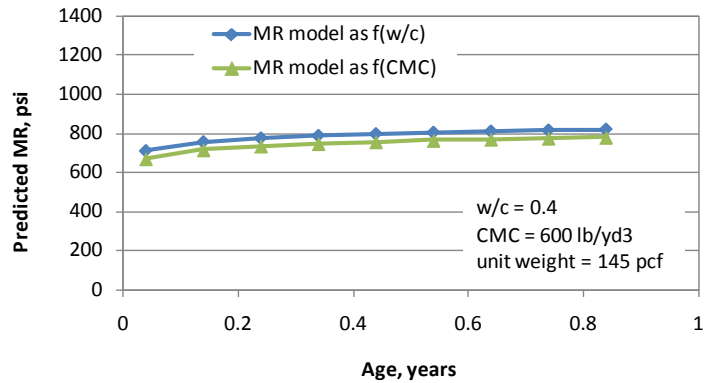


Figure 185. Graph. Sensitivity of flexural strength predictions to age.

PCC Elastic Modulus Models

As with flexural strength, the development of PCC elastic modulus models required a detailed data assembly appropriate for statistical analyses. These analyses also entailed the validation of existing models as well as the development of new models. Model forms of existing models were utilized to fit the data assembled in this study for the validation. The development of new models was not as straightforward as for the other PCC models, primarily because the physical characteristics of a PCC mixture that affect the elastic modulus are not fully captured within the data used for building a mathematical relationship.

The following are key points to note about flexural strength data:

- Elastic modulus test results were available for SPS and GPS sections.
- Test data were collected at 28 days and 1 year for most of the SPS sections. In addition, two SPS-2 sections and two SPS-8 sections had data at 10 and 4.5 years, respectively. Compressive strength data also were present for corresponding specific ages. The data were matched for these specific age categories.
- SPS-2 sections representing the two mix designs targeting low (550 psi) and high (900 psi) strengths showed marginal differences in the elastic modulus results.
- After data reduction, a majority of the observations used in the statistical models belonged to GPS sections. Multiple sections at SPS-2 sites were averaged to produce a single observation, thereby reducing the number of SPS-2 observations.

Validation of Existing Models

Existing models correlate elastic modulus to compressive strength and unit weight. Although more recent models have attempted to introduce lithological type of the coarse aggregate and admixture parameters, within the context of this study, there were not adequate data to validate them. Figure 186 to figure 189 summarize the regressed models using LTPP data.

$$E_c = a * \sqrt{f'_c}$$

Figure 186. Equation. E_c as a function of square root of compressive strength.

Regressed coefficients for figure 186 are as follows:

- $a = 55,294.$

Regression statistics for figure 186 are as follows:

- $N = 514.$
- $R^2 = 11.8$ percent.

$$E = a * \sqrt{f'_c} + b$$

Figure 187. Equation. Model form for E as a function of compressive strength with slope and intercept.

Regressed coefficients for figure 187 are as follows:

- $a = 31,624.6.$
- $b = 2,013,192.$

Regression statistics for figure 187 are as follows:

- $N = 514$.
- $R^2 = 11.8$ percent.

$$E_c = a * f'_c{}^b$$

Figure 188. Equation. E_c .

Regressed coefficients for figure 188 are as follows:

- $a = 388,082$.
- $b = 0.2809$.

Regression statistics for figure 188 are as follows:

- $N = 514$.
- $R^2 = 12.3$ percent.

$$E = a * (UW)^b * (f'_c)^c$$

Figure 189. Equation. E as function of unit weight and compressive strength.

Regressed coefficients for figure 189 are as follows:

- $a = 80,849.3$.
- $b = 0.3648$.
- $c = 0.2527$.

Regression statistics for figure 189 are as follows:

- $N = 514$.
- $R^2 = 10.8$ percent.

The quality of prediction in the validated models is poor, as indicated by the R^2 values in figure 186 through figure 189. The predicted versus measured plots for these models have not been included in this report, but they show higher predictions for the lower modulus values and lower predictions for the higher modulus values. This trend is common with elastic modulus models, especially considering that the data used in this study were not generated from controlled laboratory experiments. Also, while compressive strength is the most commonly used strength parameter and correlations with the compressive strength can be implemented most easily, there is an inherent drawback in correlating modulus to compressive strength. Modulus does not test the material to its limits, and, as discussed in chapter 2, it is more indicative of the

elastic deformational characteristics of the material. Additionally, it often captures other ITZ characteristics and can be a good indicator of concrete durability. Finally, the data contain modulus measured at a wide range of ages. The new models developed therefore utilized other mix parameters that impact modulus including age.

Elastic Modulus Model 1: Model Based on Aggregate Type

Several mix design parameters were evaluated for the elastic modulus model 1 in addition to the compressive strength and unit weight parameters. The model development efforts particularly focused on the aggregate type, given the strong influence of the aggregate hardness on the measured elastic modulus values.

This model utilizes a subset of the data used in the model validation process and has only 71 data points compared to 514 observations in the validation models. This was primarily due to the inclusion of aggregate type in the relationship. Coarse aggregate type information is present in both the materials tables and the CTE tables of the LTPP database. Several data inconsistencies were found in comparing the aggregate types listed in these two tables; therefore, for the development of CTE models (discussed later in this chapter), only those cases with the same aggregate type in both tables were used. In other words, the two tables were used to validate the data against each other. This vastly reduced the dataset used. The dataset included both SPS and GPS sections; however, a majority of the data used in this model belonged to GPS sections.

A nonlinear analysis was performed to establish the following equation:

$$E_c = (4.499 * (UW)^{2.3481} * (f_c)^{0.2429}) * D_{agg}$$

Figure 190. Equation. Prediction model 9 for E_c .

Where:

E_c = PCC elastic modulus, psi.

UW = Unit weight, lb/ft³.

f_c = Compressive strength.

D_{agg} = Regressed constant depending on aggregate type as follows:

- = 10 for andesite.
- = 0.9286 for basalt.
- = 1.0079 for chert.
- = 0.9215 for diabase.
- = 1.0254 for dolomite.
- = 0.8333 for granite.
- = 1.0 for limestone.

- = 0.9511 for quartzite.
- = 1.0 for sandstone.

The development of the model required the use of a model form which accommodates aggregate type as categorical variables (assigned values of 1,0). The values for D_{agg} were initialized to 1.0 at the start of the analyses and allowed to iteratively determine individual values for each aggregate type. The model had 71 observations, an R^2 value of 35.8 percent, and an RMSE value of approximately 500,000 psi. The nonlinear analyses results are presented in table 39.

Table 39. Regression statistics for elastic modulus model based on aggregate type.

Parameter	Comment	Estimate	Standard Error	Approximate 95 Percent Confidence Limits	
<i>a</i>	No comment	4.499	18.6844	-32.8506	41.8485
<i>b</i>	No comment	2.3481	0.8998	0.5495	4.1468
<i>c</i>	No comment	0.2429	0.1224	-0.00173	0.4875
<i>d</i>	D_{agg} for andesite	1	N/A	N/A	N/A
<i>e</i>	D_{agg} for basalt	0.9286	0.0956	0.7374	1.1197
<i>f</i>	D_{agg} for chert	1.0079	0.0863	0.8354	1.1803
<i>g</i>	D_{agg} for diabase	0.9215	0.1858	0.5501	1.2928
<i>h</i>	D_{agg} for dolomite	1.0254	0.0624	0.9006	1.1501
<i>i</i>	D_{agg} for granite	0.8333	0.0624	0.7085	0.9581
<i>j</i>	D_{agg} for limestone	1	N/A	N/A	N/A
<i>k</i>	D_{agg} for quartzite	0.9511	0.1082	0.7349	1.1674
<i>l</i>	D_{agg} for sandstone	1	N/A	N/A	N/A

N/A = Not applicable.

The model statistics for table 39 are as follows:

- RMSE = 499,856 psi.
- $R^2 = 0.3582$ percent.
- $N = 71$.

The model form described for the statistics presented in this table is as follows:

$$E = (a * (UW)^b * (f'c)^c) * (d * \text{Andesite} + e * \text{Basalt} + f * \text{Chert} + g * \text{Diabase} + h * \text{Dolomite} + i * \text{Granite} + j * \text{Limestone} + k * \text{Quartzite} + l * \text{Sandstone})$$

Figure 191. Equation. E.

Where:

d through l were iteratively determined through the nonlinear process, and andesite, basalt, chert, diabase, dolomite, granite, limestone, quartzite, and sandstone are categorical variables with values 0, 1.

Table 39 indicates that the factor that accounts for the aggregate type, D_{agg} , has a value of 1.0 for andesite, limestone, and sandstone. Basalt, diabase, granite, and quartzite have lower D_{agg} values and therefore lower modulus values than mixes using andesite, limestone, and sandstone aggregates. Likewise, chert and dolomite have higher values. Also evident from table 39 is that to a very small extent, the statistical optimization has been compromised (note significance of parameters a and c are not within limits) in the interest of developing a model with variables relevant to elastic modulus predictions. Table 40 provides details of the range of data used to develop the model. The R^2 value is reasonable and therefore presented as a feasible model. Figure 192 and figure 193 show the predicted versus measured plot and the residual plot, respectively.

Table 40. Range of data used for elastic modulus model based on aggregate type.

Parameter	Minimum	Maximum	Average
Compressive strength	1,990	11,310	7,550
Unit weight	137	156	146
Elastic modulus	1,450,000	6,800,000	4,629,646

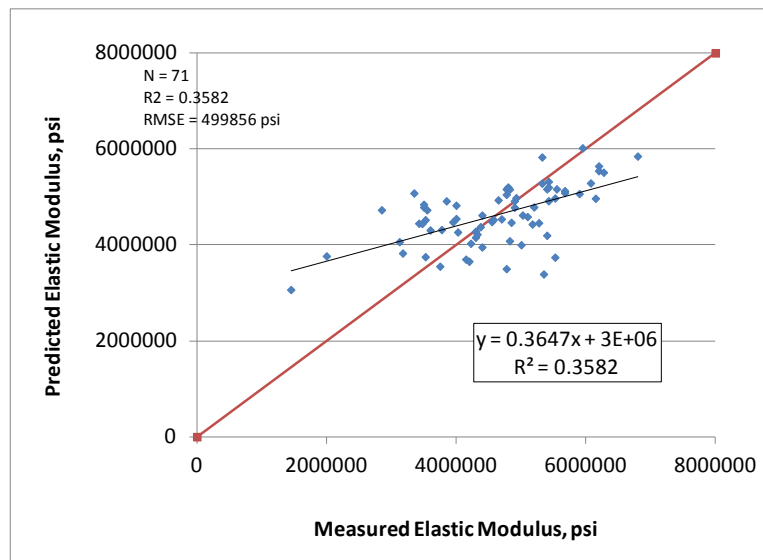


Figure 192. Graph. Predicted versus measured for elastic modulus model based on aggregate type.

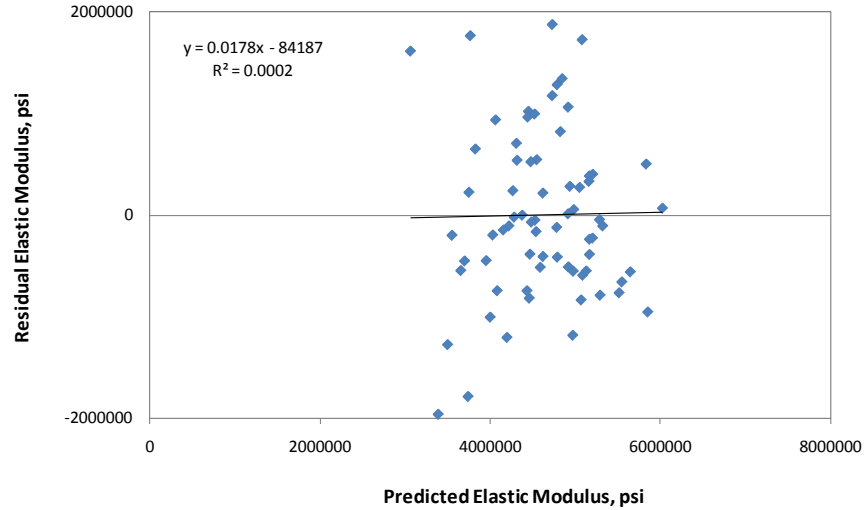


Figure 193. Graph. Residual errors for elastic modulus model based on aggregate type.

Elastic Modulus Model 2: Model Based on Age and Compressive Strength

The data used for validation were further reviewed to identify potential sources of error. Since the data covered a wide range of ages, the age parameter was considered for inclusion in the model. A model was developed to predict elastic modulus as a function of age and compressive strength at the corresponding age. The model was not entirely statistically optimized. The regressed constants were adjusted through a trial and error process to provide the best prediction (i.e., to match the measured with the predicted values as close as possible along the line of equality). The model can be expressed as follows:

$$E_{c,t} = 59.0287 * (f'c_t)^{1.3} * (\ln(\frac{t}{0.03}))^{-0.2118}$$

Figure 194. Equation. Prediction model 10 for $E_{c,t}$.

Where:

$E_{c,t}$ = Elastic modulus at age t years.

$f'c_t$ = Compressive strength at age t years.

t = Age at which modulus is determined, years.

The model used 371 data points and had an R^2 value of 26.14 percent. The RMSE value for this model is about 900,000 psi. Table 41 shows the results of the nonlinear analysis, and table 42 provides details of the range of data used to develop the model. The measured versus predicted plot and the residuals plot for this model are shown in figure 195 and figure 196, respectively.

Table 41. Regression statistics for elastic modulus model based on age and compressive strength.

Parameter Constants	Estimate	Standard Error	Approximate 95 Percent Confidence Limits	
<i>a</i>	59.0287	2.8881	53.3495	64.7079
<i>b</i>	-0.2118	0.0284	-0.2677	-0.1559

The model statistics for table 41 are as follows:

- RMSE = 949,404 psi.
- $R^2 = 0.2614$ percent.
- $N = 371$.

Table 42. Range of data used for elastic modulus model based on age and compressive strength.

Parameter	Minimum	Maximum	Average
Compressive strength	1,990	12,360	7,361
Pavement age	0.0384	45.3836	14.0900
Elastic modulus	1,450,000	6,800,000	4,586,545

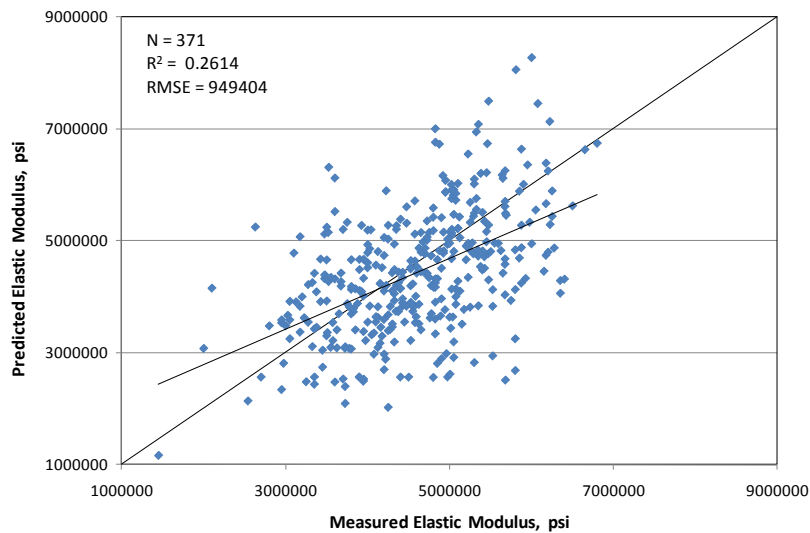


Figure 195. Graph. Predicted versus measured for elastic modulus model based on age and compressive strength.

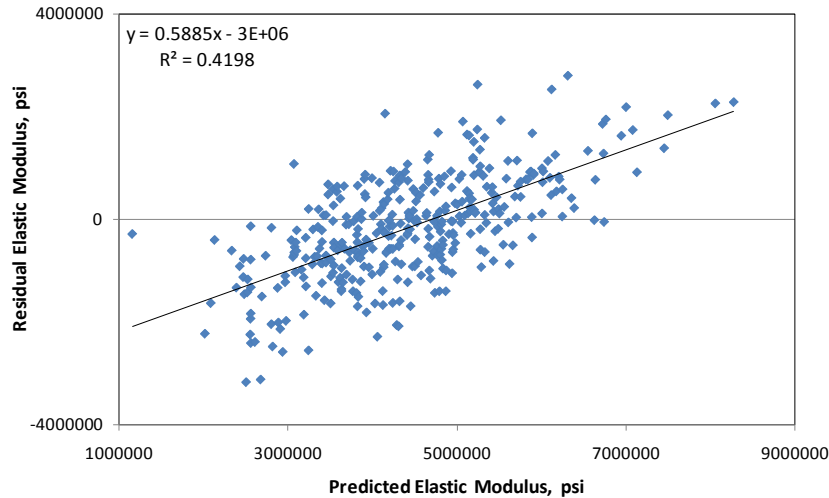


Figure 196. Graph. Residual errors for elastic modulus model based on age and compressive strength.

Elastic Modulus Model 3: Model Based on Age and 28-Day Compressive Strength

Since the 28-day compressive strength is usually available for PCC materials, a predictive model based on age and the 28-day compressive strength was developed. A relatively smaller dataset was utilized for this model with only data from SPS sections, as the 28-day compressive strength data was a necessary input. Again, this model utilized a nonlinear analysis, and beyond statistical optimization, the constants determined for this model were adjusted for closest predictions through a trial and error process. The relationship developed for these variables can be expressed as follows:

$$E_{c,t} = 375.6 * (f'c_{28-day})^{1.1} * (\ln(\frac{t}{0.03}))0.00524$$

Figure 197. Equation. Prediction model 11 for $E_{c,t}$.

Where:

$E_{c,t}$ = Elastic modulus at age t years.

$f'c_{28-day}$ = 28-day compressive strength.

t = Age at which modulus is determined, years.

The model used 46 data points and had an R^2 value of 16.32 percent. The RMSE value for this model is about 1,183,400 psi. Table 43 shows the results of the nonlinear analysis, and table 44 provides details of the range of data used to develop the model. The measured versus predicted plot and the residuals plot for this model are shown in figure 198 and figure 199, respectively.

This model uses data up to an age of 1 year. It is more appropriate for estimating the short-term modulus of a project and for supplementing strength estimates used to determine opening time for traffic.

An examination of the statistics proposed for determining elastic modulus suggests that they do not possess the predictive ability of the other material parameters presented in this study. The

models are considered fair but not excellent. They provide users with an option of moderate estimates when no information about the elastic modulus is available. It is therefore recommended that users exercise caution in using the predictive values for analyses.

Table 43. Regression statistics for elastic modulus model based on age and 28-day compressive strength.

Parameter Constants	Estimate	Standard Error	Approximate 95 Percent Confidence Limits
<i>a</i>	375.6	31.4592	312.5 to 439.3
<i>b</i>	0.00524	0.0714	-0.1388 to -0.1492

The model statistics for table 43 are as follows:

- RMSE = 1,183,400 psi.
- $R^2 = 0.1632$ percent.
- $N = 46$.

Table 44. Range of data used for elastic modulus model based on age and 28-day compressive strength.

Parameter	Minimum	Maximum	Average
28-day compressive strength	3034	7912	5022
Pavement age	0.0384	4.5288	0.9153
Elastic modulus	1,450,000	6,221,000	4,732,101

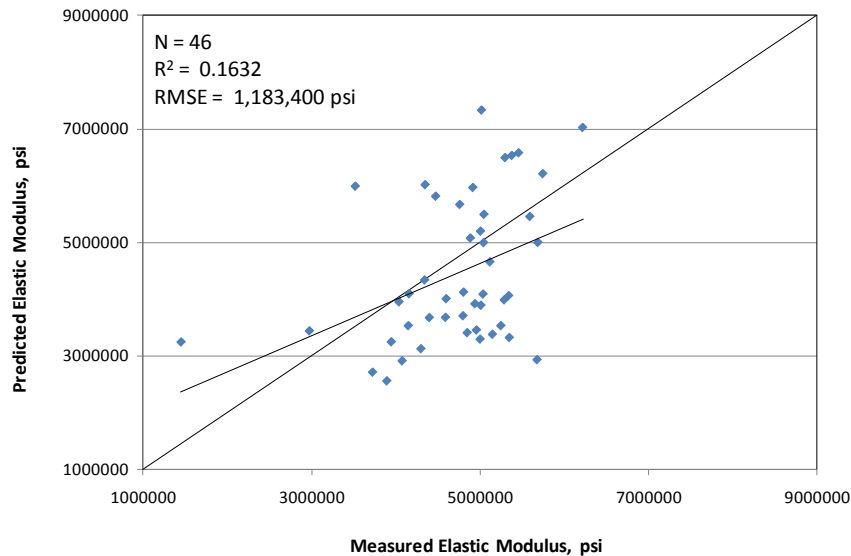


Figure 198. Graph. Predicted versus measured for elastic modulus model based on age and 28-day compressive strength.

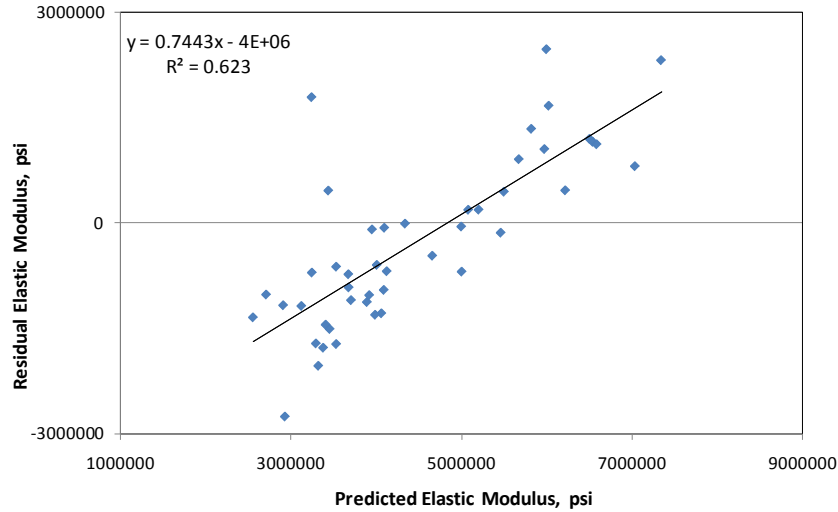


Figure 199. Graph. Residual errors for elastic modulus model based on age and 28-day compressive strength.

PCC Tensile Strength Models

The data assembly and data reduction were same as that performed for the other PCC models. Both SPS and GPS section data were used in the development of this model. PCC tensile strength is a critical input to the CRCP models in the MEPDG. It is most likely that compressive strength test results could be available for the PCC materials being used in CRCP design/construction. The intent, therefore, was to correlate PCC tensile strength data to the compressive strength. Past studies have correlated the tensile strength to the flexural strength of the mix. However, flexural strength test results are available only for the SPS sections, thereby drastically reducing the dataset that can be used to generate a tensile strength model based on flexural strength.

PCC Tensile Strength Model Based on Compressive Strength

This model development served as both a validation and development of a new correlation using the LTPP database. The model form used was a power equation and can be expressed as follows:

$$f_t = 8.9068 * (f'_c)^{0.4785}$$

Figure 200. Equation. Prediction model 12 for f_t .

Where:

f_t = Indirect tensile strength of the PCC material.

f'_c = Compressive strength of the mix determined at the same age.

The model statistics are presented in table 45. The model was developed using 541 data points, with an R^2 value of 42.1 percent and an RMSE value of 61 psi. Table 46 provides details of the range of data used to develop the model. Figure 201 and figure 202 show the predicted versus measured plot and the residual errors plot, respectively.

Table 45. Model statistics for tensile strength prediction model.

Parameter	Estimate	Standard Error	95 Percent Confidence Limits
Coefficient	8.9068	2.0204	4.9381 to 12.8756
Power	0.4785	0.0256	0.4282 to 0.5288

The model statistics for table 45 are as follows:

- RMSE = 61 psi.
- $R^2 = 0.4209$ percent.
- $N = 541$.

Table 46. Range of data used for tensile strength prediction model.

Parameter	Minimum	Maximum	Average
Compressive strength	1,990	12,360	6,763
Tensile strength	316	1,012	600

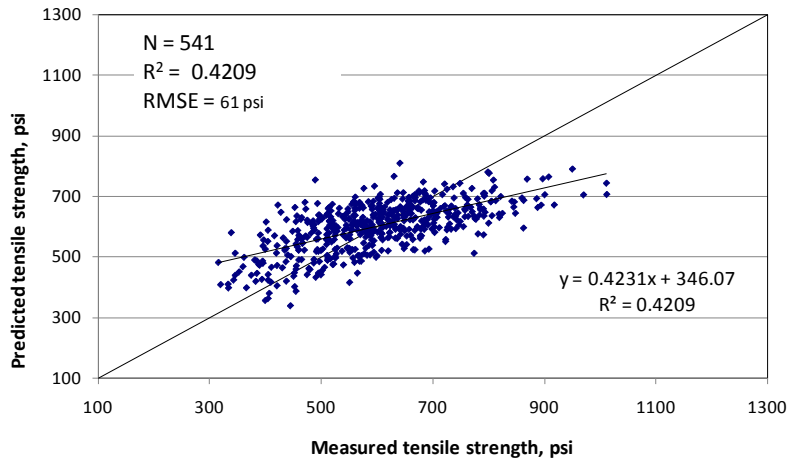


Figure 201. Graph. Predicted versus measured for tensile strength model.

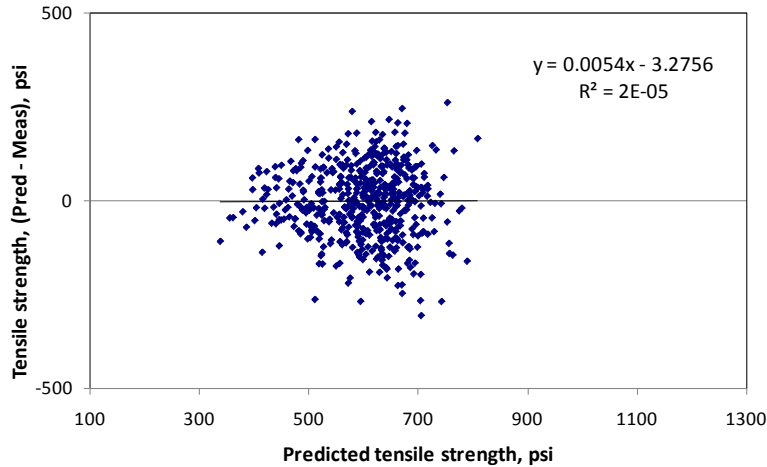


Figure 202. Graph. Residuals error plot for tensile strength model.

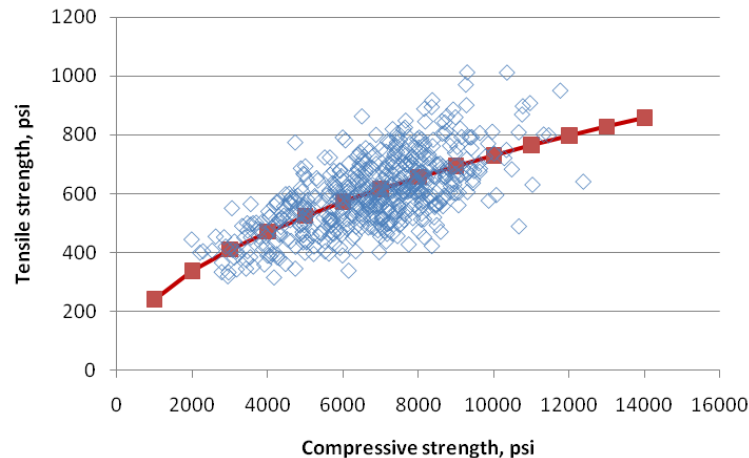


Figure 203. Graph. Sensitivity of tensile strength prediction model to change compressive strength.

Figure 203 shows the sensitivity of the model to compressive strength. The relationship developed shows that for typical ranges of compressive strength (i.e., 3,000 to 6,000 psi), the PCC tensile strength varies from about 400 to 570 psi, which is a reasonable range for this strength parameter.

PCC CTE Models

PCC CTE, which has gained higher importance in recent pavement analysis procedures as a material parameter influencing performance, has been included in the TST_PC03 table of the LTPP database for both SPS and GPS sections. The TST_PC03 table in the LTPP *Standard Data Release 23.0* contained 228 CTE test results.⁽³⁾ These test data contained multiple CTE measurements on a given 500-ft section. Each CTE test result was accompanied by the aggregate type and rock type determined by visual examination of the core used for CTE measurements. The reasons for collecting this information at the time of CTE tests can be easily perceived. Coarse aggregate mineralogy and concrete moisture content have the highest influence of all material parameters on PCC CTE values. Testing for CTE was done with the concrete saturated

so that this variable was eliminated. Additional data and corrected data have been added to the LTPP *Standard Data Release 24.0*.⁽¹⁴²⁾

Additionally, aggregate type data were obtained from the materials tables, as explained in chapter 4. It is also noted that fine aggregates in PCC are usually silica natural sand. There is no indication of fine aggregate type in the LTPP database. Specific tables from which aggregate type information were extracted and assembled in the database include SPS2_PCC_MIXTURE_DATA, RHB_PCCO_AGGR, SPS8_PCC_MIXTURE_DATA, and INV_PCC_MIXTURE for SPS-2, SPS-7, SPS-8, and GPS sections. Reviewing and comparing the aggregate type reported in the CTE and materials tables revealed the following:

- The aggregate type information was more complete in the CTE table.
- Several discrepancies exist between the reported aggregate types across the two tables (CTE values, rock type, and aggregate type are being corrected in the next release of the LTPP database).
- Multiple cores tested from the same LTPP section reported different aggregate types.

In developing CTE correlations, the following assumptions and data reduction methods were made:

- It was assumed that the aggregate types in the CTE tables were more accurate, as they were recorded from the cores used for CTE measurements.
- Multiple readings from the same section were not averaged in the preliminary analyses, as they did not necessarily represent the same aggregate type.
- Tentative models examined with the complete dataset produced very poor correlations. It was found that deleting suspect datasets from the model data resulted in better correlation statistics. Suspect datasets were those that showed multiple aggregate types within the same section and those that did not show the same material type in the materials and CTE data tables of the LTPP database.
- The data reduction process yielded 91 datasets.

Two model types were developed, either of which could be used depending on the level of information available. These models are equivalent to level 3 and level 2 MEPDG inputs. The level 3 model provides default CTE values depending on the coarse aggregate rock type used in the PCC mix. This is equivalent to the CTE values suggested by Mallela et al. but covers a larger database of CTE test results.⁽¹⁵⁾ The level 2 model provides a correlation based on mix volumetrics and uses existing model forms. The regressed constants in the model were obtained from the database assembled for this study.

Current Issue with CTE Overestimation in LTPP Data

CTE tests of the PCC specimens from LTPP sections were performed by FHWA's Turner-Fairbank Highway Research Center (TFHRC) using the AASHTO TP 60 protocol.⁽²⁴⁾ TFHRC

initiated an inter-laboratory study during which an error was discovered with the protocol and procedure used to measure concrete CTE.⁽¹⁴⁴⁾ The source of the error was in the assumption of a single CTE value for the calibration specimen. Testing performed at independent laboratories revealed that a CTE value must be determined for each calibration specimen, and the calibration specimen should be tested over the same range of temperature over which the concrete CTE is determined—50 to 122 °F. Not meeting these two conditions caused an overestimation of the reported CTE by approximately 0.83 inches/inch/°F. Since all of the initial LTPP testing for CTE had been done in one laboratory with one calibration specimen, the calibration offset can be corrected in the database, and it has been corrected in *LTPP Standard Data Release 24.0*.^(3,145,142)

This overestimation of CTE has significant ramifications, especially in light of the fact that the TFHRC has tested over 2,100 specimens for the LTPP program and the fact that the LTPP database was the primary source for the national calibration of the AASHTO MEPDG rigid pavement performance models.⁽¹⁾ The national calibration coefficients for all JPCP and CRCP performance models may be invalid, and the models may need to be recalibrated. As a result, local implementation efforts also may be delayed.

The impact of this error in the CTE values on the current study was described in an internal status report submitted to LTPP. *LTPP Standard Data Release 23.0* contained the uncorrected CTE values, and therefore, the CTE models developed in this study are not applicable for the corrected data.⁽³⁾ However, the models demonstrate the ability to develop correlations, and the procedures herein may be repeated for the corrected data.

CTE Model 1: CTE Based on Aggregate Type (Level 3 Equation for MEPDG)

CTE test data were averaged for each aggregate type, and this constituted level 3 inputs for MEPDG. These averages were determined for the entire set of LTPP data as well as for the subset developed by deleting suspect data. A summary of the data is presented in table 47. Table 47 also lists the average PCC CTE for each aggregate type as found in the literature. The data are all in general agreement, providing a degree of confidence in the level 3 MEPDG input recommendations. The average CTE values determined from the data subset are recommended by this study.

Table 47. Prediction model 13 PCC CTE based on aggregate type ($\times 10^{-6}$ inch/inch/ $^{\circ}$ F).

Aggregate Type	Average From Literature	Average From All LTPP Data	Average From Data Used in Model (Recommended)
Basalt	4.85	5.11	4.86
Chert	6.55	6.24	6.90
Diabase	4.85	5.33	5.13
Dolomite	5.75	5.79	5.79
Gabbro	4.85	5.28	5.28*
Granite	4.55	5.62	5.71
Limestone	4.25	5.35	5.25
Quartzite	6.85	6.07	6.18
Andesite	4.85	4.99	5.33
Sandstone	6.05	5.98	6.33
<i>N</i>		228	91

*There were no samples with a Gabbro aggregate type in the data used in the model. Hence, the average from the entire dataset is recommended.

Figure 204 shows a plot of recommended CTE values versus average CTE values obtained from other sources. While they are in fairly good agreement, the values recommended from this study are slightly higher for most cases. This can be explained by the overestimation of CTE during testing.

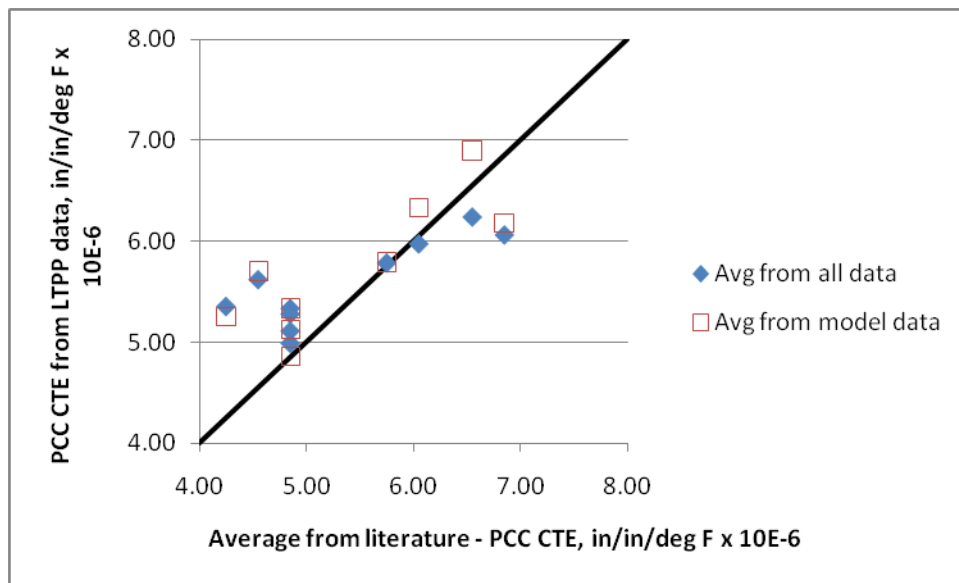


Figure 204. Graph. Comparison of average values from other sources and recommended CTE values based on aggregate type from LTPP data.

CTE Model 2: CTE Based on Mix Volumetrics (Level 2 Equation for MEPDG)

A step-wise linear regression analysis that considered all PCC variables, which performed within a 5 to 10 percent confidence limit, showed that CTE was most sensitive to aggregate types basalt, dolomite, limestone, and quartzite, as well as to coarse aggregate weight, coarse aggregate

specific gravity, and cement content. This demonstrates the influence of mix volumetrics and aggregate type on the predicted CTE values. This validated the approach of developing a model that uses the CTE of individual components with a weighted average by their volumetric proportions.

Volume proportions of each component of the PCC mix were computed using the mix proportioning and mix design data, specifically the amount of each component and the specific gravity. The specific gravities of the coarse and fine aggregates were included in the LTPP database. Air content information was available for only 72 of the 91 cases. Verification for the volumetric proportion calculation showed that for most of the sections, the volumetric proportions summed up closely to 1.0. The average was 1.007, and all values were between 0.93 and 1.08. However, two data points with extremely large coarse aggregate contents (greater than 2,700 lb/yd³) resulted in total volume proportions greater than 1.3, which were suspect data. With the deletion of these data points, the average value was 0.998.

The iterative procedures during the statistical analyses revealed that the model was handling only the volumetric proportions of the coarse aggregate adequately. Therefore, the equation was set up to consider the volumetric proportions of the coarse aggregate, V_{CA} , and that of the mortar ($1 - V_{CA}$). Because the individual aggregate CTE values were not available, aggregate CTE ranges and means from other sources of literature were used to assign a value to this parameter for each aggregate type.

The following ranges were used to determine the minimum, maximum, and mean for each aggregate type:

- Andesite: 3 to 4.5×10^{-6} inch/inch/°F.
- Basalt: 3 to 4.5×10^{-6} inch/inch/°F.
- Chert: 6.1 to 7×10^{-6} inch/inch/°F.
- Diabase: 3 to 4.5×10^{-6} inch/inch/°F.
- Dolomite: 3.9 to 5.5×10^{-6} inch/inch/°F.
- Gabbro: 3 to 4.5×10^{-6} inch/inch/°F.
- Granite: 3.2 to 5.3×10^{-6} inch/inch/°F.
- Limestone: 2 to 3.6×10^{-6} inch/inch/°F.
- Quartzite: 6.1 to 7×10^{-6} inch/inch/°F.
- Sandstone: 5.6 to 6.7×10^{-6} inch/inch/°F.

The sensitivity of the w/c ratio, a proxy variable to account for the porosity of the paste and hence its ability to expand or contract with change in temperature, was evaluated using the following model form:

$$CTE_{PCC} = A * CTE_{CA} * V_{CA} + (B * w / c + C) * V_{mortar}$$

Figure 205. Equation. CTE_{PCC} .

Where:

CTE_{PCC} = CTE of the PCC material, inch/inch/°F.

CTE_{CA} = CTE of the coarse aggregate, inch/inch/°F.

V_{CA} = Volumetric proportion of the coarse aggregate.

V_{mortar} = Volumetric proportion of the mortar ($1 - V_{CA}$).

The regression statistics of this model showed the following:

- The constant A was not significant, indicating that the value of the constant selected to represent the CTE of the coarse aggregate, CTE_{CA} , was adequate to define the effect of the volumetric proportion of the coarse aggregate.
- The constant B was not significant, indicating that the w/c ratio was not significant to the prediction.

In subsequent iterations, the analysis procedure attempted to optimize the coarse aggregate CTE value within the range provided above. The model form was reduced to figure 206 or figure 207.

$$CTE_{PCC} = CTE_{CA} * V_{CA} + C * V_{mortar}$$

Figure 206. Equation. CTE_{PCC} as a function of volumetric proportions.

$$CTE_{PCC} = CTE_{CA} * V_{CA} + C * (1 - V_{CA})$$

Figure 207. Equation. CTE_{PCC} as a function of coarse aggregate volumetric proportion.

The model statistics are presented in table 48, and details of the range of data used to develop the model are presented in table 49.

The model was established as follows:

$$CTE_{PCC} = CTE_{CA} * V_{CA} + 6.4514 * (1 - V_{CA})$$

Figure 208. Equation. Prediction model 14 for CTE_{PCC} .

Where:

CTE_{CA} = Constant determined for each aggregate type as shown in table 48.

Table 48. Statistical analysis results for CTE model based on mix volumetrics.

Parameter	Comment	Estimate	Standard Error	95 Percent Confidence Limits	
<i>c</i>	No comment	6.4514	0.1889	6.0758	6.827
<i>d</i>	CTE_{CA} for basalt	3	0	3	3
<i>e</i>	CTE_{CA} for chert	6.4	0	6.4	6.4
<i>f</i>	CTE_{CA} for diabase	3.4835	1.2824	0.9337	6.0333
<i>g</i>	CTE_{CA} for dolomite	5.1184	0.408	4.3071	5.9297
<i>h</i>	CTE_{CA} for gabbro	3.75	N/A	N/A	N/A
<i>i</i>	CTE_{CA} for granite	4.7423	0.4188	3.9096	5.5749
<i>j</i>	CTE_{CA} for limestone	3.2886	0.3579	2.5771	4.0001
<i>k</i>	CTE_{CA} for quartzite	6.1	0	6.1	6.1
<i>l</i>	CTE_{CA} for andesite	3.6243	1.4539	0.7336	6.515
<i>m</i>	CTE_{CA} for sandstone	4.5	0	4.5	4.5

The model statistics for table 48 are as follows:

- RMSE = 0.35006 psi.
- $R^2 = 0.4415$ percent.
- $N = 89$.

Table 49. Range of data used for CTE model based on mix volumetrics.

Parameter	Minimum	Maximum	Average
Coarse aggregate content	582	2730	1,811
Coarse aggregate specific gravity	2.42	2.86	2.65
w/c ratio	0	0.71	0.45
Coarse aggregate volume fraction	0.13	0.62	0.41
Mortar volume	0.38	0.87	0.59

The model has an R^2 value of 44.1 percent and an RMSE value of 0.35 psi. The predicted versus measured plot and the residual error plots are presented in figure 209 and figure 210, respectively.

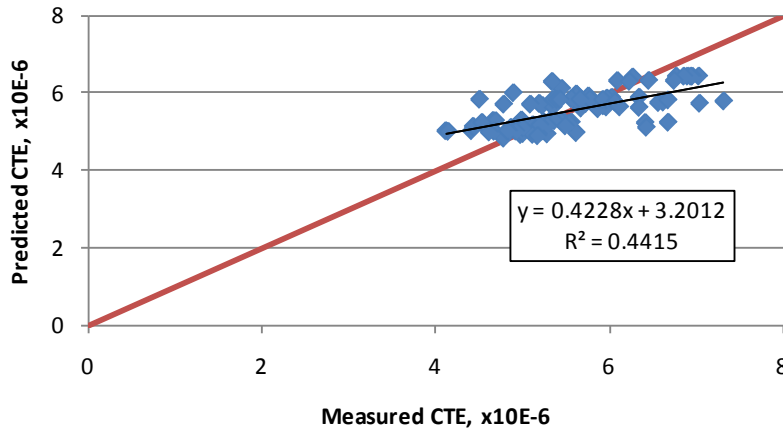


Figure 209. Graph. Predicted versus measured for CTE model based on mix volumetrics.

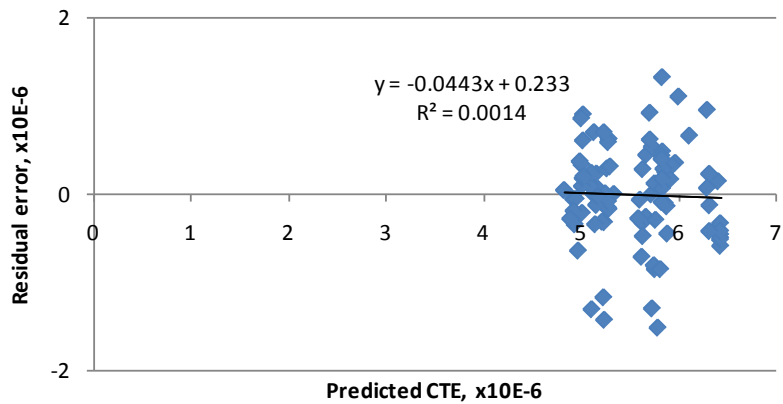


Figure 210. Graph. Residual errors for CTE model based on mix volumetrics.

The constant, C , in the model form, determined as 6.4514, is equivalent to CTE of the mortar. (At TFHRC, using the AASHTO TP 60 uncorrected values, a CTE value of 6.2 for mortar containing silica sand was determined. Hence, the value of C is in agreement with the test result.⁽²⁴⁾) Since the mortar (all components of the mix design except the coarse aggregate, as per the definition in this equation) occupies a large volume of the matrix, it was necessary for the model to predict higher CTE for increased mortar proportions (or decreasing coarse aggregate proportions). In optimizing the model and selecting the representative CTE for each aggregate type, it was ensured that the CTE of the aggregate is not above C .

Figure 211 and figure 212 show a comparison of the predicted CTE values with average values reported in literature for each aggregate type. The predictions are close, with the model showing a slight bias. The over-prediction observed can be a result of the errors in the CTE test procedure (over-measured CTEs) or could simply reflect the CTE typical of paving mixes. Figure 213 shows the sensitivity of the model to coarse aggregate content. As expected, CTE decreases as the coarse aggregate content increases (or mortar volume decreases). While this is true for most cases, it is also observed that for aggregates with high CTE values, such as chert and quartzite, CTE of the aggregate approaches CTE of mortar, thereby showing little or no sensitivity to coarse aggregate content.

As with all other models, the user is advised to verify model predictions with other sources of information. If possible, both CTE models should be evaluated simultaneously to obtain a range.

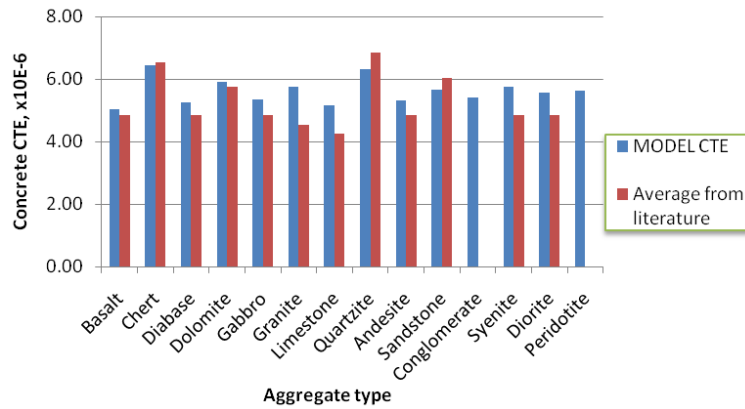


Figure 211. Graph. Comparison of CTE model prediction with average values reported in literature for each aggregate rock type.

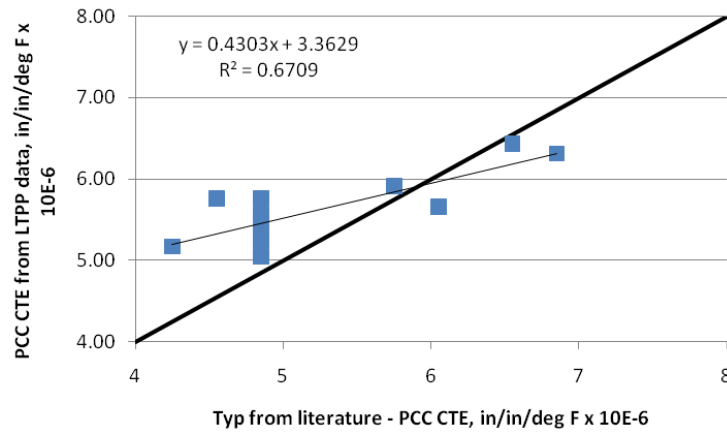


Figure 212. Graph. CTE model prediction versus average values reported in literature for each aggregate rock type.

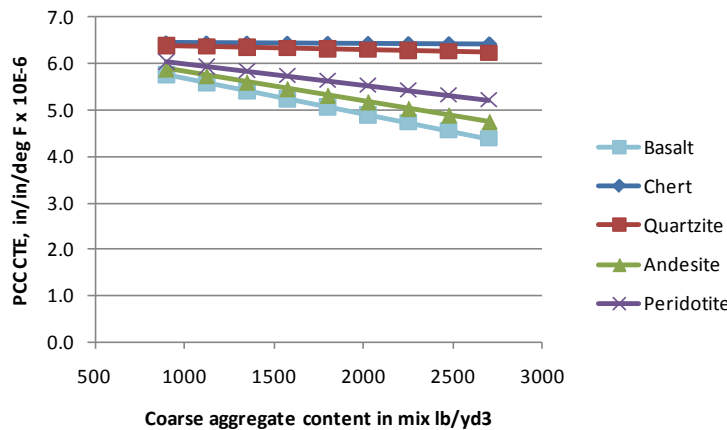


Figure 213. Graph. Sensitivity of the CTE model to coarse aggregate content.

RIGID PAVEMENT DESIGN FEATURES MODELS

The models developed for the prediction of MEPDG-specific inputs are in the design features category. As explained earlier in this chapter, it was never intended for inclusion in the LTPP database, nor was the need for inclusion clearly foreseen at the time of designing the LTPP database. The data formulation for developing these models is model type 3, wherein the dependent variable (e.g., the design feature *deltaT* for JPCP design) is determined through several trial and error runs of the MEPDG and establishing the optimum value that minimizes the error prediction.

The MEPDG design files used to generate the dependent variable data were obtained from the model calibration performed under NCHRP 1-40D, which produced the MEPDG software program version 1.0 in 2007.⁽⁴⁾ However, minor changes and software bug fixes have been performed since then, and the official version available at the time of this study was the MEPDG software version 1.1. Version 1.1 was used in the generation of the dependent variables for the models included in this study.

Therefore, the models developed to predict the design features variables are valid only for use with the distress calibration model of version 1.1 of the MEPDG software. At the time this report was written, the MEPDG is being recalibrated under ongoing project NCHRP 20-07/Task 288. This recalibration effort will make the necessary updates to the CTE values used in the rigid pavement model calibrations and will handle the various updates and software bug fixes since the release of MEPDG version 1.0.

The prediction models presented in this report for the estimation of design feature inputs therefore may not be valid once the products of NCHRP 20-07/Task 288 are released. The information provided in this section should be considered as a description of a viable method to develop design feature input models. This effort has to be repeated after the release of the NCHRP 20-07/Task 288 products.

deltaT—JPCP Design

Generating Dependent Variable Data

Both the JPCP transverse fatigue distress model and JPCP mean joint faulting were considered for use as the basis for selecting the optimum *deltaT* with minimized errors. However, JPCP transverse fatigue cracking prediction data correlated well with the material, climate, and design elements to develop the *deltaT* prediction model. The procedure used to determine the value of the dependent variable in the analysis entailed the following steps.

Step 1: Run MEPDG Calibration Files for a Range of *deltaT* Values:

The transverse cracking model in the MEPDG was calibrated using 300 design projects at a *deltaT* value of -10 °F. Each of these calibration files were run at *deltaT* values of -2.5, -5.0, -7.5, -10, -12.5, and -15 °F. The number of *deltaT* levels (six) and the range (-2.5 to -15 °F) were selected based on practical considerations of the time required to perform this analysis as well as to maintain the bounds of the predicted value within a reasonable range.

Step 2: Compile Predicted Cracking Data for All Ages:

Field-measured cracking at different ages was available for all the sections used in the calibration models. MEPDG-predicted damage and cracking data were extracted for ages corresponding to field data measurements. Table 50 shows a sample for cracking data extraction for section 01_3028.

Table 50. Summary of field measured distress and predicted distress for section 1_3028.

Pavement Age (Years)	Measured Field Cracking (Percent)	Predicted Cracking (Percent)					
		$\Delta T = -15$	$\Delta T = -12.5$	$\Delta T = -10$	$\Delta T = -7.5$	$\Delta T = -5$	$\Delta T = -2.5$
20.31507	0	20.8	4.3	1	0.7	3	12.8
21.84384	0	26.9	5.2	1.2	0.9	3.6	14.7
26.52329	4	48.9	9.3	2.2	1.6	6.8	23.3
28.87123	4	57.7	11.7	2.8	2	8.6	27.6
32.72329	8	70.1	16.8	4.2	3.1	12.7	36

Step 3: Calculate Errors and Determine Optimal ΔT for Each Section:

The predicted cracking for each level of ΔT (as shown in table 50) was compared against the field data to compute errors for each age. The sum of squared errors was then computed for each age and for each level of ΔT . Table 51 shows an example of error calculation for section 01_3028.

Table 51. Error calculations for section 1_3028.

Pavement Age (Years)	Measured Field Cracking (Percent)	Squared Error Calculation					
		$\Delta T = -15$	$\Delta T = -12.5$	$\Delta T = -10$	$\Delta T = -7.5$	$\Delta T = -5$	$\Delta T = -2.5$
20.31507	0	432.64	18.49	1	0.49	9	163.84
21.84384	0	723.61	27.04	1.44	0.81	12.96	216.09
26.52329	4	2,016.01	28.09	3.24	5.76	7.84	372.49
28.87123	4	2,883.69	59.29	1.44	4	21.16	556.96
32.72329	8	3,856.41	77.44	14.44	24.01	22.09	784
Sum of squared errors		9,912.36	210.35	21.56	35.07	73.05	2,093.38

Note: The bold text in the squared error calculation section indicates the minimum sum of squared error for all ages.

The minimum sum of squared error for all ages, a value of 21.56 as highlighted in table 51, is observed for a ΔT of -10 °F in this case. The value -10 °F is therefore the dependent variable for this section. The same procedure was repeated for all 301 JPCP sections to develop a list of optimum temperatures, or dependent variables, for each calibration file.

The example presented in table 51 used a straightforward process to select the ΔT value. The sum of squared errors reached a minimum value for a value of -10 °F. However, there were cases where the sum of squared errors did not provide a clear choice for the selection of an optimal

value. As shown in table 52, scenarios A and B are assigned a value of -10 and -12.5 °F, respectively. Scenario C represents a case where the measured cracking was zero percent for all ages, and the predicted cracking also was zero at all values of ΔT . Scenario D represents a case where the minimum error was achieved at the bounds of the selected range (i.e., at -15 °F). A higher ΔT can result in smaller errors, but the extent of data that could be appropriately included in the analyses by evaluating higher ΔT values was minimal. Therefore, all cases that resulted in error trends as represented by scenarios C and D were deleted from the dataset used for the statistical analyses. The dataset used in the statistical analyses contained 147 JPCP sections.

Table 52. Determining optimal ΔT .

Scenario	Sum of Squared Errors						ΔT at Minimum Error (°F)
	$\Delta T = -15$	$\Delta T = -12.5$	$\Delta T = -10$	$\Delta T = -7.5$	$\Delta T = -5$	$\Delta T = -2.5$	
A	19,824.72	420.7	43.12	70.14	146.1	4,186.76	-10
B	5.39	2.6	28.18	405.83	2,655.08	8,924.36	-12.5
C	0	0	0	0	0	0	Cannot be determined
D	12,600.71	13,032.5	13,097.05	13,111.56	13,111.56	13,111.56	-15

JPCP ΔT Gradient Model Development

It was observed that the data generated for the dependent variable, ΔT , correlated well with the material, design, and climate parameters when transformed from ΔT temperature differential to ΔT temperature gradient. This involved dividing the ΔT temperature differential by the slab thickness. A step-wise regression analysis and C_p analyses were performed to select the variables that are correlated to the dependent variable and to select the best combination of variables to develop the model. After an iterative process to optimize the model, the equation developed to estimate the ΔT gradient variable is as follows:

$$\frac{\Delta T}{inch} = -5.27805 - 0.00794 \times TR - 0.0826 \times SW + 0.18632 \times PCCTHK + 0.01677 \times uw + 1.14008 \times w/c + 0.01784 \times latitude$$

Figure 214. Equation. Prediction model 15 for $\Delta T/inch$.

Where:

$\Delta T/inch$ = Predicted average gradient through JPCP slab, °F/inch.

TR = Difference between maximum and minimum temperature for the month of construction, °F.

SW = Slab width, ft.

$PCCTHK$ = JPCP slab thickness, inch.

uw = Unit weight of PCC used in JPCP slab, lb/ft³.

w/c = w/c ratio.

$latitude$ = Latitude of the project location, degrees.

The model considers climate (TR , $latitude$), design (SW , $PCCTHK$), and material (uw , w/c) parameters. The model statistics are presented in table 53. The model was developed with 147 data points and has an R^2 value of 0.4967 percent and an RMSE value of 0.3199 psi. Table 54 provides details of the range of data used to develop the model. Figure 215 shows the predicted versus measured for the proposed JPCP ΔT gradient model, while figure 216 shows the residual errors. Note that the measured data here refer to the ΔT gradient determined by matching MEPDG prediction to field performance. Figure 217 shows the predicted versus measured ΔT for the model.

Table 53. Regression statistics for JPCP ΔT model.

Variable	DF	Estimate	Standard Error	t -Value	$P_r > t$	VIF
Intercept	1	-5.27805	1.06943	-4.94	< 0.0001	0
TR	1	-0.00794	0.00396	-2	0.047	1.86047
SW	1	-0.0826	0.03432	-2.41	0.0174	1.07141
$PCCTHK$	1	0.18632	0.0195	9.55	< 0.0001	1.0642
uw	1	0.01677	0.00669	2.51	0.0133	1.22792
w/c	1	1.14008	0.2914	3.91	0.0001	1.14857
$Latitude$	1	0.01784	0.0072	2.48	0.0144	1.85265

The model statistics for table 54 are as follows:

- RMSE = 0.3199 psi.
- $R^2 = 0.4967$ percent.
- $N = 147$.

Table 54. Range of data used for JPCP ΔT model.

Parameter	Minimum	Maximum	Average
Temperature range	21.2	64.5	47.4
Slab width	12.0	14.0	12.5
PCC thickness	6.4	14.3	9.6
Unit weight	134	156	147
w/c ratio	0.27	0.72	0.46
Latitude	27.93	49.60	39.58

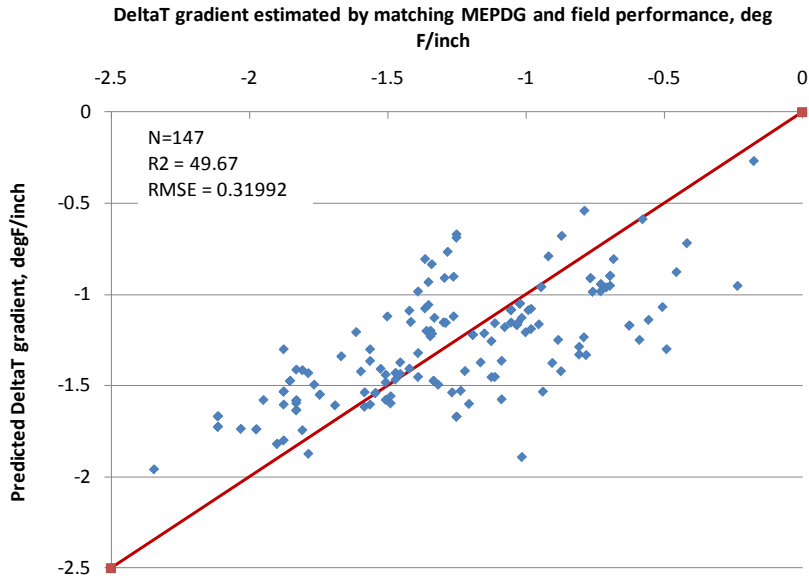


Figure 215. Graph. Predicted versus measured for JPCP *deltaT* gradient model.

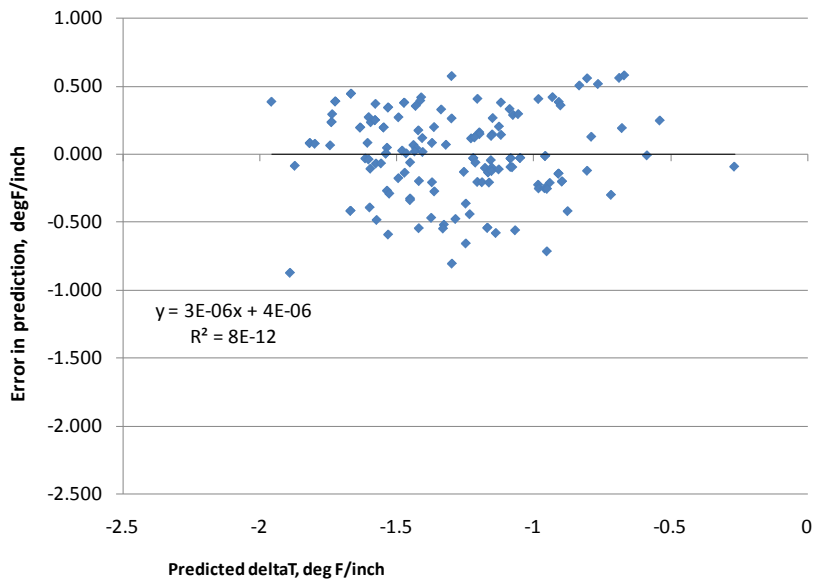


Figure 216. Graph. Residual errors for JPCP *deltaT* gradient model.

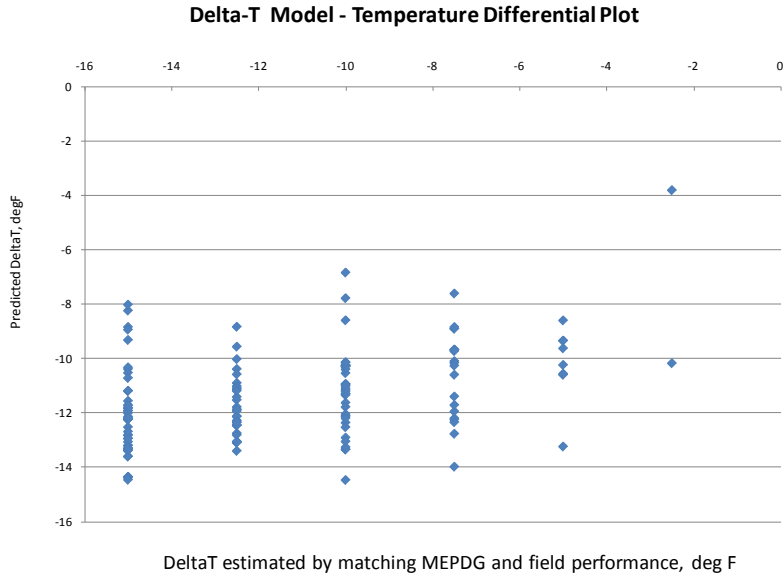


Figure 217. Graph. Predicted versus measured ΔT based on the JPCP ΔT gradient model.

Figure 218 through figure 224 present the sensitivity analysis performed to examine the impact of varying the model parameters on its prediction. The parameters included are temperature range, slab width, slab thickness, unit weight, w/c ratio, and latitude. For each sensitivity analysis, the variable of interest was varied while holding all other variables constant at their typical values. Typical values used in this analysis were 24 °F, 12-ft slab width, 10-inch slab thickness, 145 lb/ft³ PCC unit weight, 0.40 w/c ratio, and 40 degrees latitude.

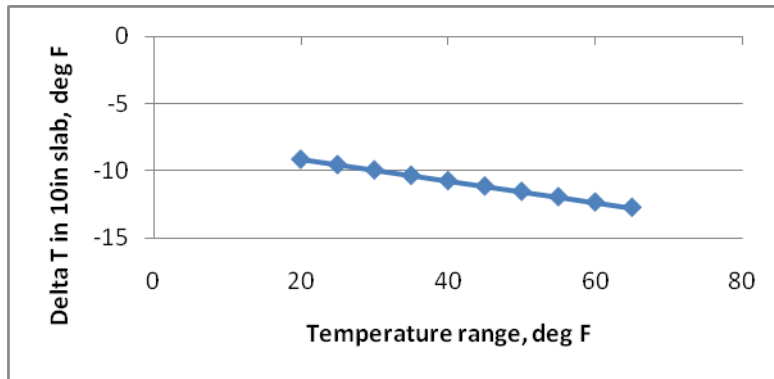


Figure 218. Graph. Sensitivity of predicted ΔT to temperature range during month of construction.

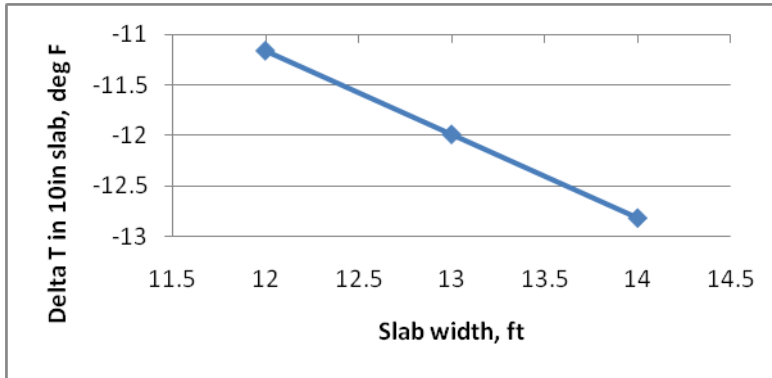


Figure 219. Graph. Sensitivity of predicted ΔT to slab width.

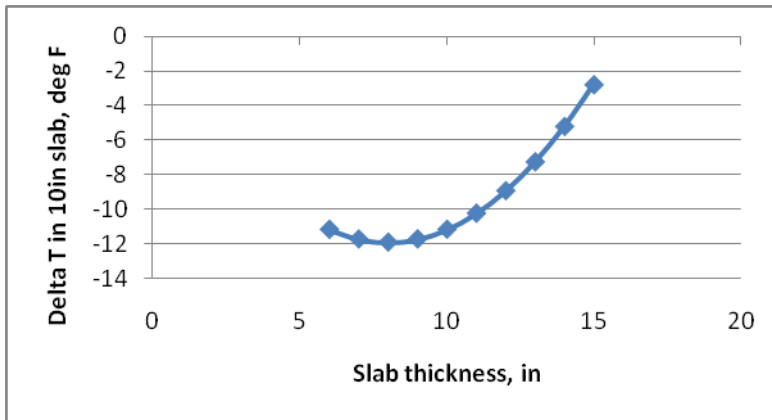


Figure 220. Graph. Sensitivity of predicted ΔT to slab thickness.

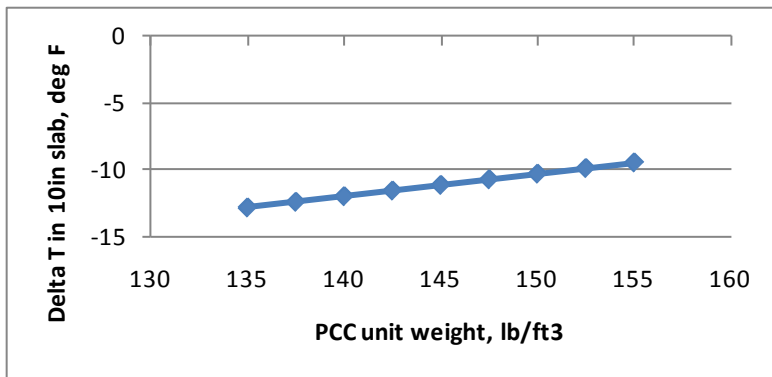


Figure 221. Graph. Sensitivity of predicted ΔT to PCC slab unit weight.

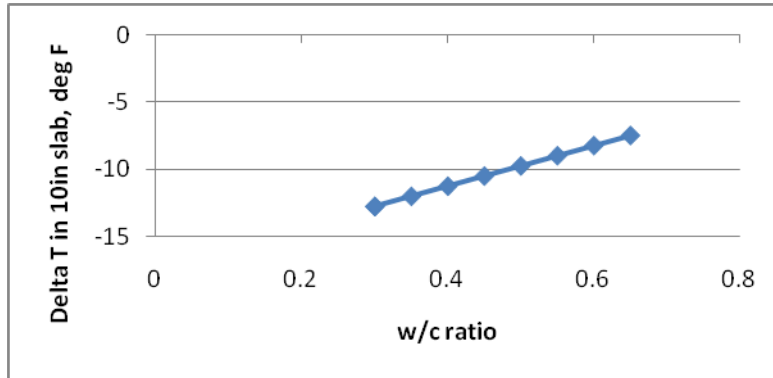


Figure 222. Graph. Sensitivity of predicted *deltaT* to PCC w/c ratio.

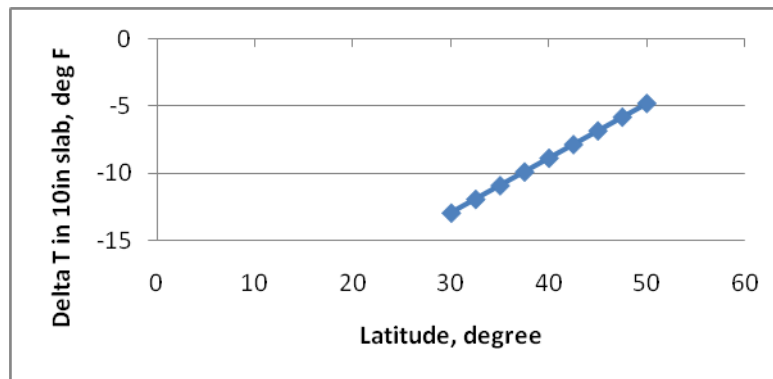


Figure 223. Graph. Sensitivity of predicted *deltaT* to latitude of the project location.

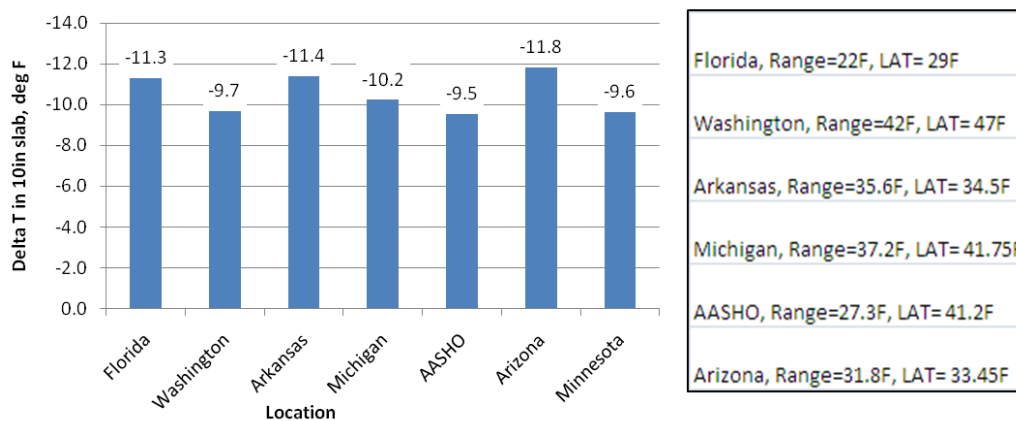


Figure 224. Graph. Predicted *deltaT* for different locations in the United States.

The following list contains brief observations from these sensitivity analyses:

- For the typical values used for each of these variables, the *deltaT* gradients estimated are in a reasonable range.
- An increase in local climate temperature range increases the temperature gradient (see figure 218). The local climate temperature range is indicative of the level of temperature drop the project location can experience. The larger the difference in the temperature

between day and night (assuming paving is performed in the daytime), the larger the negative temperature gradient locked into the slab as the slab hardens within a 24-h period.

- Wider slabs produce a larger built-in gradient (see figure 219), as has been validated in several field studies. The total thermal expansion is larger for a longer/wider slab and, therefore, the resulting curvature of the slab induces a greater lift-up at the slab corners. The data did not show a significant effect of the slab length or joint spacing parameter.
- Thicker slabs reduce the ΔT gradient, as shown in figure 220. This is the expected trend, as thicker slabs, due to a greater weight, tend to restrain the corners from curling up as the concrete hardens. This figure also shows that for very thin slabs (< 8 inches), the effect is reversed. The physical significance of this cannot be fully explained or supported with data. It is therefore necessary to evaluate the sensitivity to each parameter while selecting a ΔT for each project.
- The larger unit weight of the PCC material used in the JPCP slab also reduces the magnitude of built-in gradient, primarily because of the restraint provided by the heavier slab during hardening (see figure 221).
- Lower w/c ratios have a higher rate of hydration, and, therefore, the PCC slab remains plastic for a shorter duration of time. Strength gain offers the slab the rigidity necessary to bear against the base and does not allow the slab corners to curl up. Therefore, lower w/c ratios tend to have higher built-in gradients, as seen in figure 222. Furthermore, at low w/c ratios, the PCC mix undergoes autogenous shrinkage, which increases the potential for higher gradients in the slab.
- Figure 223 and figure 224 show the effect of latitude on predicted ΔT gradients. The United States lies between 30 and 50 degrees latitude in the Northern Hemisphere. The full range of latitudes is covered in figure 223. While this plot might appear to show ΔT 's high degree of sensitivity to the latitude parameter, for routine predictions using this model, the temperature range is a critical input. In other words, a given maximum temperature in the southern United States could have a much different temperature range relative to a location in the northern United States with the same maximum temperature. Therefore, the latitude parameter has to be evaluated combined with the temperature range parameter, as shown in figure 224. The predicted ΔT for several locations in the United States are presented.

Using the JPCP ΔT Model

This section provides an example for the use of the JPCP ΔT model developed under this study. The section used to describe the process is the LTPP SPS-2 section 04_0213 located in Maricopa County, AZ, and constructed in July 1993.

The following latitude, design, and material inputs required for the *deltaT* prediction model can be obtained from the MEPDG inputs:

- Latitude: 33.45 degrees north.
- PCC thickness: 8.3 inches.
- Slab width: 14 ft.
- PCC unit weight: 145.3 lb/ft³.
- PCC w/c ratio: 0.365.

The temperature range input to this model is the difference between the mean monthly maximum and minimum temperatures for the month of July from historical climate data records (as climate data included in the MEPDG). If the user does not have this information readily available, the data to compute the temperature range can be determined from the output file of the MEPDG analysis of this section. The output file (e.g., titled “04_0213.xls”) contains a worksheet titled “Climate” with key climate data for the specific location (or the virtual climate station created). This worksheet includes the monthly climate summary with minimum and maximum temperature by month for all years of data used under the headings “Min. Temp. (°F)” and “Max. Temp. (°F),” respectively. (Note that this summary also consists of “Average Temp. (°F),” “Max. Range (°F),” “Precip. (in.),” “Average Wind (mph),” “Average Sun (%),” “Number Wet Days,” and “Max. Frost (in.)” However, these data are not of relevance to the *deltaT* model).

For the month of July, the average minimum and maximum temperatures are 73 and 111.7 °F, respectively. The difference between these temperatures is 38.7 °F.

Using these inputs, the *deltaT* gradient can be calculated as -1.7457138 °F/inch. For the slab thickness of 8.3 inches, this is equivalent to a *deltaT* of -14.5 °F. This value is significantly higher than the default of -10 °F/inch. This input can be revised in an MEPDG file and reanalyzed to evaluate the predicted transverse cracking performance.

***deltaT*—CRCP Design**

Generating Dependent Variable Data

The procedure followed to obtain the dependent variable—the CRCP *deltaT* producing the closest prediction to field distress—shared several commonalities that followed to generate the *deltaT* for JPCP. Punchout prediction was the basis for selecting the optimum *deltaT* with minimized errors. The CRCP design files used for the calibration of the MEPDG models were run at *deltaT* values of -2.5, -5.0, -7.5, -10, -12.5, and -15 °F. The punchout predictions at all these values of *deltaT* were compared against field measured punchouts. The value corresponding to the least sum of squared errors for the prediction at all ages combined was selected as the optimum *deltaT* for that section. This selection of an optimum value for all the sections used in the calibration generated the dependent variable dataset.

CRCP *deltaT* Gradient Model Development

As with the JPCP *deltaT* gradient model, the dependent variable CRCP *deltaT* data correlated well with the material, design, and climate parameters when transformed from *deltaT* temperature differential to *deltaT* temperature gradient. Step-wise regression and C_p analyses were performed to select the variables that best correlated to the dependent variable and to select the best combination of variables to develop the model. It was observed that coarse aggregate type was significant. After an iterative process to optimize the model, the equation developed to estimate the *deltaT* gradient variable is as follows:

$$\begin{aligned} \text{deltaT / inch} = & 12.93007 - 0.15101 * \text{MaxTemp} - 0.10241 * \text{MaxTempRange} + 3.279 * \text{Chert} \\ & + 1.55013 * \text{Granite} + 1.40009 * \text{Limestone} + 2.01838 * \text{Quartzite} \\ & + 0.11299 * \text{PCCTHK} \end{aligned}$$

Figure 225. Equation. Prediction model 16 for *deltaT*/inch.

Where:

deltaT/inch = Predicted gradient in CRCP slab, °F/inch.

MaxTemp = Maximum temperature for the month of construction, °F.

MaxTempRange = Maximum temperature range for the month of construction, °F.

PCCTHK = JPCP slab thickness, inch.

Chert = 1 if PCC mix coarse aggregate is chert, or 0 if otherwise.

Granite = 1 if PCC mix coarse aggregate is granite, or 0 if otherwise.

Limestone = 1 if PCC mix coarse aggregate is limestone, or 0 if otherwise.

Quartzite = 1 if PCC mix coarse aggregate is quartzite, or 0 if otherwise.

The model considers climate (*MaxTemp* and *MaxTempRange*), design parameters (*PCCTHK*), and material (*Aggregate type*) parameters. The model statistics are presented in table 55. The model was developed with 35 data points and has an R^2 value of 82.5 percent and an RMSE value of 0.27932 psi. Table 56 provides details of the range of data used to develop the model. Figure 226 shows the predicted versus measured for the proposed CRCP *deltaT* gradient model, while figure 227 shows the residual errors. Note that the measured data refers to the *deltaT* gradient determined by matching MEPDG prediction to field performance.

Table 55. Regression statistics for CRCP *deltaT* model.

Variable	DF	Estimate	Standard Error	t-value	$P_r > t$	VIF
Intercept	1	12.93007	1.98459	6.52	< 0.0001	0
<i>MaxTemp</i>	1	-0.15101	0.01793	-8.42	< 0.0001	3.46347
<i>MaxTempRange</i>	1	-0.10241	0.01869	-5.48	< 0.0001	2.00933
Chert	1	3.279	0.30508	10.75	< 0.0001	2.24965
Granite	1	1.55013	0.22656	6.84	< 0.0001	4.96262
Limestone	1	1.40009	0.18956	7.39	< 0.0001	4.00053
Quartzite	1	2.01838	0.39449	5.12	< 0.0001	1.93773
<i>PCCTHK</i>	1	0.11299	0.0705	1.6	0.1207	1.68624

The model statistics for table 55 are as follows:

- RMSE = 0.27932 psi.
- $R^2 = 0.825$ percent.
- $N = 35$.

Table 56. Range of data used for CRCP *deltaT* model.

Parameter	Minimum	Maximum	Average
Maximum temperature	78.4	99.2	90.3
Temperature range	24.8	40.4	30.4
Chert	0	1	0.06
Granite	0	1	0.31
Limestone	0	1	0.46
Quartzite	0	1	0.03
PCC thickness	5.6	9.5	8.4

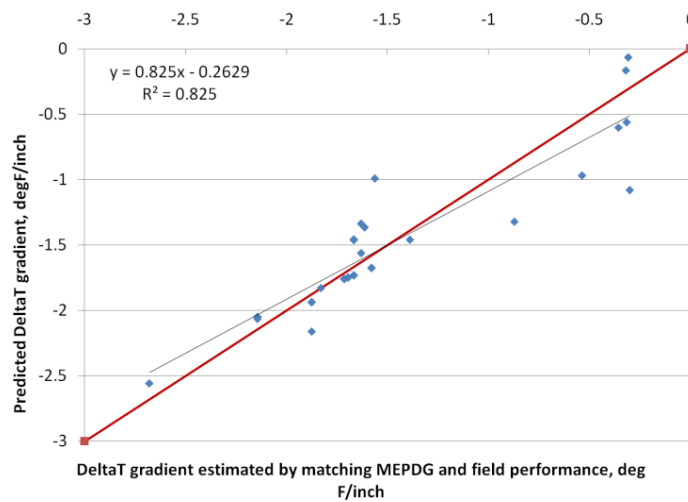


Figure 226. Graph. Predicted versus measured for CRCP *deltaT* model.

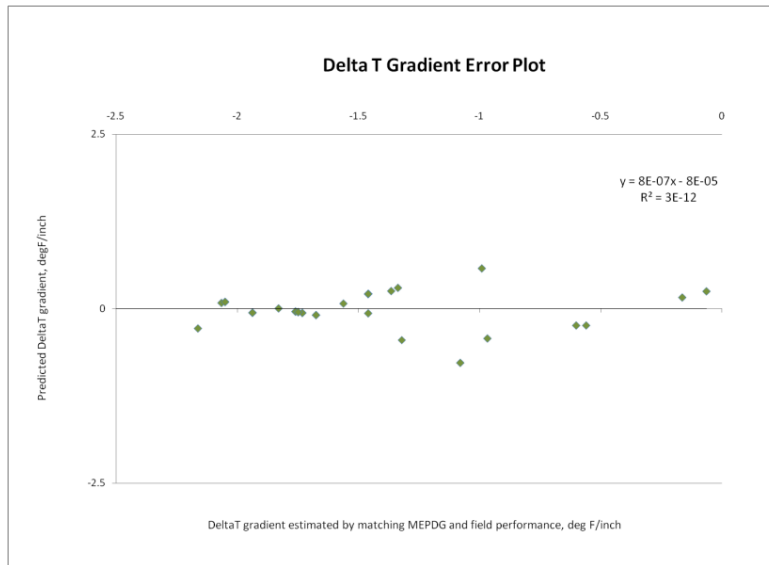


Figure 227. Graph. Residual errors for CRCP *deltaT* model.

Figure 228 through figure 231 show the sensitivity of the *deltaT* differential calculation to the parameters maximum temperature of the project location, maximum temperature range, CRCP slab thickness, and geographic location, respectively. The trends observed in the model—CRCP *deltaT* increasing with increasing maximum temperature and increasing temperature range—are reasonable. While the effect of slab thickness shows a linear relationship with the *deltaT* gradient, the magnitude of the coefficient for this variable results causes the *deltaT* differential (CRCP *deltaT* gradient \times thickness) to assume a nonlinear relationship with the *deltaT* differential, peaking at about 10 inches. Figure 231 shows the *deltaT* predictions for projects selected from LTPP sites in Texas, Illinois, Virginia, Mississippi, Oregon, and Georgia.

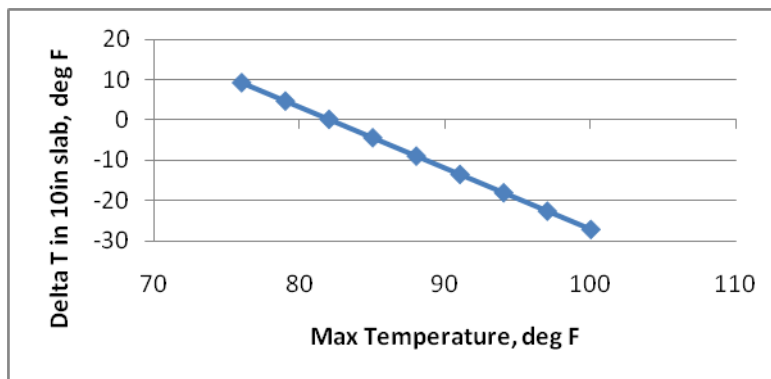


Figure 228. Graph. Effect of maximum temperature on CRCP *deltaT* prediction model.

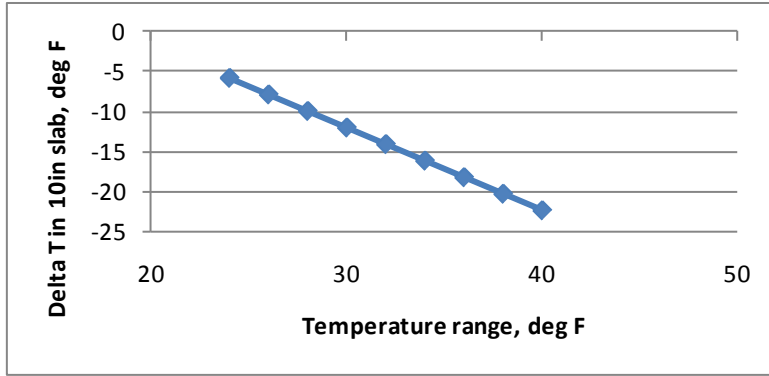


Figure 229. Graph. Effect of temperature range on CRCP ΔT prediction model.

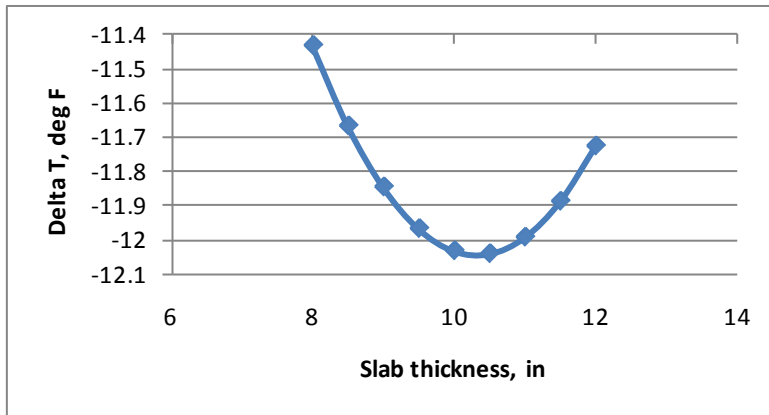


Figure 230. Graph. Effect of slab thickness on CRCP ΔT prediction model.

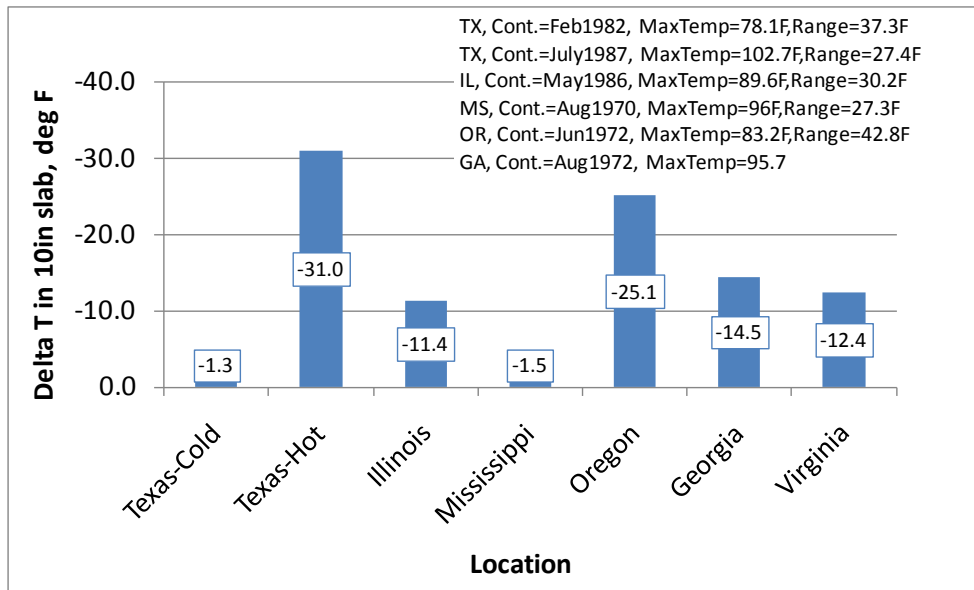


Figure 231. Graph. Effect of geographic location on CRCP ΔT prediction.

The sensitivity analyses show reasonable trends but do not demonstrate that the model is robust. From an engineering standpoint, it is not clear if the range of predicted values and their magnitudes are practical and realistic. The wide range of ΔT will have a significant effect on

design thickness. The data used to develop the model show very strong correlations, and it is likely that the predictions are valid, at least within a certain range of inputs. The current analyses and the data available are not adequate to determine these ranges. It is therefore recommended that this model be used with extreme caution.

Using the CRCP ΔT Model

The use of the CRCP ΔT model shares similarities with the JPCP ΔT model. The section used to describe the process is the LTPP GPS section in Illinois, 17_5020. This was constructed in May 1986. The CRCP thickness is 8.6 inches, and the PCC mix used a limestone aggregate. Several of the following inputs can be directly obtained from the MEPDG input file:

- *PCCTHK*: 8.6 inches.
- Chert: 0.
- Granite: 0.
- Limestone: 1.
- Quartzite: 0.

The maximum temperature and maximum temperature range can be obtained by running the design file and deriving this input from the worksheet titled “Climate.” For the month of May, the maximum temperature and maximum temperature range for this location are 89.6 and 39.2 °F, respectively. Using these inputs, the CRCP ΔT gradient can be calculated as -1.3214 °F/inch. For the slab thickness of 8.6 inches, this is equivalent to a ΔT of -11.36 °F. This value is comparable to the -10 °F default. This input can be revised in an MEPDG file and reanalyzed to predict punchout development over time.

Erosion for CRCP Design

The erosion model in the MEPDG was developed during the calibration of the punchout distress model. The erosion model is an empirical model that is a function of the base type, the quality of the base, precipitation at the project location, and the erosion potential of the subgrade. The erosion calculation was an upgrade provided to the CRCP distress model during changes made under NCHRP 1-40D.⁽⁴⁾ This model was examined under this study and found to adequately consider several parameters known to affect erosion. It also was recognized that within the limitations of the analysis procedures of the MEPDG and available LTPP data, the model considered all parameters that can possibly be included in the model. No changes are suggested for this model. Please note that this model was not developed under the current study but simply verified for adequacy.

EI for JPCP Design

EI is a design feature input used in the faulting prediction model of JPCP. The MEPDG recommends a rating system for different base types. The CRCP erosion model was used to develop a correlation between the calculated erosion values and EI used in the calibration files

of the faulting model. The correlation was poor. However, developing a new basis for the calculation of EI for each JPCP section would necessitate the recalibration of the JPCP model, which is beyond the scope of this study. No specific recommendations are therefore made for the EI model.

STABILIZED MATERIALS MODELS

As stated in chapter 4, the LTPP database does not contain adequate data on modulus values and index properties of stabilized materials. It was therefore not within the scope of this project to develop predictive models for most of the stabilized materials. Nonetheless, the data could be used to develop a single model for predicting the elastic modulus of LCB materials, and that model is included in this section.

LCB Elastic Modulus Model

The modulus values of stabilized materials are not contained in the LTPP database. However, the database does include the compressive strength test results for LCB materials. For the SPS-2 sections, compressive strength data are available at 14 days, 28 days, and 1 year. Additionally, version 24.0 of the LTPP database software was reviewed.⁽¹⁴²⁾ It was found that this version contains the elastic modulus data for SPS-2 sections and that the tests were conducted on samples greater than 10 years in age, which can be more or less considered the long-term elastic modulus for the material. A predictive model correlating the elastic modulus to the 28-day compressive strength can be helpful in using this as a design input. Averaging the data by each site resulted in only 11 data points.

The data available for this model were not considered adequate to establish a new model form; therefore, the most common existing model form (i.e., correlating modulus to the square root of the compressive strength) was used. The model was established as follows:

$$E_{LCB} = 58156\sqrt{f'_{c,28d}} + 716886$$

Figure 232. Equation. Prediction model 17 for E_{LCB} .

Where:

E_{LCB} = Elastic modulus of the LCB layer.

$f'_{c,28d}$ = 28-day compressive strength of the LCB material.

The predicted versus measured and the residual errors plots for this relationship are presented in figure 233 and figure 234, respectively. The model has an R^2 value of 41.24 percent, an RMSE value of 541,600 psi, and uses 11 data points.

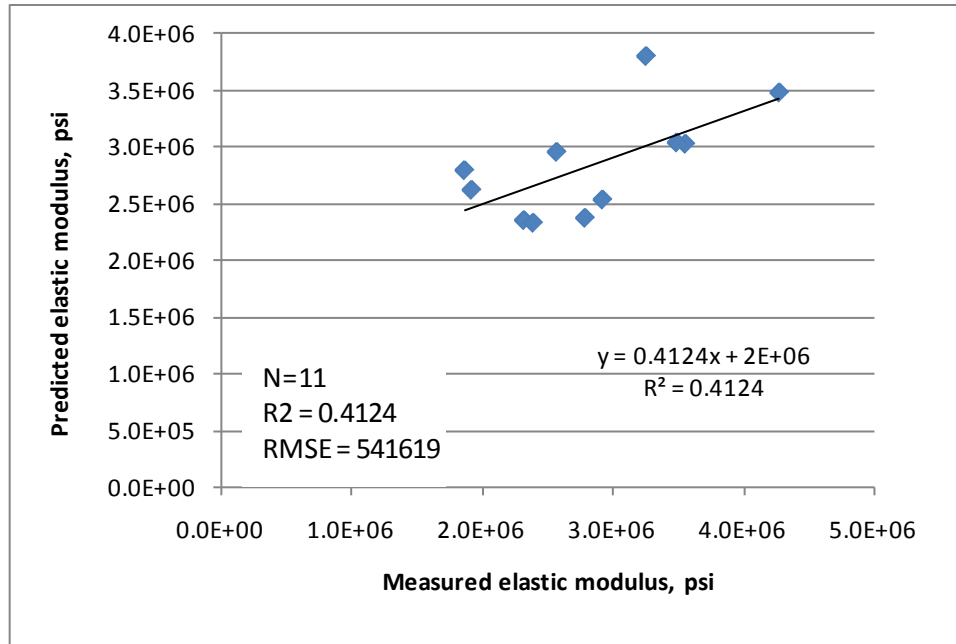


Figure 233. Graph. Predicted versus measured for the LCB elastic modulus model.

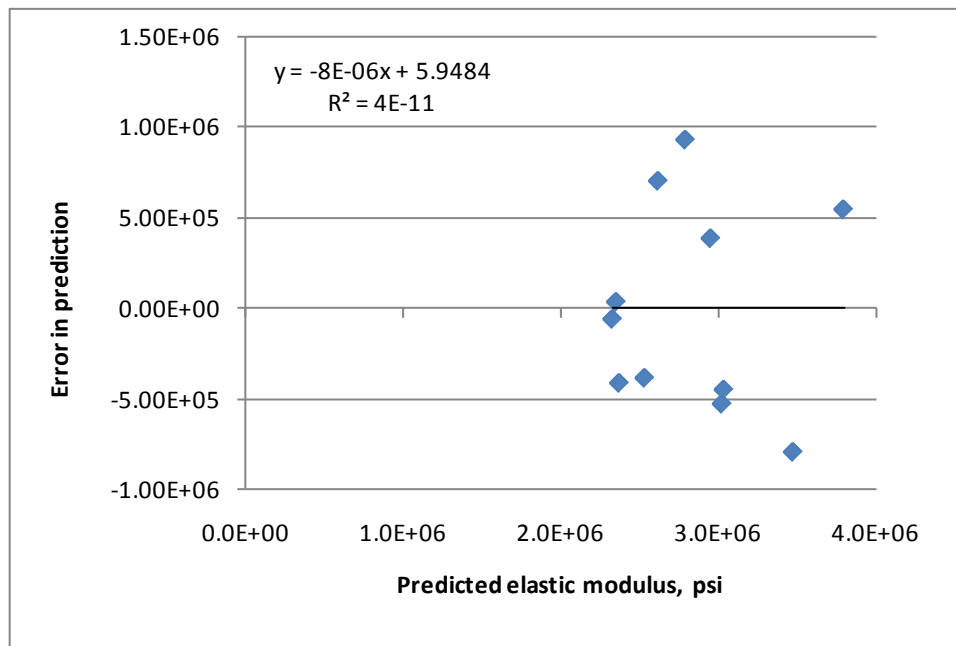


Figure 234. Graph. Residual errors for the LCB elastic modulus model.

UNBOUND MATERIALS MODELS

A key requirement in conducting M-E design or analysis of pavements is to estimate stresses, strains, and deflections within unbound base, subbase, embankment, and subgrade layers. The critical stresses, strains, and deflections are then used in empirical models to forecast future pavement conditions. Mostly, critical stresses, strains, and deflections within all pavement layers (including unbound base, subbase, embankment, and subgrade layers) are determined using finite

element analysis (FEA) or layered elastic analysis (LEA). A key input required for determining critical stresses, strains, and deflections using LEA or FEA techniques is unbound layer material resilient modulus.

Resilient modulus is a dynamic response of unbound layer materials to continuous dynamic loading of a pavement by vehicles. It is defined as the ratio of the repeated axial deviator stress to the recoverable axial strain and is determined in the laboratory by means of a triaxial testing. Because resilient modulus is sensitive to the stress state the unbound material is subjected to (combination of confining stress (σ_1) and deviator stress (σ_3)), testing typically is done over a range of confining and deviator stresses. A mathematical model is then fitted to the resilient modulus and confining and deviator stress data for use in estimating resilient modulus for any reasonable combination of confining and deviator stresses.

Developing correlations between resilient modulus and basic unbound granular/coarse-grained and fine-grained materials for use in pavement analysis and design was one of the objectives of this study. As with the other models described in this report, the LTPP database contained adequate data to develop a resilient modulus model for unbound materials.

Data Assembly for Resilient Modulus Model Development

The literature review included several models developed for the use in predicting resilient modulus using unbound material index properties. From this literature review, a list was developed of all unbound material properties that impact resilient modulus and thus could potentially be included in a resilient modulus prediction model.

Unbound material properties of interest, along with resilient modulus data required for model development as determined through the literature review, were obtained from the LTPP database and assembled in a model development database. Also included in this database were actual resilient modulus test results and the range of confining and deviator stresses at which resilient modulus was determined.

Assembly of Resilient Modulus Model Development Database

Individual LTPP material database tables were merged to develop the resilient modulus model development database. Because the LTPP database is a relational database (i.e., it is composed of separate but related data tables), data assembly was performed by linking data stored in a simple row/column format in tables using unique primary keys to identify LTPP test sections or projects. For many of the data tables, the primary keys were the combination of STATE_CODE, SHRP_ID, and CONSTRUCTION_NO.

The next step was to determine the AASHTO soil classification for each unbound material of the database. The gradation and Atterberg limits were used to determine the soil classification.

Data Review

The assembled data were reviewed thoroughly to identify anomalies and missing data elements, as well as to assess the reasonableness of the data. While this review was performed for all models developed, the review was more in-depth for the resilient modulus data because of the

sheer size of the database and because of the potential for large model errors for relatively small data discrepancies.

Examples of plots summarizing the assembled data used to assess data reasonableness are presented in figure 235 through figure 247. The data were assembled and reviewed by each AASHTO soil class to assess if the trends in the data were reasonable.

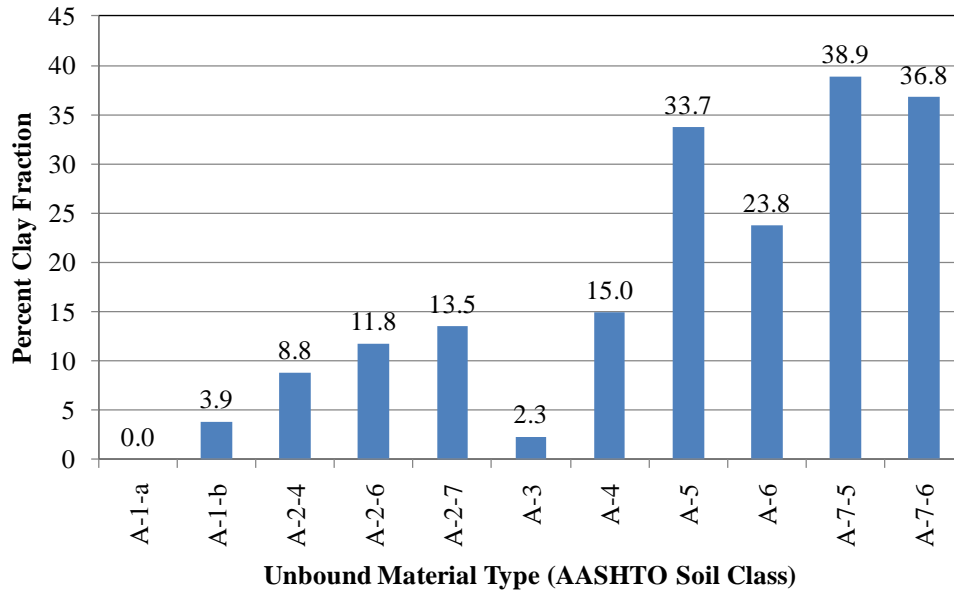


Figure 235. Graph. Mean percent clay fraction for unbound material types included in the model development database.

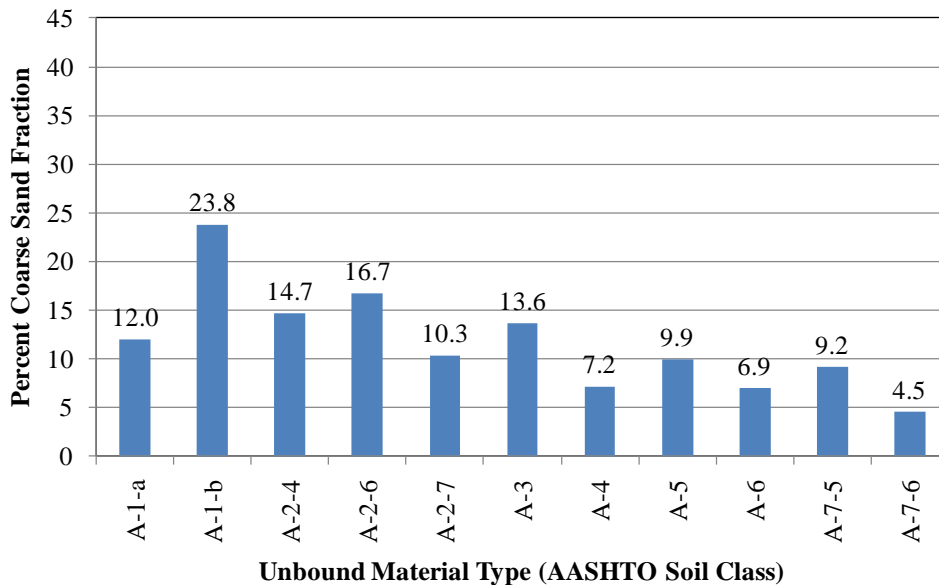


Figure 236. Graph. Mean percent coarse sand fraction for unbound material types included in the model development database.

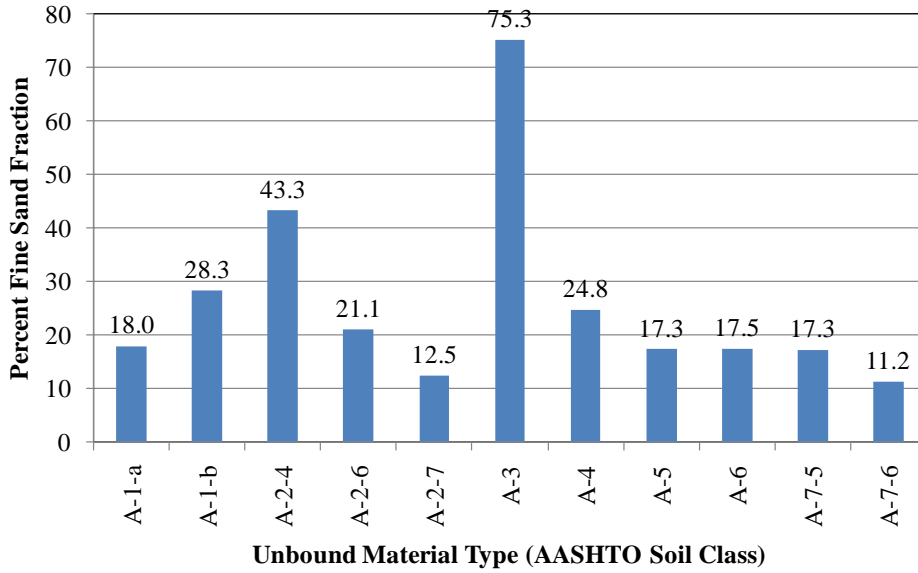


Figure 237. Graph. Mean percent fine sand fraction for unbound material types included in the model development database.

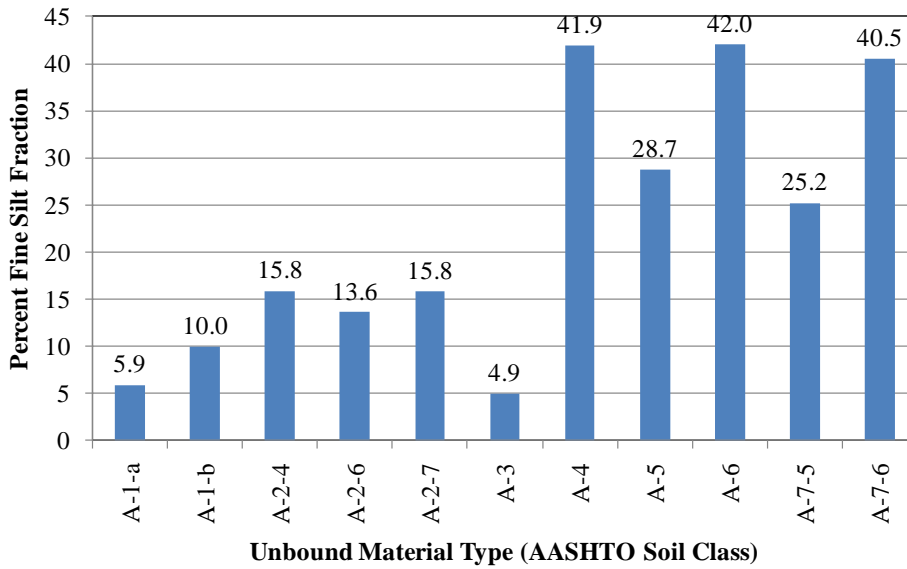


Figure 238. Graph. Mean percent silt fraction for unbound material types included in the model development database.

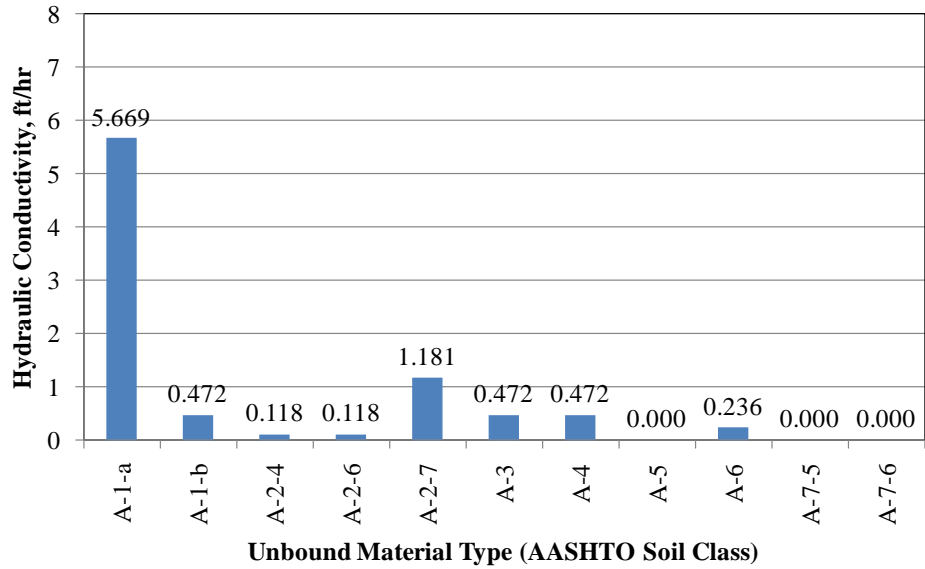


Figure 239. Graph. Mean hydraulic conductivity for unbound material types included in the model development database.

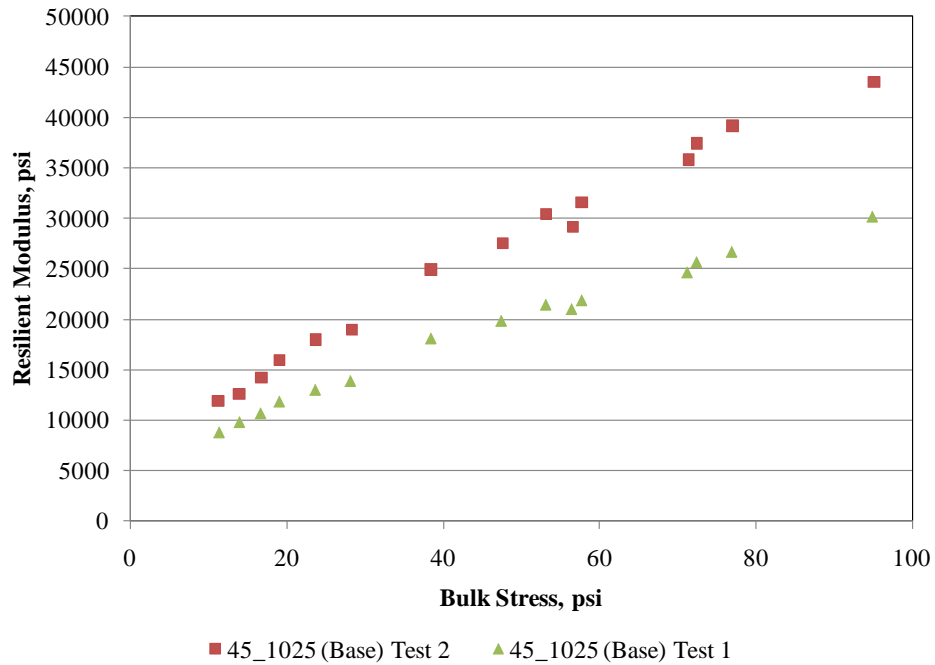


Figure 240. Graph. Plot of bulk stress versus lab tested resilient modulus for section 45_1025 (base layer).

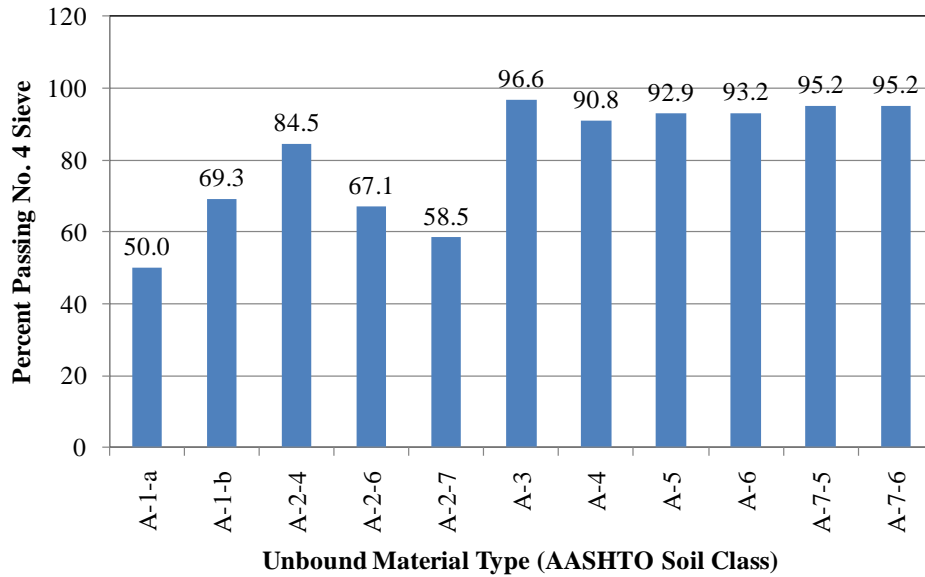


Figure 241. Graph. Percent passing No. 4 sieve for unbound material types included in the model development database.

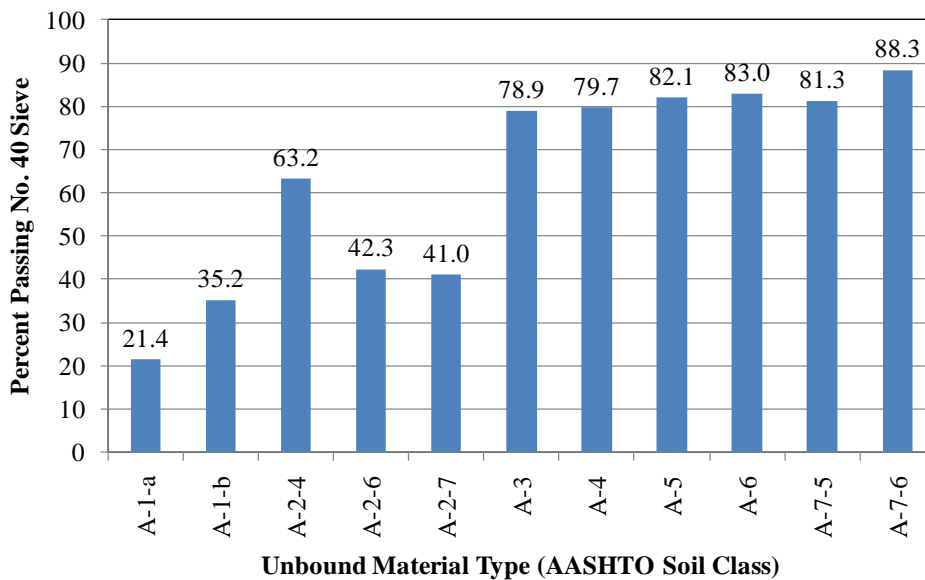


Figure 242. Graph. Percent passing No. 40 sieve for unbound material types included in the model development database.

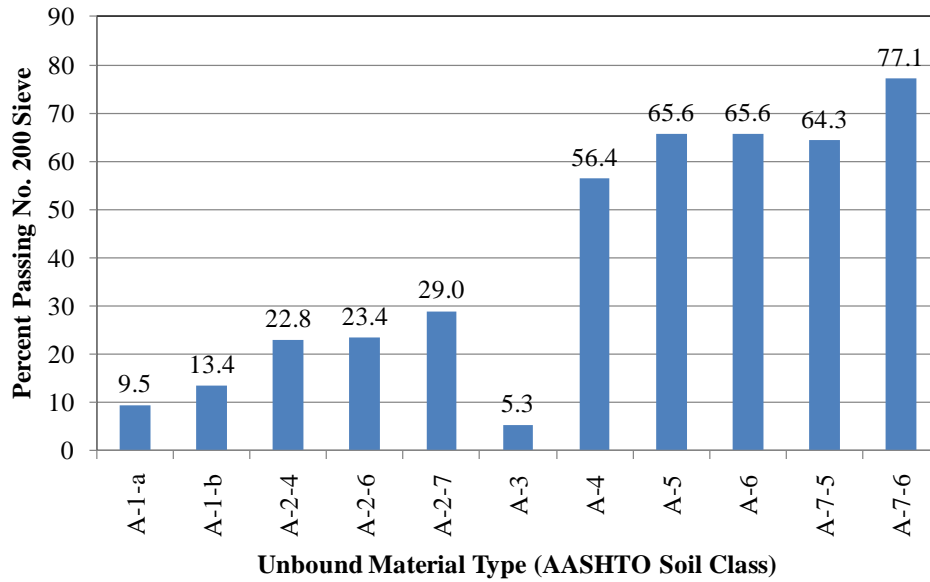


Figure 243. Graph. Percent passing No. 200 sieve for unbound material types included in the model development database.

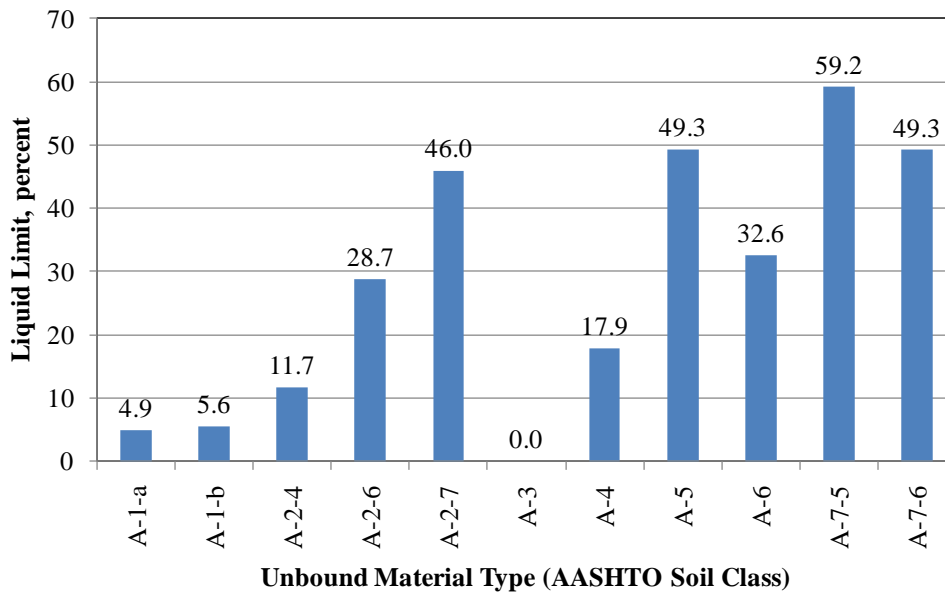


Figure 244. Graph. Liquid limit for unbound material types included in the model development database.

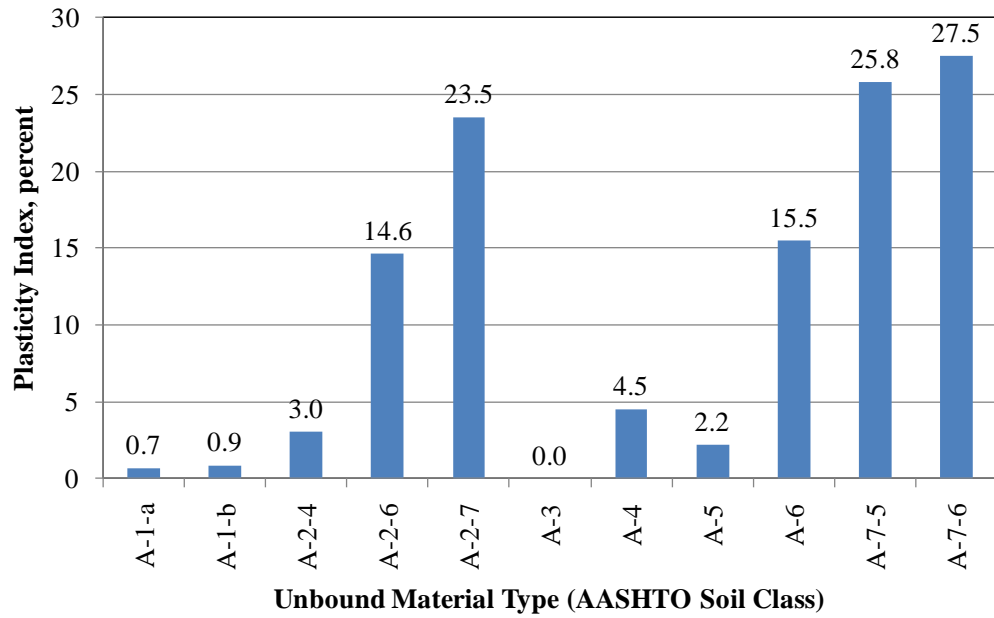


Figure 245. Graph. Plasticity index for unbound material types included in the model development database.

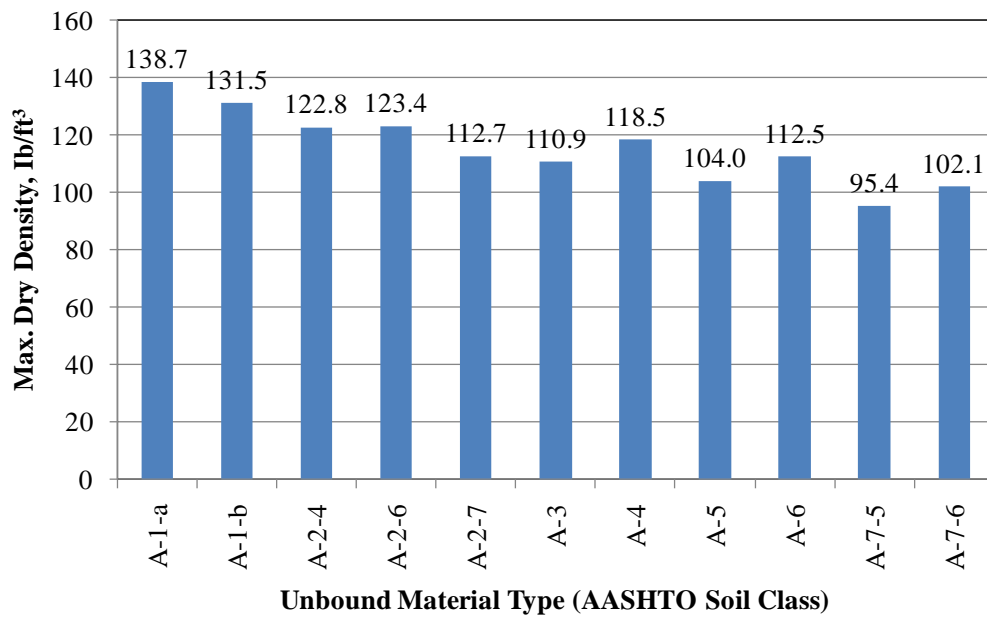


Figure 246. Graph. Maximum dry density for unbound material types included in the model development database.

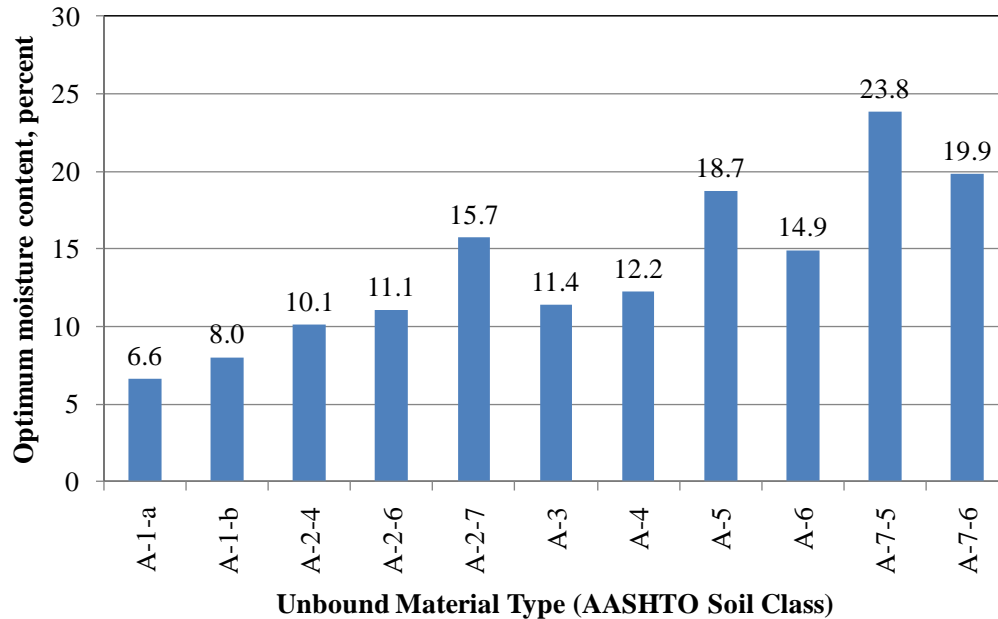


Figure 247. Graph. Optimum moisture content for unbound material types included in the model development database.

The following conclusions were made based on the review of assembled data:

- All key data elements required for resilient modulus model development were available.
- Data available were of adequate quality and completeness for use in model development.
- Resilient modulus data were available for a range of confining and deviator stresses. Thus, there was no single test result that represented the typical unbound base and subgrade soil stress state within a pavement structure. Note that stress state within the pavement structure varies considerably according to pavement type, layer types and thicknesses, layer modulus, applied truck loading, etc.

The following anomalies were identified when matching material properties data elements to M_r data for subgrade soils:

- Sampling of unbound soil/granular materials for performing resilient modulus tests and for determining other soil properties may have occurred at different depths of the subgrade, depending on how the test sample was obtained (i.e., from test pits, coring/boring, auger pits, etc).
- Highly variable subgrade soils at a given site could lead to significant differences in materials used for different types of testing.
- Lack of uniformity in test materials types could lead to mismatching of resilient modulus and soil properties data.

Resolving Identified Anomalies

Over half the test sections did not have all the data elements (e.g., hydraulic conductivity) required to fully characterize the pavement subgrade. However, sufficient data were available for key subgrade material properties (e.g., gradation and Atterberg limits). Data elements for which little data were available were not used in model development.

A significant anomaly was differences in subgrade soil materials used for different types of testing due to sampling location. This anomaly was resolved by matching resilient modulus data to other soil test data only when the sample location could be certified as being as close as possible (i.e., same depth/strata, same test pit, etc.).

A second anomaly was the lack of a single representative resilient modulus value for a given unbound material sample (i.e., series of resilient modulus values corresponding to a combination of deviator and confining stresses used during testing process). This situation has been resolved in the past by fitting the series of resilient modulus values corresponding to a combination of deviator and confining stresses used during testing process with a constitutive equation that models resilient modulus behavior for both granular and fine-grained materials.

As defined in chapter 3, the AASHTO *Mechanistic-Empirical Pavement Design Guide, Interim Edition: A Manual of Practice* proposes the constitutive equation for modeling resilient modulus behavior when subjected to various stress states the following:⁽¹⁾

$$M_r = k_1 P_a \left(\frac{\theta}{P_a} \right)^{k_2} \left(\frac{\tau_{oct}}{P_a} \right)^{k_3}$$

Figure 248. Equation. M_r .

Where:

θ = Bulk stress = $\sigma_1 + \sigma_2 + \sigma_3$.

σ_1 = Principal stress.

σ_2, σ_3 = Confining pressure.

P_a = Atmospheric pressure.

τ_{oct} = Octahedral normal stress = $1/3 (\sigma_1 + 2 \sigma_3)$.

k_1, k_2, k_3 = Regression constants that are a function of soil properties, as defined in figure 75, through figure 77.

This model can be used for various soil types, and the model attributes (k_1, k_2 , and k_3) for a given soil type remain the same regardless of stress state. Developing models to predict constitutive model attributes for a given set of soil properties is thus an effective approach to modeling resilient modulus behavior, rather than developing models individually for each possible combination of expected stress states.

Estimating Resilient Modulus Constitutive Model Parameters k_1 , k_2 , and k_3

Figure 33 presents the constitutive equation that models resilient modulus behavior for both granular and fine-grained materials recommended by the AASHTO *Mechanistic-Empirical Pavement Design Guide, Interim Edition: A Manual of Practice*.⁽¹⁾ The parameters k_1 , k_2 , and k_3 were calculated for all datasets based on the soil properties. Histograms showing the distribution of k_1 , k_2 , and k_3 values by soil class are shown in figure 249 through figure 251, respectively.

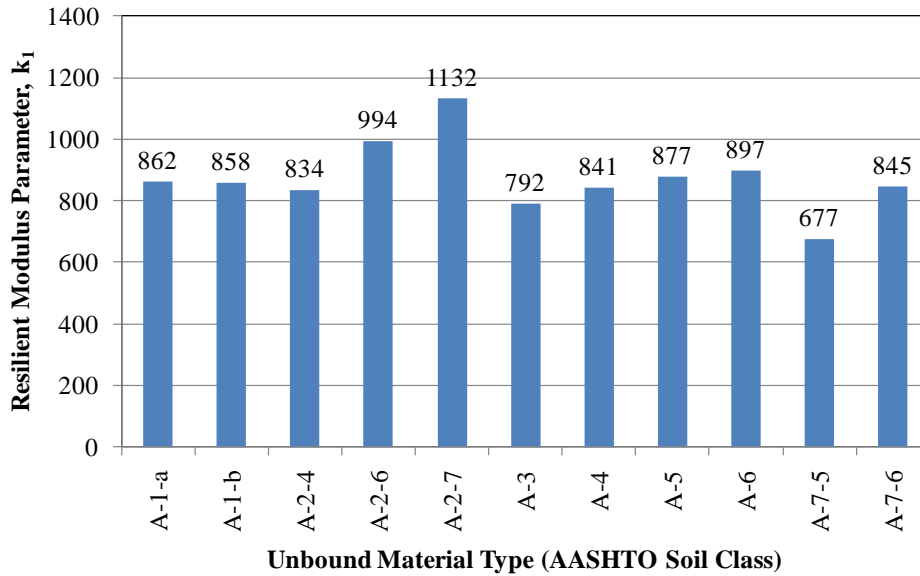


Figure 249. Graph. Resilient modulus parameter k_1 for unbound material types included in the model development database.

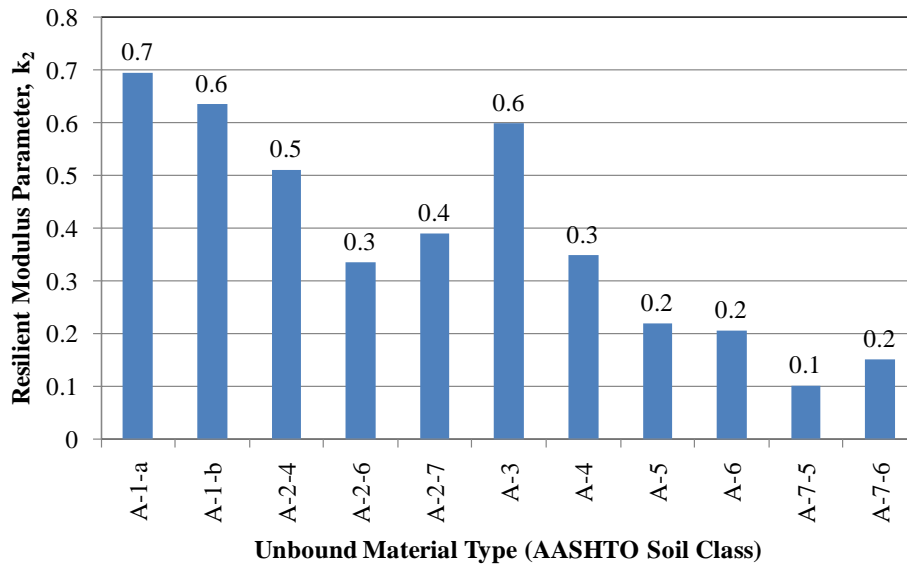


Figure 250. Graph. Resilient modulus parameter k_2 for unbound material types included in the model development database.

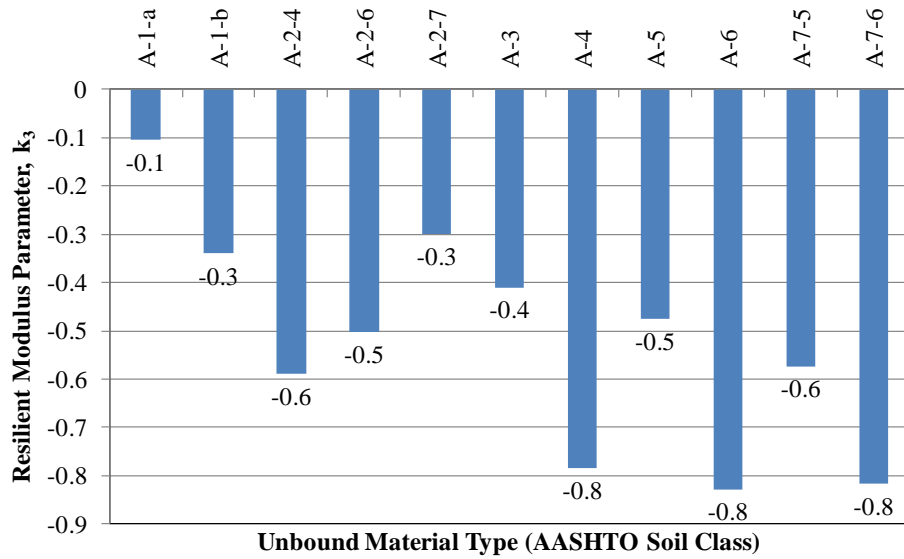


Figure 251. Graph. Resilient modulus parameter k_3 for unbound material types included in the model development database.

This model was fitted to all soil samples with resilient modulus available for a range of confining and deviator stresses. Model fitting was done individually for each unbound material sample in the LTPP database. For each of the soil samples, calculated k_1 , k_2 , and k_3 and the constitutive equation were used to predict resilient modulus at the lab test confining and deviator stresses for comparison. The results of the comparison showed a good fit of predicted and measured resilient modulus with a high R^2 value and low standard error of estimate (SEE), as presented in figure 252.

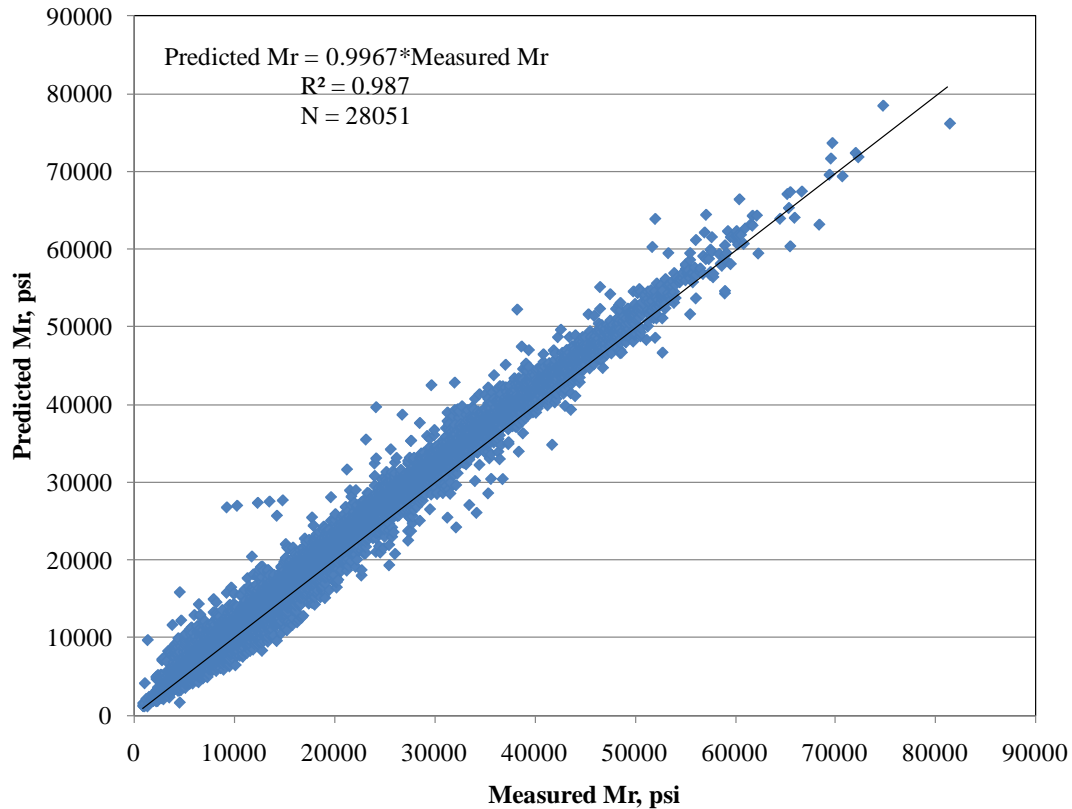


Figure 252. Graph. Plot of measured versus calculated resilient modulus (using k_1 , k_2 , and k_3 computed from constitutive model).

Resilient Modulus Model Development

The following five-step procedure using regression analysis was used to develop multiple linear regression models relating resilient modulus to unbound material properties:

1. Determine appropriate model form.
2. Develop inputs for regression analysis.
3. Perform separate regression analyses for each soil class as follows:
 - Partition assembled data for use in actual model development and validation of tentative models.
 - Perform regression analysis and develop tentative models.
 - Verify tentative model by validating with “set aside” data and checking various model diagnostic statistics to determine the suitability of tentative models developed.
 - Select optimal model inputs and establish k_1 , k_2 , k_3 and material properties relationship.

4. Perform regression with full dataset and determine optimal model coefficients and diagnostic statistics.
5. Perform sensitivity analysis and determine final model coefficients.

Details of the procedure are explained in the following sections.

Step 1: Select Appropriate k_1 , k_2 , k_3 Prediction Model Form

Various forms of mathematical relationships have been used for relating constitutive model parameters k_1 , k_2 , and k_3 to simple material properties. The two most commonly applied, and hence most promising, model forms are as follows:

- $k_i = f(\text{material properties})$.
- $\log(k_i) = f(\text{material properties})$.

Where k_i is k_1 , k_2 , and k_3 . Because both of these mathematical equations have been used successfully, they were both deemed appropriate and were adopted for model fitting in this project.

Step 2: Develop Inputs for Regression Analysis

The data assembled contained all inputs required for model development. Details are as previously described.

Steps 3 and 4: Perform Regression Analyses

Numerous preliminary multivariable regression runs were performed to produce the “best” model. The goal was to determine the optimal set of independent variables (material properties) that, when included in the model, will maximize adjusted R^2 values and minimize errors (SEE). Other diagnostic statistics, such as the level of significance of the regression coefficient of each independent variable, COLLIN (used to check for multicollinearity) in SAS[®], and VIF were made to determine the goodness of fit for the model.

Independent variables with regression coefficients significant at the 0.05 significance level (determined through performing t -tests) were retained in the models developed. The t -test threshold was set at this level so that only variables that impacted k_1 , k_2 , and k_3 were significantly included in the models. The resulting models developed through regression analysis for constitutive model parameters k_1 , k_2 , and k_3 are described below.

Constitutive Model Parameter k_1 :

$$k_1 = 1446.2 - 4.56764 * PCTHALF + 4.92 * LL - 27.73 * OPTMOIST$$

Figure 253. Equation. Prediction model 18 for k_1 .

Model statistics for k_1 are as follows:

- $R^2 = 0.16$ percent.
- $SEE = 237.4$.
- $N = 1,029$.

Constitutive Model Parameter k_2 :

$$k_2 = 0.45679 - 0.00073376 * PCTNO80 - 0.00269 * LL + 0.00060555 * PCTGRVL + 12.97 * D_{10}$$

Figure 254. Equation. Prediction model 19 for k_2 .

Model statistics for k_2 are as follows:

- $R^2 = 0.67$ percent.
- $SEE = 0.0934$.
- $N = 1,032$.

Constitutive Model Parameter k_3 :

$$k_3 = -0.188 \text{ (for fine grained soils)}$$
$$k_3 = -0.153 \text{ (for coarse grained materials)}$$

Figure 255. Equation. Prediction model 20 for k_3 .

Where:

$PCTHALF$ = Percent passing $1/2$ -inch sieve.

LL = Liquid limit, percent.

$OPTMOIST$ = Optimum moisture content, percent.

$PCTNO80$ = Percent passing No. 80 sieve.

$PCTGRVL$ = Percent gravel fraction (0.078- to 2.36-inch size).

D_{10} = Maximum particle size of the smallest 10 percent of soil sample.

Model prediction accuracy and reasonableness were evaluated by reviewing the plot of predicted and measured resilient modulus for all individual resilient modulus test values used in model development as presented in figure 256. Note that the plot presents actual measured resilient modulus for each individual sample and stress state and resilient modulus computed using predicted k_1 , k_2 , and k_3 based on actual material properties for each individual sample and the resilient modulus constitutive model and stress state. Figure 257 presents a plot of measured and predicted resilient modulus versus bulk stress for all fine- and coarse-grained materials included in model development database. Note that mean measured k_1 , k_2 , and k_3 for coarse- and fine-grained materials and predicted k_1 , k_2 , and k_3 using the equations in figure 70 through figure 72 and mean input values for fine- and coarse-grained materials were used for developing this plot. A review of the plots presented in figure 256 and figure 257 shows a reasonable prediction of resilient modulus.

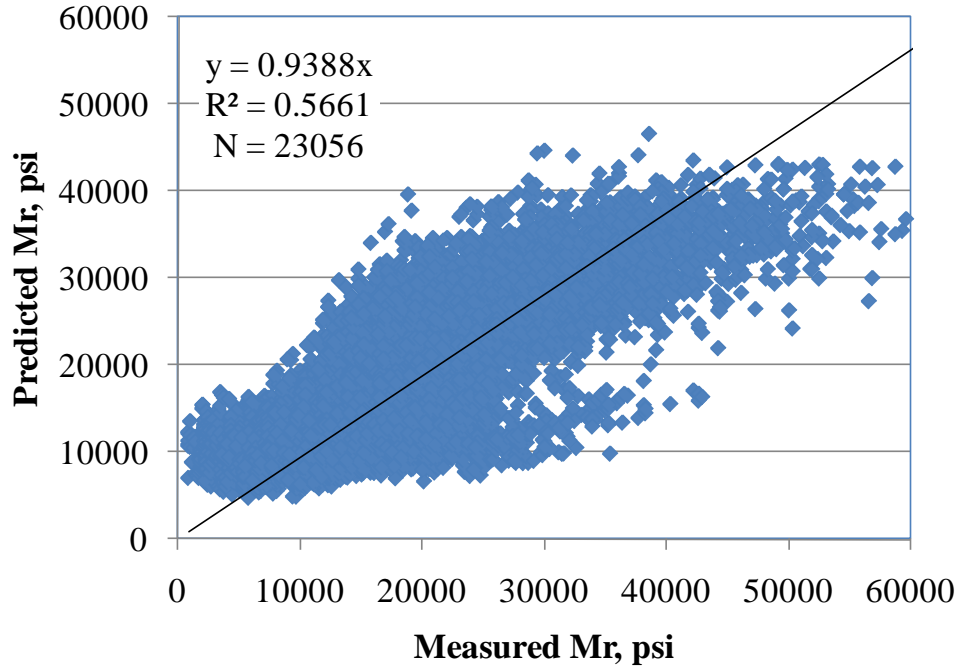


Figure 256. Graph. Measured versus predicted resilient modulus (using k_1 , k_2 , and k_3 from figure 70 through figure 72).

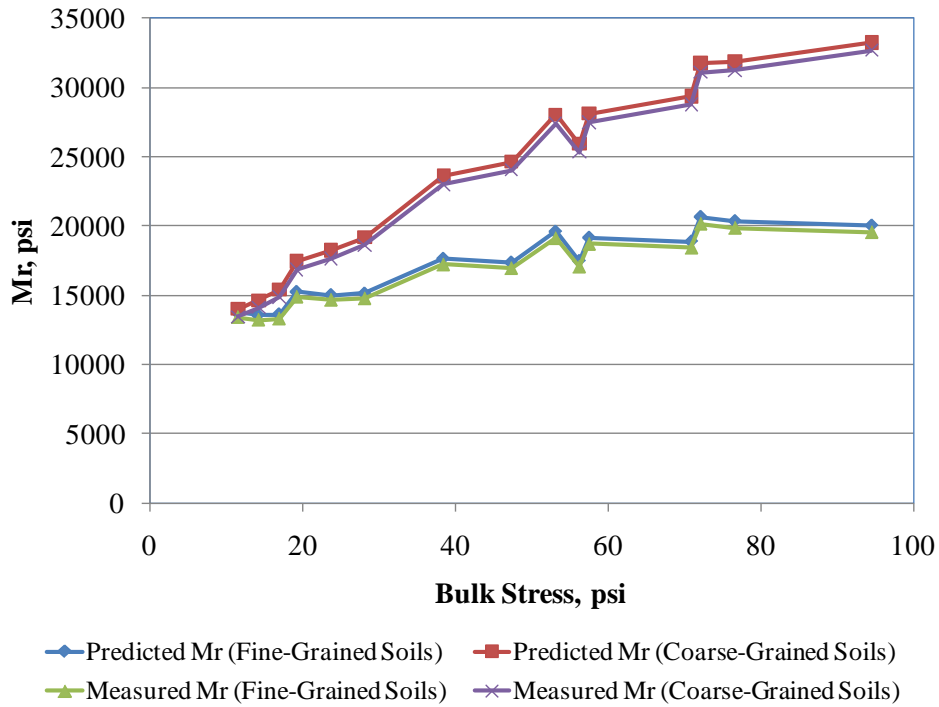


Figure 257. Graph. Predicted and measured resilient modulus versus bulk stress for fine- and coarse-grained soils.

Step 5: Conduct Sensitivity Analysis

The tentative models were further evaluated by conducting a comprehensive sensitivity analysis. The goal was to determine if the model behaves as expected based on engineering principles. Sensitivity analysis results are presented in figure 258 through figure 264. The results of the sensitivity analysis are summarized as follows:

- Soil type had a significant impact on predicted resilient modulus. Coarse-grained materials show significantly higher levels of resilient modulus with increasing bulk stress.
- Increasing the amount of finer materials resulted in a decrease in resilient modulus.
- Increasing the amount of gravel resulted in increased resilient modulus.
- Increasing effective size increases resilient modulus.
- Increasing optimum moisture content resulted in reduced values of resilient modulus.
- Increasing liquid limit resulted in an increase in resilient modulus.

Overall, the trends observed were deemed reasonable, and the proposed model was established as the recommended model for resilient modulus prediction.

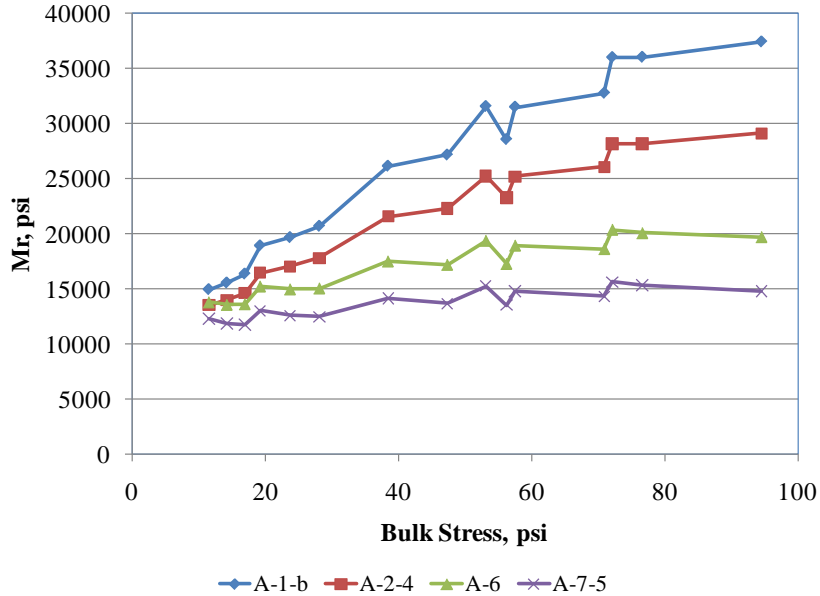


Figure 258. Graph. Effect of material type (AASHTO soil class) on predicted resilient modulus.

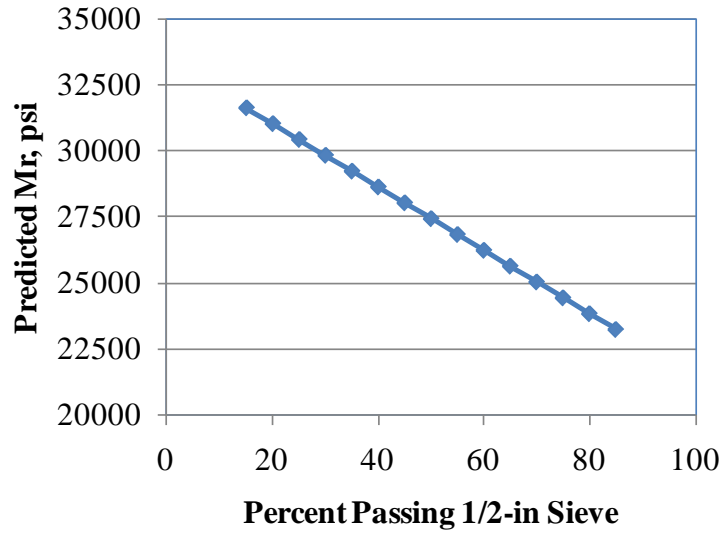


Figure 259. Graph. Effect of percent passing 0.5-inch sieve on predicted resilient modulus.

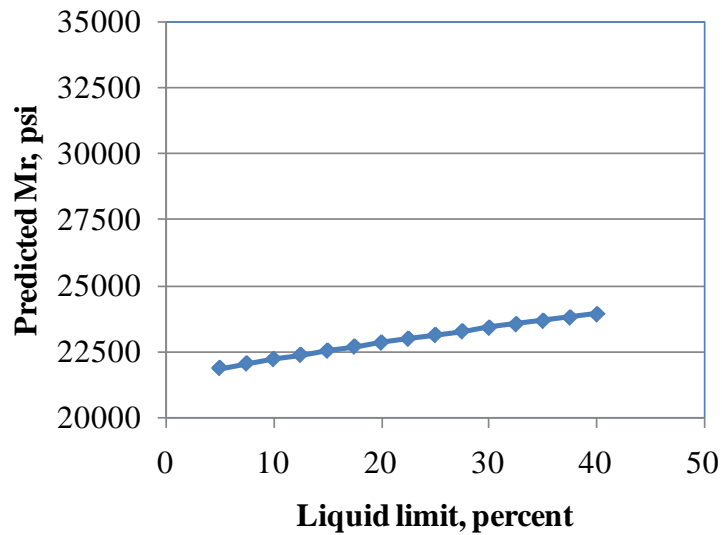


Figure 260. Graph. Effect of liquid limit on predicted resilient modulus.

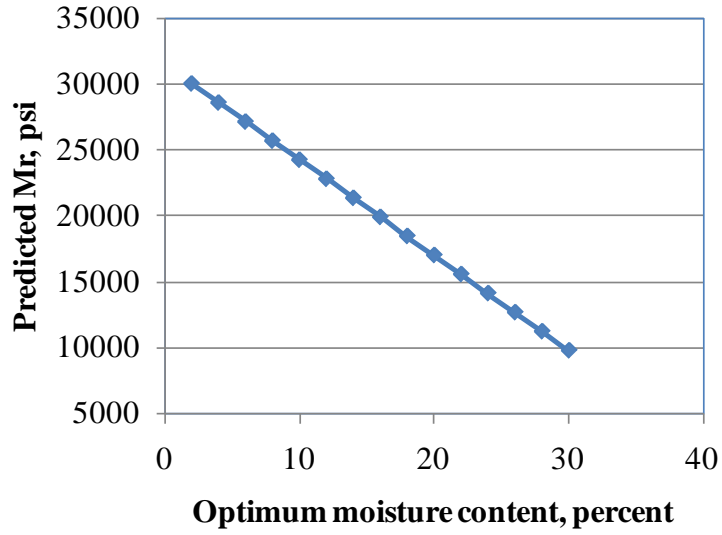


Figure 261. Graph. Effect of optimum moisture content on predicted resilient modulus.

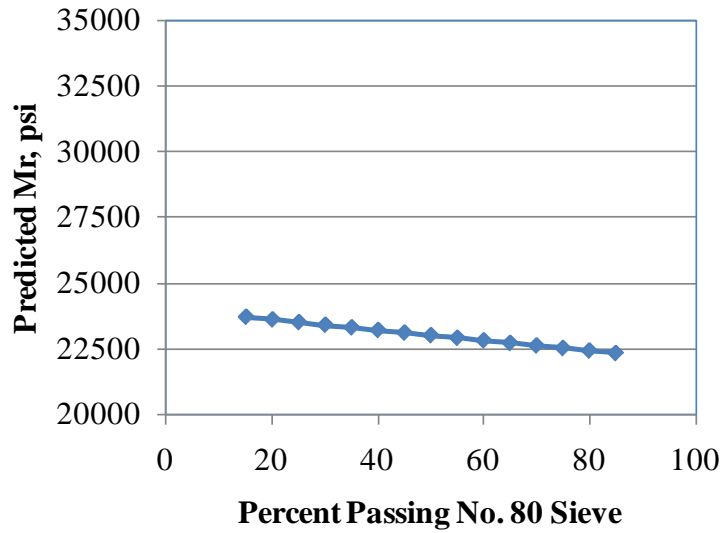


Figure 262. Graph. Effect of No. 80 sieve on predicted resilient modulus.

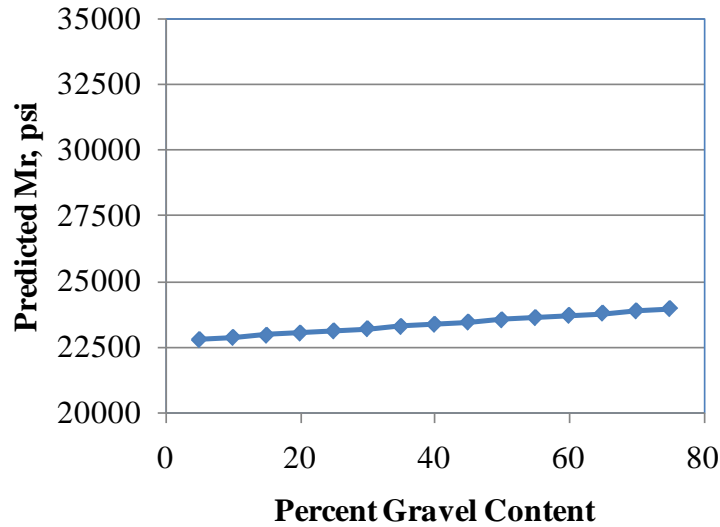


Figure 263. Graph. Effect of gravel content on predicted resilient modulus.

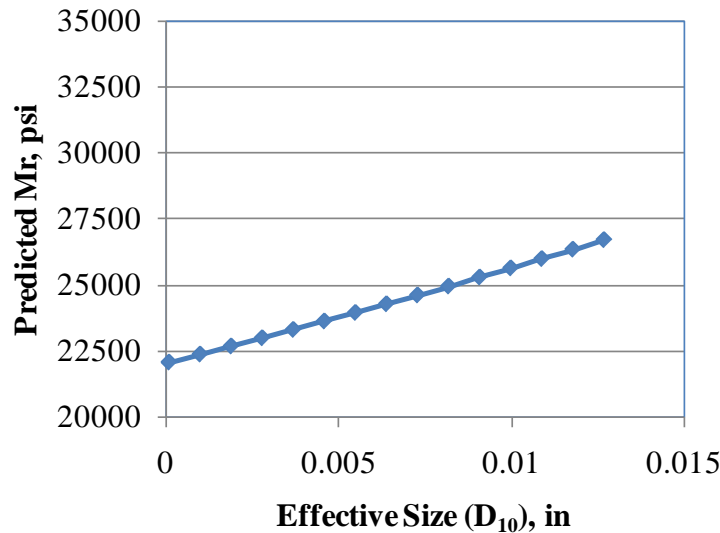


Figure 264. Graph. Effect of effective size on predicted resilient modulus.

PRACTICAL GUIDE AND SOFTWARE PROGRAM

The models developed under this study have been incorporated into a user-friendly software program, *Correlations*, which can be used independently from the MEPDG. The software, developed under this study, was developed on the Microsoft.NET platform to be compatible with the latest versions of the Microsoft Windows® operating systems. It is programmed in the C# language and uses a modern user interface library to provide a familiar look and feel. It features multiple windows on the user interface that are initially docked inside the main window. These windows can be moved separately from the main window for better viewing of the inputs or results.

The program interface features tabs for PCC, design features, stabilized materials, and unbound materials. Models that belong to each of these categories are made available through a series of radio button selections placed in an accordion control. This placement not only provides the ability to make multiple selections, but it also conserves screen space so that the results of the calculations can be placed for easy viewing. Once a model is selected, the entry area adds controls for the available inputs of the model.

Throughout the software, tooltips are used to provide feedback for each of the areas where data can be entered. Calculations occur after all necessary values have been input. Information about each of the models is available in an information window initially located at the bottom of the screen. This information is context-sensitive to the specific selections that the software user has made. Results of each calculation are displayed prominently in the results area window, initially placed on the right side of the main window.

The software program may be requested from the LTPP Customer Support Service Center at ltpinfo@dot.gov.

CHAPTER 6. SUMMARY AND FUTURE WORK

SUMMARY

Material characterization has gained increasing importance in pavement engineering, mainly due to the development of analyses and design procedures that are capable of considering material properties to predict pavement performance. This becomes crucial not only in the initial design phase, but also in QA practices and in pavement management throughout the pavement service life. Materials behave differently depending on the material type (PCC materials, unbound fine-grained materials, unbound coarse-grained materials, etc.), the type of loading (loading under compression, under flexure, under thermal differentials, etc.), and the testing conditions (rate of loading, level of loading, etc). Therefore, materials are characterized by different properties to capture the behavior of the material under different conditions. Procedures like the MEPDG use various material property inputs to model pavement response and to predict pavement performance.

Consequently, there is a need for more information about material properties, which is addressed only to a limited extent in currently available resources. Reliable correlations between material parameters and index properties offer a cost-effective alternative and are equivalent to the level 2 MEPDG inputs. The LTPP database, which contains material property test results as well as material index properties, offers an opportunity to develop such correlations for PCC materials, stabilized materials, and unbound materials.⁽⁵⁾ Furthermore, because these data come from real-world materials, workmanship, and construction practices instead of from controlled laboratory experiments, correlations developed from LTPP data can be considered suitable for use in pavement-related applications.

The MEPDG also requires certain design-related inputs, commonly called design feature inputs, which are influenced by material properties as well as climate and construction-related parameters. The *deltaT* values for JPCP and CRCP design are prime examples of design feature inputs. These inputs are not directly available from simple test results. In combination with the data available from the MEPDG calibration models, the LTPP database offers the potential to provide the much-needed guidance to estimate these inputs.

This study involved developing predictive models to estimate material and design parameters. The main objectives of this study were as follows:

- Identify a set of material engineering properties for which predictive relationships would be useful in pavement design, construction QC/QA, and pavement management applications.
- Establish and/or validate relationships between the identified engineering properties and routine test results, index properties, and/or other readily available information.
- Develop a practical guide accompanied by user friendly software incorporating the recommendations.

A thorough review of the literature was performed to identify material properties for which predictive models would be required and to identify the index properties that have a significant impact on each material property of interest. This was followed by an evaluation of the data available in the LTPP database to assess the availability of data essential for developing these correlations. Based on the review of the database, the following material categories and material properties were selected for developing predictive relationships:

- PCC materials.
 - Compressive strength.
 - Flexural strength.
 - Elastic modulus.
 - Tensile strength.
 - CTE.
- Rigid pavement design features.
 - ΔT in JPCP design.
 - ΔT in CRCP design.
 - Erosion and EI in CRCP and JPCP design, respectively.
- Stabilized materials.
 - Elastic modulus of LCB layers.
- Unbound materials.
 - Resilient modulus of base and subgrade layers.

The LTPP database has an extensive record of material test results. Also, test data are available for SPS and GPS sections, which have distinctly different levels of detail for material index properties and cover different pavement age ranges. Therefore, multiple models were developed for each material property if suitable data were available. The data required to develop models under the rigid pavement design features category were obtained partly from the LTPP database and partly by conducting multiple analysis runs of the LTPP sections used in the calibration of the MEPDG distress models. All models were developed under rigorous statistical analysis procedures, and a uniform set of criteria was used across all models. The statistical significance was discussed in detail throughout the report.

The following is a summary of the models developed under this study, grouped by material type and material property.

PCC MATERIALS

PCC Compressive Strength Models

Compressive Strength Model 1: 28-Day Cylinder Strength Model

$$f_{c,28d} = 4028.41841 - 3486.3501 * w/c + 4.02511 * CMC$$

Figure 265. Equation. Prediction model 1 for $f_{c,28d}$.

Where:

$f_{c,28d}$ = 28-day compressive strength, psi.

w/c = Water to cement ratio.

CMC = Cementitious materials content, lb/yd³.

Compressive Strength Model 2: Short-Term Cylinder Strength Model

$$f_{c,t} = 6358.60655 + 3.53012 * CMC - 34.24312 * w/c * uw + 633.3489 * \ln(t)$$

Figure 266. Equation. Prediction model 2 for $f_{c,t}$.

Where:

$f_{c,t}$ = Compressive strength at age t years, psi.

CMC = Cementitious materials content, lb/yd³.

w/c = Water to cement ratio.

uw = Unit weight, lb/ft³.

t = Short-term age, years.

Compressive Strength Model 3: Short-Term Core Strength Model

$$f_{c,t} = 98.92962 + 5.70412 \times CMC + 28.48527 \times uw + 2,570.13151 \times MAS \times w/c - 199.84664 \times FM + 611.30879 \times \ln(t)$$

Figure 267. Equation. Prediction model 3 for $f_{c,t}$.

Where:

$f_{c,t}$ = Compressive strength at age t years, psi.

CMC = Cementitious materials content, lb/yd³.

uw = Unit weight, lb/ft³.

MAS = Maximum aggregate size, inch.

w/c = Water to cement ratio.

FM = Fineness modulus of fine aggregate.

t = Short-term age, years.

Compressive Strength Model 4: All Ages Core Strength Model

$$f_{c,t} = -6,022.44 - 854.46 \times w/c + 4.8656 \times CMC + 68.5337 \times uw + 533.15 \times \ln(t)$$

Figure 268. Equation. Prediction model 4 for $f_{c,t}$.

Where:

$f_{c,t}$ = Compressive strength at age t years, psi.

w/c = Water to cement ratio.

CMC = Cementitious materials content, lb/yd³.

uw = Unit weight, lb/ft³.

t = Short-term age, years.

Compressive Strength Model 5: Long-Term Core Strength Model

$$f_{c,LT} = -3467.3508 + 3.63452 * CMC + 0.42362 * uw^2$$

Figure 269. Equation. Prediction model 5 for $f_{c,LT}$.

Where:

$f_{c,LT}$ = Long-term compressive strength, psi.

CMC = Cementitious materials content, lb/yd³.

uw = Unit weight, lb/ft³.

PCC Flexural Strength Models

Flexural Strength Model 1: Flexural Strength Based on Compressive Strength

$$MR = 22.7741 * f_c^{0.4082}$$

Figure 270. Equation. Prediction model 6 for MR .

Where:

MR = Flexural strength, psi.

f_c = Compressive strength determined at the same age, psi.

Flexural Strength Model 2: Flexural Strength Based on Age, Unit Weight, and w/c Ratio

$$MR_t = 676.0159 - 1120.31 * w/c + 4.1304 * uw + 35.74627 * \ln(t)$$

Figure 271. Equation. Prediction model 7 for MR_t .

Where:

MR_t = Flexural strength at age t years, psi.

w/c = water to cement ratio.

uw = Unit weight, lb/ft³.

t = Pavement age, years.

Flexural Strength Model 3: Flexural Strength Based on Age, Unit Weight, and CMC

$$MR_t = 24.15063 + 0.55579 * CMC + 2.96376 * uw + 35.54463 * \ln(t)$$

Figure 272. Equation. Prediction model 8 for MR_t .

Where:

MR_t = Flexural strength at age t years, psi.

CMC = Cementitious materials content, lb/yd³.

uw = Unit weight, lb/ft³.

t = Pavement age, years.

PCC Elastic Modulus Models

Elastic Modulus Model 1: Model Based on Aggregate Type

$$E_c = (4.499 * (UW)^{2.3481} * (f'_c)^{0.2429}) * D_{agg}$$

Figure 273. Equation. Prediction model 9 for E_c .

Where:

E_c = PCC elastic modulus, psi.

uw = Unit weight, lb/ft³.

f'_c = Compressive strength at same age, psi.

D_{agg} = Regressed constant depending on aggregate type as follows:

- = 1.0 for andesite.
- = 0.9286 for basalt.
- = 1.0079 for chert.
- = 0.9215 for diabase.
- = 1.0254 for dolomite.
- = 0.8333 for granite.
- = 1.0 for limestone.
- = 0.9511 for quartzite.
- = 1.0 for sandstone.

Elastic Modulus Model 2: Model Based on Age and Compressive Strength

$$E_{c,t} = 59.0287 * (f'_c)_t^{1.3} * (\ln(\frac{t}{0.03}))^{-0.2118}$$

Figure 274. Equation. Prediction model 10 for $E_{c,t}$.

Where:

- $E_{c,t}$ = Elastic modulus at age t years
- $f'c_t$ = Compressive strength at age t years.
- t = Age at which modulus is determined, years.

Elastic Modulus Model 3: Model Based on Age and 28-day Compressive Strength

$$E_{c,t} = 375.6 * (f'c_{28-day})^{1.1} * (\ln(\frac{t}{0.03}))^{0.00524}$$

Figure 275. Equation. Prediction model 11 for $E_{c,t}$.

Where:

- $E_{c,t}$ = Elastic modulus at age t years.
- $f'c_{28-day}$ = 28-day compressive strength.
- t = Age at which modulus is determined, years.

PCC Indirect Tensile Strength Models

PCC Indirect Tensile Strength Model: Model Based on Compressive Strength

$$f_i = 8.9068 * (f'c)^{0.4785}$$

Figure 276. Equation. Prediction model 12 for f_i .

Where:

- f_i = Indirect tensile strength of the PCC material.
- $f'c$ = Compressive strength of the mix determined at the same age.

PCC CTE Models

CTE Model 1: CTE Based on Aggregate Type (Level 3 Equation for MEPDG)

Table 57. Model 13. CTE based on aggregate type.

Aggregate Type	Average From Data Used in Level 2 Model
Basalt	4.86
Chert	6.90
Diabase	5.13
Dolomite	5.79
Gabbro	5.28
Granite	5.71
Limestone	5.25
Quartzite	6.18
Andesite	5.33
Sandstone	6.33

CTE Model 2: CTE Based on Mix Volumetrics (Level 2 Equation for MEPDG)

$$CTE_{PCC} = CTE_{CA} \times V_{CA} + 6.4514 \times (1 - V_{CA})$$

Figure 277. Equation. Prediction model 14 for CTE_{PCC} .

Where:

CTE_{PCC} = CTE of the PCC material, $\times 10^{-6}$ inch/inch/°F.

V_{CA} = Volumetric proportion of the coarse aggregate (value between zero and 0.6).

CTE_{CA} = Constant determined for each aggregate type as follows:

- CTE_{CA} for basalt: 3.
- CTE_{CA} for chert: 6.4.
- CTE_{CA} for diabase: 3.4835.
- CTE_{CA} for dolomite: 5.1184.
- CTE_{CA} for gabbro: 3.75.
- CTE_{CA} for granite: 4.7423.
- CTE_{CA} for limestone: 3.2886.
- CTE_{CA} for quartzite: 6.1.
- CTE_{CA} for andesite: 3.6243.
- CTE_{CA} for Sandstone: 4.5

RIGID PAVEMENT DESIGN FEATURES MODELS

***deltaT*—JPCP Design**

$$\begin{aligned} \text{deltaT} / \text{inch} = & -5.27805 - 0.00794 * TR - 0.0826 * SW + 0.18632 * PCCTHK \\ & + 0.01677 * uw + 1.14008 * w/c + 0.01784 * latitude \end{aligned}$$

Figure 278. Equation. Prediction model 15 for $\text{deltaT}/\text{inch}$.

Where:

$\text{deltaT}/\text{inch}$ = Predicted gradient in JPCP slab, °F/inch.

TR = Difference between maximum and minimum temperature for the month of construction, °F.

SW = Slab width, ft.

$PCCTHK$ = JPCP slab thickness, inch.

uw = Unit weight of PCC used in JPCP slab, lb/ft³.

w/c = Water to cement ratio.

$latitude$ = Latitude of the project location, degrees.

ΔT —CRCP Design

$$\begin{aligned} \Delta T / \text{inch} = & 12.93007 - 0.15101 * \text{MaxTemp} - 0.10241 * \text{MaxTempRange} + 3.279 * \text{Chert} \\ & + 1.55013 * \text{Granite} + 1.40009 * \text{Limestone} + 2.01838 * \text{Quartzite} \\ & + 0.11299 * \text{PCCTHK} \end{aligned}$$

Figure 279. Equation. Prediction model 16 for $\Delta T/\text{inch}$.

Where:

$\Delta T/\text{inch}$ = Predicted gradient in CRCP slab, °F/inch.

MaxTemp = Maximum temperature for the month of construction, °F.

MaxTempRange = Maximum temperature range for the month of construction, °F.

PCCTHK = JPCP slab thickness, inch.

Chert = 1 if PCC mix coarse aggregate is chert, or 0 if otherwise.

Granite = 1 if PCC mix coarse aggregate is granite, or 0 if otherwise.

Limestone = 1 if PCC mix coarse aggregate is limestone, or 0 if otherwise.

Quartzite = 1 if PCC mix coarse aggregate is quartzite, or 0 if otherwise.

Erosion for CRCP Design

There were no modifications to the existing MEPDG erosion model.

EI for JPCP Design

No model was developed for this parameter.

STABILIZED MATERIALS MODELS

LCB Elastic Modulus Model

$$E_{LCB} = 58156\sqrt{f'_{c,28d}} + 716886$$

Figure 280. Equation. Prediction model 17 for E_{LCB} .

Where:

E_{LCB} = Elastic modulus of the LCB layer.

$f'_{c,28d}$ = 28-day compressive strength of the LCB material.

UNBOUND MATERIALS MODELS

Resilient Modulus of Unbound Materials

Resilient modulus will be determined using the following constitutive model:

$$M_r = k_1 \left(\frac{\theta}{P_a} \right)^{k_2} \left(\frac{\tau_{oct}}{P_a} \right)^{k_3}$$

Figure 281. Equation. M_r .

The constitutive model parameters are defined as follows:

$$k_1 = 1,446.2 - 4.56764 \times PCTHALF + 4.92 \times LL - 27.73 \times OPTMOIST$$

Figure 282. Equation. Prediction model 18 for k_1 .

$$k_2 = 0.45679 - 0.00073376 \times PCTNO80 - 0.00269 \times LL + 0.00060555 \times PCTGRVL + 12.97 \times D_{10}$$

Figure 283. Equation. Prediction model 19 for k_2 .

$$k_3 = -0.188 \text{ (for fine-grained soils)}$$

$$k_3 = -0.153 \text{ (for coarse-grained materials)}$$

Figure 284. Equation. Prediction model 20 for k_3 .

Where:

PCTHALF = Percent passing $1/2$ -inch sieve.

LL = Liquid limit, percent.

OPTMOIST = Optimum moisture content, percent.

PCTNO80 = Percent passing No. 80 sieve.

PCTGRVL = Percent gravel fraction (0.078- to 2.36-inch size).

D₁₀ = Maximum particle size of the smallest 10 percent of soil sample.

FUTURE WORK

The models presented in this report, for most part, were developed from LTPP materials tables that are comprehensive and have been cleared through rigorous data screening and reviews (level E). The CTE values in the database are a relatively recent addition. Over the past year, some issues were identified with the accuracy of these data, and FHWA has made other efforts to correct the CTE test data. The CTE models developed in this study, therefore, need to be updated to reflect the recent changes.

Additionally, the *deltaT* models for JPCP and CRCP design are based on the calibration in the MEPDG version 1.0 software. The MEPDG rigid pavement models are being updated to account for changes in CTE values and to address software bugs identified since the release of version 1.0 in 2006. This version was completed in 2011. Therefore, the *deltaT* models presented here will not be applicable in the new version. These models will require updating. The procedures followed to develop these models are valid and can be used in a framework for future revisions.

REFERENCES

1. American Association of State Highway and Transportation Officials. (2008). *Mechanistic-Empirical Pavement Design Guide, Interim Edition: A Manual of Practice*, American Association of State Highway and Transportation Officials, Washington, DC.
2. National Cooperative Highway Research Program. (2004). *Mechanistic-Empirical Pavement Design Guide*, NCHRP Project 1-37A, Transportation Research Board, Washington, DC. Obtained from: <http://www.trb.org/mepdg/guide.htm>. Site last accessed April 2010.
3. Federal Highway Administration. (2009). *Long-Term Pavement Performance Program Standard Data Release 23.0*, VR2009.01, DVD Version, Federal Highway Administration, Washington, DC.
4. National Cooperative Highway Research Program. (2006). *Research Results Digest 308: Changes to the Mechanistic Empirical Pavement Design Guide Software Through Version 0.900*, NCHRP Project 1-40D, Transportation Research Board, Washington, DC.
5. Turner-Fairbank Highway Research Center. *How to Get LTPP Data*, Federal Highway Administration, Washington, DC. Obtained from: <http://www.fhwa.dot.gov/research/tfhrc/programs/infrastructure/pavements/ltpp/getdata.cfm>.
6. National Cooperative Highway Research Program. (2009). *User Manual and Local Calibration Guide for the Mechanistic-Empirical Pavement Design Guide and Software*, Final Report, Project NCHRP 1-40B, Transportation Research Board, Washington, DC.
7. Irick, P.E., Seeds, S.B., Myers, M.G., and Moody, E.D. (1990). *Development of Performance-Related Specifications for Portland Cement Concrete Pavement Construction*, Final Report, Report No. FHWA-RD-89-211, Federal Highway Administration, Washington, DC.
8. Okamoto, P., Wu, C.L., Tarr, S.M., Darter, M.I., and Smith, K.D. (1993). *Performance Related Specifications for Concrete Pavements*, Report No. FHWA-RD-93-044, Federal Highway Administration, Washington, DC.
9. Hoerner, T.E., Darter, M.I., Khazanovich, L., Titus-Glover, L., and Smith, K.L. (2000). *Improved Prediction Models for PCC Pavement Performance-Related Specifications, Volume I: Final Report*, Report No. FHWA-RD-00-130, Federal Highway Administration, Washington, DC.
10. Rao, C., Darter, M.I., Smit, A.F., Mallela, J., Smith, K.L., Von Quintus, H.L., and Grove, J. (2006). *Advanced Quality Systems: Guidelines for Establishing and Maintaining Construction Quality Databases*, Report No. FHWA- HRT-07-019, Federal Highway Administration, Washington, DC.

11. Hoerner, T.E. and Darter, M.I. (2000). *Improved Prediction Models for PCC Pavement Performance-Related Specifications, Volume II: PaveSpec 3.0 User's Guide Report*, Report No. FHWA-RD-00-131, Federal Highway Administration, Washington, DC.
12. AASHTO. (1993). *Guide for Design of Pavement Structures*, American Association of State Highway and Transportation Officials, Washington, DC.
13. Rao, C., Mallela, J., Darter, M.I., and Titus-Glover, L. (2007). *Concrete Mix Properties to Optimize Concrete Pavement Performance Using the MEPDG*, Proceedings for International Conference on Optimizing Paving Concrete Mixtures and Accelerated Concrete Pavement Construction and Rehabilitation, Atlanta, GA.
14. Bazant, Z.P. (2000). "Criteria for Rational Prediction of Creep and Shrinkage of Concrete," *Adam Neville Symposium: Creep and Shrinkage—Structural Design Effects*, ACI SP-194, A. Al-Manaseer, Ed., American Concrete Institute, Farmington Hills, MI.
15. Mallela, J., Titus-Glover, L., Ayers, M.E., and Wilson, T.P. (2001). *Characterization of Mechanical Properties and Variability of PCC Materials for Rigid Pavement Design*, Proceedings from the 7th International Conference on Concrete Pavements, Orlando, FL.
16. Mallela, J., Abbas, A., Harman, T., Rao, C., Liu, R., and Darter, M.I. (2005). "Measurement and Significance of the Coefficient of Thermal Expansion of Concrete in Rigid Pavement Design," *Transportation Research Record 1919*, Transportation Research Board, Washington, DC.
17. AASHTO T 22. (2006). *Standard Test Method for Compressive Strength of Cylindrical Concrete Specimens*, American Association of State Highway and Transportation Officials, Washington, DC.
18. ASTM C 469. (2010). "Standard Test Method for Static Modulus of Elasticity and Poisson's Ratio of Concrete in Compression," *Annual Book of Standards Volume 04.02*, ASTM International, West Conshohocken, PA.
19. AASHTO T 97. (2010). *Standard Method of Test for Flexural Strength of Concrete (Using Simple Beam with Third-Point Loading)*, American Association of State Highway and Transportation Officials, Washington, DC.
20. AASHTO T 198. (2002). *Standard Method of Test for Splitting Tensile Strength of Cylindrical Concrete Specimens*, American Association of State Highway and Transportation Officials, Washington, DC.
21. AASHTO T 121. (2005). *Standard Method of Test for Density (Unit Weight), Yield, and Air Content (Gravimetric) of Concrete*, American Association of State Highway and Transportation Officials, Washington, DC.
22. AASHTO T 152. (2005). *Standard Method of Test for Air Content of Freshly Mixed Concrete by the Pressure Method*, American Association of State Highway and Transportation Officials, Washington, DC.

23. AASHTO T 196M/T 196. (2005). *Standard Method of Test For Air Content of Freshly Mixed Concrete by the Volumetric Method*, American Association of State Highway and Transportation Officials, Washington, DC.
24. AASHTO TP 60. (2000). *Standard Test Method for the Coefficient of Thermal Expansion of Hydraulic Cement Concrete*, American Association of State Highway and Transportation Officials, Washington, DC.
25. ASTM E1952. (2006). "Standard Test Method for Thermal Conductivity and Thermal Diffusivity by Modulated Temperature Differential Scanning Calorimetry," *Annual Book of ASTM Standards*, Vol. 14.02, ASTM International, West Conshohocken, PA.
26. ASTM D2766. (2009). "Standard Test Method for Specific Heat of Liquids and Solids," *Annual Book of Standards Volume 05.01*, ASTM International, West Conshohocken, PA.
27. ASTM D4694. (2009). "Standard Test Method for Deflections with a Falling-Weight-Type Impulse Load Device," *Annual Book of Standards Volume 04.03*, ASTM International, West Conshohocken, PA.
28. AASHTO T 307. (1999). *Standard Method of Test for Determining the Resilient Modulus of Soils and Aggregate Materials*, American Association of State Highway and Transportation Officials, Washington, DC.
29. National Cooperative Highway Research Program. (2004). *Research Results Digest No. 285: Laboratory Determination of Resilient Modulus for Flexible Pavement Design*, National Cooperative Highway Research Program, Washington, DC.
30. AASHTO T 180. (2010), *Standard Method of Test for Moisture-Density Relations of Soils Using a 4.54-kg (10-lb) Rammer and a 457-mm (18-in.) Drop*, American Association of State Highway and Transportation Officials, Washington, DC.
31. AASHTO T 100. (2006), *Standard Method of Test for Specific Gravity of Soils*, American Association of State Highway and Transportation Officials, Washington, DC.
32. AASHTO T 215. (2003), *Standard Method of Test for Permeability of Granular Soils (Constant Head)*, American Association of State Highway and Transportation Officials, Washington, DC.
33. AASHTO T 99. (2010), *Standard Method of Test for Moisture-Density Relations of Soils Using a 2.5-kg (5.5-lb) Rammer and a 305-mm (12-in.) Drop*, American Association of State Highway and Transportation Officials, Washington, DC.
34. ASTM D5858. (2008). "Standard Guide for Calculating In Situ Equivalent Elastic Moduli of Pavement Materials Using Layered Elastic Theory," *Annual Book of Standards Volume 04.03*, ASTM International, West Conshohocken, PA.
35. The Transtec Group. *HIPERPAV: High-Performance Paving Software*, Austin, TX. Obtained from: www.hiperpav.com.

36. ASTM C 39. (2012). "Standard Test Method for Compressive Strength of Cylindrical Concrete Specimens," *Annual Book of Standards Volume 04.02*, ASTM International, West Conshohocken, PA.
37. Ozyildirim, C. and Carino, N.J. (2006). "Concrete Strength Testing," *Significance of Tests and Properties of Concrete & Concrete Making Materials*, Chapter 3, ASTM STP 169D, West Conshohocken, PA.
38. Carino, N.J. (2006). "Prediction of Potential Concrete Strength at Later Ages," *Significance of Tests and Properties of Concrete & Concrete Making Materials*, Chapter 4, ASTM STP 169D, West Conshohocken, PA.
39. Mehta, P.K. and Monteiro, P.J.M. (2005). *Concrete*, 3d Edition, McGraw Hill Companies, New York, NY.
40. Neville, A.M. (1996). *Properties of Concrete*, 4th Edition, John Wiley & Sons, New York, NY.
41. Abrams, D.A. (1918). *Design of Concrete Mixtures*, Structural Materials Research Lab, Lewis Institute Bulletin No. 1, Chicago, IL.
42. Colak, A. (2006). "A New Model for the Estimation of Compressive Strength of Portland Cement Concrete," *Cement and Concrete Research*, Netherlands 36(7).
43. Alexander, M.G. and Mindess, S. (2005). *Aggregates in Concrete*, Taylor & Francis, New York, NY.
44. Gilkey, H.J. (1961). "Water-Cement Ratio Versus Strength—Another Look," *ACI Materials Journal*, 57(4), Farmington Hills, MI.
45. Bloem, D.L. and Gaynor, R.D. (1963). "Effects of Aggregate Properties on Strength of Concrete," *ACI Materials Journal*, 60(10), Farmington Hills, MI.
46. Kaplan, M.F. (1959). "Flexural and Compressive Strength of Concrete as Affected by the Properties of Coarse Aggregates," *Proceedings ACI*, 55, Farmington Hills, MI.
47. Bennett, E.W. and Khilji, Z.M. (1964). "The Effect of Some Properties of the Coarse Aggregate in Hardened Concrete," *Journal of the British Granite and Whinstone Federation*, 3(2).
48. De Larrard, F. and Bellock, A. (1997). "The Influence of Aggregate on the Compressive Strength of Normal and High Strength Concrete," *ACI Material Journal*, 94(5), Farmington Hills, MI.
49. ACI 318-05. (2005). *Building Code Requirements for Structural Concrete and Commentary*, American Concrete Institute, Farmington Hills, MI.

50. Namyong, J., Sangchun, Y., and Hongbum, C. (2004). "Prediction of Compressive Strength of In Situ Concrete Based on Mixture Proportions," *Journal of Asian Architecture and Building Engineering*, 3(1), Farmington Hills, MI.
51. Committee Euro-International du Beton (CEB-FIP). (1993). *CEB-FIP Model Code 1990*, Thomas Telford, London, United Kingdom.
52. Ruiz, J.M., Rasmussen, R.O., Chang, G.K., Dick, J.C., Nelson, P.K., Schindler, A.K., Turner, D.K., and Wilde J.W. (2006). *Computer-Based Guidelines for Concrete Pavements, Volume III: Technical Appendices*, Report No. FHWA-HRT-04-127, Federal Highway Administration, Washington DC.
53. Wang, K., Hu, J., and Zhi, G.E. (2008). *Task 4: Testing Iowa Portland Cement Concrete Mixtures for the AASHTO Mechanistic-Empirical Pavement Design Procedure*, CTRE Project 06-270, Ames, IA.
54. Powers, T.C. (1949). *The Nonevaporable Water Content of Hardened Portland Cement Paste—Its Significance for Concrete Researchers and Its Method of Determination*, ASTM Bulletin No. 158, West Conshohocken, PA.
55. Tango, C.E.S. (2000). *Time-Generalization of Abrams' Model for High-Performance Concrete and Practical Application Examples*, Proceedings of the International Symposium on High-Performance Concrete, Hong Kong, China.
56. Forster, S.W. (1997). *Concrete Materials and Mix Design for Assuring Durable Pavements*, Volume 1, Sixth International Purdue Conference on Concrete Pavement Design and Materials for High Performance, Indianapolis, IN.
57. Mohamed, A.R. and Hansen, W. (1999). "Micromechanical Modeling of Crack-Aggregate Interaction in Concrete Materials," *Journal of Cement and Concrete Composites*, 21, 349–359.
58. ASTM C 78-02. (2006). "Standard Test Method for Flexural Strength of Concrete (Using Simple Beam with Third-Point Loading)," *Annual Book of Standards Volume 04.02*, ASTM International, West Conshohocken, PA.
59. Kaplan, M.F. (1959). *Ultrasonic Pulse Velocity, Dynamic Modulus of Elasticity, Poisson Ratio, and Strength of Concrete Made with Thirteen Different Coarse Aggregates*, RILEM Bulletin No. 1, Bagnaux, France.
60. ASTM C 496-90. (1995). "Standard Test Method for Splitting Tensile Strength of Cylindrical Concrete Specimens," *Annual Book of Standards Volume 04.02*, ASTM International, West Conshohocken, PA.
61. Wood, S.L. (1992). "Evaluation of the Long-Term Properties of Concrete," Research and Development Bulletin RD102T, Portland Cement Association, Skokie, IL.

62. Teychenne, D.C. (1954). *Discussion on the Design of Concrete Mixes on the Basis of Flexural Strength*, Proceedings of a Symposium on Mix Design and Quality Control of Concrete, 153, Cement and Concrete Association, London, United Kingdom.
63. The Concrete Society. (2003). *Concrete Industrial Ground Floors—A Guide to Their Design and Construction*, Technical Report 34, Third Ed, Crowthorne, Berkshire, UK.
64. Carrasquillo, R.L., Nilson, A.H., and Slate, F.O. (1981). “Properties of High-Strength Concrete Subjected to Short-Term Loads,” *ACI Materials Journal*, Proceedings, 78(3), Farmington Hills, MI.
65. Legeron, F. and Paultre, P. (2000). “Prediction of Modulus of Rupture of Concrete,” *ACI Materials Journal*, 97(2), Farmington Hills, MI.
66. Sozen, M.A., Zwoyer, E.M., and Siess, C.P. (1959). *Strength in Shear of Beams Without Web Reinforcement*, University of Illinois Engineering Experiment Station Bulletin No. 452, Urbana, IL.
67. Mindess, S. and Young, J.F. (1981). *Concrete*, Prentice-Hall, Inc., Englewood Cliffs, NJ.
68. Iravani, S. (1996). “Mechanical Properties of High-Performance Concrete,” *ACI Materials Journal*, 93(5), Farmington Hills, MI.
69. Gardner, N.J. and Poon, S.M. (1976). “Time and Temperature Effects on Tensile, Bond, and Compressive Strengths,” *ACI Materials Journal*, 73(7), Farmington Hills, MI.
70. Oluokun, F.A. (1991). “Prediction of Concrete Tensile Strength From Compressive Strength: Evaluation of Existing Relations for Normal Weight Concrete,” *ACI Materials Journal*, 88(3), Farmington Hills, MI.
71. Kim, J-K., Han, S.H., and Song, Y.C. (2002). “Effect of Temperature and Aging on the Mechanical Properties of Concrete—Part I: Experimental Results,” *Cement and Concrete Research*, Netherlands.
72. Kim, J-K., Han, S.H., and Song, Y.C. (2002). “Effect of Temperature and Aging on the Mechanical Properties of Concrete—Part II: Prediction Model,” *Cement and Concrete Research*, Netherlands.
73. La Rue, H. (1946). “Modulus of Elasticity of Aggregates and Their Effect on Concrete,” *ASTM Proceedings*, 46, West Conshohocken, PA.
74. Meininger, R.C. (2006). “Degradation Resistance, Strength, and Related Properties of Aggregates,” *Significance of Tests and Properties of Concrete & Concrete-Making Materials*, ASTM STP 169D, West Conshohocken, PA.
75. Hashin, Z. (1962). “The Elastic Moduli of Heterogeneous Materials,” *Journal of Applied Mechanics*, 29(1), Santa Barbara, CA.

76. Hirsh, T.J. (1962). "Modulus of Elasticity of Concrete affected by Elastic Moduli of Cement Paste Matrix and Aggregate," *Journal Proceedings*, 59(3), Farmington Hills, MI.
77. Counto, U.J. (1964). "The Effect of Elastic Modulus of the Aggregate on the Elastic Modulus, Creep, and Creep Recovery of Concrete," *Magazine of Concrete Research*, 16.
78. Hansen, T.C. and Nielsen, K.E.C. (1965). "Influence of Aggregate Properties on Concrete Shrinkage," *Journal ACI*, 63(7), Farmington Hills, MI.
79. Hobbs, D.W. (1971). "The Dependence of Bulk Modulus, Young's Modulus, Creep, Shrinkage and Thermal Expansion of Concrete upon Aggregate Volume Concentration," *Materials and Structures*, 4.
80. Ahmad, S.H. (1994). "Short Term Mechanical Properties," *High-Performance Concrete and Applications*, London, United Kingdom.
81. Alexander, M.G. and Davis, D.E. (1991). "Aggregate in Concrete—New Assessment of Their Role," *Concrete Beton*, 59, 10–20.
82. Alexander, M.G. and Davis, D.E. (1992). "The Influence of Aggregates on the Compressive Strength and Elastic Modulus of Concrete," *The Civil Engineer in South Africa*, 34.
83. Noguchi, T., Tomosawa, F., Nemati, K., Chiaia, B., Fantilli, A. (2009). "A Practical Equation for Elastic Modulus of Concrete," *ACI Structural Journal*, 106(5), Farmington Hills, MI.
84. Tomosawa, F., Noguchi, T., and Onoyama, K. (1990). *Investigation of Fundamental Mechanical Properties of High-Strength Concrete*, Summaries of Technical Papers of Annual Meeting of Architectural Institute of Japan, 497–498.
85. TS 500 Ankara. (2000). *Turkish Standardization Institute Requirements for Design and Construction of Reinforced Concrete Structures*, Turkish Standards Institute, Ankara, Turkey.
86. Westergard, H.M. (1927). "Analysis of Stresses in Concrete Pavements Due to Variations of Temperature," *Highway Research Board Proceedings*, 6, 201–215, Transportation Research Board, Washington, DC.
87. AASHTO T 336. (2009), *Standardized Test Method for the Coefficient of Thermal Expansion of Hydraulic Cement Concrete*, American Association of State Highway and Transportation Officials, Washington, DC.
88. Al-Ostaz. (2007). *Inputs of Portland Cement Concrete Parameters Needed for the Design of New and Rehabilitated Pavements in Mississippi*, Report No. FHWA/MSDOT-RD-07-177, Federal Highway Administration, Washington, DC.

89. ACI. (1971). *Temperature and Concrete*, ACI SP-25, American Concrete Institute, Detroit, MI.
90. Lane, D.S. (1994). "Thermal Properties of Aggregates," *Significance of Tests and Properties of Concrete and Concrete-Making Materials*, ASTM STP 169C, West Conshohocken, PA.
91. Neekhara, S. (2004). *A New Mineralogical Approach to Predict the Coefficient of Thermal Expansion of Aggregate and Concrete: A Thesis*, Texas A&M University, College Station, TX.
92. Powers, T.C. (1971). "Fundamental Aspects of Concrete Shrinkage," *Materials and Structures/Materiaux et Constructions*, (545), 79–85.
93. Troxell, G.E., Raphael, J.M., and Davis, R.E. (1958). "Long-Time Creep and Shrinkage Tests of Plain and Reinforced Concrete," *ASTM Proceedings*, 58, 1–20, West Conshohocken, PA.
94. Bazant, Z.P. and Baweja, S. (2000). "Creep and Shrinkage Prediction Model for Analysis and Design of Concrete Structures: Model B3," *Adam Neville Symposium: Creep and Shrinkage—Structural Design Effects*, ACI SP-194, American Concrete Institute, Farmington Hills, MI.
95. Arellano, D. and Thompson, M.R. (1998). *Final Report: Stabilized Base Properties (Strength, Modulus, Fatigue) for Mechanistic-Based Airport Pavement Design*, COE Report No. 4, University of Illinois at Urbana-Champaign, Urbana, IL.
96. Thompson, M.R. (1986). *Mechanistic Design Concept for Stabilized Base Pavements*, Transportation Engineering Series No. 46, Illinois Cooperative Highway and Transportation Series No. 214, University of Illinois, Urbana, IL.
97. ASTM D1633. (2007). "Standard Test Methods for Compressive Strength of Molded Soil-Cement Cylinders," *Annual Book of Standards Volume 04.08*, ASTM International, West Conshohocken, PA.
98. American Coal Ash Association. (1991). *Flexible Pavement Manual*, American Coal Ash Association, Washington, DC.
99. ASTM C593. (2006). "Standard Specification for Fly Ash and Other Pozzolans for Use With Lime for Soil Stabilization," *Annual Book of Standards Volume 04.01*, ASTM International, West Conshohocken, PA.
100. Little, D.N. (2000). *Evaluation of Structural Properties of Lime Stabilized Soils and Aggregates, Volume 3: Mixture Design and Testing Protocol for Lime Stabilized Soils*, National Lime Association, Arlington, VA.

101. ASTM D5102. (2009). "Standard Test Method for Unconfined Compressive Strength of Compacted Soil-Lime Mixtures," *Annual Book of Standards Volume 04.08*, ASTM International, West Conshohocken, PA.
102. National Cooperative Highway Research Program. (2008). *NCHRP Synthesis 382: Estimating Stiffness of Subgrade and Unbound Materials for Pavement Design*, Transportation Research Board, Washington, DC.
103. Transportation Research Board. (2003). *Harmonized Test Methods for Laboratory Determination of Resilient Modulus for Flexible Pavement Design*, NCHRP Project 1-28A, National Cooperative Highway Research Program, Washington, DC.
104. Carmichael III, R.F. and Stuart, E. (1985). "Predicting Resilient Modulus: A Study to Determine the Mechanical Properties of Subgrade Soils," *Transportation Research Record 1043*, Transportation Research Board, Washington, DC.
105. Drumm, E.C., Boateng-Poku, Y., and Johnson Pierce, T. (1990). "Estimation of Subgrade Resilient Modulus from Standard Tests," *Journal of Geotechnical and Geoenvironmental Engineering*, 116(5), Reston, VA.
106. George, K.P. (2004). *Prediction of Resilient Modulus from Soil Index Properties*, Report No. FHWA/MS-DOT-RD-04-172, Federal Highway Administration, Washington, DC.
107. Heukelom, W. and Klomp, A.J.G. (1962). *Dynamic Testing as a Means of Controlling Pavements During and After Construction*, Proceedings of the First International Conference on Structural Design of Asphalt Pavements, Ann Arbor, MI.
108. Asphalt Institute. (1982). *Research and Development of the Asphalt Institute's Thickness Design Manual*, Report No. 82-2, Ninth Edition, Asphalt Institute, Lexington, KY.
109. Webb, W.M. and Campbell, B.E. (1986). *Preliminary Investigation into Resilient Modulus Testing for New AASHTO Pavement Design Guide*, Georgia Department of Transportation, Atlanta, GA.
110. Yeh, S.T. and Su, C.K. (1989). *Resilient Properties of Colorado Soils*, Report No. CDOH-DH-SM-89-9, Colorado Department of Highways, Denver, CO.
111. Jones, M.P. and Witzak, M.W. (1972). "Subgrade Modulus on the San Diego Test Road," *Transportation Research Record 641*, Transportation Research Board, Washington, DC.
112. Thompson, M.R. and LaGrow, T.G. (1988). *A Proposed Conventional Flexible Pavement Thickness Design Procedure*, Report No. FHWA-IL-UI-223, Illinois Department of Transportation, Springfield, IL.
113. Thompson, M.R. and Robnett, Q.L. (1979). "Resilient Properties of Subgrade Soils," *Journal of Transportation Engineering*, 105(1), Reston, VA.

114. Elliot, R.P., Thornton, S.I., Foo, K.Y., Siew, K.W., and Woodbridge, R. (1988). *Resilient Properties of Arkansas Subgrades*, Report No. FHWA/AR-89/004, Arkansas Highway and Transportation Research Center, Little Rock, AK.
115. Rahim, A.M. (2005). "Subgrade Soil Index Properties to Estimate Resilient Modulus for Pavement Design," *The International Journal of Pavement Engineering*, 6(3), London, England.
116. Farrar, M. and Turner, J. (1991). *Resilient Modulus of Wyoming Subgrade Soils*, Report No. MPC 91-1, Mountains-Plains Consortium, Fargo, ND.
117. Hudson, J.M., Drumm, E.C., and Madgett, M. (1994). *Design Handbook for the Estimation of Resilient Response of Fine-Grained Subgrades*, 4th International Conference on the Bearing Capacity of Roads and Airfields, Minneapolis, MN.
118. Li, D. and Selig, E.T. (1994). "Resilient Modulus for Fine-Grained Subgrade Soils," *Journal of Geotechnical and Geoenvironmental Engineering*, 120(6), Reston, VA.
119. Gupta, S., Ranaivoson, A., Edil, T., Benson, C., and Sawangsuriya, A. (2007). *Pavement Design Using Unsaturated Soil Technology*, MN/RC-2007-11, Minnesota Department of Transportation, St. Paul, MN.
120. Berg, R.L., Bigl, S.R., Stark, J.A., and Durell, G.D. (1996). *Resilient Modulus Testing of Materials from Mn/ROAD: Phase 1*, CRREL Special Report 96-19, Minnesota Department of Transportation, St. Paul, MN.
121. Pezo, R.F. and Hudson, W.R. (1994). "Prediction Models of Resilient Modulus for Nongranular Materials," *Geotechnical Testing Journal*, 17(3), Washington, DC.
122. Powell, W.D., Potter, J.F., Mayhew, H.C., and Nunn, M.E. (1984). *Transport and Road Research Laboratory: The Structural Design of Bituminous Roads*, TRRL Report 1132, Department of Transport, Berkshire, United Kingdom.
123. Asphalt Institute. (1999). *Thickness Design: Asphalt Pavements for Highways and Streets*, Series No. 1, Asphalt Institute, Lexington, KY.
124. Buu, T. (1980). "Correlation of Resistance R-Value and Resilient Modulus of Idaho Subgrade Soil," *Special Report No. ML-08-80-G*, Idaho Department of Transportation, Boise, ID.
125. Lee, W., Bohra, N.C., Altschaeffl, A.G., and White, T.D. (1997). "Resilient Modulus of Cohesive Soils," *Journal of Geotechnical and Geoenvironmental Engineering*, 123(2), Reston, VA.
126. Hassan, A. (1996). *The Effect of Material Parameters on Dynamic Cone Penetrometer Results for Fine-Grained Soils and Granular Materials*, Ph.D. Dissertation, Oklahoma State University, Stillwater, OK.

127. Chen, J.Z., Mustaque, H., and LaTorella, M.T. (1999). "Use of Falling Weight Deflectometer and Dynamic Cone Penetrometer in Pavement Evaluation," *Transportation Research Record 1655*, Transportation Research Board, Washington, DC.
128. George, K.P. and Uddin, W. (2000). *Subgrade Characterization for Highway Design*, FHWA/MS-DOT-RD-00-131, Mississippi Department of Transportation, Jackson, MS.
129. Chen, D.H., Lin, D.F., Liao, P.H., and Bilyeu, J. (2005). "A Correlation Between Dynamic Cone Penetrometer Values and Pavement Layer Moduli," *Geotechnical Testing Journal*, 28(1), Washington, DC.
130. Mohammad, L.N., Herath, A., Gaspard, K., Abu-Farsakh, M.Y., and Gudishala, R. (2007). "Prediction of Resilient Modulus of Cohesive Subgrade Soils from Dynamic Cone Penetrometer Test Parameters," *Journal of Materials in Civil Engineering*, 19(11), Reston, VA.
131. Mohammad, L.N., Titi, H.H., and Herath, A. (2000). *Investigation of the Applicability of Intrusion Technology to Estimate the Resilient Modulus of Subgrade Soil*, FHWA/LA-00/332, Louisiana Transportation Research Center, Baton Rouge, LA.
132. Von Quintus, H. and Killingsworth, B. (1998). *Analyses Relating to Pavement Material Characterizations and Their Effects on Pavement Performance*, Report No. FHWARD-97-085, Federal Highway Administration, Washington, DC.
133. Dai, S. and Zollars, J. (2002). "Resilient Modulus of Minnesota Road Research Project Subgrade Soil," *Transportation Research Record 1786*, Transportation Research Board, Washington, DC.
134. Santha, B.L. (1994). "Resilient Modulus of Subgrade Soils: Comparison of Two Constitutive Equations," *Transportation Research Record 1462*, Transportation Research Board, Washington, DC.
135. Yau, A. and Von Quintus, H.L. (2002). *Study of LTPP Laboratory Resilient Modulus Test Data and Response Characteristics*, Final Report, Report No. FHWA-RD-02-051, Federal Highway Administration, Washington, DC.
136. Larson, G. and Dempsey, B.J. (1997). *Enhanced Integrated Climatic Model, Version 2.0*, Final Report, Contract DTFA MN/DOT 72114, University of Illinois at Urbana-Champaign, Urbana, IL.
137. Zapata, C. and Houston, W.N. (2008). *NCHRP Report 602: Calibration and Validation of the Enhanced Integrated Climatic Model for Pavement Design*, NCHRP Project 9-23, Transportation Research Board, Washington, DC.
138. Titi, H., Elias, M.B., and Helwany, S. (2006). *Determination of Typical Resilient Modulus Values for Selected Soils in Wisconsin*, Report No. WHRP 0092-03-11, Wisconsin Department of Transportation, Madison, WI.

139. Rahim, A.M. and George, K.P. (2005). "Models to Estimate Subgrade Resilient Modulus for Pavement Design," *The International Journal of Pavement Engineering*, 6(2), London, England.
140. Mohammad, L.N., Huang, B., Puppala, A.J., and Allen, A. (1999). "Regression Model for Resilient Modulus of Subgrade Soil," *Transportation Research Record 1687*, Transportation Research Board, Washington, DC.
141. Titus-Glover, L., Mallela, J., Jiang, J., Ayres, M.E., and Shami, H.I. (2001). *Assessment of Selected LTPP Material Data Tables and Development of Representative Test Tables*, Report No. FHWA-RD-02-001, Federal Highway Administration, Washington DC.
142. Federal Highway Administration (2010). *Long-Term Pavement Performance Program—Standard Data Release 24.0*, VR2010.0, DVD Version, Federal Highway Administration, Washington, DC.
143. Mallows, C.L. (1973). "Some Comments on CP," *Technometrics*, 15(4), Alexandria, VA.
144. Crawford, G., Gudimettla, J., and Tanesi, J. (2010). "Inter-Laboratory Study on Measuring Coefficient of Thermal Expansion of Concrete," *Paper 10-2068*, Presented at the Annual Meeting of the Transportation Research Board, Washington DC.
145. Tanesi, J., Crawford, G., Nicolaescu, M., Meininger, R., Gudimettla, J. (2010). "How Will the New AASHTO T336-09 CTE Test Method Impact You?," *Paper 10-1631*, Presented at the Annual Meeting of the Transportation Research Board, Washington DC.

